DATA COMPRESSION OF ECG RHYTHMS

Ph.D. THESIS

by

SHANTI CHANDRA

DEPARTMENT OF ELECTRICAL ENGINEERING
INDIAN INSTITUTE OF TECHNOLOGY ROORKEE
ROORKEE-247667 (INDIA)
July, 2019

DATA COMPRESSION OF ECG RHYTHMS

A THESIS

Submitted in partial fulfilment of the requirements for the award of the degree

of

DOCTOR OF PHILOSOPHY

in

ELECTRICAL ENGINEERING

by

SHANTI CHANDRA

DEPARTMENT OF ELECTRICAL ENGINEERING
INDIAN INSTITUTE OF TECHNOLOGY ROORKEE
ROORKEE-247667 (INDIA)
July, 2019

©INDIAN INSTITUTE OF TECHNOLOGY ROORKEE, ROORKEE - 2019
ALL RIGHTS RESERVED

INDIAN INSTITUTE OF TECHNOLOGY ROORKEE
ROORKEE

CANDIDATE'S DECLARATION

I hereby certify that the work which is being presented in the thesis entitled "**DATA COMPRESSION OF ECG RHYTHMS**" in partial fulfilment of the requirements for the award of the Degree of Doctor of Philosophy and submitted in the Department of Electrical Engineering of the Indian Institute of Technology Roorkee, Roorkee is an authentic record of my own work carried out during a period from July, 2015 to July, 2019 under the supervision of Dr. A. Sharma, Assistant Professor and Dr. G. K. Singh. Professor, Department of Electrical Engineering, Indian Institute of Technology Roorkee, Roorkee.

The matter presented in this thesis has not been submitted by me for the award of any other degree of this or any other Institution.

(SHANTI CHANDRA)

This is to certify that the above statement made by the candidate is correct to the best of our knowledge.

(Ambalika Sharma)
Supervisor

(G. K Singh)
Supervisor

The Ph.D. Viva-Voce Examination of Shanti Chandra, Research Scholar, has been held on _____

Chairman, SRC

Signature of External Examiner

This is to be certified that the student has made all the correction in the thesis.

Signature of Supervisor(s)

Head of the Department

ABSTRACT

Heart diseases, such as coronary heart disease, congestive heart failure, and congenital heart disease, are the leading cause of deaths for men and women all over the world. The continuous monitoring for twenty-four-hour is necessary to detect heart abnormalities for the critical cardiac patient. Therefore, recent developments in Electrocardiogram (ECG) signal processing, information technology and communication has brought a new dimension to the medical world. ECG is a quasi-periodic and non-stationary signal that is generated by the action of depolarization and repolarization of the cardiac cells. The analysis of ECG signal is very significant for feature extraction and interpretation of heart diseases. Timely diagnosis is an important factor in the treatment of cardiac abnormalities; however, it is not possible for every cardiac patient. Therefore, incorporation of wireless communication technology in the field of telemedicine, especially tele-cardiological systems has played an incredible role in the timely monitoring of a heart patient. However, these technologies are resource-constrained applications with limited bandwidth and power. Transmission /transfer of large amount of physiological data to healthcare /e-healthcare centers is very expensive. Therefore, these systems require efficient data reduction before transmission.

In many cases, cardiologists need observation of the continuous heart activity of the patient after release from the hospital. In these cases, ambulatory monitoring or Holter monitoring system plays an important role. In these systems, data recording and storing is done for twenty-four-hour. For effective data storing, data size must be as less as possible. Therefore, ECG data compression is an essential part of these types of devices. As a result, ECG data compression is an important area of research for the last few decades. Data compression is the process of converting the bits structure of data in such a way that it consumes less space on disk. The major aim of every data compression method is to accomplish maximum data volume reduction while preserving the important features of the signal morphology during reconstruction.

Data compression techniques can be divided into four major types, direct data compression (DDC), transform based data compression, feature extraction based data compression, and two dimensional (2D) data compression. In DDC techniques, data is compressed in time domain, therefore, these methods do not provide efficient results in terms of compression ratio (CR) and signal reconstruction quality. In feature extraction

based data compression techniques, useful features are extracted and used for reconstructing the signal. These methods provide a good CR; however, the signal reconstruction quality is very poor. In 2D data compression techniques first, 1D ECG signal is converted into 2D, then 2D data compression techniques such as joint photographic experts group (JPEG) and set partitioning in the hierarchical trees (SPHIT) are employed for data reduction. These techniques provide good results in terms of CR and signal reconstruction quality both. However, conversion of signal from 1D to 2D is a time taking and complex process for the non-stationary signals such as ECG, and hence these techniques cannot be used for real-time processing. Therefore, for the last two decades, several studies have been carried out to compress the ECG rhythms, in which researchers have used transform based techniques. are generally used to compress the data compression of ECG rhythms. In these techniques, data is transformed from time domain to frequency domain. Among all transform based techniques, wavelet and filter bank based techniques are preferred, because of multi-resolution property of them. Therefore, the aim of this thesis is to develop an ECG signal compression algorithm that has a high compression ratio while guaranteeing signal quality.

A wavelet filter bank is a tree-structured filter bank that decomposes the signal into sub-bands, and the power of time and frequency based parallel signal processing is exploited. Modulated filter banks (MFBs) is a cost-effective way to design and implement filter banks. Amongst all modulated filter banks, cosine modulated filter banks (CMFBs) provide the best results in terms of computational efficiency with small number of optimization parameters. Computational efficiency can be improved further by using computationally efficient prototype filter. An interpolated finite impulse response (IFIR) filter is a highly efficient filter in terms of computational complexity. Hence, in the present research work, the mammoth task of signal compression has been accomplished using computationally efficient CMFB, which also provides low implementation cost, higher compression ratio, and good signal reconstruction quality.

Noise elimination is the first step of this work, because feature extraction and comparison is utilized here to examine the data decompression performance, and presence of noise may lead to false feature extraction. Therefore, in this work, elimination of noise is carried out using IFIR and frequency response masking (FRM) techniques. This filtering technique provides linear phase, inherently stable output with low computational complexity, which are the important factors for any signal processing.

The design of nearly perfect reconstructed 4, 8, 16 and 32 channel uniform and 3, 4 and 5 channel non-uniform cosine modulated filter banks are done. A nearly perfect filter bank suffers from three types of distortions; a) amplitude distortion, b) aliasing distortion and c) phase distortion. Phase distortion can be eliminated completely using linear phase filters (FIR or IFIR), aliasing distortion and amplitude distortion can be minimized by suitable optimization technique. Here, for designing the filter banks, three approaches are used such as: a) a simple and proficient linear iterative technique, b) Schittkowski algorithm, and c) passband edge iteration to minimize the cost function. In technique (a), the cut-off frequency of the model filter is optimized to satisfy the perfect reconstruction condition in CMFB. Different fixed (Blackman, rectangular, Bartlett, Hanning and hamming) and adjustable (Kaiser, Dolph-Chebyshev, Saramaki, ultraspherical, symmetric exponential, symmetric hyperbolic cosine, symmetric Nuttall, extended Norton-beer, modified Kaiser, Gaussian and Taylor) window functions are used for designing the linear phase IFIR prototype filter for the CMFB. 8-channel uniform and 5 channel non-uniform filter bank are used for feature extraction and data compression, respectively. The non-uniform CMFB /QMF /WT is used for ECG data compression by decomposing the ECG signal into various frequency bands. Subsequently, thresholding is applied for truncating the insignificant coefficients. The estimation of threshold value is performed by examining the significant energy of each band. Encodings (RLE /Huffman /LZW) are utilized for the compression. In this work, performance is measured in terms of CR and signal reconstruction quality (peak mean square difference (PRD), signal to noise ratio (SNR), mean square error (MSE), mean error (ME), peak mean square difference normalized (PRDN) and quality score (QS). And also signal reconstruction quality is measured by extracting and comparing the features of both signals (original signal before the compression and reconstructed signal after decompression). R-peak extraction through wavelet transforms using bi-orthogonal mother wavelet and 8-channel uniform CMFB is done. The extraction of other features, *viz*., Q waves, S waves, P waves, T waves, P wave onset & offset points, T wave onset & offset points, QRS onset and offset points are identified using rule-based algorithms developed for the study. In this work, weighted diagnostic distortion (WDD) a measure of signal reconstruction quality and accuracy, has been used.

In addition to eighteen, two new features (number of P waves and ventricular late potential) are used to compute the value of WDD. The tabular results show that the filter

banks provide better results as compared to other related work (in terms of computational complexity) without affecting the other fidelity parameters. The data compression performance of the method based on CMFB provides efficient results in terms of CR and preserving diagnostic information (WDD).

Finally, it can be stated that the work contributes significantly to the area of ECG data compression techniques. The developed methods are very much useful for telemedicine, especially in telecardiology. The overall work done in this thesis may be considered a positive and significant contribution for effective healthcare services to remotely located patients. In the current open society and with the growth of human rights, people are more concerned about the privacy of their information and other important data. Water marking and compression of ECG data can protect the individual identification and information. An ECG signal cannot be only used to analyse disease, but also to provide biometric information for identification and authentication. Integrating ECG water marking and compression approach can be taken as an area for future study, as ECG water marking can ensure the confidentiality and reliability of users' data while reducing the amount of data.

ACKNOWLEDGEMENTS

I express my deepest sense of gratitude towards my supervisors Dr. A. Sharma, Assistant Professor, Department of Electrical Engineering of Indian Institute of Technology Roorkee, and Prof. G. K. Singh, Professor, Department of Electrical Engineering of Indian Institute of Technology, Roorkee for their inspiring guidance, constant encouragement, moral support, and keen interest in minute details of the work.

I am thankful to Prof. G. N. Pillai, Professor Department of Electrical Engineering of Indian Institute of Technology, Roorkee Dr. M. Felix Orlando Assistant Professor, Department of Electrical Engineering of Indian Institute of Technology Roorkee for their invaluable encouragement and support, and above all the noblest treatment extended by them.

I am extremely thankful to my fellow researchers Miss. Prachi Tripathi, Mrs. Sneha Singh, Mr. Ashish Rohela, Mr. Gaurav Shukla, Mr. Prateek Singh and Mr. K. A. Chinmaya.

I express my deep sense of gratitude to my father, Late Shri. Ram Chandra and to my beloved mother Smt. R. P. Channdra and my in-laws Sri. Amar Singh and Smt. Usha Rani for their moral support, encouragement and care which provided the necessary impetus and strength to achieve this work. I will also remain grateful to my brother Mr. Mukesh Chandra. I acknowledge with utmost warmth the everlasting love and unending support of my Husband Vikash Singh.

Lastly, I owe a deep sense of gratitude to the All-pervading, All-sustaining Spirit whose Divine light and warmth provided me the perseverance, guidance, inspiration, faith and strength to carry on even when the going got tough.

(**Shanti Chandra**)

CONTENTS

ABSTRACT I
ACKNOWLEDGMENTS V
CONTENTS VII
LIST OF FIGURES XIII
LIST OF TABLES XVIII
LIST OF ABBREVIATIONS XX
LIST OF SYMBOLS XXVI

CHAPTER 1: INTRODUCTION

1.1. Overview 1
1.2. The Heart 2
1.2.1. Cardiovascular System 2
1.2.2. Impulse Conduction System 5
1.2.3. ECG Signal 5
1.2.3.1. Application of ECG Signal 6
1.2.3.2. Cardiac Vectors and Lead System 7
1.2.3.3. MIT-BIH Database 8
1.3. ECG Data Compression 9
1.3.1. The Need for ECG Signal Compression 9
1.3.1.1. Telemedicine and e-healthcare System 9
1.3.1.2. Holter Monitor Systems 12
1.3.1.3. Reducing the Storage Requirements 12
1.4. Digital Filters 13
1.4.4. IFIR Filter 13
1.4.2. Filter Bank 15
1.5. Literature Review 15
1.5.1. Data Compression 15
1.5.1.1. Direct Data Compression 16
1.5.1.2. Transformation Compression Techniques 18
1.5.1.3. Parameter Extraction Compression 24
1.5.2. Noise Elimination 25
1.5.3. Feature Extraction 28
1.5.4. IFIR Filter and Filter Bank 31

1.6. Author’s contribution 36
1.6. Research Objectives 38
1.7. Thesis Outlines 40

CHAPTER 2: ECG SIGNAL NOISE REDUCTION TECHNIQUES

2.1. Overview 41
2.2. Filtering 42
2.2.1. Infinite Impulse Response Filter 42
2.2.2. Finite Impulse Response Filter 43
2.2.2.1.Windowing Method 44
2.2.2.1.1. Fixed Window Functions 44
2.2.2.1.1.1. Blackman window function 44
2.2.2.1.1.2. Rectangular Window Function 45
2.2.2.1.1.3. Bartlett Window Function 45
2.2.2.1.1.4. Hanning Window Function 45
2.2.2.1.1.5. Hamming Window Function 46
2.2.2.1.1.6. Blackman-Harris Window Function 46
2.2.2.1.1.7. Flat Top Window Function 46
2.2.2.1.1.8. Modified Bartlett-Hann Window Function 47
2.2.2.1.1.9. Nuttall Window Function 47
2.2.2.1.1.10. Parzen Window Function 47
2.2.2.1.2. Adjustable Window Functions 48
2.2.2.1.2.1. Kaiser Window Function 48
2.2.2.1.2.2. Dolph–Chebyshev Window Function 48
2.2.2.1.2.3. Saramaki Window Function 49
2.2.2.1.2.4. Roark’s Transitional Window Function 51
2.2.2.1.2.5. Ultraspherical Polynomials Window Function 51
2.2.2.1.2.6. Exponential or Poisson window Function 52
2.2.2.1.2.7. Gaussian Window Function 52
2.2.2.1.2.8. Tapered Cosine Window Function 54
2.2.2.1.2.9. Hyperbolic Cosine Window Function 54
2.2.2.2. Weighted Least Squares Method 55
2.2.2.3. Parks–McClellan Method 55

2.2.3. IFIR Filters 56
2.2.4. Adaptive Filters 60
2.3. Multirate Signal Processing 61
2.3.1. M-fold Decimator 61
2.3.2. L-fold Expender 63
2.3.3. Multirate Filter Bank 63
2.3.3.1. Types of Multirate Filter Bank 65
2.3.3.1.1. Two-channel Filter Bank 65
2.3.3.1.2. *M*-channel Filter Bank 65
2.3.3.1.2.1. Uniform *M*-channel Filter Bank 67
2.3.3.1.2.2. Non-uniform M-channel Filter Bank 68
2.3.3.2. Cosine Modulated Filter Bank 68
2.3.3.2. Wavelet Transform 68
2.3.3.3. Maximal Overlap Discrete Wavelet Transform 71
2.4. Summary 72

CHAPTER 3: NOISE REDUCTION OF ECG SIGNAL

3.1. Overview 73
3.2. Noise Reduction using IFIR Filter 73
3.2.1. Baseline Wander Noise Reduction 74
3.2.2. High-Frequency Noise Reduction 77
3.2.3. Powerline Interference Minimization 82
3.3. Proposed IFIR Filter 82
3.3.1. Analysis of Time Domain Coefficients of The FIR and IFIR Filters 82
3.3.2. Performance Evaluation of the Proposed Technique 87
3.4. Noise Elimination using Proposed Filters 90
3.5. Noise Reduction using WT 93
3.5.1. High-frequency Noise Minimization 93
3.5.2. Baseline Wander Removing 93
3.6. Discussion 95
3.6. Summary 95

CHAPTER 4: ECG DATA COMPRESSION TECHNIQUES

4.1. Overview 97
4.2. Direct Data Compression Techniques 99
4.2.1. Amplitude Zone Time Epoch Coding (AZTEC) 99
4.2.2. Turning Point (TP) 99
4.2.3. Co-ordinate Reduction Time Encoding System (CORTES) 100
4.2.4. Fan Algorithm 100
4.2.5. Scan Along Polygonal Approximation (SAPA) 101
4.2.6. Encoding Methodologies 101
4.2.6.1. Run-Length Encoding (RLE) 101
4.2.6.2. Huffman Coding 101
4.2.6.3. LZW Encoding 102
4.3. Transform Based Techniques 102
4.3.1. Hilbert Transform 104
4.3.2. Fourier Transform 104
4.3.3. Discrete Cosine Transform 105
4.3.4. Empirical Mode Decomposition (EMD) 106
4.3.5. Discrete Wavelet Transform (DWT) 107
4.3.6. Empirical Wavelet Transform (EWT) 108
4.4. Parameter Extraction Techniques 110
4.5. 2- Dimensional Compression Techniques 111
4.6. Performance Parameters 111
4.7. Summary 112

CHAPTER 5: DATA COMPRESSION OF ECG SIGNAL USING WAVELET FILTER BANK

5.1. Overview 113
5.2. Data Compression using Wavelet Packet Decomposition and RLE 114
5.3. Data Compression using Two-Channel Filter Bank 122
5.4. ECG Data Compression using Wavelet Transform and RLE 130
5.5. ECG Data Compression using Wavelet Transform and Huffman coding 130
5.6. ECG Data Compression using Wavelet Transform and LZW 130
5.7. ECG Data Compression using Empirical Wavelet Transform 134
5.8. Discussion 135

5.9. Summary 138

CHAPTER 6: DATA COMPRESSION OF ECG SIGNAL USING COSINE MODULATED FILTER BANK

6.1. Overview 139
6.2. Near-Perfect-Reconstruction Pseudo-QMF Banks using IFIR Filter 140
6.3. CMFB Design using Window Function 144
6.3.1. CMFB Design using Fixed Window Function 148
6.3.2. CMFB Design using Adjustable Window Function 151
6.3.3. CMFB Design Using Other Optimum Convex Method of Equiripple Filter 158
6.4. Compression of ECG Rhythms using CMFB 162
6.4.1. Data Reconstruction 165
6.4.2. Compression of ECG Rhythms using CMFB and LZW Encoding 171
6.5. Summary 174

CHAPTER 7: PERFORMANCE EVALUATION

7.1. Overview 175
7.2. Beat Detection using WT 175
7.3. R-Peaks Detection using CMFB 177
7.4. Feature Extraction 177
7.5. Experiments and Results 181
7.6. Performance Measurement of Data Decompression 185
7.6.1. Performance Evaluation using Function WDD 190
7.7. Discussions 193
7.8. Summary 194

CHAPTER 8: CONCLUSIONS

8.1. Overview 195
8.2. Main Findings 195
8.2.1. Methodologies used for the Design of Filter and Filter Bank 195
8.2.2. ECG Data Compression 196
8.3. Future Scope 197

PUBLICATIONS 199

BIBLIOGRAPHY 201

List of Figures

Figure No.	Caption	Page No.
Fig. 1.1	The heart [2]	3
Fig. 1.2	Flow diagram of circulatory system [7]	3
Fig. 1.3	Circulatory system [2].	4
Fig. 1.4	Flow diagram of impulse conduction system	4
Fig. 1.5	Impulse conduction system [2].	4
Fig. 1.6	Normal ECG signal [54].	5
Fig. 1.7	12-lead system [2].	10
Fig. 1.8	Telemedicine /e-health care system.	11
Fig. 1.9	Holter monitor system [48].	11
Fig. 1.10	Ideal low pass [1].	12
Fig. 1.11	IFIR structure [22].	14
Fig. 1.12	Two stages IFIR structure [24].	14
Fig. 2.1	Lowpass filter response.	43
Fig. 2.2	Comparison of Shape of Different Fixed Windows.	50
Fig. 2.3	Comparison of normalized magnitude spectrum of different fixed windows.	53
Fig. 2.4	Comparison of the shape of different adjustable windows.	53
Fig. 2.5	Comparison of normalized magnitude spectrum of different adjustable windows.	55
Fig. 2.6	IFIR structure [3].	56
Fig. 2.7	Two stages IFIR structure [22].	59
Fig. 2.8	Frequency response of (a) FIR filter, (b) Model filter, (c) Modal filter after Up-sampling, (d) Interpolator/Image suppression filter and (e) Final response of IFIR filter [227].	59
Fig. 2.9	An FRM filter structure [227].	59
Fig. 2.10	Block diagram of an adaptive filter [158].	61
Fig. 2.11	M-fold decimator [23].	62
Fig. 2.12	Down-sampling in frequency domain [23].	62
Fig. 2.13	L-fold expender [23].	62
Fig. 2.14	(a) Input signal and (b) Up-sampled signal [24].	62
Fig. 2.15	M-channel filter bank [259].	64
Fig. 2.16	Classification of the filter [285].	64
Fig. 2.17	Two-channel filter bank [264].	66
Fig. 2.18	Two-Channel filter bank response [265].	66
Fig. 2.19	Block diagram of M-channel FB [254].	66
Fig. 2.20	Tree Structured NUFB [285]	69
Fig. 2.21	Parallel structured NUFB [285]	69
Fig. 2.22	Wavelet decomposition for a signal [6].	69
Fig. 3.1	(a) Noise-free original ECG (record MIT-BIH 100) signal, (b) Baseline wander is introduced in the original signal (linearly incremented), (c) Baseline wander is removed completely	75

Fig. 3.2 (a) Baseline wander is introduced in the original signal (linearly decremented) and (b) Baseline wander is removed 75

Fig. 3.3 (a) Baseline wander is introduced in the original signal (sine wave 0.57 Hz) and (b) Baseline wander is removed 75

Fig. 3.4 FIR filter structure of 5 tap. 78

Fig. 3.5 (a) Original signal (MIT-BIH dataset record no. 103), (b) High-frequency noise (450 to 1000 Hz) is present in the signal and (c) Noise is removed 80

Fig. 3.6 (a) Original signal (MIT-BIH dataset record no. 106), (b) Multiple frequencies with multiple amplitude noise (450 to 1000 Hz) is present in the signal and (c) Noise is removed 81

Fig. 3.7 (a) Notch filter structure, (b) Response of notch filter using IFIR technique (c) Power line interferences present in ECG signal (MIT-BIH arrhythmia record no. 121) and (d) Noise is eliminated using notch filter 81

Fig. 3.8 Design of IFIR filter using conventional approach $A_s = 100$ dB, $\omega_{ss} = 0{:}0555\pi$ and $\omega p = 0{:}0413\ \pi$. Magnitude response: (a) FIR model filter, (b) modal filter, (c) up-sampled model $G(z^L)$, (d) Interpolator filter, (e) IFIR filter and (f) Comparison of FIR and IFIR filter. 85

Fig. 3.9 Coefficient plots of FIR and IFIR, using (a) Conventional method and (b) Proposed method 85

Fig. 3.10 Relationship plot between (a) Up-sampling factor and transition width, (b) Transition width and filter orders of FIR and IFIR filter and (c) Up-sampling factor and computational complexity reduction. 88

Fig. 3.11 (a) Response of proposed IFIR filter, (b) Comparison of responses of FIR, conventional IFIR and proposed IFIR filter and (c) Comparison of *DFD* of FIR, conventional IFIR and proposed IFIR filter 88

Fig. 3.12 (a) Response of proposed two-stage IFIR filter, (b) Comparison of responses of FIR, conventional two-stage IFIR and proposed two-stage IFIR filter and (c) Comparison of *DFD* of FIR, conventional two-stage IFIR and proposed two stage IFIR filter. 89

Fig. 3.13 (a) Noisy ECG signal (MIT-BIH-118e00) and (b) Noise is removed using proposed IFIR filter. 89

Fig. 3.14 50 Hz noise reduction from MIT-BIH record no. 123 using notch filter designed by proposed. 91

Fig. 3.15 (a) MIT-BIH record no. 224 with Baseline wander reduction and (b) Baseline wander is removed using IFIR filter. 91

Fig. 3.16 (a) Noise present in the ECG signal (MIT-BIH arrhythmia record no. 232) and (b) Noise is eliminated using MODWT. 94

Fig. 3.17 (a) 60 seconds ECG signal (MIT-BIH noise stress test database record no.118e24m) with baseline wander and (b) Signal after baseline wander removal. 94

Fig. 4.1 Broad classification of data [36]. 98

Fig. 4.2 Classification of data compression. 98

Fig. 4.3 LZW encoding algorithm [307]. 97

Fig. 4.4	EWT decomposition representation using low pass and band pass filters [18].	102
Fig. 5.1	Modified RLE	115
Fig. 5.2	ECG data compression methodology	115
Fig. 5.3	Signal decomposition of lower frequency bands	120
Fig. 5.4	Signal decomposition of higher frequency	121
Fig. 5.5	(a) Original signal, (b) Reconstructed signal after decompression, (c) Beat detection in the original signal and (d) Beat detection in the reconstructed signal.	121
Fig. 5.6	Proposed data compression technique	123
Fig. 5.7	Signal reconstruction steps	124
Fig. 5.8	(a) Analysis filter bank response and (b) Synthesis filter bank	124
Fig. 5.9	Decomposition of signal	126
Fig. 5.10	Original and reconstructed signal	126
Fig. 5.11	R-peaks detection in the original and reconstructed signal	128
Fig. 5.12	ECG compression using wavelet and RLE	129
Fig. 5.13	ECG compression using wavelet and Huffman's coding.	131
Fig. 5.14	ECG compression using wavelet and LZW encoding	132
Fig. 5.15	Steps used in data compression methodology	133
Fig. 5.16	Threshold value measurement	133
Fig. 5.17	MIT-BIH arrhythmia database (100m signal) and 3 mode signals.	136
Fig. 5.18	Compression ratio on different detailed energy packing efficiencies	136
Fig. 5.19	PRD on different detailed energy packing efficiencies	136
Fig. 5.20	(a) Original and (b) Reconstructed signal	137
Fig. 6.1	(a) Frequency response of analysis filters and (b) Reconstruction error in dB	145
Fig. 6.2	(a) Frequency response of analysis filters and (b) Reconstruction error in dB	145
Fig. 6.3	Block diagram of optimization of prototype filter	147
Fig. 6.4	(a) Magnitude response of prototype filter, (b) Analysis filters response, and (c) Reconstruction error in dB using the iterative algorithm by utilizing fixed window function	149
Fig. 6.5	Response of (a) Prototype low pass filter, (b) 4-band analysis filter bank (c) Reconstruction error.	153
Fig. 6.6	Response of (a) Prototype low pass filter, (b) 8-band analysis filter bank and (c) Reconstruction error.	155
Fig. 6.7	Response of (a) Prototype low pass filter, (b) 5-band non-uniform analysis filter	156
Fig. 6.8	Response of a) Prototype low pass filter, b) 8-band analysis filter bank and c) Reconstruction error	160
Fig. 6.9	(a) Uniformly distribution of the signal, (b) 16-channel UFB and (c) 5-channel NUFB	161
Fig. 6.10	Steps of (a) Proposed data compression technique and (b) Data reconstruction	162
Fig. 6.11	(a) Original and (b) reconstruction signal	169
Fig. 6.12	Data compression technique using LZW and RLE	170

Fig. 6.13	Signal Reconstruction Steps	172
Fig. 6.14	Original and reconstructed MIT/BIH record n0.101	173
Fig. 6.15	Data compression performance of different encoding with CMFB	173
Fig. 7.1	Wavelet decomposition of MIT-BIH record no. 100	183
Fig. 7.2	Feature detection in ECG signal	187
Fig. 7.3	(a) Peak detection of decomposed ECG signal (MIT-BIH record no. 222) and (b) Actual R peak detection of signal	187
Fig. 7.4	(a) Original data and (b) Reconstruction signal	191

List of Table

Table No.	Caption	Page No.
Table 3.1	Measured values of correlation coefficient (original and signal after noise elimination).	76
Table 3.2	Computational complexity cost reduction measurement for different design specification.	76
Table 3.3	Computed values of SNR and CC using IFIR filter.	76
Table 3.4	Coefficients representation of FIR and IFIR filter.	84
Table 3 6	Delayed coefficients and SNR measurement using designed IFIR filters	91
Table 3.5	Comparative analysis of FIR, proposed single stage IFIR and Two-Stage IFIR using different fidelity parameters.	92
Table 5.1	Signals naming before and after thresholding	117
Table 5.2 (a)	Fidelity parameters of proposed data compression technique (using bior2.8)	117
Table 5.2 (b)	Fidelity parameters of proposed data compression technique (using bior1.5)	117
Table 5.2 (c)	Fidelity parameters of proposed data compression technique (using bior3.5)	118
Table 5.2 (d)	Fidelity parameters of proposed data compression technique (using bior6.8)	118
Table 5.2 (e)	Fidelity parameters of proposed data compression technique (using sym, Fk and db)	119
Table 5.3	Various performance indices of the QMF and RLE based method	127
Table 5.4	Comparison of diagnostic features of original and reconstruction signal	128
Table 5.5	Various ECG compression methods and their reported performance	128
Table 5.6	WT decomposition	128
Table 5.7	Performance of compression ratio using wavelet transform and RLE	129
Table 5.8	Performance comparison of different wavelet and Huffman's coding base algorithm	131
Table. 5.9	Performance of compression ratio using wavelet transform and LZW encoding	132
Table 5.10	Fidelity assessment parameters in the EWT and RLE based method	137
Table 5.11	Comparative analysis of the performance of the proposed method with other methods	137
Table 6.1	Performance of cosine modulated filter bank using fixed window function	150

Table 6.2	Performance of cosine modulated filter bank using adjustable window functions	152
Table 6.3	Performance parameters of IFIRs filter for UFBs.	155
Table 6.4	Performance parameters of IFIRs filter for NUFBs	157
Table 6.5	Comparisons of proposed work with other methods	157
Table 6.6	Performance of cosine modulated filter bank with other optimization	161
Table 6.7	Energy distribution in the bands of MIT-BIH record no- 100	163
Table 6.8	Performance parameters of compression using MIT-BIH arrhythmia dataset I	167
Table 6.9	Performance parameters of compression using MIT/ BIH arrhythmia dataset II	168
Table 6.10	Performance comparison of proposed data compression method with several existing methods	168
Table 6.11	Performance comparison of proposed data compression method with several existing methods	173
Table 7.1	Tabular results of beat detection using bi-orthogonal WT	182
Table 7.2	Beat detection performance comparison with other methods	186
Table 7.3	Tabular results of feature detection.	186
Table 7.4	(a) Performance measurement of data decompression using features comparison	188
Table 7.4	(b) Performance measurement of data decompression using features comparison	188
Table 7.5	Diagnostic parameters for WDD measurement	189
Table 7.6	Morphologies of features for WDD extraction	191
Table.7.7	Measured values of WDDs	192

LIST OF ABBREVIATIONS

ABC	Artificial Bee Colony
ADPCM	Adaptive Delta Pulse Code Modulation Asymmetric
AI	Artificial Intelligence
AFD	Adaptive Fourier Decomposition
AHMES	Adaptive Hermite Model Estimation System
ASEC	Analysis by Synthesis ECG Compressor
ANN	Artificial Neural Network
AV	Atrioventricular
AZTEC	Amplitude Zone Time Epoch Coding
BFO	Bacterial Foraging Optimization
BW	Baseline wander
CC	Cross-Correlation
CM	Cosine-Modulated
CMFB	Cosine-Modulated Filter Bank
CLS	Constrained Least Square
CORTES	Coordinate Reduction Time Encoding System
CPBC	Cycle Pool Based Compression
CR	Compression Ratio
CRC	Complexity Reduction Cost
CS	Cuckoo Search
CSE	Sub-Expression Technique
CSD	Cosine Signed-Digit Code
CTC	Cycle -to- Cycle
CWT	Continuous Wavelet Transform
DCT	Discrete Cosine Transform
DDC	Direct Data Compression
DE	Difference Equation
DFT	Discrete Fourier Transform
DLT	Discrete Legendre Transform

DPCM	Delta Pulse Code Modulation
Db	Daubechies
DSP	Digital Signal Processing
DWT	Discrete Wavelet Transform
EBP	Errorback Propagation
ECG	Electrocardiogram
EEG	Electroencephalogram
EMG	Electromyogram
EMD	Empirical Mode Decomposition
EP	Evolution Program
EPE	Energy Packing Efficiency
ESPIHT	Enhanced Set Partitioning in Hierarchical Trees
EWT	Empirical Wavelet Transform
EZW	Embedded Zerotree Wavelet
FB	Filter Bank
FD	Fourier Descriptor
fECG	Fetal ECG
FFT	Fast Fourier Transform
FIR	Finite Impulse Response
FRM	Frequency-Response Masking
FT	Fourier Transform
FL	Fuzzy Logic
HM	Holter Monitor
HR	Heart Rate
HT	Haar Transform
IMF	intrinsic mode function
ICA	Independent Component Analysis
IIR	Infinite Impulse Response
IFIR	Interpolated Finite Impulse Response
ISI	Inter-Symbol Interference
LBB	Left Bundle Branch
LPC	Linear Prediction Coding
KLT	Karhunen-Loeve Transform

LL	Left Leg
LA	Left Arm
LPC	Linear Prediction Coding
LPF	Low-Pass Filter
LSPIHT	Layered Set Partitioning in The Hierarchical Trees
LTP	Long-Term Prediction
LZW	Lempel ZivWelch
MCS	Modified Cuckoo Search
MDFT	Modified Discrete Fourier Transform
ME	Maximum Error
MEZW	Modified Embedded Zero-Tree Wavelet
MIT-BIH	Massachusetts Institute of Technology/Beth Israel Hospital
MOS	Mean Opinion Score
MODWT	Maximal Overlap Discrete Wavelet Transform
MMF	Modified Morphological Function
MR	Magnitude Response
MRD	Magnitude Response of Design Prototype
MSE	Mean Square Error
MSP	Multirate Signal Processing
MWI	Moving Window Integral
NOI	Number of Iterations
NLMS	Normalized Least Mean Square
NPR	Nearly Perfect Reconstruction
NRDPWT	Non-Recursive 1-D Discrete Periodized Wavelet Transform
NUFB	Non-Uniform Filter Banks
SF	Sampling Frequency
RL	Right Leg
NSR	Normal Sinus Rhythm
OZWC	Optimal Zonal Wavelet Coding Picture
QMF	Quadrature Mirror Filter
QS	Quality Score
PCR	Principal Component Regression
PLI	Power Line Interference

PR	Perfect Reconstruction
PRDN	Peak Mean Square Difference Normalized
PRE	Peak Reconstruction Error
PT	Polynomial Transform
PCA	Peripheral Component Analysis
PRD	Percent Root Mean Square
PT	Polynomial Transform
RBB	Right Bundle Branch
RF	Radio Frequency
RLE	Run-Length Encoding
RLS	Recursive Least Square
SOT	Swarm Optimization Technique
STFT	Short-Time Fourier Transform
SA	Sinoatrial
SAPA	Scan Along Polygonal Approximation
SBC	Subband Coding
SPIHT	Set Partitioning in Hierarchical Trees
SS	Symbol Substitution
SNR	Signal-to-Noise Ratio
SSRLS	State Space Recursive Least Square
TP	Turning Point
TF	Transfer Function
TW	Transition Width
USZZQ	Uniform Scalar Zero Zone Quantizer
VHDL	VHSIC Hardware Description Language
VCG	Vector-cardiogram
VQ	Vector Quantization
WLS	Weighted Least Square
WP	Wavelet Packet
WT	Wavelet Transform
WHOSC	Wavelet Transform Higher Order Statistics Based Coding

List of Symbol

A_s	Stopband Attenuation (dB)
ω	Frequency
ω_p	Passband Edge Frequency
ω_s	Stopband Edge Frequency
ω_c	Cut-off Frequency
D	Normalized Passband Edge Frequency
e_{am}	Amplitude Distortion
e_a	Aliasing Distortion
Noi	Number of Iterations
CPUs:	Computational Time (Sec)
$H(e^{j\omega})$	Filters in Frequency Domain
$H(\mathbf{z})$	Filters in Z- Domain
$F(\mathbf{z})$	Modal Filters in Z- Domain
$I(\mathbf{z})$	Interpolator Filters Transform in Z- Domain
L	Up-Sampling Factor
$x(n)$	Input Signal
y(n)	Output Signal
$L_{\max}$	Maximum Value of Up-Sampling Factor
M	Number of Channel
N	Filter Order
δ_s	Stopband Ripple
δ_p	Passband Ripple
$\Delta\omega$	Transition Width
$h_{id}(n)$	Ideal Impulse Response of The Filter
$w(n)$	Window Function
β	Controlling Parameters

$I_0[.]$	Modified Zeroth-Order Bessel Function
γ	Additional Shape Adjusting Parameter
r	Ripple Ratio
μ	Window Shape Parameter
σ	Slandered Deviation
$h_i(z)$	Analysis Filters
$g_i(z)$	Synthesis Filters
j_0	Level of Decomposition
$e(n)$	Error Function
$d(n)$	Desired Function
$A_l(z)$	Gain for Aliasing Term
$\varphi(t)$	Mother Wavelet
$d_j(k)$	Detailed Signals
γ_{xy}	Correlation Coefficient
$Multi_{FIR}$	Multiplier of FIR Filter
$Multi_{IFIR}$	Multiplier of IFIR Filter
M_{zeros}	Number of Zero Valued Coefficients
DFD	Distortion in The Frequency Domain
$n(t)$	Noisy Signal
$s(t)$	Noise Contaminated ECG Signal
$p(k)$	Frequency Domain Coefficient of The Filter (dB)
$W_f^e(n,t)$	Empirical Wavelet Transform
$\boldsymbol{N}_{\mathbf{x}}$	The Number Of Bits nn *X(n)*
Nv	Number of Bits used to Code the Significant Coefficients
thr_i	Signals after Thresholding
bior	Bi-orthogonal Mother Wavelet
sym	Symlet Mother Wavelet
Fk	Fejér-Korovkin Mother Wavelet
a_i	Approximation Bands
d_i	Detail Bands

S_n	Constant Matrixes
β_i	Relative Weight
ϕ	Error Function
Tol	Tolerance Range
MLII	Modified Lead Two
Tuv	Universal Thresholding
$\hat{\sigma}$	Estimate of the Noise Level
QRS_{offi}	Offset Values of QRS Complex
QRS_{oni}	Onset Values of QRS Complex
S_e	Sensitivity
$+P$	Positive Predictivity
E_r	Error
TB	Total Number of Beats Present in the Signal
FP	False Positive
FN	False Negative
TP	True Positive
$Tdur$	Average T-Wave Durations
$Pdur$	Average P-Wave Durations
$QRSdur$	Average QRS Complex Durations
P_{offi}	Offset Values of P-Waves
T_{offi}	Offset Values of T-Waves
T_{oni}	Onset Values of T-Waves
P_{oni}	Onset Values of P-Waves
$\Delta\beta$	Normalized Difference Vector

CHAPTER 1

INTRODUCTION

1.1. Overview

Biomedical signal has characteristics of changing with respect to time. Signals can be classified into different types, *viz.*, a) continuous, discrete and digital signals, b) random and deterministic signals, c) even and odd signals, d) periodic and aperiodic signals, e) energy and power signals and e) real and imaginary signals, *etc.*, [1]. A signal is categorized as a biomedical signal, if it is recorded from a living system. The biomedical signals convey information about the state or behavior of the human being [2]. Some of the biomedical signals represent the collective electrical information accomplished from an organ, signifying a physical variable of interest, and can be expressed with respect to time /amplitude /frequency /phase. Different types of signals are generated from a living system. An electrocardiogram (ECG) signal is one of the most vital and important biomedical signals, which represents electrical activity of the heart. It is the measure of bioelectrical information produced at the surface of human body due to the action of polarisation and depolarization of different parts of the heart. It depicts the cardiac condition of a human being [3].

The incorporation of wireless communication technology in the field of telemedicine especially tele-cardiological system has played a very important role in the timely monitoring of a biomedical signal. However, these technologies are resource-constrained applications with limited bandwidth and power. Transmission /transfer of large amount of physiological data to healthcare /e-healthcare centers is also very expensive. Therefore, these systems require efficient data reduction before transmission. As a result, ECG data compression has become an important area of research for the last few decades [4,5].

Multirate signal processing is needed in some specific types of signal and image processing such as; ECG signal, the speech signal, wireless communication, *etc,*. The Wavelet transform (WT) and filter banks based technique are more preferable to process a non-stationary signal than other signal processing technique, because of multi-

resolution property. Several authors have used wavelet-based techniques for noise elimination, data compression and feature extraction of ECG signal [6].

In this chapter, human heart, ECG signal and cosine modulated filter bank is described briefly. It also presents a literature survey on ECG data compression, ECG noise elimination, feature extraction, and filter bank design techniques developed so far. In addition this chapter also contains a brief discussion about the overall thesis work including the research objectives.

1.2. The Heart

The heart is a hollow muscular organ that pumps blood through a network of blood vessels. It consists of four chambers; a) right atrium, b) left atrium, c) right ventricle, and d) left ventricle. These chambers are separated by four valves. The two valves between the atria and ventricles are called the atrioventricular valves. The valve between the left atrium and the left ventricle is also known as the mitral valve, and valve between the right atrium and right ventricle is named as tricuspid valve. Other two valves, *i.e*, **aortic** and **pulmonic valves** are located between the ventricles and major blood vessels. These parts are depicted in Fig. 1.1. The roles of these parts are very important in circulation of blood in the body *i.e*., cardiovascular system is described in the next section [7].

1.2.1. Cardiovascular System

The cardiovascular system is also known as circulatory or vascular system. The complete cycle of blood circulation of the human body takes place through this system. This system is also involved in the purification of blood *i.e*., the addition of oxygen and elimination of carbon dioxide in the blood. It consists of heart, blood, two lungs and a closed system of blood vessels known as arteries, veins, and capillaries. Impure blood is collected from different parts of the body and goes to the right atrium. Impure blood passes to the right atrium through superior and inferior vena cava. Superior vena cava is a large vein that receives impure blood from upper parts of the body, such as head, neck, thorax, and *arms*. Inferior vena cava takes de-oxygenated blood from lower and middle parts of the body. This impure blood enters into the right ventricle when right atrioventricular or tricuspid valve is opened. Then, the blood is pumped to both the lungs for purification (*i.e*, oxygen is added and carbon dioxide is removed) using pulmonary artery. After that the pure blood is pumped to left part of the heart (*i.e*, left atrium) using pulmonary veins. The wall

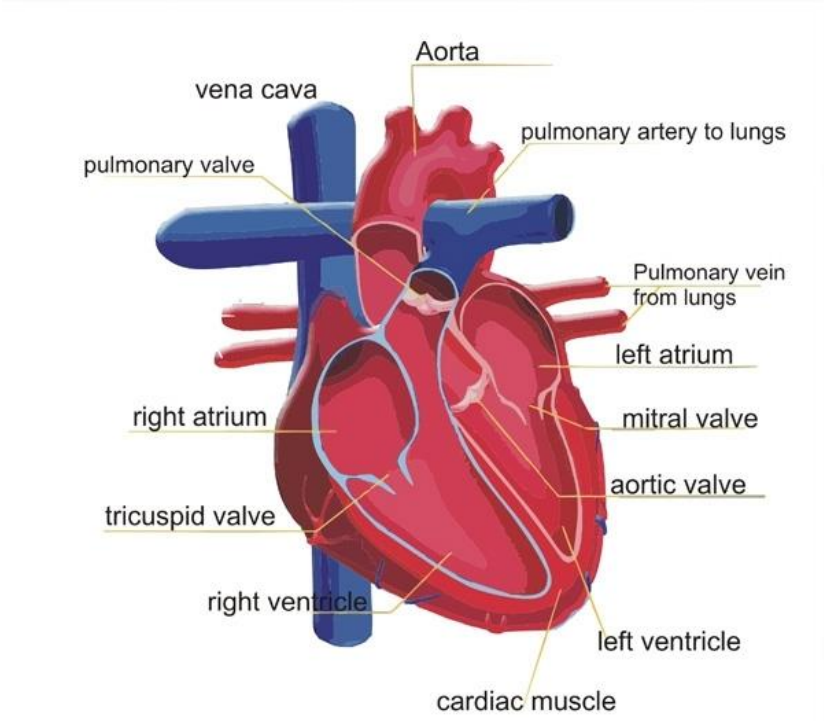

Fig. 1.1 The heart [2].

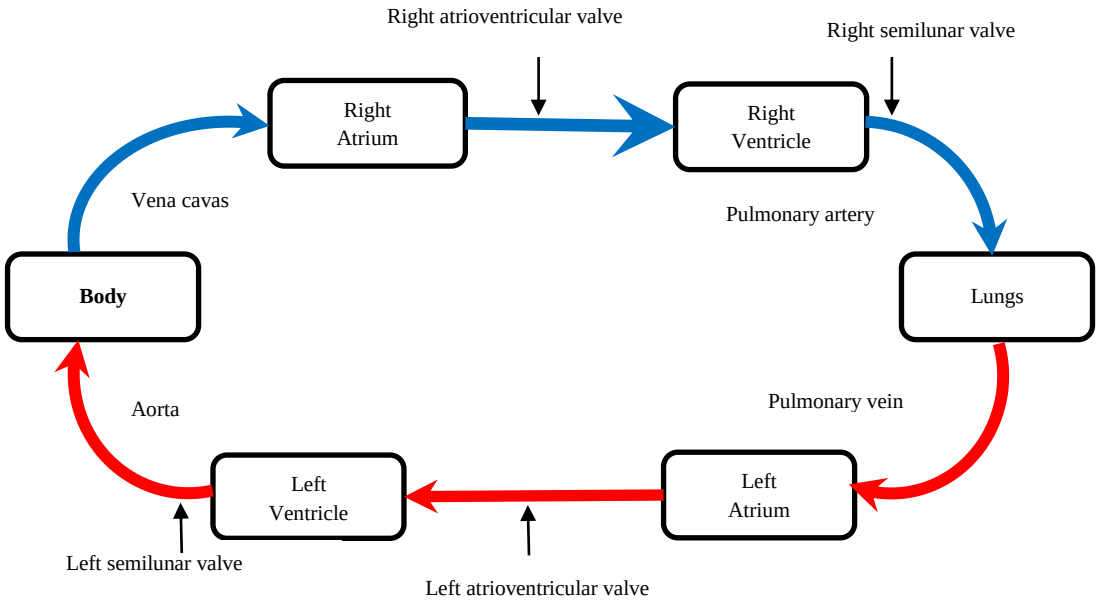

Fig. 1.2 Flow diagram of circulatory system [7].

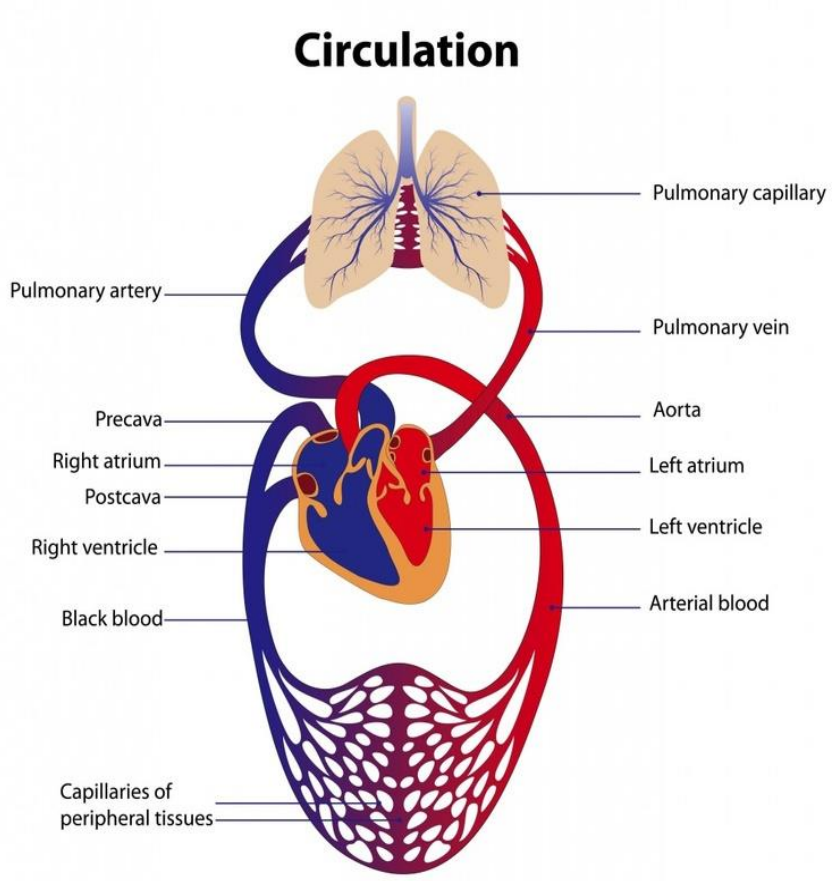

Fig. 1.3 Circulatory system [2].

SA node

AV

Bundle of Hiss

LBB and RBB

Purkinje fibers

Ventricles contraction

Fig. 1.4 Flow diagram of impulse conduction system

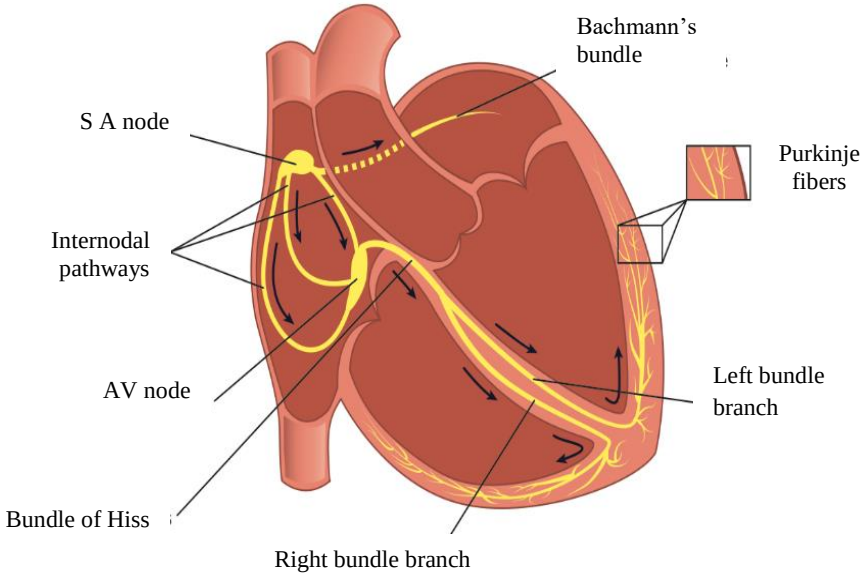

Fig. 1.5 Impulse conduction system [2]

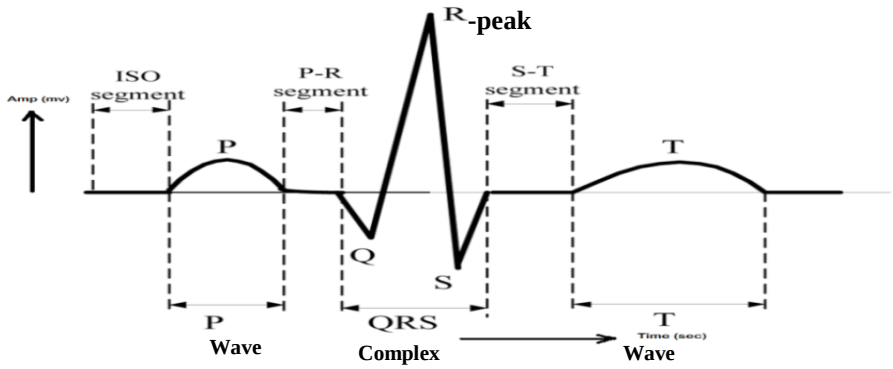

Fig.1.6 Normal ECG signal [54].

of left atrium is thicker than the right atrium. Sub-sequentially blood enters into the left ventricle by the opening of the mitral/bicuspid valve. Further, oxygenated blood goes to several parts of the body. It is the aorta (largest artery of the body), which originates from the left ventricle and extended down to the abdomen and it distributes oxygenated blood to several parts of the body. Fig. 1.2 and Fig. 1.3 show cardiovascular system of the human. In these diagrams, the blue part depicts the impure blood flow and oxygenated blood flow is shown by red color [8].

1.2.2. Impulse Conduction System

The electrical conduction system of the heart is the phenomenon of transmitting the impulses, which are generated by contraction of the muscles. The generation of these signals is initiated from the node that is located on the junction of superior vena cava and right atrium. This node is called the sinoatrial (SA) node. It is also called as natural pacemaker. Generated signals are propagated from the SA node along the surface of both atria in all direction and move towards the atrioventricular (AV) node. AV node is the junction of atria and ventricles. Here the little amount of delay is produced to provide proper timing for the pumping action between the atria and ventricles. After AV nodes, these impulses are transmitted to the bundle of hiss and divided into two branches (left bundle branch (LBB) and right bundle branch (RBB)). From these bundle branches, the signals fan out into Purkinje fibers, which are the widely distributed network of conducting fibers. And finally, propagates over both ventricles that causes the ventricles to contract. This phenomenon is depicted in Fig. 1.4 and Fig. 1.5 [9].

1.2.3. ECG Signal

A normal ECG signal is a quasi-periodic and non-stationary signal, which is illustrated in Fig. 1.6. Here, P wave, QRS complex and T wave indicate the depolarization of atria,

depolarization of ventricles and repolarization of ventricles, respectively. The PR segment begins from the offset point of P wave and ends at the onset point of QRS complex. It denotes the electrical conduction period of electrical impulses from AV node to LBB, RBB and Purkinje fibers. Under the normal conditions, this segment is an isoelectric line. ST segment starts from the offset point of S wave and ends to the onset point of T wave. It represents the time to relax atria and ventricles after contraction. It is also an isoelectric line in normal circumstances. ISO segment is also called as TP segment, and commences at the end of T wave and ends to the onset point of P wave. It is used as the baseline for reference when assessing the other segments. The duration between the onset points of two consecutive P waves is the one beat duration. However, the duration of two consecutive R peak points is considered as the one beat duration, because it is easy to detect. Any change in these components (*i.e.*, amplitude, duration, and shape) can indicate an arrhythmia (abnormal cardiac condition). Heart rate is the number of heart beats in one minute. The heart rate between the 60 to 100 beats per minute is considered as normal heart rate or normal sinus rhythm (NSR). However, the heart rate of fewer than 60 beats per minute is called bradycardia and when it is greater than 100 beats per minute, it is known as tachycardia [10].

Different kinds of noises are also presented in this signal. For analysis of ECG signals, the first step is to remove these noises, because the noise present in the signal can lead to an inaccurate diagnosis. Power line interference, baseline wander, motion artifacts, muscle contractions, electrode contact noise and instrumentation noise generated by the electronic circuit are various noises present in the ECG signal [11].

1.2.3.1. Application of ECG Signal

ECG is very important for the clinical diagnosis of a heart patient. Since different systems of the human body are interconnected each other, sometimes it is also important in the diagnosis of other diseases (other than cardiac patients). As a result, it has a significant role for engineers to be conscious of the kinds of abnormalities and their biomedical/biochemical/physical characteristics, which are of clinical interest [12]. Cardiac disease can be classified into two major categories; such as based on changes in QRS morphology (contour) and based on the variation in rhythm *i.e.*, heart rate variability (HRV) [11]. Changes arising from abnormalities as a result of cardiac generator and volume conductor can be imminent. By performing a statistical analysis of the normal ECGs data, the normal and abnormal conditions can be identified. It can be assumed that

the clinical abnormalities are reflected by the electrical abnormalities (amplitude, time and shape) of ECG signal. On the contrast, if the objective criteria for abnormal ECGs are present, clinical interpretation is less definite. The clinical judgment, experience, and surety of biomedical data are very important in cardiac diagnosis, for human identification [10, 13,14]**.**

1.2.3.2. Cardiac Vectors and Lead Systems

A cardiac vector represents electromotive forces (EMF) of the heart cycle. The magnitude, direction, and polarity of a cardiac vector can be identified. At any given instant, when the process of repolarization and depolarization takes place, the bioelectrical potentials are propagated in different directions in the space. These bioelectric potentials are canceled out by the opposing forces; therefore, only 20% of the signal can be recorded. The recorded potential can be represented by an instantaneous vector for a given instant [2]. An average vector of a given portion of the cardiac cycle denotes the direction, polarity and average magnitude for that period (QRS period). Polarization and depolarization of atria and ventricles can be depicted by a vector. To receive bioelectric potential, electrodes are used, which are called bioelectrodes. These electrodes are connected directly to a device (amplifier /resistive networks), which amplifies the potential. The recording of these potentials is done in different manners that is called lead system [14].

The lead system was introduced by Einthoven. Limb leads are classified into three categories; a) lead I, lead II, and lead III. These leads include the configurations of left arm (LA), right arm (RA), left leg (LL) and right leg (RL). Lead I is the configuration of RA with negative polarity and LA with positive polarity. In lead II, RA and LL are connected with negative and positive polarities, respectively; and in lead III, LA with negative polarity and LL with positive polarity are used. In the limp lead system, RL is used as a common point in all the configurations. Another combination of electrodes proposed by Goldberger is called augmented leads. Augmented leads are also classified into 3 types; a) aV_R, b) aV_L and c) aV_F [2]. These are the unipolar leads. When positive electrodes for these leads are positioned on the right arm, left arm, and left leg, the configuration is to be said (aV_R), (aV_L) and (aV_R), respectively. Another class of leads given by Wilson are called unipolar chest leads, which originate potentials from six different chest locations (V1,V2, V3, V4,V5 and V6). In this system, a reference input is

used to the amplifier in these cases known as the Wilson central terminal. It is formed by a resistive network that pays equally weighted signals from each of the three limb electrodes (LA, RA, LL). For acquisition of ECG signal from a human being, 12 lead system is used (limp, augmented and chest leads). Patient monitoring can be done by one lead ECG signal. Generally, Lead II is used for monitoring purpose. In Fig. 1.7, 12 lead system is depicted [2,14].

1.2.3.3. MIT-BIH Database

In this database, several ECG recordings are included, extended over 200 hours. Each recording includes one, two or three signals. The range of these signals is from 20 seconds to nearly 24 hours in length. Majority of the dataset has two signals of about 30 minutes long. Annotated beat-by-beat is given for most of the signals. This database is classified into the following types;

a) MIT-BIH Normal Sinus Rhythm Database
b) MIT-BIH Polysomnographic Database
c) MIT-BIH Arrhythmia Database.
d) MIT-BIH ST Change Database
e) MIT-BIH Atrial Fibrillation Database
f) MIT-BIH ECG Compression Test Database
g) MIT-BIH Long-Term Database
h) MIT-BIH Malignant Ventricular Arrhythmia Database
i) MIT-BIH Supraventricular Arrhythmia Database
j) MIT-BIH P-wave Annotations

In this work, MIT-BIH Arrhythmia database is used to evalute the performance of proposed methodologies for data compression, noise elimination, and feature detection. The details of the database are given below. This database has two series (series 100 and series 200). Series 100 included record numbers; 100 101 102 103 104 105 106 107 108 109 111 112 113 114 115 116 117 118 119 121 122 123 124. And series 200 included record numbers: 200 201 202 203 205 207 208 209 210 212 213 214 215 217 219 220 221 222 223 228 230 231 232 233 234.This database has 48 annotated records, acquired from 47 persons, and studied during 1975 and 1979 in the Arrhythmia Laboratory of Beth Israel Hospital in Boston. 60% of the records were obtained from the patients who lived in the hospital while under treatment. The number of 200 series records were chosen in detail, because of QRS morphology and other features of the rhythm. The signals of this

database are 30 minutes in length and the sampling frequency is 360 Hz. The information about the leads (*i.e*, I, II, V1, V2, V3, V4, V5 and V6), the patient's sex, age, and medications are included in the header files [15,16].

1.3. ECG Data Compression

The process of encoding, modifying or converting the construction of a given signal /data in such a manner that it takes less memory or space on a disk is called signal /data compression. Techniques used to extract the reliable and important information from a signal or data, and also remove the irrelevant data are known as data compression techniques [17].

1.3.1. The Need for ECG Signal Compression

Data compression is very important in the following areas; a) Telemedicine and e-healthcare system, b) Holter monitor systems and c) Reducing the storage requirements.

1.3.1.1. Telemedicine and e-healthcare System

The field of telemedicine has changed drastically from its inception. Originally, telemedicine is initiated from the telecommunications technology, in which the information is sent in the form of electromagnetic signals over a distance. In the early 20th century, various technologies were developed in the field of medicine. In telemedicine and e-healthcare systems, information of the physiological parameters is obtained in one location and the interpretation of disease is done in another location. It has many advantages, such as; patient convenience (*w.r.t.*, time and travel), it plays an important role in rural areas, it reduces the problem of a low ratio of doctor /patient, it is important for the treatment of a number of critically ill patients due to factors like floods, tsunami, earthquake *etc*., it is helpful in a quick and timely follow-up of patients discharged after palliative care and it also plays an important role in continuing education or training through video conferencing periodically *etc*,. In these systems, the acquisition of physiological data is performed at the patient site and this data is transferred to doctor site using a suitable transmitting channel. For efficient data transmission, data size should be less; therefore, data compression is very important prior to data transmission [18]. In Fig. 1.8, telemedicine /e-healthcare system is depicted. [18,19].

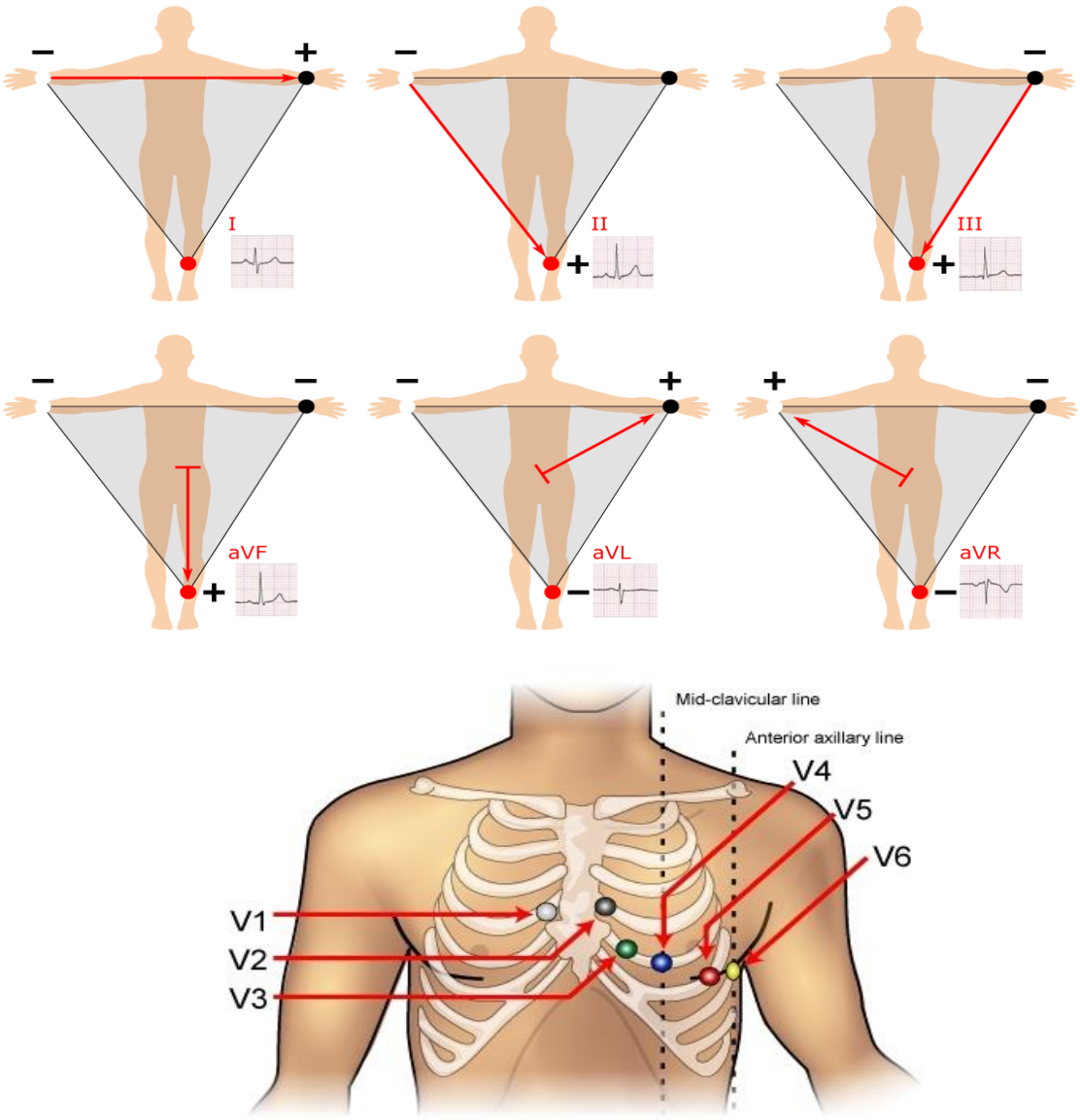

Fig. 1.7 12-lead system [2].

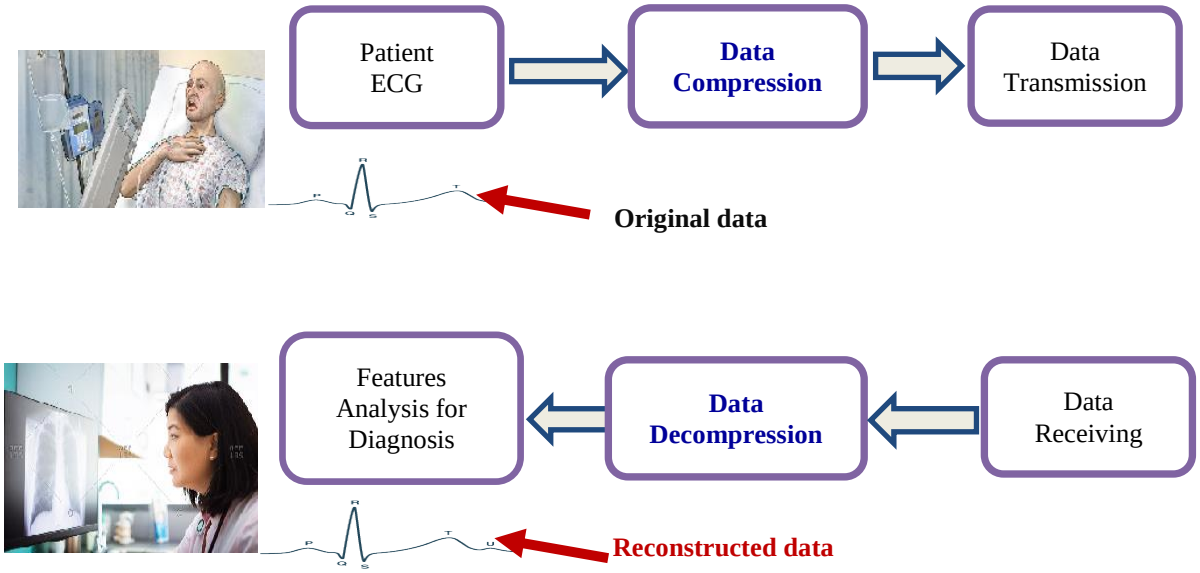

Fig.1.8 Telemedicine /e-health care system.

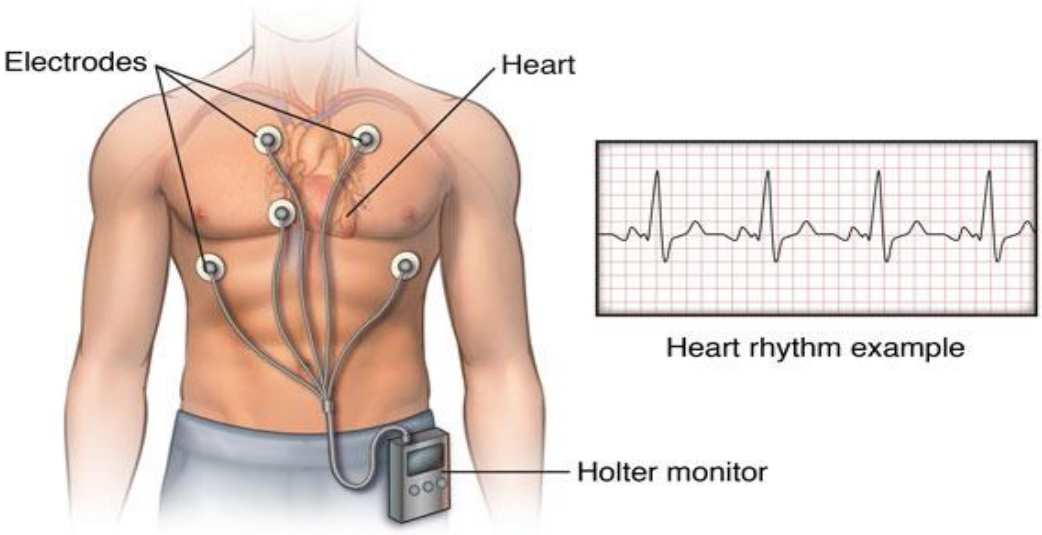

Fig.1.9 Holter monitor system [48].

1.3.1.2. Holter Monitor Systems

A Holter monitor (HM) is a battery-powered, small, medical device. It is used to measure the activity of heart, such as heart rate and rhythm. HM records hearts activity continuously for 24 hours. It is also known as ambulatory electrocardiography. It contains two parts; a) electrodes used to record the signal from the skin and b) recording unit, in this unit, recorded signal is stored. For efficient data storage, data compression is needed in this system. In Fig.1.9, HM system is depicted. It is very helpful for the patient who is suffering from a heart attack. In this case, the doctor needs to observe the continuous heart activity after release from the hospital also [28,29].

1.3.1.3.Reducing the Storage Requirements

The digital ECG data is needed for:

a) Future diagnosis of patients
b) In research and development in the field of healthcare
c) In educational institutes.

The human body is composed of several closed systems such as; respiratory system, nervous system digestion system, and the cardiological system. These systems are interconnected to each other. The physiological parameter of one system may represent the conditions of other systems. Therefore, stored data can also help in another disease diagnosis. Healthcare system is one of the most important areas of research from the last few decades. In research, physiological data is needed to perform different experiments. However, the recording of new data is not possible everywhere. Therefore, recorded data can be used in several research areas by storing and transmitting to several places [20]. Form the above discussion, it can be seen that ECG signal analysis is the essential part in diagnosis of a cardiac patient. Before the analysis of an ECG signal, noise reduction is mandatory. In several situations, timely diagnosis of a cardiac patient can be achieved by

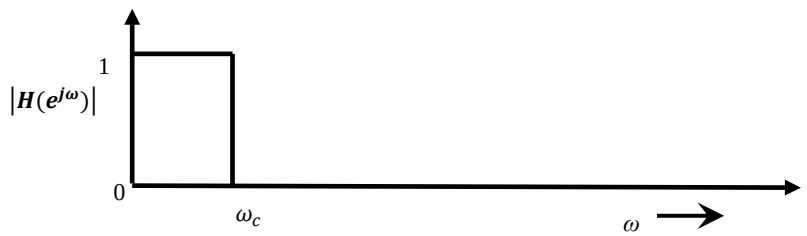

Fig.1.10 Ideal low pass filter response [1].

telemedicine system, where data compression is always needed. These operations can be achieved by applying suitable digital signal processing (DSP) methodology. Digital filter is basic unit of the DSP. Therefore, in the next section digital, filter is described in brief.

1.4. Digital Filters

Digital filters are the systems that boost or reduce certain features of a discrete time signal using a mathematical operation. The fundamental function of a filter is to reject a range of frequency. Filters are an essential part of the signal processing. Digital filters are classified into four categories, *viz*., low pass, high pass, band pass, and band reject filter. Digital filters have applications in a large number of areas such as; image processing, data communications, noise elimination in the biomedical signal, beat detection in ECG signal, digital video processing and analysis, and in voice communications. Digital filters are mainly classified into two categories; a) finite impulse response (FIR) filters and b) infinite impulse response (IIR) filters. FIR filters have finite length of impulse response *i.e.*, the coefficients of FIR filters are set to zero value at the finite time, these are recursive in nature. In case of IIR filter, length of the impulse response is infinite [1]. Selection of these filters is based on the applications. FIR filter can be designed using the IIR filter by truncating some coefficients of IIR filter. In Fig. 1.10, the ideal magnitude response of low pass filter is depicted and the mathematical expressed in Eqn. (1.1) of this filter is given in Here,

$$H(e^{j\omega})\begin{cases}1 & |\omega| < \omega_c \\ 0 & \text{otherwise.}\end{cases} \tag{1.1}$$

where, ω_c is the cut off edge frequency and $H(e^{j\omega})$ is the magnitude response [3].

1.4.1. IFIR Filter

Linear phase and stable nature are the main advantages of the FIR filters. Therefore, instead of using IIR filters, FIR filters are preferred. However, in case of FIR filters, computational complexity is more due to a large number of adders and multipliers. Therefore, Neuvo *et al.*, introduced the interpolated finite impulse response (IFIR) filters for narrowband and sharp transition band, which have linear phase, stable nature and low computational complexity [21]. In IFIR filters, two FIR filters (modal and interpolator filter) are connected in the cascading form. The orders of these filters are very less in

comparison to desired FIR filter. The basic structure of IFIR filter is shown in Fig. 1.11 and can be defined in Eqn. (1.2) [21];

$$H(\mathbf{z}) = F(\mathbf{z}^L)\, I(\mathbf{z}) \tag{1.2}$$

where, *x(n)* is the input signal, *y(n)* is the output signal, *F*(z) is the modal filter, which is up-sampled by up-sampling factor *L* and *I*(z) is the interpolator filter. The maximum value of *L* can be evaluated using Eqn. (1.3)

$$L_{\max} = \frac{2 \times \pi}{\omega_s + \omega_p + \sqrt{(\pi(\omega_s - \omega_p)}} \tag{1.3}$$

where, ω_s and ω_p are the stopband and passband edge frequencies respectively of the desired FIR filter ($H(z)$).

IFIR filters reduce the computational complexity significantly. The complexity can be reduced further by using multistage IFIR filter, where, two or more up-sampling factors are used. In two stages IFIR filter, two up-sampling factors are used. In Fig. 1.12, two-stage IFIR filter is depicted, here instead of two, three filters are used. In Eqn. (1.4), two-stage IFIR filter is defined.

$$H(z) = F(z^L) I_1(z^{L_1}) I_2(z) \tag{1.4}$$

where, $I_1(z)$ is used as a model filter for $I(z)$ that is up-sampled by L_1 and $I_2(z)$ is an image suppression filter. The maximum value of L_1 is also calculated using Eqn. (1.3) by replacing ω_s by stopband edge frequency of $I(z)$ [22].

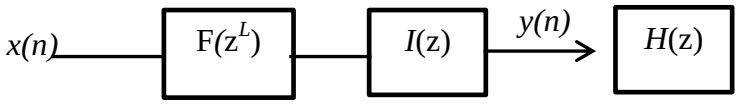

Fig. 1.11 IFIR structure [22].

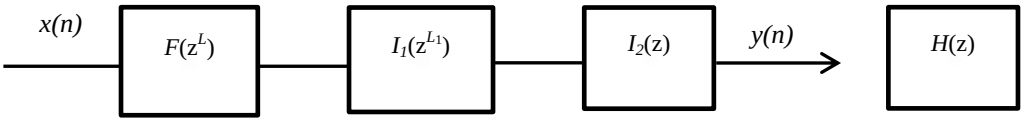

Fig. 1.12 Two stages IFIR structure [24].

1.4.2. Filter Bank

Signal processing is divided into two types on the basis of sampling frequency; single rate signal processing and multirate signal processing (MSP). In MSP, the sampling rate is different throughout the system. Multirate signal processing has several advantages over single rate signal processing, such as higher bit rate, less memory requirement and less computational cost for the specific application. The filter bank is one of the important tools of (MSP).

It divides the input signal into the number of frequency bands using bandpass filters and down-sampling factors. A filter bank consists of two sections; analysis and synthesis section. Analysis section includes down-sampling and filters (low, high or band pass) to decompose the input signal, and the synthesis section consists of up-sampling and filers for recombining the output signal [23].

Filter bank can be classified into two types on the basis of signal decomposition, *viz*,. Two-channel filter bank and M-channel /Multi-channel filter bank. In two-channel filter bank, the signal is decomposed into two frequency bands, and in M-channel filter bank input signal is divided into M number of frequency bands. M-channel filter banks are further classified into two types; uniform filter banks (UFBs) and non-uniform filter banks (NUFBs). In UFBs, the input signal is uniformly distributed into *M* number of frequency bands. However, in case of NUFBs, the input signal is decomposed into *M* number of frequency bands with different bandwidth [24].

1.5. Literature Review

In this section, the literature survey of data compression, feature extraction, noise elimination, and multirate filter bank is presented.

1.5.1. Data Compression

In the past five to six decades, several methodologies have been proposed for the ECG signal compression [20]. Compression ratio is the main factor used to show the performance of compression. Value of compression ratio is based on the number of original and compressed samples. Therefore, this does not depend on factors such as sampling frequency, bandwidth, reconstruction error threshold, lead selection, and noise level, *etc*., [25]. This section includes the literature review of data compression techniques.

1.5.1.1. Direct Data Compression

Initially, direct data compression techniques are developed to compress the ECG signal. Cox *et al*., developed the amplitude zone time epoch coding (AZTEC) algorithm for preprocessing the real-time ECG signal analysis. This is a very popular data compression method used for the reduction of ECG data. In this technique, the low amplitude signal is suppressed to reduce the data. It reduces the data about ten times. It also involves coding of the resultant signal into a convenient form, which helps in the analysis [26]. However, this technique is not acceptable to the cardiologist due to discontinuities and distortion presented in the reconstructed signal. This problem is reduced by utilizing a smoothing parabolic filter, which reduces the discontinuities significantly [27]. Furht & Perez have modified the AZTEC algorithm, by using an error threshold. This algorithm is an adaptive real-time algorithm, which can be used for on-line transmission and compression of the ECG signal [28]. In another study, discontinuities in the reconstructed signal is alleviated to remove the problem of AZTEC algorithm [29]. Another approach *i.e*., turning point (TP) is proposed for reducing the sampling frequency of ECG signal. In this algorithm, the sampling frequency is reduced to 100 Hz from 200 Hz, without affecting the amplitude of QRS complexes [30]. The saved points of this algorithm are not having equally spaced time intervals, which is the main drawback of this algorithm. It gives a fixed compression ratio, *i.e*., 2:1.

A hybrid combination of AZTEC and TP algorithm is called a coordinate reduction time encoding system (CORTES) [31]. It incorporates the advantages of AZTEC and TP by applying both algorithms parallelly to the incoming samples. Implementation and reconstruction procedure of CORTES algorithm has been described in detail by Tompikns and Webster [32]. Gardenhire developed another algorithm of ECG signal compression known as fan and scan along polygonal approximation (SAPA) algorithm [33,34]. This algorithm involves first order interpolation with two degree of freedom. Three new algorithms are introduced by Ishijima *et al*., for compression of ECG signal [35]. These algorithms are based on SAPA, and provide efficient performance in terms of computational complexity [35].

An efficient methodology has been developed for compression of ECG data. Here, basic concept of modified AZTEC technique has used and named as improved modified AZTEC [36]. Wolf *et al*., and Bertrand *et al*., have proposed and implemented an ECG

delta coding system, respectively [37,38]. Stewart *et al.*, have modified delta coding by applying thresholding for the data reduction of three leads ECG signal [39]. Delta pulse code modulation (DPCM) is also used for ECG signal compassion, which is more complex and employs the linear predictor of different orders [40,41].

Huffman coding is one of the most popular coding system used to compress a signal. As a result, Huffman and variable coding have been used for compression of ECG signal by several researchers [42-44]. However, in variable code length coding, serious decoding error possibility is presented due to the transmission. This problem is minimized by data block coding with known error control techniques [45]. A new algorithm "SLOPE" is presented by Tai [46]. It is a real-time algorithm, which considers some adjacent coefficients as an information vector. Later the same author has proposed the CORNER algorithm for real-time ECG data compression [47]. This algorithm locates the relevant coefficients, and encodes using linear interpolation simultaneously which provide linear segmentation. Therefore, this technique codes the data more accurately.

Another high-performance technique "cycle-to-cycle (CTC)" has been used to compress ECG rhythms by Holterm [48]. In the CTC technique, QRS complex detection is required. Improvement in the performance of CTC technique can be done by combining it with FAN or SAPA. The combination of CTC and SAPA is called as SAPA-CTC [49]. Kulkarni *et al.*, has presented a study, which shows the effect of sampling frequency on the performance of compression done by direct data compression techniques. The resulted data shows that by increasing the sampling frequency, the percentage root mean square difference decreases and the compression ratio increases [50]. Another technique of direct data compression has been given by Saxena *et al.*, [51]. In this technique, compression is achieved by down-sampling and non-redundant template (NRT). Here, data compression is done by applying down-sampling and store the data in data array as NRT and for the reconstruction of data, the interpolation process is performed. This technique is called NRT-DDC. Zigel *et al.* proposed a new algorithm of ECG data compression called analysis by synthesis ECG compressor (ASEC). In this algorithm, long and short-term predictors, beat codebook, an adaptive residual quantizer is utilized [52]. A new idea to evaluate the performance of data decompression is weighted diagnostic distortion (WDD) proposed in [53]. In WDD, features of the original and reconstructed signal are used to check the quality of reconstruction.

1.5.1.2. Transformation Compression Techniques

Another class of data compression techniques is transformation compression techniques, which involves linear orthogonal transformation and encoding. For signal reconstruction, decoding and inverse transformation are used. In this method, irrelevant information is removed to improve the performance of compression, however, these methods do not reconstruct signal exactly same as the original input signal [20]. Several studies have been done to compress the ECG data using transformation techniques [54]. Examples of transformation compression techniques are Fourier transform (FT), orthonormal exponentials, Karhunen-Loeve transform (KLT), cosine transform (CT), Walsh transform and Haar transform (HT) [20]. Vectorcardiogram data compression has been done using discrete Karhunen-Loeve expansion by Womble *et al*., [55]. Researchers have used 1000 data files having sampling frequency 250 Hz. Compression performance of this method is high with an acceptable range of error. In a study, the discussion of real-time data compression based on microprocessor processing using fast Walsh transform has been done [56]. This work investigates the reconstruction quality of the signal using linear filter. Fourier descriptors (FDs) have been used for ECG signal compression by Reddy & Murthy [57]. In this work, two lead ECG database have been taken. Here, firstly, the data is segmented into QRS complex and S-T segment by *L* point forward FFT with FD, and then for obtaining the reconstructed data, *L* point inverse FFT is applied. This method is simple and very resistant to noisy signals. Multilead ECG rhythm compression using a linear transform has been addressed by Cetin *et al*., [58]. In this work, researchers first linearly transformed the highly correlated standard ECG lead signals, then after various coding methods are applied to the resulted signals to reduce the data size. This method providess a high compression ratio and better reconstruction quality. In another work, high degree polynomial based ECG data compression has been introduced [59]. This method is also known as polynomial transform (PT). This method provides better results than the discrete cosine transform (DCT).

A new adaptive compression technique is developed in [60]. In this technique, the representation of R-R interval using an optimally time warped polynomial is done. The performance of this work is superior to other techniques, such as DCT and DLT. Jane *et al*., have proposed a technique based on orthogonal transform on Hermite function for ECG signal compression. Here, authors have used four windows *viz.*, for p wave, QRS complex, ST segment, and T wave. The differences between the automatic measures in

the original signal and in the reconstructed signals has been compared that showed good results for compression [61].

Wavelet transform (WT) is the most important tool of data compression from last 3 decades. Several researchers have used WT for a signal compression and analysis [20]. In a study, WT is used to compress ECG data along with vector quantization (VQ). VQ is applied to wavelet coefficients to achieve the compression by choosing scales of long durations low dynamic range retains the features integrity of the ECG with a very low bit per sample rate [62]. Another study is done by Ramakrishnan & Saha for ECG data compression by utilization of WT. Here, authors first did beat normalization using multirate signal processing, and then WT is applied to each beat. Then after, residual sequence achieved by linear prediction of the significant wavelet coefficients. And then resultant coefficients are transmitted to decoder to increase the compression ratio [63]. In another work, wavelet based hybrid method used to compress the ECG data [64]. Wavelet packet (WP) algorithm is also a powerful tool for signal processing and analysis. Single lead ECG data compression is performed using WP by Bradie [65]. WP is used, because of its high efficiency and flexibility.

In a study, detection of R peaks, R-R interval and ECG data compression is done using discrete wavelet transform (DWT). Here, researchers have developed a methodology based on orthogonal WT and adaptive quantization. This work provides a high compression ratio and low implementation complexity [66]. Subsequentially, DCT is used for ECG signal compression. In this work, researcher has used the MIT-BIH database to test the developed algorithm. 2-D DCT is used to compress the ECG signal, because it probides better results than single 1D. Here, two types of redundancies *i.e.*, a) between the adjacent sample and b) adjacent beats are removed in this work [67]. ECG data compression by wavelet code on the set partitioning in hierarchical trees (SPIHT) has been done by Lu *et al.,* [68]. Here, the researchers have achieved the exact bit rate control and created a bit stream progressive in quality. Further in another study, wavelet choise to compress the rhythms of ECG is given[69]. Two other methods *i.e.,* a) optimal zonal wavelet coding (OZWC) and b) wavelet transform higher order statistics based coding (WHOSC) have been proposed by Istepanian *et al*., [70].

An efficient coding has been proposed by Rajoub [71]. First, the author has used WT to decompose the signal into a number of frequency bands, and then applied a new efficient coding. This method provides better performance than other methods in terms of CR and PRD. Kulkarni *et al*., have discussed the diagnostic acceptability of FFT based ECG signal compression. Here, two important parameters (CR and PRD) have been used to examine the

performance of compression besides visual comparison [72]. Fast Walsh transform is used for ECG data compression in order to study the clinical acceptability of reconstructed peaks amplitude and locations [73]. Another new algorithm for compression of ECG rhythms has been given by Chagas *et al*., [74]. The main aim of this methodology is to reduce the bit rate without affecting the reconstruction quality of the signal. The methodology is based on the compression of linearly predicted residuals of the coefficients of wavelet. Compression of the signal also involves two coding methods, such as; modified run-length and Huffman coding. Another method based on wavelet and iterative thresholding are given by Benzid *et al*., [75]. After application of thresholding, all the coefficients are coded using Huffman coding. This work also shows that the compression ratio is increased, significantly. Hwang *et al*., have proposed a novel method for compression of biomedical data. The name of this algorithm is layered set partitioning in the hierarchical trees (LSPIHT) [76]. The 3-D integer wavelet transform is used to study the lossy to lossless medical data compression by Xiang *et al*., [77]. First, the 3-D integer packet transform is designed; after this the designed methodology is applied to the signal, and then arithmetic coding is utilized to achieve better compression performance. In another work, use of wavelet transform for data compression with vector quantization is done. Here, authors have investigated and fixed the coding inefficiency problem in lossless compression *i.e*., overall, a new and unified coding framework is designed. Additionally, a novel coding strategy is proposed to enhance the coding efficiency of SPIHT at the less significant bit representation of the WT coefficients [78]. Subsequently, in another work, 2-D wavelet technique is used to compress the ECG signal. In this work, the researchers have used the modified SPIHT. The methodology is tested by using several records of MIT-BIH arrhythmia database [79]. Other researchers have also used SPIHT and subband energy compression methodology for data compression of ECG signal. They have utilized 2-D ECG data, in which each row of the array indicates one or more period and amplitude of normalized ECG beats. The overall method is superior than the 1D ECG signal compression [80]. A joint use of different fidelity parameters, in order to examine the performance of coding and decoding for ECG signal, has been done in [81]. The aim of this study is to improve the performance of CR value without the expense of quality of the reconstructed signal. Another work has been reported by Moazami-Goudarzi & Moradi, in which multiwavelet transform is used for the compression of ECG signal. Here, authors have investigated the optimum wavelet to perform ECG data compression. Different parameters have been used to examine the performance of data compression and decompression such as; CR, percent root difference (PRD), distortion (D), root mean square error (RMSE) and cross-correlation (CC) [82].

A novel method for compression of ECG rhythms has been reported by Manikandn & Dandapat using discrete sinc interpolation (DSI) technique. Here, the realization of DSI is done by an efficient discrete Fourier transform (DFT). The performance of this methodology is compared with the performance of other widely used ECG data compression methodologies, *vis*., FAN, AZTEC, Hilton and Djohan technique. Authors have observed that in case of DSI based method, higher CR is achieved with a relatively lower percentage of RMS and PRD value. Here, diagnostic distortion is also computed in terms of average absolute error (AAE), which is lower than the other methods (FAN and AZTEC) [83]. A new wavelet-based quality measure is introduced by Al-Fahoum. This approach is based on the division of interest segment in the repeated band, where a score is given based on dynamic range and diagnostic significance. Quantitative and qualitative measurement of the performance is done, which shows that given approach is insensitive to error variation, and provides an accurate comparison in original and reconstructed diagnostic features [84]. A low-delay ECG compression algorithm for continuous ECG transmission is done in a research work. Here, wavelet partitioning and adaptive frame size adjustment based methodology is employed to attain the low delay. Another novel approach used to compress the ECG data is reported by Ku *et al.*, This methodology uses the full wavelet coefficients with mean value in the termination. Here, the reversible round-off non-recursive 1-D discrete periodized wavelet transform (NRDPWT) is utilized to resist the truncation error propagation. Further, quantization is used to compress the data using octave coefficients [84]. A hybrid approach based on wavelet, uniform scalar zero zone quantizer (USZZQ) and Huffman coding on differencing significance map (DSM) is done for compression of ECG signal. Here, the thresholding value selection is done using the energy packing efficiency (EPE) of each subband; after this, the quantization process is utilized. Then after storing process of the indices of significant coefficients is done by creating a significance map. Finally, the Huffman coding is used to encode the map [86]. Another approach of ECG signal compression is done based on the modified embedded zero-tree wavelet (MEZW). Two different thresholding values are applied to decomposed coefficients to improve the values of CR and PRD [87]. A methodology for the compression of biomedical signals, such as ECG, electromyogram, electroencephalogram, *etc*., is done with mother wavelet optimization and best-basis WP selection. Here, the researchers have used the discreet WP for decomposing the ECG waveform. The optimization process is involved to acquire the optimum wavelet decomposition [88].

An improved wavelet-based 2-D algorithm is proposed for the compression of ECG data, which employs a double stage compression. In the first stage, SPIHT algorithm is utilized to compress the 2-D data ECG data, and in the second stage, VQ is used to the residual image gained from the preceding stage. This methodology uses both inter-beat and inter-sample redundancies present in the data [89]. Arnavut has developed a methodology for compression of ECG data using Burrows-Wheeler transformation and inversion ranks of linear prediction. The methodology yields better compression gain in terms of weighted average bit per sample than several existing methods [90]. A constrained ECG compression algorithm using the block-based DCT is given by Benzid *et al*., This algorithm controls quality criterion in terms of PRD [91]. SPIHT algorithm is modified to provide better performance of compression called enhanced set partitioning in hierarchical trees (ESPIHT). This method is faster than the conventional SPIHT. This method also reduces the number of bits in a bit stream. The ESPIHT is applied to the multichannel ECG data [92]. Another wavelet-based method is used for ECG signal compression, in which first, the DWT is applied to the digitized ECG signal; and then, uniform scalar dead-zone quantizer is applied to the DWT coefficients. After this, these coefficients are decomposed into four symbol streams, representing a binary significance stream, the signs, the positions of the most significant bits, and the residual bits. An adaptive arithmetic coder with several different context models is employed for the entropy coding of these symbol streams [93]. Lee & Lee have introduced an algorithm to compress the ECG signal for holter monitoring. This algorithm involves different steps, such as; ECG signal differentiation, R-R interval division and classification, DCT application, window filtering, signal assembling, and Huffman coding. This algorithm provides a good value of CR and PRD [94]. Another work has been reported, in which a new 2-D wavelet-based ECG signal compression algorithm is introduced [95]. An ECG signal (1-D) is first segmented and aligned to a 2-D signal (array), consequently, the two types of correlation of heartbeat signals can be fully utilized. Then after, 2-D WT is applied to the created 2-D ECG data array. After this, a modified VQ is applied to the resultant coefficients of previous stage. DCT and Laplacian pyramid based compression method for ECG signal is proposed in [96], where first, the transformation is done using DCT algorithm, then after, a thresholding is applied based on bisection algorithm. Then after, the binary lookup table is formulated for storing the position map. In another work, a new modified SPIHT algorithm is used to code the coefficients of ECG after WT decomposition [97]. In another study, ECG data compression is done using DCT based discrete orthogonal Stockwell transform [98].

A new cyber-physical measurement process model is proposed with applying compressive sensing, where the packet loss in a wireless link is modeled as a random sampling process [99]. In a comparative study, transform based methods, *viz*., FFT, DCT, and WT are analyzed for ECG data compression. Researchers have observed that the DCT based method increases CR by 58.97% than FFT. And WT methods further improve the value of CR by 31% than DCT with low PRD value [100]. Bendifallah *et al*., have introduced an algorithm in which improvement in the DCT method is done first; and then, the improved DCT algorithm is applied to the ECG signal. DCT coefficients are then quantized using a uniform scalar dead zone quantizer. After this, quantized coefficients are coded using arithmetic encoding method [101]. A new approach based on compressive sensing (CS) is formulated for data compression of ECG signal [102]. Lee *et al*., have developed a real-time signal compression technique for e-healthcare terminals. This methodology includes five procedures, such as; downsampling, classification of one rhythmic period, DCT, filtering using the windowing method and coding using Huffman coding [103]. Another work is presented by Sharma *et al*., for data compression of multichannel ECG signal. Here, researchers have used the wavelet transform to decompose all channel coefficients, and then multichannel principle component analysis is used. Multichannel compression is implemented using uniform quantizer and entropy coding of principal component analysis (PCA) coefficients [104]. Kumar *et al*., have used optimized wavelet filter bank based methodology for the compression of ECG rhythms. Authors first, designed the wavelet filter bank using a Kaiser window function, which is optimized using the linear iterative algorithm. Then applied it to ECG signal for frequency division. Further, they have used RLE technique to encode the wavelet coefficients [105]. An improved wavelet-based technique is proposed by Huang *et al*., for data compression of ECG signal. Here, first, DWT is applied to the ECG signal, which provides tree structure decomposition. Then, the quantization of the decomposed coefficients is done using vector-scalar quantizer. And then, the context modeling arithmetic coding is applied to quantized coefficients [106]. Another approach of ECG data compression is given by Kumar *et al*., by using WT. Here, researchers have used beta wavelet and lossless coding. The threshold value estimation is done in such a way that the low PRD value can be achieved [107].

A new scheme based on wavelet is proposed in [108]. In this work, wavelet coefficients quantization is done, for which the evolution program (EP) is proposed, which can formulate a check stationary relationship between the quantization scales of multi-resolution levels. Researchers have tested the proposed method by using the MIT-BIH and PTB database. A novel methodology is designed for the compression of ECG signal for telemedicine and e-

healthcare application. Here, researchers have used the adaptive Fourier decomposition (AFD) and symbol substitution (SS) based hybrid technique. This Methodology of compression includes two stages such as; a) AFD is executed for efficient lossy compression with high fidelity and b) SS is performed for the lossless compression, which enhances the compression performance and encrypts the built-in data [109]. Padhy *et al*., have introduced data compression of multi-lead ECG signals. Here, singular value decomposition in the wavelet domain is performed. A new technique for estimating the suitable value of thresholding is also given in this work, which is based on multiscale root fractional energy contribution [110]. Another hybrid technique based A hybrid ECG compression technique based on DWT and removal of interbeats and intrabeats correlations is introduced for the ECG signal compression [111]. Wavelet and coding based other methods are also used for ECG signal compression [112]. WT is used for data compression and decompression of audio and ECG Signals in [113].

1.5.1.3. Parameter Extraction Compression

In parameter extraction compression techniques, extraction of a set of parameters from the original signal is done, and these extracted parameters are used to reconstruct the signal. The process is used to quantize a small set of extracted diagnostic features; sufficiently enough to reduce the data size, and provides almost invisible distortion. In the peak peaking compression techniques, the data reduction is based on the sampling of the continuous signal at all the significant peaks [114]. ECG data reduction using peak peaking method is done in [115,116]. Here, data reconstruction is done using a spline function. The ECG signal compression is presented by utilizing the predictionary interpolation and entropy coding by Ruttimann & Pipberger [117]. The main objective of this work is to attain the data by application of stationary time series analysis. This algorithm has economic implementation by using the available hardware. However, the study has contained the basic problems of DSP, for example, interpolation, linear prediction coding (LPC), least square estimation, estimation of the auto-regressive coefficient, *etc*. [118,119,120].

In a research work, ambulatory ECG data is compressed using the methodology, which includes the average beat subtraction and first differentiation of residual data [121]. Another algorithm is proposed by Nave & Cohen to compress the ECG signal, which is based on a long-term prediction (LTP) model [122]. Subsequently, Cohen & Zigel have presented the multichannel ECG data compression using multichannel LTP [123]. Barlas & Skodalkis have proposed an innovative class of data compression methodologies called a cycle pool based

compression (CPBC) algorithm [124]. These methodologies have been designed for exploiting the redundancy of 1-D semi periodical biological signals, which have the cyclic nature, for example, ECG signal. Another method is given by Hamilton *et al*., in which beat division is performed after QRS complexes identification. Here, researchers have used the artificial neural network (ANN). This work has presented an improvement in the compression methodology based on ANN [125,126]. Another method is proposed for data compression of ECG rhythms, which is more suitable than the average beat subtraction algorithm [127]. A detailed study of training different topologies of errorback propagation (EBP) ANN *w.r.t* variation in a number of hidden layers is given by Saxena *et al*., [128]. This work shows the best topology for ECG data compression. It deals with a composite and efficient method for signal retrieval, data compression and feature extraction. Non-linear quantizer based ECG signal compression method is developed by Cassen & English [129]. This method is a computationally efficient method, in which the compressed data is presented in form of codes or numerals. Other methods are also used for ECG data compression [130-147].

1.5.2. Noise Elimination

For the analysis of ECG signals, the first step is to remove the noises, because noises can lead to an inaccurate diagnosis. An efficient method to clean the ECG signal has been presented by Ahlstrom & Tompkins [148], in which a set of real-time digital filters to denoise ECG waveform is proposed. Hanning filter is used to remove the 60Hz power line interference. After removing 60Hz frequency, the high pass filter is designed to remove dc offset. These researchers also used bandpass filter for the detection of QRS complex. Linear phase filters to remove the baseline drift during the exercise designed by Alsti *et al*., work in real time ECG signal processing [149]. Impulsive noise is removed, using a morphological operator [150]. In this study, researchers have used the basic morphological operator such as erosion and dilation for removing impulsive noise, and removed the baseline drift by applying opening operation followed by closing operation. Further, background normalization has been carried out using drifting and subtraction.

Adaptive filtering is also used to reduce the noise in a biomedical signal. The technique [151], is used for baseline wander drift elimination. Also, these researchers employed the adaptive recurrent filters for noise cancellation of ambulatory ECG data, which includes environmental noise, power line noise, radio frequency noise, and other noises. After

cleaning the signal, arrhythmia detection was done, accomplished with the specialty of QRS-T complexes and ectopic beat detection, P-wave and atrial fibrillation detection. Cascaded structure of adaptive filter has been used to remove the baseline wander [152]. A new technique employing IIR notch filter that not only suppresses the transient state(s) in the output, but also improves the performance in noise reduction as compared to other methods is proposed by Pei *et al*., [153]. Hamilton has compared the adaptive and non-adaptive filtering methods to remove noise in the ECG signal, and has applied adaptive and non-adaptive notch filter to remove 60Hz signal and concluded that the adaptive filtering technique is less complex [154]. In a study, the interval based wavelet denoising method for denoising the ECG signals are used [155]. WT is very often used to denoise the ECG signals, since the past 2 decades. In the same context, Tikkenen used wavelet transform to denoise the ECG signal using a new wavelet packet based algorithm [156]. The research involved the quantitative comparative study of several denoising approaches by means of visual inspection and optimized error measures and the error signal of the denoised ECG data.

Statistical threshold estimator is used to completely eliminate the noise from ECG signal by Agante [157]. Motion artifact in stress is removed from ECG signals by Raya et al. by using adaptive noise cancellation [158], the stress being created by the accelerometer. Modified morphological function (MMF) is used for conditioning the ECG signal [159], where the aim of the research is to improve the performance of signal conditioning to achieve reliable ECG signal analysis in terms of low computational burden, low distortion ratio and good signal to noise ratio. In another study, 60Hz noise is reduced using a notch filter [160]. Authors first, designed the FIR filter using Parks-McClellan method, and then compared the different notch filter results. A new approach to remove baseline wander is proposed by Zhang [161]. DWT is used to remove the baseline wander noise, and the high-frequency noise component is eliminated using the wavelet shrinking method. In another approach, the nonlinear filter bank is used to remove noise components from the ECG signal [162]. Nonlinear filtering improves the performance in terms of less distortion and less computational complexity. In yet another study, researcher employed the elliptical filter for elimination of noise [163]. Blanco-Velasco *et al.,* proposed a new method to enhance the diagnostic value of ECG signal. This method is based on empirical mode decomposition (EMD) to remove baseline wander and high-frequency noise [164].

A novel method to suppress noise, based on unbiased and normalized adaptive noise reduction (UNANR), has been proposed by Wu *et al*., [165]. The performance of this method is better in terms of SNR in the range of 5–20 dB over the 48 ambulatory ECG recordings tested, and analyzed using standard MIT-BIH arrhythmia database. Independent component analysis (ICA) and principal component analysis (PCA) are investigated to denoise ECG signal in [166]. The author has applied 8- channel PCA & ICA to eliminate the unwanted signal. Chand & Lu have proposed an algorithm that is an improvement of EMD algorithm to remove Gaussian white noise [167]. The authors also used FIR Wiener filter for performing the task. A hybrid scheme consisting of Genetic algorithm and wavelet transform has been used by El-Dahshan for ECG signal denoising [168]. The performance of this hybrid scheme is evaluated in terms of SNR and percentage root mean squire difference method (PRD). In another study [169], researchers have presented and compared different technique, *viz.*, IIR high pass filter, IIR zero phase, FIR filter, moving average, wavelet, polynomial filter etc. for removal of baseline wander from the noisy ECG data.

A hybrid method is introduced by Kabir & Shahnaz to denoise ECG data [170]. Authors combine two mass valuable algorithms that are wavelet transform and EMD to improve the processing of ECG signal. Comparative analysis is made in terms of PRD and SNR. In another technique, authors improved the principal component regression (PCR) approach for processing maternal ECG [171]. The aim of this work was to remove maternal ECG signal from the abdomen signal with high accuracy. The non-stationary nature of noise contaminating the ECG signal and the spectral overlapping of noise with diagnostic ECG wave complexes prompted the researchers to undertake another study [172] based on an adaptive filtering approach taking into account two major techniques, *viz*., discrete wavelet transform and artificial neural network (ANN). Authors developed a new combination of multiresolution property of wavelet decomposition with the rationale of adaptive learning ability of ANNs. The study could provide significant SNR improvement as compared to another algorithm that is capable of only removing a fewer number of noises. Another comparatively simple, effective and computationally undemanding method has been proposed that performs noise reduction to increase the accuracy of ECG interpretation [173]. In this work, the researchers have computed the discrete Fourier series of sampled ECG data and calculated the Fourier coefficients for the segmented signal. Eventually, the coefficient corresponding to the noise frequency is eliminated and by using an inverse

operation the processed coefficients are transformed back to time-domain to retrieve the original ECG signal, noiseless and reliable for the analysis and interpretation. The method yielded suitable SNR improvement for high-frequency noise. Liu & Luan proposed a novel integrated adaptive algorithm to separate the fECG (fetal ECG) from the maternal ECG data [174]. The adaptive integrated algorithm is based on ensemble empirical mode decomposition (EEMD), independent component analysis (ICA) and wavelet shrinkage (WS) denoising criteria, denoted by the authors as ICA-EEMD-WS technique for noise elimination and fECG separation. Researchers concluded that the integrated adaptive algorithm gives better result in terms of high SNR, R wave amplitude and smaller mean square error values as compared to conventional algorithm in signal denoising.

A new methodology is proposed by Mirza *et al*., to suppress impulsive noise [175]. In this work, an enhanced adaptive impulsive noise cancellation technique is proposed. This technique is based on State Space Recursive Least Square (SSRLS) algorithm and used to eliminate the impulsive noise that causes catastrophic effects in electrocardiography. The method exhibits better results, as regards impulsive noise cancellation in ECG signal, in comparison to Recursive Least Square (RLS) and Normalized Least Mean Square (NLMS) techniques. The proposed scheme not only demonstrates the fastest convergence, but also excellent tracking characteristics leading to desired and effective results

In another study, by Goel *et al*., [176], white noise has been removed for obtaining the diagnostic information in the ECG signal acquired from MIT-BIH database. The authors used Welch and Blackman Nuttall window functions to design low pass FIR filters. The performance of the two windows based FIR filters are compared by computing Total Harmonic Distortion (THD) and energy levels of the signal. Finally, the authors concluded that Blackman Nuttall window performed better. Another efficient technique, based on VHDL (VHSIC hardware description language) implementation, is introduced by Belchandan et al., [177]. In this research work, researchers used FIR filter and IIR filter for reducing artifacts in ECG data

1.5.3. Feature Extraction

A number of studies have been done for the last six decades for accurate features extraction of ECG signal, especially the QRS segment. QRS complex detection techniques are classified into four groups, *viz.*, (a) transformative approach, (b) syntactic approach, (c) non-syntactic approach and (d) combined or hybrid approach. Several researchers have detected QRS complex, because it is a fiducial point and can be

extracted easily [178-182]. The studies of feature extraction of ECG signal involves different processes, *viz.*, squaring, filtering and differentiation, by applying the decision rules like amplitude and time thresholds, zero crossings, sharp consecutive peaks (P, R, Q point), QRS complex duration, and R-R interval duration [183]. However, several techniques face difficulties in extracting exact features due to a number of dissimilarities in cardiovascular activities, these similerties are reflected in time durations, amplitudes, and slopes of the different parts of ECG wave. Therefore, it is very difficult to extract features of an ECG signal.

In the syntactic approach, pattern recognition is done for QRS complex estimation. Here, the input wave of ECG is segmented into a set of small patterns, *viz*., durations, slopes peaks, and other interwave parts, after that rule-based steps are applied. The signal is shown as a combined unit of durations, slopes, peaks, and interwave segments. The patterns are utilized to determine the QRS complexes. However, these techniques are consuming more time and require inference grammar in each step of execution for the estimation of QRS complex [184-186]. A bottom-up method is used for the recognition of ECG waveforms [187]. This method is based on the assumption that ECG waveforms are the overall units that can be broken into other simple units, and in other simple ones, and so on, up to the peak pattern and segment pattern.

Non-syntactic ECG feature detection techniques are most widely used for the detection of features. These types of techniques involve time duration, slope, amplitude, and threshold values by using different, model, mathematical functions and filters. In a study, the five-step digital filter has been used to detect the QRS complex of ECG signal [188]. Thakor *et al.*, have done a study, in which the power spectral analysis of ECG signal is carried out along with the separate QRS complexes and episodes of noise and artifacts [189].

A real-time algorithm has been proposed by Pan & Tompkins for detection of QRS complex of ECG signal [190]. This algorithm is a reliable technique, because it is based on the digital analysis of width, amplitude, and slope of the segments of the signal. In another work, the standard database (MIT-BIH arrhythmia database) is used to perform the quantitative effects of a number of common elements of rules of QRS complex [191]. Laguna *et al*., have proposed an automatic technique for determination of onsets and offsets points of P, QRS, and T waves. Researchers have used multi-lead ECG signals from the CSE DS-3 database [192]. Another wavelet-based machine learning techniques

for detection of features of ECG signal is done in [193]. A fast expert system is design for electrocardiogram arrhythmia detection [194]. Here, also researchers have used MIT-BIH ECG datasets for analyzing the performance of given method. A method based on mid prediction (MIDP) has been used to extract the spikes of a biomedical signal [195]. Multirate digital signal processing based ECG signal analysis is done by Afonso *et al*., [196]. In this method, authors have designed the filter bank, then decomposed the ECG signal into uniformly distributed sub-bands. Several mathematical approaches are also used to determine the features of ECG signal, *viz*., mathematical models, averaging techniques, mathematical morphology, mixed mathematical basis functions, and spatial velocity function.

Another study includes a new mathematical model, which is used to extract the QRS segment. Here, the researchers have considered that the QRS segment of ECG signal as a pulse-like structure and the number of P-peaks, amplitudes, arrival time and width [197]. The mixed mathematical functions like exponential, Gaussian and straight line have been also utilized to show the amalgamated ECG waveform. A mathematical model has been considered for the occurrence of pulse-shaped waveforms corrupted with colored Gaussian noise [198]. In this work, QRS wave is also determined using the thresholding. A new method, to denoise weak ECG signal based on fuzzy thresholding and wavelet packet analysis is given by Üstündağ *et al*., [199]. In the first method, the diverse mathematical functions are used, and in the second method, a spline function is utilized to extract the QRS complex. Researchers have also identified the P and T waves. Another method is suggested by Trahnias, based on the morphology of QRS complex detection [200]. In this work, a morphological operator is used for peak-valley extractor. A new method based on spatial velocity is suggested by Maheshwari *et al*., for detection of QRS complexes, P and T waves [201]. Several new techniques have been proposed for detection of QRS complex based on fuzzy logic (FL), ANN and genetic algorithms (GA) [202]. However, the accuracy of these methods depends upon the type of used training set. In another study, ANN based methodology is employed to detect the QRS complex in ECG [203].

The artificial neural network (ANN) based method developed by Vijaya *et al*., works on high prediction error to indicate the occurrence of QRS complexes [202]. A number of studies have been done to improve the performance of QRS detection by using adaptive techniques QRS detection [203-208]. Application of higher order cumulate is utilized for

features extraction and cardiac health diagnosis using ECG signals [209]. Here, the linear matched filter is used to detect high frequency QRS complex energy. Two types of problem are found for this method, a) in the detection of QRS complex of a different subject, different passband is required, this problem may come for the same subject in the detection of QRS complex of a different beat and (b) sometimes QRS complex and noise are overlapped. Laguna *et al.,* have presented a method for on-line beat-to-beat extraction known as Adaptive Hermite Model Estimation System (AHMES) [210].

The hybrid methods are the combination of syntactic and non-syntactic approaches used to estimate the QRS segment, and the transformative methods involve transformation of the signal from time domain to other. The examples of these techniques are Fourier transform, sine transform, cosine transform, differentiator transform pole-zero transform, Hilbert transform and wavelet transform. Several studies have been done in which authors have used transformable method to detect the QRS complex [211-220]. In a study, a solution to the basic problem occurring in analyzing the ECG signal has given, for example, the delineation of the signal into its component [221]. Here, the researchers used a pole-zero methodology to analyze the ECG waveform. From the last two decades, the use of WT in QRS estimation has shown the upper edge, because it provides good accuracy in less preprocessing requirement and also easy to implement. [222].

DWT and PCA based method is given by Martis *et al*., for the detection of Feature Extraction of ECG signal [223]. The main advantage of the method based on DWT is that no assumptions are required for ECG signal analysis. Multiresolution analysis of ECG signal based on Maxima of WT is given by Sahambi *et al.,* [224]. A method based on WT is used for the detection of QRS complex by zero crossings [225]. This method is robust to time-varying QRS complex morphology and noise.

1.5.4. IFIR Filter and Filter Bank

IFIR filter is developed by Neuvo *et al.,* to reduce the complexity in linear filtering [21]. A structure, with flat passband and equiripple stopband attenuation using Remez exchange algorithm has been developed by Vaidyanathan [126]. Another methodology, based on iterative method, has been used for designing computationally efficient IFIR filters [227]. Subsequently, Pawel & Chau have further improved the IFIR filter response in terms of computational complexity [228]. In this study, a delta cosine signed-digit code (CSD) truncation method for designing of IFIR filter has been used to obtain a simple

structure for improving the response in passband region. In another study, frequency-response masking (FRM) technique was used for efficiently improving the filter response [229]. A new procedure for implementing fully adaptive IFIR filter has been presented in [230]. In this method, the border effects have been removed with an improvement in mean square error (MSE). Since then, further improvements in the response of passband region of IFIR filters have been made by several researchers [231-234].

In the design of IFIR filter, up-sampling factor (L) is a dominant parameter of IFIR filter as all other specifications of the sub-filters (model and interpolator filter) are directly derived from L. Thus, the selection of L is an essential step in designing an IFIR filter. So far, the value of L has been expressed as the reciprocal of stopband frequency of original desired FIR filter. For further reducing the computational complexity, researchers have introduced techniques for obtaining suitable values of L. For instance, Richard has suggested an optimum value of L on the basis of the relation between the complexity reduction cost (*CRC*) and transition width (*TW*) [235]. In another study, a mathematical relation for obtaining an optimum value of L is proposed by Mahernia & Willison [236] that improves CR significantly.

In a recent study, a new filter design approach is presented based on interpolation function. Here, researchers have designed close form linear phase filter using convolution window spectrum interpolation that improves the transfer function characteristics. The proposed filter is having a good response in terms of ripples, large stopband attenuation and high efficiency [237]. Mehrnia & Willson have proposed a new design method for constructing FIR filters which are significantly superior to other methods of implementations in terms of hardware realization. In this study, optimally factored IFIR filters are formulated, which are also easily pipelined, thereby allowing the operation at higher data-rates [238]. Other works are also presented for improving the performance of IFIR filter [239-242]

A new design method based on interpolation function is introduced for designing narrow-band sparse FIR filters. The proposed filter is superior than the conventional IFIR filter, because it generates sparser solutions [243]. Another approach is introduced to design a low complexity reconfigurable IFIR filter for software defined radio channelizers. Here, the researchers have used farrow structure to implement the IFIR filter [244]. A simple design technique of a baseband filter for inter-symbol interference (ISI) cancellation is obtained by using a structure based on the IFIR approach. Unlike the classical IFIR

scheme, in this filter, the interpolator is designed first as; simple multiplier less filter composed by cascaded subfilters with unitary coefficients [245].

For additional improvement in the computational complexity, the concept of multistage IFIR filter has been used. As a result of low computational complexity, IFIR filter is more preferable than FIR filter for narrowband and sharp transition width. Therefore, it has many applications in various fields such as image processing, communication systems, radar systems, multirate signal processing, biomedical signal processing and speech processing [246-256]. In designing of a digital filter, following two points are important a) passband of the filter should have approximate a constant amplitude, in the manner of equiripple, namely, the maximum deviation from a constant is minimized; and b) the amplitude of stop-band, should approximate zero in the manner of equiripple, namely, the maximum deviation from zero is minimized [257].

The filter bank is one of the most important tools of multirate signal processing. Among different types of filter banks, cosine modulated filter banks (CMFBs) are the most important. Koilpilai & Vaidyanathen have given perfect reconstruction (PR) condition for CMFB [258]. In this work, PR condition is obtained using power complementary condition. However, practically PR condition cannot be achieved due to the ideal filter requirement due to high computational complexity. Therefore, Nguyen has introduced a new perfect reconstruction condition called as, nearly perfect condition [259]. Here, the filter bank suffers from three types of distortion, which can be removed by considering some point. Here, the authors have used optimization of several parameters to reduce the reconstruction error. However, this approach is complicated, because of large number of iterations. This problem is removed by Creusere & Mitra, by using optimization of single parameter instead of multiparameter [260]. Here, authors linearly change the passband edge frequency to optimize the response of prototype filter. Prototype filter designed by window function can remove the error present in the stop band. However, the window function method generates ripples in the passband and stopband [261-265]. Minimization of ripple length has been done by using the weighted least square method for designing the prototype filter [266]. Here, researchers have considered a factor known as error ratio, it is the ratio of passband energy to stopband energy. Authors have used different values of roll of factor for different error ratio value to get efficient results. A close-form technique is applied to design an optimum prototype filter for cosine modulated filter

bank [267,268]. In this method, the authors have removed the optimization by eliminating the iteration process which reduces the computational time.

In a study, a near-perfect reconstructed trans-multiplexer is designed [269]. Here, the researchers have used the windowing method for the design of linear phase prototype filter, and different modulation techniques have been exploited for designing a suitable transmultiplexer. Sharma *et al*., have been designed a multiplier-less near perfect reconstruction CMFB [270]. In this work, adjustable window functions have been used to design a prototype filter, and cuckoo search (CS) optimization technique is applied to obtain the magnitude response of *0.707* at frequency $\omega=\pi /2M$. Recently, Shaeen and Elias have done a study of literature of several techniques of CMFB and their performance comparisons [271]. Authors have also prosed FRM based technique for designing a computationally efficient filter bank. In another work, M-channel multiplierless CMFB has been designed by utilizing sub-expression technique (CSE) [272]. In this work, a hybrid method is also used to obtain the optimum response of filter using roll- off factor and A_S. Sharma & Sharma have designed CMFB for spectrum sensing application in Cognitive Radio [273]. In this work, windowing method has been used by the researchers. Kaiser window function is used to design the prototype filter. Instead of optimization method, here authors have used closed form method. Baderia *et al*., have proposed an efficient Multi-channel MFB [274]. Here, the researchers have optimized the prototype filter by utilizing the polyphase components. For this purpose, CS, modified cuckoo search (MCS) and swarm optimization techniques (SOTs) based algorithms are used to improve the performance of FB. A multiplier-less tree-structured NPR FB is proposed by Bindiya & Elias [275]. The aliasing distortion generated between the adjacent bands is reduced by using a sharp transition band filter. For this purpose, FRM technique is used which provides the low computational complexity, linear phase and sharp transition width. The authors have also compared the performance of proposed filter bank with several existing FBs, and concluded that the proposed FB is better in terms of number of multipliers.

In another work, discrete Fourier transform (MDFT) filter bank is proposed using canonic signed digit space-based methodology [276]. Here, FRM technique is used to obtain sharp transition width and less computational complexity. Further, the performance of designed FB has been increased using modified meta-heuristic algorithms. Prema & Dasgupta have proposed a method for optimizing a prototype filter for designing the

CMFB [277]. In this methodology, NPR CMFB is designed, which have low distortion (amplitude and aliasing). Low value of these distortions is obtaining by coshing an objective function. The designed approach is systematic and self-controlled. Kalathil & Elias have presented a new methodology to design an NPR CMFB [278]. In this study, CSD coefficients methodology has been used to design an efficient CMFB. Further the authors have designed the non-uniform FB by merging the bands of uniform FB. Here three methodologies are used to design the prototype filter i.e., weighted Chebyshev approximation, window method and weighted constrained least square approximation [279]. Further, authors have given another study of designing VMFB. Here, the authors have designed the hybrid methodology, which has combined the qualities of two meta-heuristic algorithms. A novel methodology of recombination of filter bank for obtaining the NUFB has been given by Kalathil [280]. Here the researcher first designed the uniform FB and transmultipexer by applying cosine modulating technique. The nature-inspired optimization algorithm is used to achieve multiplier free FB in CSD, and the overall CMF has less computational complexity.

Another hybrid methodology is given by Kuldeep *et al*., to design an m-channel CMFB [281]. Here, the researchers have used a combination of Lagrange multiplier method and cuckoo search optimization. Verma & Singh have recently proposed a methodology to design a multi-channel CMFB [282]. Here, authors have used bacterial foraging optimization (BFO) and CSD technique to minimize error in the response of the filter. This approach has reduced up-to 22% of time of completion. Another recent approach for the design of a CMFB is given by Ozdemir_ & Karaboga [283]. Artificial bee colony (ABC) algorithm has been used by the researcher to optimize the filter response.

Since the filter bank has a variety of applications in various fields. The research is continued from the last two decades to design efficient multirate filter bank, and the non–uniform filter bank is more remarkable than uniform FB, because it is suitable for complex applications. A non-uniform filter bank can be used for the audio system and biomedical systems [284,285]. A substantial amount of research has been done to design non-uniform filter bank and detailed by different authors. [286-295]. for reducing the computational complexity of prototype filter, Zijing & Yun have used IFIR filter instead of FIR filter. This method gives a significant reduction in computational complexity. Authors have designed non-uniform cosine modulated filter bank. Parks-McClellan has used an algorithm for designing model and interpolated filter [296]. Soni *et al*., [297]

have designed the prototype filter with IFIR by using the windowing technique. Kaiser window function has been used to design uniform CMFB and optimization of prototype filter has been done using linear gradient optimization technique [298]. Authors [299] have designed a trans-multiplexer by using IFIR filter. In this work, minimization of parameters has been done by applying a single variable bisection type optimization technique. The improvement of the response of prototype filter has been done by different algorithms. Others researchers have also presented the design of digital filter and filter bank [300, 303].

1.6. Author's contribution

The Author has developed an algorithm for designing computational linear phase filters. In coefficient reduction method, the numbers of unwanted coefficient have been removed by using suitable mathematical relations between filter tap of IFIR and FIR. Several filter design method are used to design model and interpolated filter, which shows that the methodology used in this work can be applicable for all type of filter design technique and provide efficient results in terms of computational cost and filter response. And these filters can be used to denoise any signal without phase distortion and complexity. Another advantage of the designed method is it provides less delay in comparison to conventional IFIR and FIR filter.

M-channel filter bank has been designed by using single stage and two staged IFIR filter, which reduces the computational complexity. Further, the computational cost is reduced by apply cosine modulation technique. The perfect reconstruction condition has been achieved using linear optimization of cut off frequency of model filter by calculating the filter coefficients at 3dB cut-off frequency. The designed filter bank can be used in several signal compression, signal analysis and signal processing.

The designed uniform filter bank is used to compress the ECG data along with encoding methodology. Here, the author has been used several combinations of filter bank and encoding to obtained performance comparisons of these combinations in different terms, *viz*., compression ratio and signal reconstruction quality parameters. The designed methodologies can be used for the real time ECG signal compression.

Designed non-uniform filter bank is used for the R-peak detection. Other features are also obtained using some rule based techniques. These features are important in the diagnosis of a cardiac patient. the performance of data decompression is obtained by extracting the

diagnostic features from the denoised original and reconstructed data and performing the comparative analysis of these features. The comparative analysis shows that the methodology can reconstruct the compressed data, with diagnostic information loss. Therefore, design methodology can play an important role in the diagnosis of patient using telemedicine and holter monitor systems, which are very important in several emergency cases.

1.7. Research Objectives

Several techniques have been developed for compression of ECG rhythms. Amongst all filter bank based data compression methods are more popular, because they provide better performance in terms of compression ratio (CR) and signal reconstruction quality (peak mean square difference (PRD), signal to noise ratio (SNR), mean square error (MSE), mean error (ME), peak mean square difference normalized (PRDN) and quality score (QS). In these methods, signal is transformed from time domain to frequency domain, and then irrelevant components are removed using suitable thresholding to achieve compression.

The performance of data compression and decompression is measured using different parameters. However, in order to justify diagnostic relevance, the performance of data decompression of a biomedical signal should be examined by the comparative analysis of features of both signals, *i.e.*, original input signal before compression, and reconstructed signal after decompression. Also, a new performance parameter; WDD has been introduced by researchers for measuring the performance of data reconstruction. WDD utilizes the features of the both signals.

The computational complexity of an IFIR filter is very low in comparison to FIR filter. IFIR filters are designed using FIR filters that provide inherent stability and linear phase, rendering them preference in most of the signal processing applications.

After an exhaustive literature survey carried out in the present study, the following challenges were encountered that motivated for pursuing the present research work; a) data compression of biomedical signals, specially the ECG signal is highly sensitive, significant and cumbersome task that is very helpful in telemedicine, e-healthcare and holter monitor systems. b) among all data compression methods, filterbank based methods are more suitable for ECG signal compression, c) hybrid combination of transform based methods and lossless coding can improve the data compression and reconstruction performance, d) selection of thresholding is a very important part of data compression, e) for a biomedical signal, data decompression, performance should be evaluated by comparing the features of both the signals, f) IFIR filters are computationally efficient, these are linear phase filters having stable characteristics, g) among all the categories of filter banks, CMFBs are computationally efficient and simple to design, h) computational complexity of CMFBs can be further reduced by using single stage and two stage IFIR prototype filters and i) for reducing the reconstruction error, the

optimization of prototype filter is very important, Therefore, the following objectives are addressed in this work:

Objective 1: To design a ripple free IFIR filter, which has an identical filter response to the FIR filter, to acquire less computational complexity, stable nature and linear phase.

Objective 2: Design and development of computationally efficient CMFB using suitable prototype filter which would provide optimum performance by applying suitable optimization technique.

Objective 3: To compress ECG rhythms using efficient filter bank(s) and if necessary, other compatible compression technique(s) in addition, to enhance the performance w.r.t. WDD and other respective indices.

Objective 4: To extract features from denoised original ECG signal and decompressed ECG signal, and then perform the comparative analysis of extracted features in both the original and decompressed data.

1.8. Organization of Thesis

The work carried out in this thesis can be broadly classified into two sections. The first section mainly deals with the implementation of filter and filter banks using cosine modulated filter bank. And in the second part, implementation of ECG data compression using the designed filterbank and their performance evaluations is given. In the first chapter, the introduction of the heart, generation of ECG signal, 12-lead system used to record the ECG data from a human body, MIT-BIH databases, IFIR filter, and filter bank is presented. The major part of this chapter is the literature review of the methods of ECG data compression, noise elimination from ECG signal, feature extraction, IFIR filter, and filter bank design. In the second chapter, several techniques for noise elimination from an ECG signal are described in detailed. Chapter three includes the noise elimination from MIT/BIH database using different methods. This chapter also has the implementation of IFIR filter and noise elimination using IFIR filter. In the fourth Chapter, different methods of data compression in general and lastly for ECG data particularly are described in detail. In chapter five, data compression of ECG rhythms is done using wavelet transform, wavelet packet, QMF filter bank, and empirical wavelet transform. The developed algorithms are evaluated using the MIT/BIH databases. Chapter six deals with the implementation of uniform and non uniform CMFBs design using IFIR prototype filter. Further, designed filter banks are applied to MIT/BIH database for compression and decompression. In Chapter seven, the performance of data compression using features comparison is done. The conclusions of the overall work, the findings and the guidelines for the future work are given in the last chapter.

CHAPTER 2

ECG SIGNAL NOISE REDUCTION TECHNIQUES

2.1. Overview

Biomedical signal processing is one of the most important branch of biomedical engineering. The main objective of biomedical signal processing is to extract significant information from the biomedical signals. For a bio-medical engineer and doctor, the first and the foremost part is to acquire signal from the human body [2]. However, acquiring a signal from a living being without noise contamination is almost impossible task. A human body generates different signals, *viz*., electrocardiogram (ECG), electroencephalogram (EEG), electromyogram (EMG), electro-dermal activity (EDA) signals, *etc.* The detailed information about the ECG signal is presented in Chapter 1. The normal frequency range of this signal is 0.05–100 Hz. Similar to other biomedical signal, this signal is also contaminated with several types of noises, such as; high frequency noise, power line interference (PLI) 50/60Hz, EMG noise (<10 KHz), baseline wander (<1 Hz), channel noise generated due to poor channel conditions, motion artifacts, *etc*. Elimination of these noises must be done before the analysis to obtain accurate interpretation of the disease. In general, the noise is consisted of chaotic processes [170]; and hence, accurate prediction of dynamic as well as other characteristics of the noise is impossible. Therefore, estimation of noise is not an easy task especially for a non-stationary signal such as ECG signal. This is due to two reasons, a) properties of deceptive noise, and b) subtle and fine characteristics of the ECG signal. Several researchers have developed techniques to eliminate these noises without affecting the cardiac information. These techniques are classified into a) linear filtering, b) nonlinear filtering, c) adaptive filtering, d) time-frequency resolution methodologies and e) artificial intelligent based methodologies [160-165]. In this chapter, noise elimination techniques are discussed in details.

2.2. Filtering

Filtering is a process of removing of un-useful information from a signal. In digital signal processing, digital filters are used to perform the filtering operation. Digital filters are mainly divided into two categories; infinite impulse response filters (IIR) and finite impulse response filters (FIR) [1]. Digital filters are used in a number of areas, such as communication system, power system, image processing, radar system, biomedical system, *etc*. In this section, several filter design methodologies are described.

2.2.1. Infinite Impulse Response Filter

Infinite Impulse Response (IIR) filters are having impulse response for the infinite duration. IIR filters perform better in comparison to FIR filters under the same set of design specifications. These types of filters have a feedback connection and also known as recursive digital filters. Due to recursive property, these filters provide good frequency response at low filter order. The transfer function of an IIR filter includes both zeros as well as poles, which are depicted in Eqn. (2.1) [24].

$$H(z) = \frac{\sum_{k=0}^{M} b_k z^{-k}}{1 + \sum_{k=1}^{N} a_k z^{-k}} \tag{2.1}$$

where, a_k, b_k M and N are the feedback filter coefficients, feed forward fitter coefficients, feed forward filter order and feedback filter order, respectively.
Butterworth, Bessel, and Chebyshev filters are the main examples of IIR filters. IIR filters are mainly used in the systems, in which linear phase and stability is not needed. Therefore, applications of these filters are in audio processing such as speakers and for sound processing applications, biomedical signal processing, radar signal processing, *etc*., [153].

IIR filters are used to remove the stationary power line interference (PLI). The notch filter provides a noble performance at higher attenuation level, in removing the PLI. However, there are three major difficulties encountered in case of IIR filter design such as; a) non-convex optimization problem, due poles position, b) non-linear phase, and c) stability constraint [177].

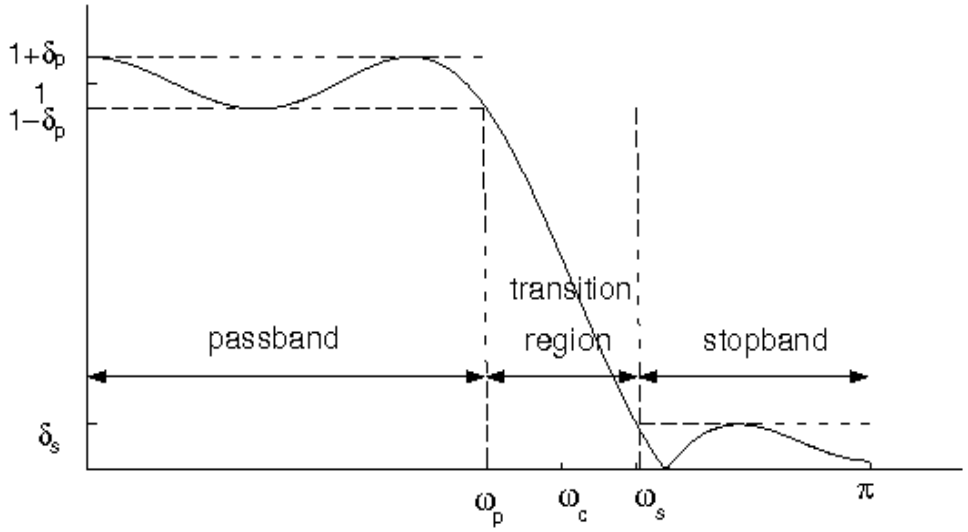

Fig. 2.1 Lowpass filter response [24].

2.2.2. Finite Impulse Response Filter

FIR filters are the filters, which have the impulse response of finite duration *i.e.*, they settle to zero in the finite time. An FIR filter has *N+1* sample. The transfer function of an FIR filter includes only zeros. It is based on a feed-forward difference equation (DE) as shown in Eqn. (2.2).

$$y(n) = \frac{1}{3}(x[n+1] + x[n] + x[n-1]) \tag{2.2}$$

where, $x(n)$ and $y(n)$ are the input and output signal, respectively.

The lowpass practical FIR filter response is illustrated in Fig. 2.1. For designing a filter design important specifications are required, *viz.*, stopband edge frequency (ω_s), passband edge frequency (ω_p), stopband ripple (δ_s) and passband ripple (δ_p). In some methods, cut off edge frequency (ω_c) is used, which is calculated as:

$$\omega_c = \frac{\omega_s + \omega_p}{2\pi} \tag{2.3}$$

In general, FIR filters are more desirable in comparison to IIR filters due to linear phase and inherent stable nature [226]. The transfer function (TF) of FIR filter is given in Eqn. (2.4) [1]

$$H(z) = \sum_{n=0}^{N-1} h(n) z^{-n} \tag{2.4}$$

This function includes only zeros, here, *N* is the order of filter, which is calculated as:

$$N = \frac{A_s - 7.95}{14.36\Delta\omega} \tag{2.5}$$

where, $\Delta\omega$ is the transition width, which can be estimated as:

$$\Delta\omega = \frac{1}{2}\left(\omega_s - \omega_p\right) \tag{2.6}$$

An FIR filter can be designed using several methodologies such as: windowing, weighted least squares, Parks-Mc-Clellan, spline method, *etc*., [4,176]. In this section, these methodologies are described.

2.2.2.1. Windowing Method

Selection of methodology to design an FIR filter is done according to the requirement of filtering, for example, a windowing technique is superior to other filter design techniques in terms of time taken and simplicity. In this method, a function known as window function is used to obtain the desired filter response. Here, the coefficients of ideal filter are truncated using window function. A window function tapers smoothly to zero at both ends. In this method, Eqn. (2.7) is used to obtain filter response.

$$h(n) = h_{id}(n)w(n) \tag{2.7}$$

here, $h_{id}(n)$ represents the ideal impulse response of the filter that can be computed as:

$$h_{id}(n) = \frac{\sin(\omega_c(n - N/2))}{\pi(n - N/2)} \tag{2.8}$$

and $w(n)$ is the window function.

Window functions are mainly classified into two types: a) fixed window functions and b) adjustable window functions [1-3].

2.2.2.1.1. Fixed Windowing Function

The fixed window function is a window function that uses only one controlling factor to adjust the side lobe and main lobe (width and height) shape. Several types of fixed window functions have been used for designing the FIR filters. One of the commonly used fixed window function is the Blackman window function.

2.2.2.1.1.1. Blackman Window Function

Blackman window reduces the effects of secondary lobes using two cosine terms. The mathematical expression of this function is given in Eqn. (2.9) [176].

$$w(n) = 0.42 + 0.5\cos\left(\frac{2\pi n}{2M+1}\right) + 0.08\cos\left(\frac{4n\pi}{2M+1}\right), \text{ for } -M \le n \le M \quad (2.9)$$

where, *M* is the length of the window function.

2.2.2.1.1.2. Rectangular Window Function

A very simple window function is the Rectangular window function that has unit magnitude for the specified length and has zero magnitude for rest of the length. The rectangular window gives a smaller main lobe width than other fixed type windows and provides fixed ripple ratio *i.e*., 13.1 dB. The mathematical expression of the rectangular window function is given below [137]:

$$w(n) = \begin{cases} 1, & -\frac{M-1}{2} \le n \le \frac{M-1}{2} \\ 0, & \text{otherwise} \end{cases} \quad (2.10)$$

2.2.2.1.1.3. Bartlett Window Function

Bartlett has introduced a new window function that removes the problem of ripple presented in the rectangular window, *i.e*., nearer to the band edges of the designed filters. This window function is also known as a triangular window function, because the shape of this window function is triangular. It gives a wider main lobe width than the rectangular window and provides better ripple ratio *i.e*., 26.5 dB [1]. The mathematical expression of the Bartlett window function is depicted in Eqn. (2.11)

$$w(n) = \begin{cases} \frac{2n}{M}, & 0 \le n \le \frac{M}{2} \\ 2 - \frac{2n}{M}, & \frac{M}{2} \le n \le M \end{cases} \quad (2.11)$$

2.2.2.1.1.4. Hanning Window Function

Hanning window is also known as a raised cosine window or Hann window. This window has the same main lobe width as the Bartlett window ($8\pi/(M+1)$). It gives more attenuated side-lobes with ripple ratio equal to 31.5 dB [5].

$$w(n) = 0.5\left(1 - \cos\left(2\pi\frac{n}{M}\right)\right), \quad 0 \le n \le M \quad (2.12)$$

2.2.2.1.1.5. Hamming Window Function

Hamming window is obtained by linear combination of rectangular and Hanning window. This window function is used for minimizing the maximum side lobe amplitude. The main lobe width of this window is larger than the rectangular window, and the ratio of the amplitude of main lobe to secondary lobes is much larger than the rectangular window. This window provides batter stopband attenuation in comparison to Rectangular, Bartlett and Hanning window, *i.e.*, 42.7 dB [5]. In Eqn. (2.13), mathematical expression of Hamming window is given.

$$w(n) = 0.54 - 0.46\cos\left(2\pi\frac{n}{M}\right), \quad 0 \le n \le M \tag{2.13}$$

2.2.2.1.1.6. Blackman-Harris Window Function

This window functions is the modified version of Blackman window function. In this window, more than one shifted sinc functions are added to minimize the side lobe levels. The mathematical expression of this window function is:

$$w(n) = a_0 - a_1\cos\left(\frac{2\pi n}{M}\right) + a_2\cos\left(\frac{4\pi n}{M}\right) - a_3\cos\left(\frac{6\pi n}{M}\right) \tag{2.14}$$

where, a_0 , a_1, a_2 and a_3 are the constant and have magnitude of *0.35875*, *0.48829*, *0.14128* and *0.01168*, respectively.

2.2.2.1.1.7. Flat Top Window Function

A flat top window has a wide main lobe, minimal scalloping loss in the frequency domain, and positive and partial negative amplitude. For designing a flat top window function, either low-pass filter design methods or cosine-sum methodologies are used. Cosine-sum function used to define this window function is presented in Eqn. (2.15).

$$w(n) = a_0 - a_1\cos\left(\frac{2\pi n}{M}\right) + a_2\cos\left(\frac{4\pi n}{M}\right) - a_3\cos\left(\frac{6\pi n}{M}\right) + a_4\cos\left(\frac{8\pi n}{M}\right) \tag{2.15}$$

In this Eqn., values of a_0, a_1, a_2, a_3 and a_4 are *0.21557895, 0.41663158, 0.277263158, 0.083578947* and *0.006947368*, respectively

2.2.2.1.1.8. Modified Bartlett-Hann Window Function

Modified Bartlett-Hann Window is a linear combination of Hanning and Bartlett window. The near sidelobes of this window are lower than the near sidelobes of Bartlett or Hanning window. In this window, the mainlobe width is not increased as compared to mainlobes of Bartlett or Hanning window. The mathematical function of this window is given in the following equation.

$$w(n) = 0.62 - 0.48\left|\left(\frac{n}{M} - 0.5\right)\right| + 0.38\cos\left(2\pi\left(\frac{n}{M} - 0.5\right)\right) \tag{2.16}$$

where, window length is $L = M + 1$ and $0 \le n \le M$.

2.2.2.1.1.9. Nuttall Window Function

Nuttall window is also a fixed window, which is the combination of more than one cosine terms. The mathematical expression of this window is:

$$w(n) = \sum_{m=0}^{M-1} (-1)^m b_m \cos\left(\frac{2\pi nm}{L}\right) \tag{2.17}$$

where, b_m are the coefficients of window, L is the length of the window and M is the number of terms used.

2.2.2.1.1.10. Parzen Window Function

This window is also known as the 4^{th} order B-spline window that can be defined as:

$$w(n) = w_0\left(n - \frac{M}{2}\right), \qquad 0 \le n \le M \tag{2.18}$$

where,

$$w_0(n) = \begin{cases} 1 - 6\left(\dfrac{n}{L/2}\right)^2\left(1 - \dfrac{|n|}{L/2}\right), & 0 \le |n| \le \dfrac{L}{4} \\ 2\left(1 - \dfrac{|n|}{L/2}\right)^3 & \dfrac{L}{4} < |n| \le \dfrac{L}{2} \end{cases} \tag{2.19}$$

and $L = M + 1$.

Comparison of normalized magnitude responses and frequency responses of different fixed window functions is shown in Fig. 2.2 and Fig. 2.3, respectively.

2.2.2.1.2. Adjustable Window Functions

Another class of window functions is the adjustable window functions. These type of window functions have more than one parameters for controlling the ripple ratio. Kaiser and Dolph–Chebyshev window are famous examples of the adjustable window function.

2.2.2.1.2.1. Kaiser Window Function

Kaiser Window function uses two controlling parameters. It can be defined by using Eqn. (2.20) to Eqn. (2.22) [105];

$$w(n) = \frac{I_0\left[\beta\sqrt{1-\left(1-\frac{2n}{M-1}\right)^2}\right]}{I_0[\beta]}, \quad \text{for } 0 \le n \le (M-1) \tag{2.20}$$

where,

$$I_0(x) = 1 + \sum_{r=1}^{\infty}\left[\frac{(x/2)^r}{r!}\right]^2 \tag{2.21}$$

and

$$\beta = \begin{cases} 0, & \text{for } A_s \le 21 \\ 0.5842(A_s - 21)^{0.4} + 0.07886(A_s - 21), & \text{for } 21 \le A_s < 50 \\ 0.1102(A_s - 8.7), & \text{for } A_s > 50 \end{cases} \tag{2.22}$$

where, N and β are two controlling parameters used to control the length and shape of window, respectively. The term $I_0[.]$ is the modified zeroth-order Bessel function. The Kaiser window function is also modified by using one more shape controlling parameter (γ). The Expression of this modified Kaiser window is given as:

$$w(n) = \frac{I_0\left[\beta\sqrt{1-\left(1-\frac{2n}{M-1}\right)^2}\right]^{\gamma}}{I_0[\beta]}, \quad \text{for } 0 \le n \le (M-1) \tag{2.23}$$

where, γ is the additional shape adjusting parameter.

2.2.2.1.2.2. Dolph-Chebyshev Window Function

Dolph-Chebyshev window function is used to produces equeripple frequency response of a filter. It has a minimum main-lobe width for a given side-lobe attenuation. Since, the

height of all side-lobes are equal [3].

Mathematically, it is defined by Eqn. (2.24) to Eqn. (2.27).

$$w(n) =, \begin{cases} \frac{1}{M+1}\left(\frac{1}{r} + 2\sum_{i=1}^{M/2} C_M\left[x_0 \cos\left(\frac{i\pi}{M+1}\right)\cos\left(\frac{2\pi ni}{M+1}\right)\right]\right), & \text{for } |n| \le \frac{M}{2} \\ 0, & \text{for } |n| > \frac{M}{2} \end{cases} \quad (2.24)$$

where, x_0 is obtained by using expression given below:

$$x_0 = \cosh\left((1/M)\cosh^{-1}(1/r)\right) \quad (2.25)$$

and r is the ripple ratio that can be obtained as:

$$r = (A_s / A_p), \quad (2.26)$$

$$C_M(x) = \begin{cases} \cos\left(M\cos^{-1}(x)\right), & \text{for } |x| \le 1 \\ \cosh\left(M\cosh^{-1}(x)\right), & \text{for } |x| > 1 \end{cases} \quad (2.27)$$

2.2.2.1.2.3. Saramaki Window Function

Dolph-Chebyshev window does not provide a decent side-lobe roll-off ratio. Saramaki has introduced another adjustable window function that is known as Saramaki window. When Saramaki window is compared to Kaiser window, it is observed that both have identical performance in the time and frequency domain. There is no need of power series expansion for estimating window coefficient in both the cases. In Eqns. (2.28) to (2.32), Saramaki window function is presented [291].

$$w(n) = v_0(n) + 2\sum_{k=1}^{M} v_k(n) \qquad 0 \le n \le M-1 \quad (2.28)$$

where, $v_k(n)$ can be calculated using the following recursion relation:

$$v_0(n) = \begin{cases} 1, & n = 0 \\ 0, & otherwise \end{cases} \quad (2.29)$$

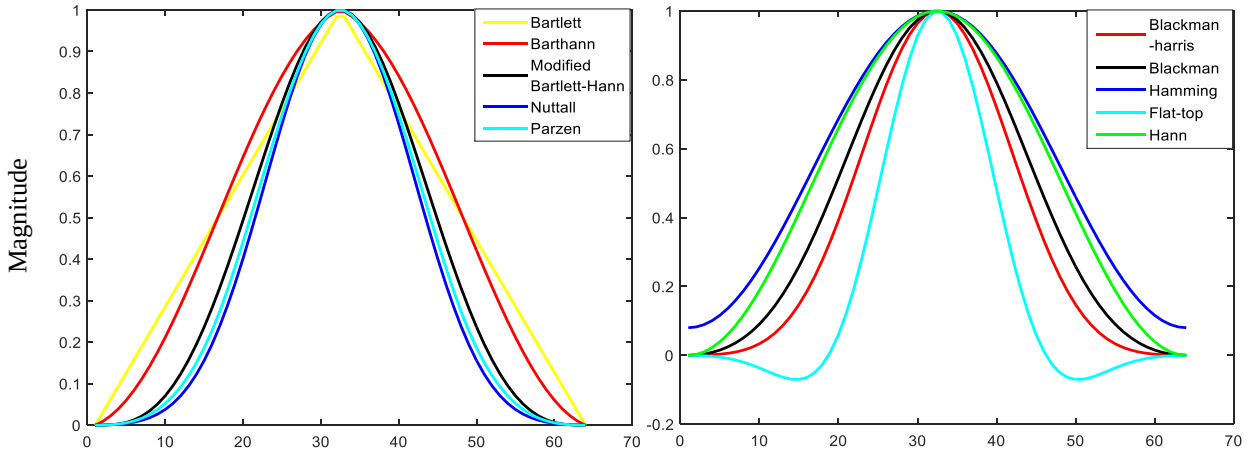

Fig. 2.2 Comparison of Shape of Different Fixed Windows.

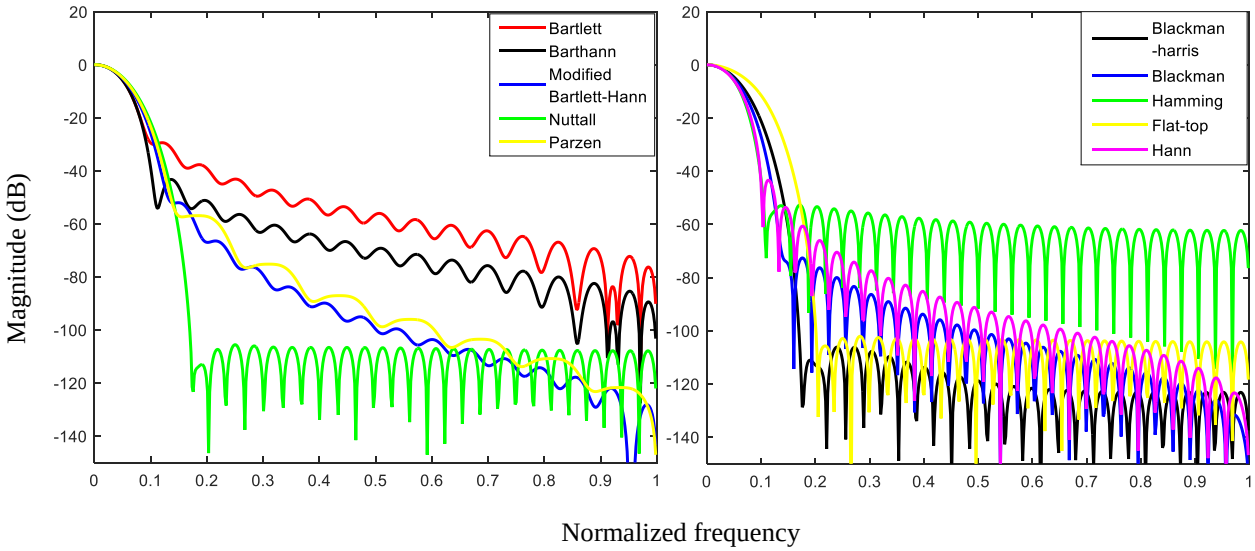

Fig. 2.3 Comparison of normalized magnitude spectrum of different fixed windows.

and $v_1(n)$ is;

$$v_1(n)=\begin{cases}\gamma-1, & n=0\\ \dfrac{\gamma}{2}, & |n|=1\\ 0, & otherwise\end{cases} \tag{2.30}$$

Therefore, $v_k(n)$ can be estimated as;

$$v_k(n)=\begin{cases}2(\gamma-1)v_{k-1}(n)-v_{k-2}(n)+\gamma\left[v_{k-1}(n-1)+v_{k-1}(n+1)\right] & |n|\le k\\ 0; & otherwise\end{cases} \tag{2.31}$$

here, the value of γ is measured by the following expression;

$$\gamma=\frac{1+\cos(2\pi/2M+1)}{1+\cos(2\pi\beta/2M+1)} \tag{2.32}$$

2.2.2.1.2.4. Roark's Transitional Window Function

In FIR filter designing, for a given stopband attenuation and filter order, any adjustable window such as Kaiser, Saramaki and Dolph-Chebyshev gives minimum transition width in the window spectrum. However, it gives large amplitude error in passband. Three response criterions: minimum transition width, high stopband attenuation, and passband flatness cannot be attained concurrently through any adjustable window function. Therefore, Roark's transitional window function is designed using a B-spline function in the transition region. This window has more degree of freedom through, which compromise three parameters easily. Roark's transitional window is also known as a maximally flat window [284].

In digital filter design, transitional window gives better smoothness than all above windows in passband and stopband region both.

$$w(n)=\begin{cases}\left(\dfrac{\left(\sin\left[\pi n/M+1\right]\right)}{\pi n/M+1}\right)^{\rho}, & for\ \ -M\le n\le M\\ 0, & otherwise\end{cases} \tag{2.33}$$

2.2.2.1.2.5. Ultraspherical Polynomials Window Function

Ultraspherical Window is also known as Gegenbauer window. The mathematical expression of this window is based on the Gegenbauer/ultraspherical orthogonal polynomials. The mathematical function of this window is depicted in Eqn. (2.34).

$$w(n)=\frac{1}{M}\left[C_{M-1}^{\alpha}(x_0)\sum_{i=1}^{(M-1)/2}C_{M-1}^{\alpha}(x_0\cos\frac{i\pi}{M}\cos(\frac{2n\pi i}{M})\right] \quad (2.34)$$

In this expression, x_0 is the side-lobe controlling parameters and $C_N^{\alpha}(x)$ is the M^{th} degree ultraspherical polynomial, which can be obtained using recursion relationship as depicted in Eqn. (2.35) .

$$C_N^{\alpha}(x)=\frac{1}{N}\left[2(N+\alpha-1)xC_{N-1}^{\alpha}(x)+(N+2\alpha-2)C_{N-2}^{\alpha}(x)\right] \quad (2.35)$$

Here, $C_0^{\alpha}=1$, $C_1^{\alpha}=2\alpha x$, and $C_2^{\alpha}=-\alpha+2\alpha(1+\alpha)x^2$.

2.2.2.1.2.6. Exponential or Poisson window Function

This window function involves exponential terms. In comparison to ultraspherical window function, this window provides better ripple ratio by utilizing the fixed length of window, side lobe roll-off ratio and mainlobe width. The mathematical expression of this window function is:

$$w(n)=\frac{e^{[\mu\sqrt{1-(1-(2n/(M-1)))^2}]}}{e^{\mu}}\ ,\quad \text{for } 0<n<M-1 \quad (2.36)$$

where, μ (window shape parameter) is used to control the ripple ratio, which can be calculated as:

$$\mu=-1.552\times10^{-5}\rho^3-2.923\times10^{-3}\rho^2-0.3211\rho-3.763,\ \text{for } \rho\le-13.25 \quad (2.37)$$

2.2.2.1.2.7. Gaussian Window Function

One of the important properties of a Gaussian function is that, when it transform into the Fourier domain the resulted function is also has Gaussian form. This property can be utilized to design a window for the filter design purpose. The Gaussian window function is depicted in Eqn. (2.38).

$$w[n]=e^{-\frac{1}{2}\left(\alpha\frac{n}{(L-1)/2}\right)^2}=e^{-n^2/2\sigma^2}\ ,\quad \text{for } -(L-1)/2\le n\le(L-1)/2 \quad (2.38)$$

where, σ is slandered deviation, which is computed as:

$$\sigma=(L-1)/2\alpha \quad (2.39)$$

and α is the width factor.

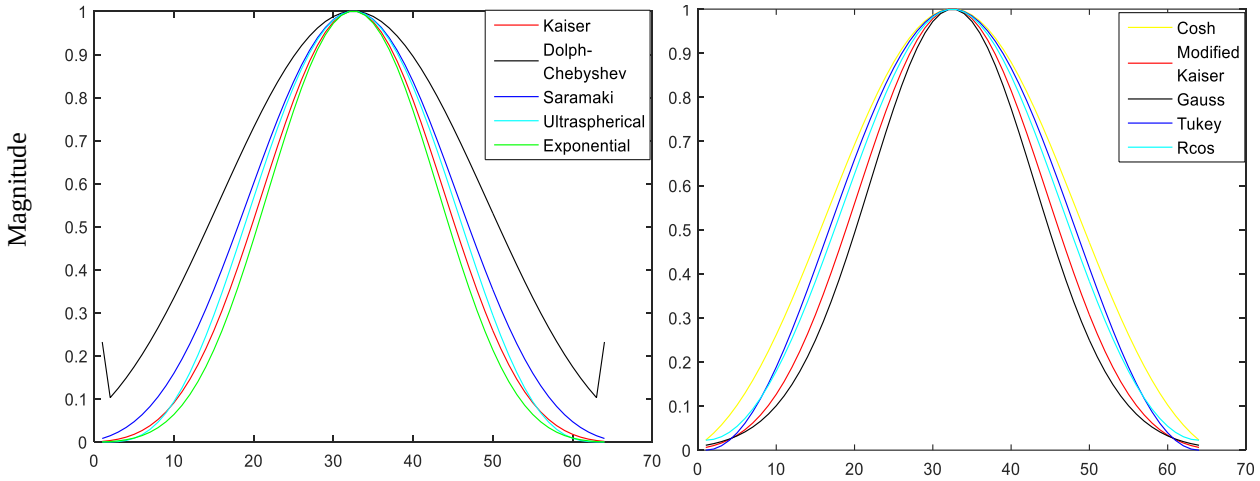

Fig. 2.4 Comparison of the shape of different adjustable windows.

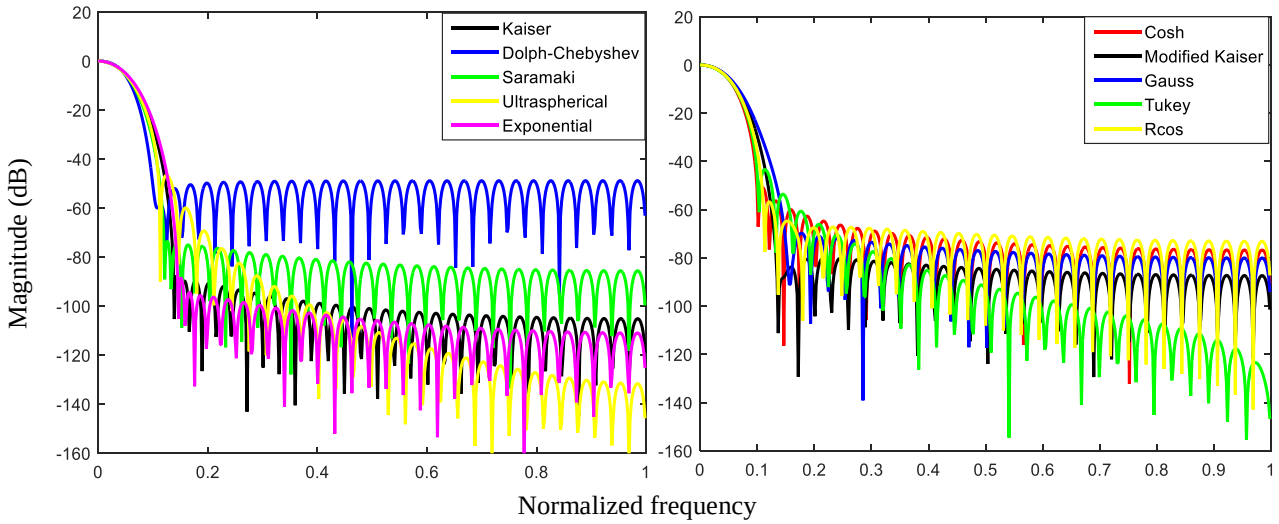

Fig. 2.5 Comparison of normalized magnitude spectrum of different adjustable windows.

2.2.2.1.2.8. Tapered Cosine Window Function

Tapered Cosine Window is also named as Tukey window, which is a rectangular window with the first and last *r/2* present of the samples equal to parts of a cosine. The mathematical function of this window is presented in Eqn. (2.40) [292].

$$w(n)=\begin{cases}\dfrac{1}{2}\left[1+\cos\left(\pi\left(\dfrac{2n}{\alpha M}-1\right)\right)\right] & 0\le n\le\dfrac{\alpha M}{2}\\ & \dfrac{\alpha M}{2}\le n\le M\left(1-\dfrac{\alpha}{2}\right)\\ \dfrac{1}{2}\left[1+\cos\left(\pi\left(\dfrac{2n}{\alpha M}-\dfrac{2}{\alpha}+1\right)\right)\right] & \mathrm{M}\left(1-\dfrac{\alpha}{2}\right)<n\le M\end{cases} \tag{2.40}$$

where, α is the shape parameter, when the value of *it =0* then shape will be rectangular and when it *is =1*, then shape will be the same as shape of Hanning window.

2.2.2.1.2.9. Hyperbolic Cosine Window Function

This window function is the modified form of Kaiser window, where cosine hyperbolic term is used, instead of Bessel function. The hyperbolic function is expressed as [292]:

$$\cosh(s)=\frac{e^{x}+e^{-x}}{2} \tag{2.41}$$

Therefore, the cosh window function can be written as:

$$w(n)=\begin{cases}\dfrac{\cosh\left(\beta_c\sqrt{1-\left(\dfrac{2n}{M-1}\right)^2}\right)}{\cosh\beta_c}, & |n|\le\dfrac{M-1}{2}\\ 0 & \text{otherwise}\end{cases} \tag{2.42}$$

where, β_c is the shape parameter that can be computed as:

$$\beta_c=\begin{cases}0, & \text{for } A_s\le -13\\ 0.4611(-A_s-13.26)^{0.4}-0.1165(A_s+13.26), & \text{for } -50\le A_s<-13.26\\ 0.1469A_s-0.1461, & \text{for } -120\le A_s\le -50\end{cases} \tag{2.43}$$

Comparison of normalized magnitude responses and frequency responses of different adjustable window functions is shown in Fig. 2.4 and Fig. 2.5, respectively. Filter design using windowing technique is an easy and reliable task with an insignificant amount of computation cost. In this technique, only three parameters are needed as a design specification. However, it also has some drawback such as: design filters are suboptimal,

for explicit specifications requirement, large value of filter order is needed; therefore, complexity is increased, and also slow process and less efficient for real-time applications [292].

2.2.2.2. Weighted Least Squares Method

Weighted least squares (WLS) regression method is widely used technique for filter design. It is useful for assessing the parameters of model filter. Here, the predictive values are varied on the basis of reaction values. In this method, an objective function is minimized, which is given in Eqn. (2.44) [266]

$$p(x) = \sum_{i=m}^{m} (z_i - h_i(x)^2) / R_{ii} = [z - h(x)]^T R^{-1} [z - h(x)] = 0 \tag{2.44}$$

For the least value, the first-order optimality conditions have to fulfill the compact form, which is expressed as:

$$g(x) = \frac{\partial p(x)}{\partial x} = -H^T(x) R^{-1} [z - h(x)] = 0 \tag{2.45}$$

Taylor series expansion of *g(x)* around x_k will be:

$$g(x) = g(x_k) + G(x_k)(x - xk) + \ldots = 0 \tag{2.46}$$

therefore, the solution will be:

$$x_{k+1} = x_k - [G(x_k)]^{-1} g(x_k) \tag{2.47}$$

where, k and x_k are the iteration index and solution vector respectively.

$$G(x_k) = \frac{\partial g(x_k)}{\partial x} = H^T(x_k) R^{-1} H^T(x_k) \tag{2.48}$$

WLS method is a robust method that provides suitable filter response; however, this method cannot capture the time-history of data, and only considers one set of measurements.

2.2.2.3. Parks-McClellan Filter

Another efficient method of digital filter design is given by McClellan. In this method, a maximal ripple algorithm is formulated. It imposes a flashing error by the interpolation condition. Rather than reducing the worst case error, the maximum ripple algorithm solves a set of equations that had to satisfy the alternative solution, which is given in the following expression:

$$D(\omega_i) + (-1)^i \in = \sum_{k=0}^{M} a_k \cos(\omega_i k) \tag{2.49}$$

where, $|\in|$ and D is the Chebyshev error and desired filter response, respectively.

The factor $(-1)^i$ forces $|\in|$ to alternate on the range of frequencies (ω_i) (*i.e.*, *0* to π). a_k are the M number of coefficients that are estimated by finding the solution of a group of simultaneous linear equations. The error value can be measured by using expression given below [302];

$$E(\omega) = D(\omega) - \sum_{k=0}^{M} a_k \cos(\omega_k) \tag{2.50}$$

here, the order of filter must be odd and can be computed using Eqn. (2.51).

$$N = 2M + 1 \tag{2.51}$$

where, the filter length is N, which must be odd for this form to hold. In this method, the frequency adjustment is required, if the actual maximum error exceeds the desired maximum error. This can be done by iterating the error value until a suitable value is obtained [302].

2.2.3. IFIR Filters

A brief introduction of IFIR filter is given in Chapter 1. IFIR filter consists of two or more FIR filters connected in a cascade form. As a consequence of the interpolation process and characteristics of FIR filter, these type of filters are known as interpolated FIR filters. IFIR filters are categorized into two types: a) single stage IFIR filter, where only one up-sampling factor is used and b) multistage IFIR filter, which involves two or more up-sampling factors. In single stage IFIR filter, two FIR filters (model filter, which is up-sampled by L and interpolator filter) are connected in a cascade form as shown in Fig. 2.6 and defined by Eqn. (2.52). The order of these filters are very less as compared to those of FIR filter with the same design specifications [254].

$$H(z) = G(z^L) I(z) \tag{2.52}$$

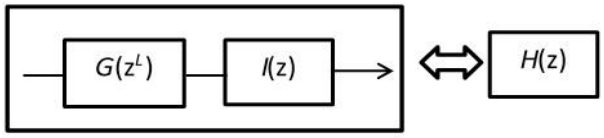

Fig. 2.6 IFIR structure [3].

where, $H(z)$ is desired FIR filter, $G(z)$ and $I(z)$ are the model and interpolator/image suppression filter in z-domain.

The design specifications of $G(z)$ and $I(z)$ are derived from the design specifications of the $H(z)$ [246].

$$G(z) = \sum_{n=0}^{N_m} g(n) z^{(-n)} \tag{2.53}$$

where, $g(n)$ and N_m are the impulse response and order of model filter, respectively. The design specifications of the model filter can be calculated using Eqns. (2.54), and (2.55) [3]:

(i) Stopband edge frequency $(\omega_{sm}) = L \times \omega_s$. (2.54)

(ii) Passband edge frequency $(\omega_{pm}) = L \times \omega_p$. (2.55)

In Eqns. (2.54) and (2.55), ω_s and ω_p are the stopband and passband edge frequencies of $H(z)$. $I(z)$ is defined as [6]:

$$I(z) = \sum_{o}^{N_i} i(n) z^{(-n)} \tag{2.56}$$

where, *i(n)* and N_i are the impulse response and order of the interpolator filter, respectively. The stopband and passband edge frequencies of this filter are computed as [240]:

(i) Stopband edge frequency $(\omega_{si}) = \frac{2\pi}{L} - \omega_s$ (2.57)

(ii) Passband edge frequency $(\omega_{pi}) = \omega_p$ (2.58)

and the up-sampling factor L is calculated using Eqn. (2.59). [241];

$$L_{\max} = \frac{2 \times \pi}{\omega_s + \omega_p + \sqrt{(\pi(\omega_s - \omega_p)}} \tag{2.59}$$

In case of a very narrow band filter design, the value of L becomes large and computational complexity reduction is also accomplished, because the order of model filter is very small. However, large ordered interpolator filter is required to remove $L-1$ unwanted images. In such a case, the computational complexity can be reduced further by using a multistage IFIR filter, in which two or more up-sampling factors are required [235]. The structure of two-

stage IFIR filter is illustrated in Fig. 2.7. Eqn. (2.60) represents the mathematical expression for this IFIR filter [236].

$$H(z) = G(z^{L}) I_1(z^{L_1}) I_2(z) \tag{2.60}$$

where, $I_1(z)$ is used as a model filter for $I(z)$ that is up-sampled by L_1 and $I_2(z)$ is an image suppression filter, and the value of L_1 is also calculated using Eqn. (2.59) by replacing ω_s by ω_{si}; where, ω_{si} is the stopband frequency of $I_1(z)$. The following steps are to be undertaken while designing the IFIR filter [2-7]:

Step 1: The design specifications of $H(z)$ is selected as; ω_s, ω_p stopband attenuation (A_s) and passband attenuation (A_p). Stopband ripple (δ_s) and passband ripple (δ_p) are calculated using Eqns. (2.61) and (2.62), respectively.

$$\delta_s = 10^{-0.05A_s} \tag{2.61}$$

$$\delta_p = 10^{-0.05A_p} - 1/10^{-0.05A_p} + 1 \tag{2.62}$$

Step 2: Up-sampling factor L is calculated using Eqn. (2.59).

Step 3: Next, ω_{sm}, ω_{pm}, ω_{si} and ω_{pi} are computed.

Step 4: In this step, N_m and N_i are calculated.

Step 5: Impulse responses of the model and interpolator filters are obtained.

Step 6: In this step, the model filter is up-sampled by L.

Step 7: Here, the up-sampled model filter is convolved with the interpolator filter.

The above steps are illustrated in Fig. 2.8. Fig. 2.8(a) shows the response of desired FIR filter $H(z)$, while Fig. 2.8(b) depicts the response of model filter. In this case, $L = 4$, As a result, three undesirable images are generated that cause distortion in the process of filtering as illustrated in Fig. 2.8(c). To remove these images, the image suppression filter is connected to up-sampled model filter. The Response of image suppression filter is displayed in Fig. 2.8(d) and in Fig. 2.8(e), the final response of IFIR filter is presented, which is identical to the desired original FIR filter (Fig. 2.8(a)). The main drawback of IFIR filters is that these types of filters are not designed to wideband filtering. Therefore, frequency-response masking (FRM) technique based filters are proposed for wideband filtering and low complexity.

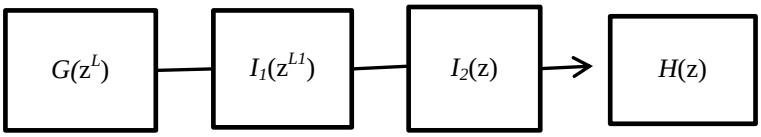

Fig. 2.7 Two stages IFIR structure [22].

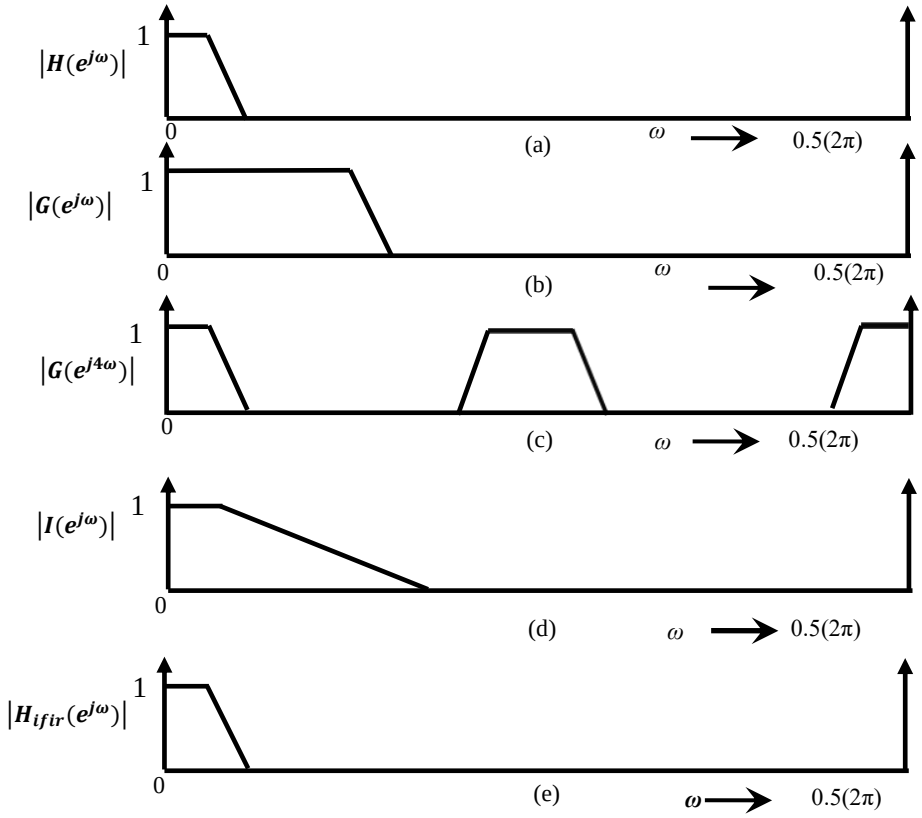

Fig. 2.8 Frequency response of (a) FIR filter, (b) Model filter, (c) Modal filter after Up-sampling, (d) Interpolator/Image suppression filter and (e) Final response of IFIR filter [228].

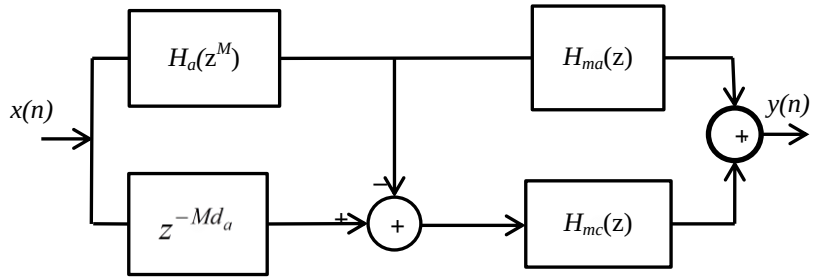

Fig. 2.9 An FRM filter structure [227].

The FRM technique yields a filter network, which includes more than a few sub-filters with very sparse coefficient values. It is an efficient technique for designing a linear phase filter with sharp transition width. Similar to IFIR filter, the realization of this filter is also efficient, and hence the number of multiplier and adders are very less than an FIR filter. In Fig. 2.9, realization structure of FRM filter is depicted and mathematically defined in Eqn. (2.63) [21].

$$H(z) = H_{Ma}(z)H_a(z^M) + H_{Mc}(z)[z^{-M(N_a-1)/2} - H_a(z^M)] \tag{2.63}$$

where, H_{Ma}, H_a , and H_a are FIR filters with very low valued filter order. The specifications of these filters are obtained using specifications of *H(z)* given in [22]

2.2.4. Adaptive Filters

Adaptive filtering is also utilized to remove the noise from a biomedical signal. In adaptive filtering, adaptive filters are used, which are the computational devices and use an iterative method to model the relationship between two signals in real-time. These filters perform filtering in two manners, *i.e.*, a) by the realization on an arithmetic processing device such as microprocessor /microcontroller using a set of programs, and b) by using very large scale integration (VLSI) or field-programmable gate array (FPGA) device by performing set of logic operations. To define an adaptive filter, the following point must be considered; a) properties of signals should be known, b) the structure of filter should be defined that can process an operation to obtain output signal from the input signal, c) the important parameters must be initialized, that change their values iteratively to alter the filter's input-output relationship and d) the adaptive algorithms are performed, that are used to define how the parameters are tuned from time to time. These filters have the ability to adjust filter response according to the signal. Fig. 2.10 shows the basic block diagram of the adaptive filter.

where, $e(n)$ and $d(n)$ are error and desired response of the filter, respectively.

Adaptive digital filters have applications in numerous areas, such as: bio-signal de-noising, system identification, sonar signal processing, channel equalization for communications, acoustic echo cancellation, clutter rejection in radars, and networking systems interference [158].

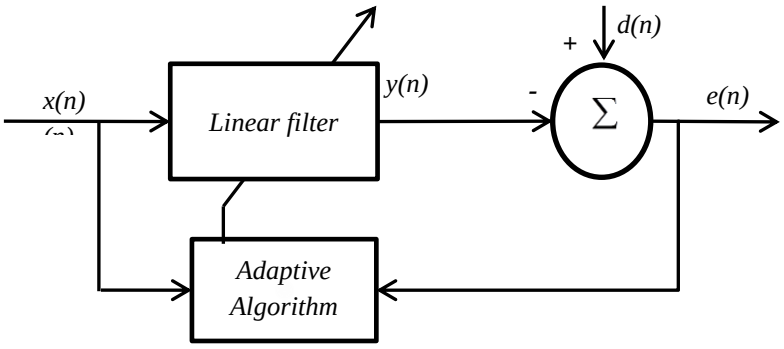

Fig. 2.10 Block diagram of an adaptive filter [158].

2.3. Multirate Signal Processing

On the basis of sampling frequency utilization, the signal processing is classified into two types a) single rate signal processing (SRSP) and b) multirate signal processing (MSP). In signal rate signal processing, the sampling rate is the same at all significant nodes of the system; and in MSP systems, more than one sampling rates are used. In some applications, to process a signal, MSP is preferred over single rate signal processing, because it has some advantages over SRSP, *viz*., higher bit rate, less memory requirement, and less computational cost. In MSP systems, the sampling rate is changed using two basic operations such as: a) down-sampling and b) up-sampling. Down-sampling is done using decimator and up-sampling is done by using up-sampler [1].

2.3.1. M-fold Decimator

The down-sampling process decreases the sampling rate by using decimator. In Fig. 2.11, *M*-fold decimator is depicted. Here, the sampling rate is decreased by *M* times, *M* is called as down-sampling factor. In Eqn. (2.64), a time domain expression of the down-sampling operation is depicted [24]:

$$y(n) = x(nm), \tag{2.64}$$

in z-domain,

$$y(n) = \frac{1}{M}\sum_{k=0}^{M-1} X(z^{1/M} W_M^k) \ , \tag{2.65}$$

and frequency domain

$$y(e^{j\omega}) = \frac{1}{M}\sum_{k=0}^{M-1} X(z^{j(\omega-2\pi k)/M}) \tag{2.66}$$

The frequency domain spectrum of the signal $x(n)$ and its decimated output are given in

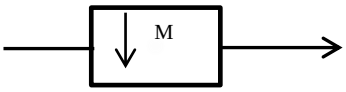

Fig. 2.11 M-fold decimator [23].

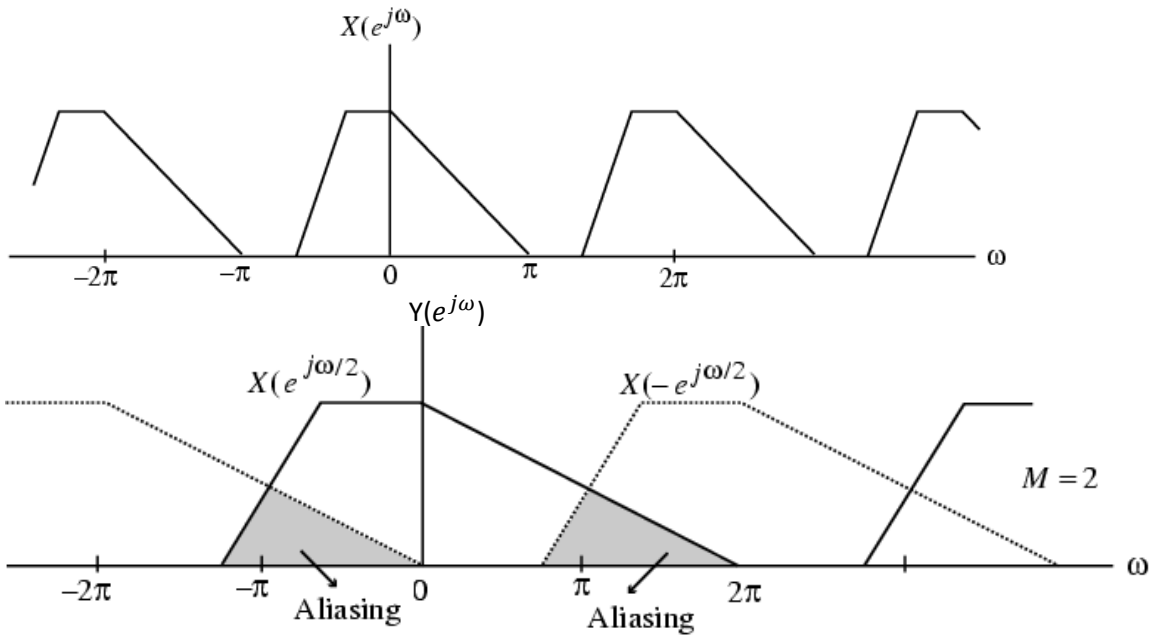

Fig. 2.12 Down-sampling in frequency domain [23].

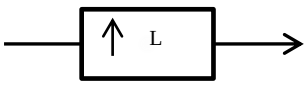

Fig. 2.13 L-fold expender [23].

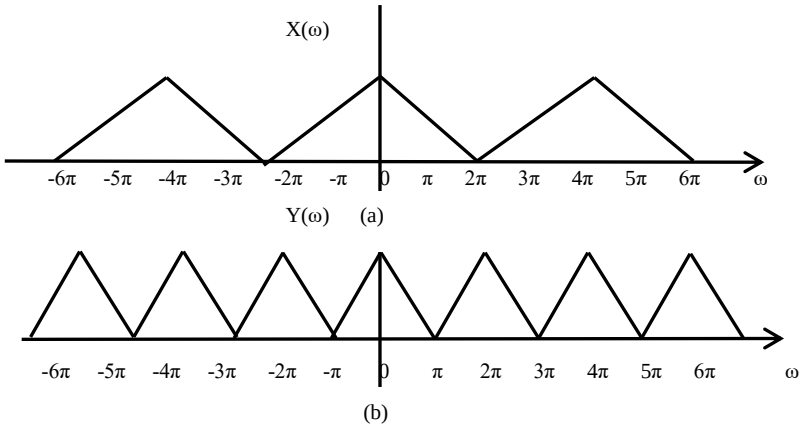

Fig. 2.14 (a) Input signal and (b) Up-sampled signal [24].

Fig. 2.12(a) and 2.12(b), respectively. In this operation, overlapping between two consecutive bands is generated, due to which the information can be lost. This effect is known as aliasing effect. In this diagram, *x(n)* is down-sampled by factor 2 (*i.e.*, $M = 2$). Here, the shaded area shows the overlapping between two bands. It can be removed by connecting a low pass filter known as anti-aliasing filter before the down-sampling [191].

2.3.2. *L*-fold Expender

L-fold expender is used for increasing the sampling rate *L* times. It is also known as interpolator, up-sampler and sampling rate expander. *L* is called the up-sampling factor. Fig 2.13 shows the block diagram the *L*-fold expender. The mathematical output of this block diagram are expressed in Eqns. (2.67), (2.68) and (2.69) in the time domain, z-domain and frequency domain, respectively [24].

$$y(n) = \begin{cases} x(n/L), & \text{if } n \text{ is a multiple of } L \\ 0, & \text{otherwise} \end{cases} \tag{2.67}$$

$$Y(z) = X(z^L) \tag{2.68}$$

$$Y(e^{j\omega}) = X(e^{jL\omega}) \tag{2.69}$$

While performing an interpolation process, $L-1$ unwanted images are generated in the frequency domain, which must be removed. To avoid these images, a low pass filter is connected after the up-sampling block. This filter is known as anti-imaging filter. The process of up-sampling is presented in Fig. 2.14 in the frequency domain. In this case, $L = 2;$ therefore, one image is generated due to the imaging effect which is presented in Fig. 3.14(b) [303].

2.3.3. Multirate Filter Bank

Subband coding (SBC) is the process of decomposition of the frequencies of a signal. Filter bank (FB) is one of the important tools of MSP used to perform SBC. In SBC, $x(n)$ is divided into different frequency signals. It consists of down-sampling, filtering, up-sampling, and summing process. In Fig 2.15, filter bank structure is depicted. A filter bank has two sections a) analysis section and b) synthesis section. Analysis section consists of down-sampling and filtering elements. This section divides the signal into the number of frequency bands to process each band separately, while the synthesis section consists of up-sampling and filtering elements for reconstruction of input signal [283].

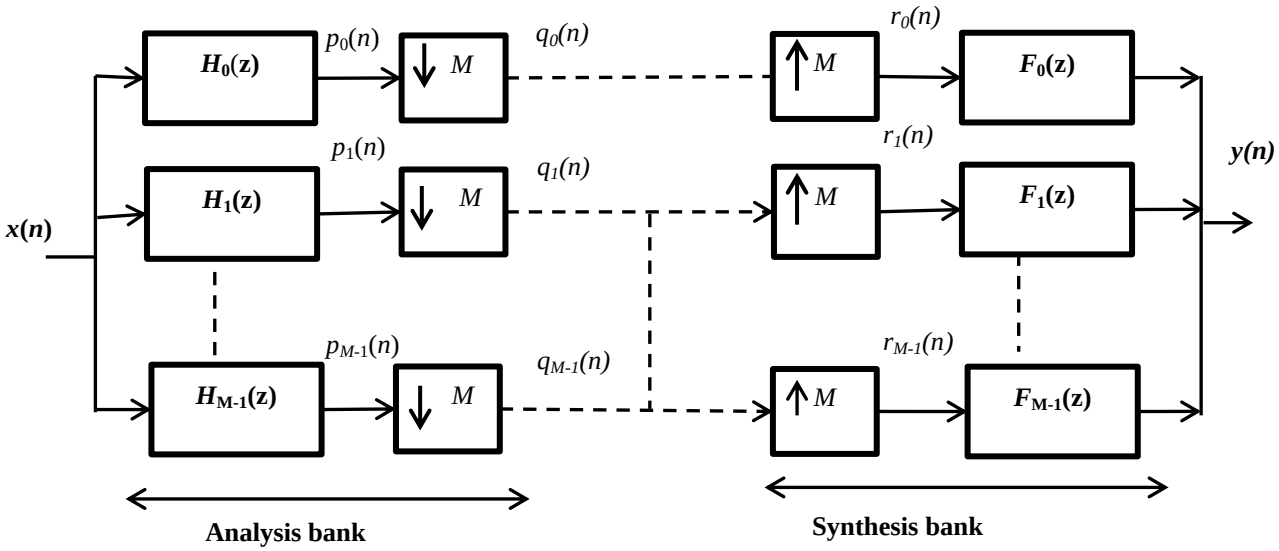

Fig. 2.15 M-channel filter bank [259].

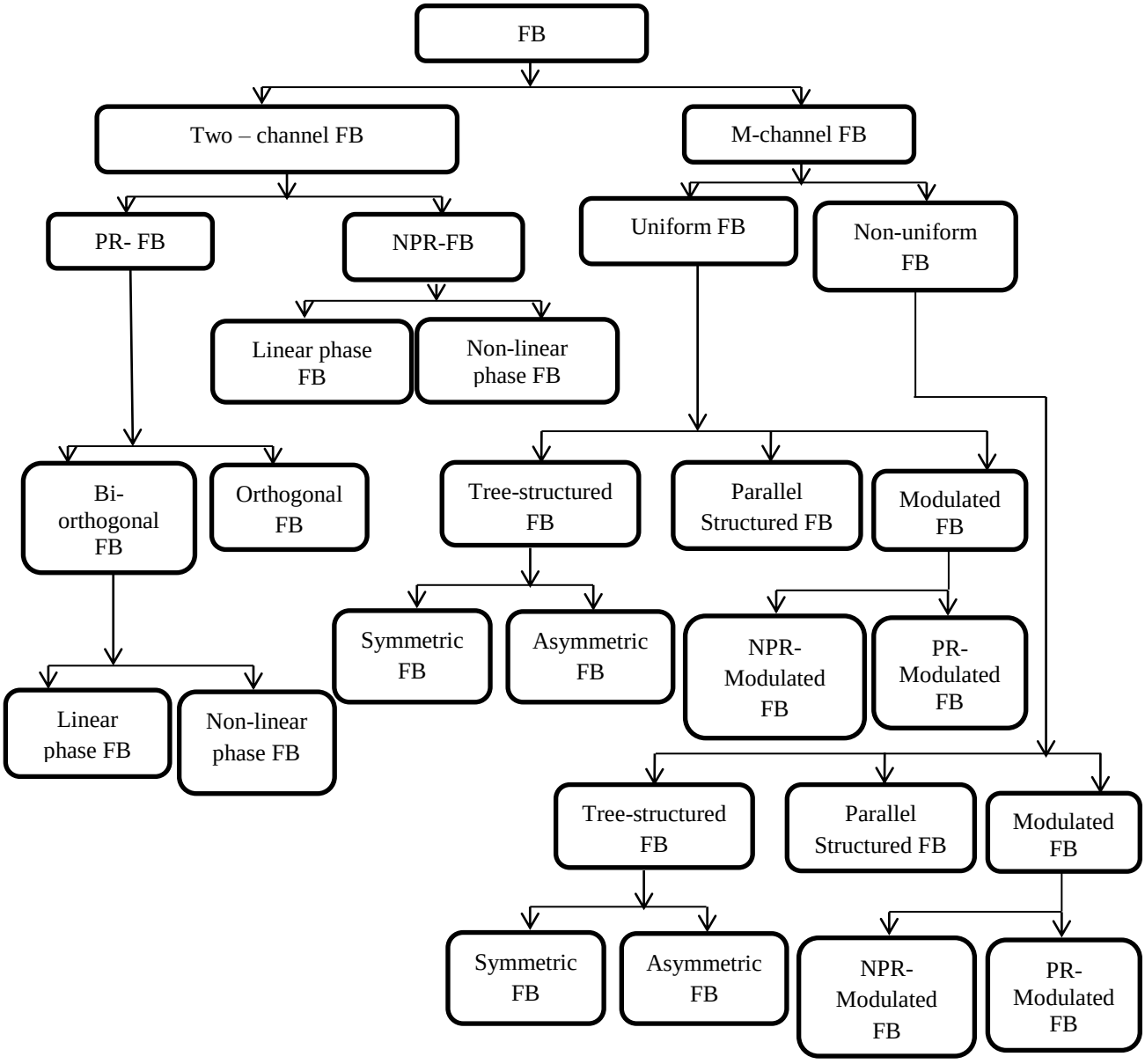

Fig. 2.16 Classification of the filter bank [285].

2.3.3.1. Types of Multirate Filter Bank

Filter banks (FBs) can be classified into different groups as depicted in Fig. 2.16. Here, it is shown that a filter bank is mainly classified into two categories a) two-channel filter bank and b) M-channel filter bank. In this section, the division of the FBs is described.

2.3.3.1.1. Two-channel Filter Bank

The two-channel filter bank is used to decompose the input signal into two equal frequency bands using low pass and high pass filters. In Fig. 2.17, the block schematic of two-channel filter bank is presented. Here, $x(n)$ is the input signal, which is divided into two signals: $v_0(n)$ & $v_1(n)$, and followed by down-sampling by factor 2. This portion is called as analysis bank. The signals obtained by down-sampling stage are $u_0(n)$ and $u_1(n)$. Then after, $u_0(n)$ and $u_1(n)$ are up-sampled by factor 2 and pass to low pass and high pass filter, and finally, obtained signals are recombined to reconstruct the signal. The frequency response of this bank is presented in Fig. 2.18. A two-channel filter bank, which provides reconstructed output exactly the replica of input signal, without applying any channel coding is known as perfect reconstruction (PR) two-channel FB. When exact replica of the input signal is not obtained, then this type of FB is known as nearly perfect reconstruction (NPR) two-channel FB. PR two-channel FBs are further divided into two categories PR orthogonal and PR bi-orthogonal FB. In PR orthogonal FBs, regularities of the analysis and synthesis part are equal, while in case of bi-orthogonal FBs, regularities of the analysis part depend on lowpass analysis filter and the regularities of synthesis part depend on the lowpass synthesis filter. Another class of FBs is linear and non-linear phase FBs, when a FB is designed by using filters that have linear phase property then it is called linear phase FB, whereas when non-linear phase filters are used to design a FB, it is known as non-linear phase FB [294].

2.3.3.1.2. *M*-channel Filter Bank

In a FB, if the input signal is decomposed into more than 2 frequency bands then it is known as *M*-channel or multichannel filter bank. Here, *M* represents the number of signal divisions. The value of *M* is always greater than 2. In this type of FB, *M*-number of analysis and synthesis filters (lowpass, highpass, and bandpass) are used.

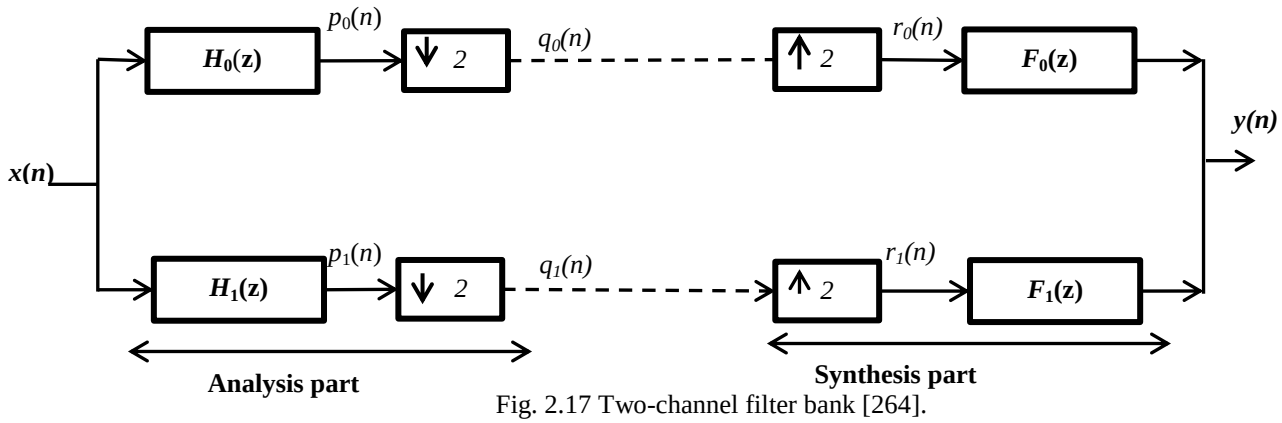

Fig. 2.17 Two-channel filter bank [264].

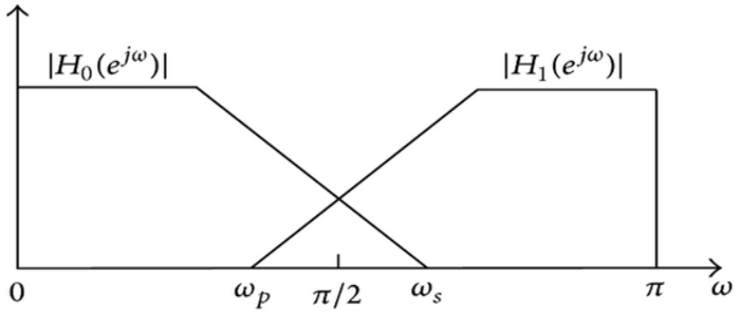

Fig. 2.18 Two-Channel filter bank response [265].

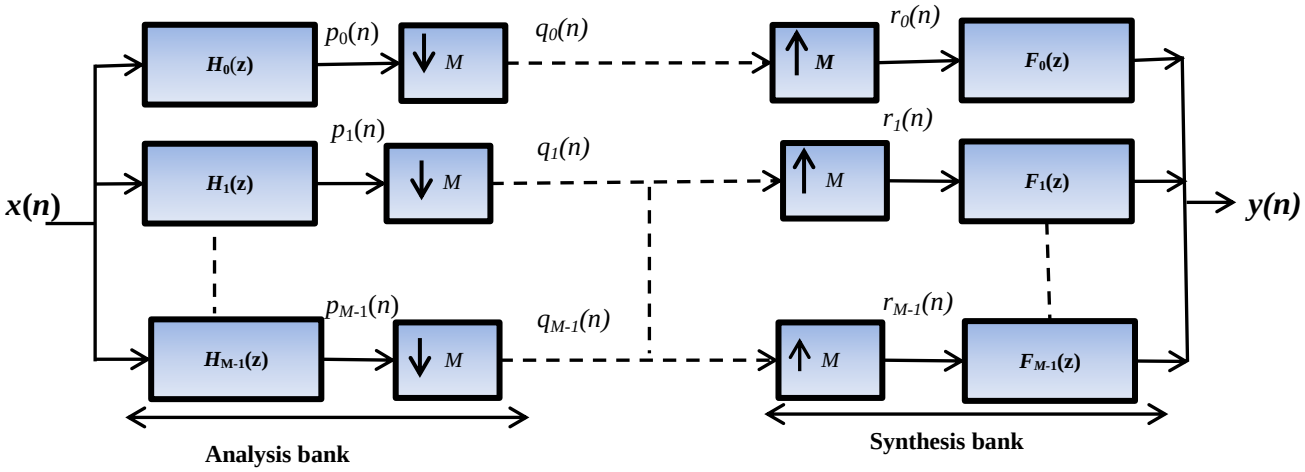

Fig. 2.19 Block diagram of M-channel FB [254].

2.3.3.1.2.1. Uniform *M*-channel Filter Bank

Uniform *M*-channel filter bank (UMFB) is used to divide a signal into *M* number of uniformly distributed frequency bands. In Fig. 2.19, the parallel structure of UMFB is depicted. Here, $x(n)$ and $y(n)$ are input and output signal, respectively. $p_0(n),...,p_{M-1}(n)$, $q_0(n),...,q_{M-1}(n)$ and $r_0(n),...,r_{M-1}(n)$ are the signals achieved by intermediate operations such as; filtering, down-sampling and up-sampling process [30]. When there is no processing unit applied after down-sampling, the $y(n)$ must be same as $x(n)$ with delay.

The output of FB can be obtained by performing the stepwise analysis. The first step is: input signal is applied to filters, therefore the resultant signals are after filtering [281]:

$$P_k(z) = X(z)H_k(z) \tag{2.70}$$

These signals are then down-sampled by *M*, at this stage the obtained outputs $q_k(n)$ are:

$$Q_k(z) = \frac{1}{M}\sum_{l=0}^{M-1} H_k(z^{\frac{1}{M}}W^l)X(z^{\frac{1}{M}}W^l) \tag{2.71}$$

When there is no channel coding /processing unit, as shown in Fig. 2.19, $q_k(n)$ are pass to up-sample by the up-sampling factor *M*. The obtaining signals at this node are ($r_k(n)$):

$$R_k(z) = \frac{1}{M}\sum_{l=0}^{M-1} H_k(zW^l)X(zW^l) \tag{2.72}$$

The final output can be obtained by summing the previous stage output signals ($r_k(n)$):

$$Y(z) = \frac{1}{M}\sum_{l=0}^{M-1} X(zW^l)\sum_{k=0}^{M-1} H_k(zW^l)F_k(z) \tag{2.73}$$

$$Y(z) = \frac{1}{M}\sum_{l=0}^{M-1} A_l(z)X(zW^l) \tag{2.74}$$

$$Y(z) = \frac{1}{M}\sum_{l=0}^{M-1} A_l(z)X(zW^l), \quad 0 \le l \le M-1 \tag{2.75}$$

here, $X(zW^l)$ is the aliasing term and $A_l(z)$ is gain for aliasing term [279]. For cancelation of aliasing effect, $A_l(z)$ should be = 0.

2.3.3.1.2.2. Non-uniform M-channel Filter Bank

The non-uniform M-channel filter banks (NUMFBs) are more suitable filter banks in some applications due to better portioning of bands. Similar to UMFBs, these filter banks are also classified into three groups, a) parallel structured filter bank, b) tree structured bank and c) modulated filter bank. In Figs. 2.20 and 2.21, tree-structured NUFB and parallel-structured NUFB are presented, respectively. A parallel structured non-uniform filter bank can be designed using non-linear optimization with significant number of factors, and a tree-structured FB is designed by connecting two and more two-channel QMF banks [296].

2.3.3.1.3. Cosine Modulated Filter Bank

In a modulated FB, a specific modulation technique is used to design the FB. Among all modulation techniques, the cosine modulation technique (CMT) is the most popular and widely used technique. Cosine modulation filter banks (CMFBs) are designed using CMT. In this type of filter banks, CMT is used to design the analysis and synthesis filter bank. The expressions of deriving analysis and synthesis filters are given in Eqns. (2.76) and (2.77), respectively. The procedure includes steps; a) prototype filter design, b) optimization is applied on prototype filter and c) analysis and synthesis filter banks design. This types of FBs are superior to other types of FBs in terms of computational complexity and easy optimization [291].

$$h_i(z) = 2h(n)\cos\left(\frac{\pi}{M}\left(k+\frac{1}{2}\right)\left(n-\frac{M}{2}\right)+(-1)^k\frac{\pi}{2}\right) \tag{2.76}$$

$$f_i(z) = 2h(n)\cos\left(\frac{\pi}{M}\left(k+\frac{1}{2}\right)\left(n-\frac{M}{2}\right)-(-1)^k\frac{\pi}{2}\right) \tag{2.77}$$

2.3.3.2. Wavelet Transform

The wavelet transform (WT) has emerged as an important mathematical tool in the area of non-stationary signal analysis, because it examines the signal structures at different scales. The fundamental principle of WT is: it divides a signal into different functions by using the property of translation and dilation of mother wavelet ($\varphi(t)$), which acts as a prototype function, and can be defined as [63,69]:

$$\varphi_{ab}(t) = |a|^{-1/2}\,\varphi\left(\frac{t-b}{a}\right) \qquad a,b \in R \tag{2.78}$$

where, a and b are the dilation and translation function, respectively. When the parameters a and b are restricted to discrete values such as: $a = 2^{m/2}$, $b = n2^{-m}$, then, a new family of discrete wavelets is formulated, which is expressed as [125]:

$$\varphi_{mn}(t) = 2^{m/2}\varphi(2^{mt-n}), \tag{2.79}$$

In this expression, φ must satisfy the condition given below:

$$\int R^{\varphi(t)dt=0} \tag{2.80}$$

WT is classified into two types: continuous wavelet transform (CWT) and discrete wavelet transform (DWT). CWT can be expressed as [19]:

$$W_f(b,a) = |a|^{-1/2} \int_{-\infty}^{\infty} f(t)\varphi^*\left(\frac{t-b}{a}\right)dt \tag{2.81}$$

In the above expression, the symbol '*' represents a complex conjugate and multiplication of $|a|^{1/2}$, and it is used for stabilizing the transformed signal with the same energy at every scale. Adaptive nature and multiresolution property of WT makes analysis easy and effective. In case of CWT, the values of a and b are continuous over the real number (R), which increases the computational complexity. Therefore, DWT is used as a more efficient transform to analyze a signal. DWT is represented by Eqn. (2.82) [78].

$$Wx(m,n) = \int_{-\infty}^{\infty} x(t)\varphi_{m,n}(t)dt = Wx(m,n) = a_0^{-m/2}\int_{-\infty}^{\infty} x(t)\varphi(a_0^{-m}t - nb_0)dt \tag{2.82}$$

This expression is achieved by choosing the values: $a = a_0^m$ and $b = nb_0a_0^m$ for different values of m and n, (*i.e.*, $m{=}n = \pm 0, \pm 1, ..., \pm\infty$). For both types of wavelet transforms, condition given in Eqn. (2.83) should be satisfied [20] :

$$\int \varphi(t)dt \tag{2.83}$$

When, $a_0 = 2$ and $b_0 = 1$, a new discrete wavelet can be constructed, which is given in Eqn. (2.84). This wavelet consists of an orthogonal basis for $L^2(R)$.

$$\varphi_{m,n}(t) = 2^{-m/2}\varphi(2^{-m}t - n) \tag{2.84}$$

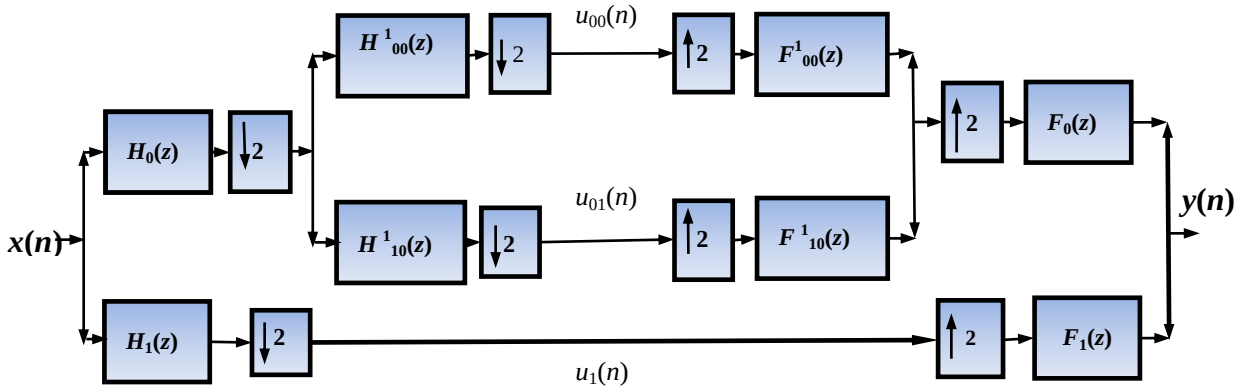

Fig. 2.20 Tree Structured NUFB [285].

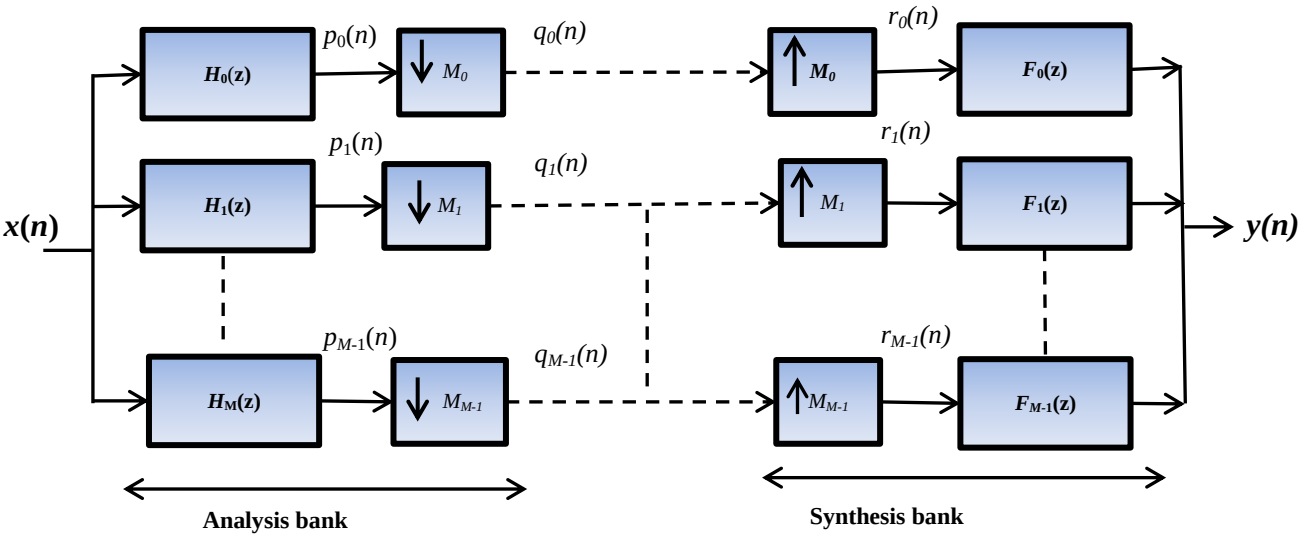

Fig. 2.21 Parallel structured NUFB [285].

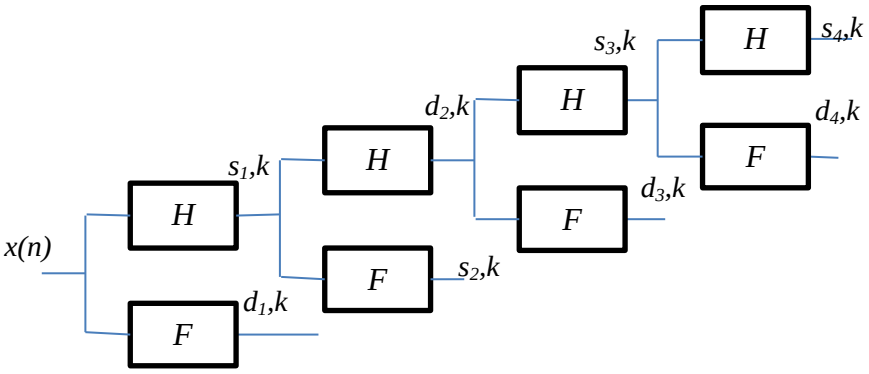

Fig. 2.22 Wavelet decomposition for a signal [6].

In DWT, the input signal is decomposed on different scales by the following expression [81]:

$$x(t)=\sum_{j=1}^{K}\sum_{k=-\infty}^{\infty}d_j(k)\varphi_{j,k}(t)+\sum_{-\infty}^{\infty}a_k(k)\psi_{K,k}(t) \tag{2.85}$$

where, $d_j(k)$, $\varphi_{j,k}(t)$ and $\psi_{K,k}(t)$ are detailed signals, discrete analysis wavelets, and discrete scaling functions, respectively. Wavelet decomposition tree is depicted in Fig. 2.21, and the implementation of DW FB can be done using Eqns. (2.86) and (2.87) [81] .

$$h(n)=\frac{1}{2}\langle\psi(t),\psi(2t-n)\rangle \tag{2.86}$$

$$g(n)=\frac{1}{\sqrt{2}}\langle\varphi(t),\psi(2t-n)\rangle=(-1)^n h(1-n) \tag{2.87}$$

The value of function $d_j(k)$ at level j can be estimated by using the mathematical function, *i.e.*, convolution function with the signal $f(n)$ at $j-1$ [82].

2.3.3.3. Maximal Overlap Discrete Wavelet Transform

Maximal overlap discrete wavelet transform (MODWT) is a variant of DWT. It also performs linear filtering. The function of MODWT is similar to DWT as it produces a set of the time-dependent wavelet, scaling coefficients. Similar to conventional WT, MODWT also appropriates to process a non-stationary signal. The MODWT is a highly redundant, non-orthogonal transform and also keeps down-sampled values at each level of the decomposition. It is superior to DWT, because it has the capability to enable a ready comparison between the series and its decomposition. MODWT decompose an infinite sequence into j_0 numbers of levels, which involves j_0 numbers of pair of low pass and high pass filters. It can be done using the expression (2.88) and (2.89) [20].

$$\overline{W}_{j,t}=\sum_{l=0}^{L_j-1}\overline{h}_{j,l}X_{t-l} \tag{2.88}$$

where, $\overline{W}_{j,t}$ are the wavelet coefficients, $\overline{h}_{j,l}$ is high pass filter X_t is an infinite sequence, $t=...,-1,0,1,...$ and j indicates the level of decomposition.

$$\overline{V}_{j,t}=\sum_{l=0}^{L_j-1}\overline{f}_{j,l}X_{t-l} \tag{2.89}$$

In this equation, $\overline{V}_{j,t}$ calculates the scaling coefficients and $\overline{f}_{j,l}$ is the low pass filter [20].

In this work, two factors are taken to measure the performance of noise reduction methodology.

a) Signal-to-noise ratio (SNR)

$$SNR = \frac{\sum_{t=0}^{L-1} y^2(t)}{\sum_{t=0}^{L-1} n^2(t)} \tag{2.90}$$

where, *y(n)* is the obtained signal after the noise elimination signal [11].

b) Correlation coefficient (γ_{xy})

$$\gamma_{xy} = \frac{\sum_{n=1}^{N}(x(n)-\bar{x}(n))(y(n)-\bar{y}(n))}{\sqrt{\sum_{n=1}^{N}(x(n)-\bar{x}(n))^2(y(n)-\bar{y}(n))^2}} \tag{2.91}$$

where, $\bar{x}(n)$ and $\bar{y}(n)$ are the mean values of input signal [1].

Correlation coefficient represents the average cross-correlation, which is a measure of how much received signal resembles the target signal at the location.

2.4. Summary

In this chapter, different types of noise elimination techniques are reviewed which includes the basic need of filtering and objectives of signal processing. First, the overview of IIR and FIR filter is done in brief. Then, methods of filter designing such as: windowing, Parks-McClennan, WLS methods are discussed. Adaptive filtering is also described in this chapter. After this, the introduction of MSP including decimation and interpolation are given. These techniques are linear time-varying operations. Then after, FB and types of FB are described, which is a powerful tool of MSP and provides very efficient results in some applications, such as ECG signal processing data compression, image compression, optical communication speech signal processing, *etc*. This chapter also includes the background of WT, which is also a very important part of signal processing especially to remove the noise from a non-stationary signal. In the last, MODWT, the variant of DWT is discussed.

CHAPTER 3

NOISE REDUCTION OF ECG SIGNAL

3.1. Overview

The ECG signal is one of the essential biological signals that represent the electrical activity of cardiovascular system. Most of the physicians and cardiologists need good quality ECG data for interpretation and identification of cardiac disease. However, it is almost impossible to extract physiological parameter without noise. As discussed in previous chapter that there are several methods that are used to eliminate the noise present in the signal. This noise can be either cardiac or extra-cardiac. For example, reduction /disappearance of the interval of isoelectric, extended repolarization and atrial flutter are accountable for the cardiac noise. The examples of extra-cardiac noise include changes of electrode-position, breathing, muscle contraction, and power line interference [147]. The elimination of these noises is mandatory, because the existing noises may lead to wrong interpretation of the signal. For example, present of muscle contraction noise can interrupt the R-peak location and amplitude, which is a very important feature used as the fiducial parameter of a signal [153].

In this chapter, noise elimination using the computationally efficient filter (IFIR and FRM filter), MOSDWT, and ripple free IFIR filter is presented. Results have been tested using the MIT-BIH arrhythmia database and MIT-BIH noise stress test database. For performance evaluation, signal to noise ratio (SNR) and correlation coefficient (CC) has been used.

3.2. Noise Reduction using IFIR Filter

In this thesis, noise is eliminated before the compression, because original data and decompressed data is compared by extracted features. Sometimes due to noise, signal reconstruction is also affected, and in several data-compression methods, during the process of compression and decompression, noise is generated due to several factors [151].

As discussed in the previous chapters, several types of noise can contaminate in an ECG signal, such as baseline wander, high-frequency noise, power line interference, *etc*. in this chapter, baseline wander, high frequency noise and power line wander are eliminated. For elimination of noises, computationally efficient filters are designed using IFIR and FRM techniques. MOSWT is also used to remove the high frequency noise.

3.2.1. Baseline Wander Noise Reduction

Baseline wander is a low-frequency (0-0.8Hz) noise. Presence of this noise can show wrong amplitudes of different features of the ECG signal. An ECG signal can have baseline wander of different morphologies, *viz*., linear, sinusoidal, linear with sinusoidal, *etc.* In this work, linear and sinusoidal baseline wander is removed by using the FRM based FIR filters. First, lowpass FRM filter structure is designed using steps given in Chapter 2. All sub-filters of this structure are designed using WLS method. It is observed that, in comparison to FIR filter, this filter is computationally very efficient for the same design specification. And then the highpass filter is derived using lowpass FRM filter, which can block the frequencies below 0.7Hz. After this, the convolution of ECG signal with designed highpass filter is performed. For evaluation of the performance of this method, MIT-BIH data is taken. In this work, first the noise is generated, and then contaminated with the original ECG signal using Eqn. (3.1) [156].

$$s(t) = ECG + n(t) \tag{3.1}$$

where, $n(t)$ is the noisy signal, that can be real or synthetic.

To investigate the performance of noise reduction method, the following points are considered: a) two sets of tests are performed over synthetic noise, where both quantitative and qualitative investigations are given and b) examining the real noise cases. The quantitative evaluation is assessed by the signal-to-noise ratio (SNR) and correlation coefficients, the mathematical expressions used for this purpose are given in Chapter 2.

FRM based filters exhibit high computational efficiency. In this type of filter, very low order filters are combined (Fig. 2.9) to make linear filter with very sharp transition width. Therefore, the multiplier and adders are reduced which reduces the designing cost [227]. For example: at ω_p =0.55π ω_s =.58 π A_s =100; M=6; In this case filter orders are 41, 161, 161 the total, filter multiplier used in this case = 41+161+161= 363, and in case of FIR filter the filter order will be 484, therefore using FRM filter design technique, 123 multipliers and adders can be reduce.

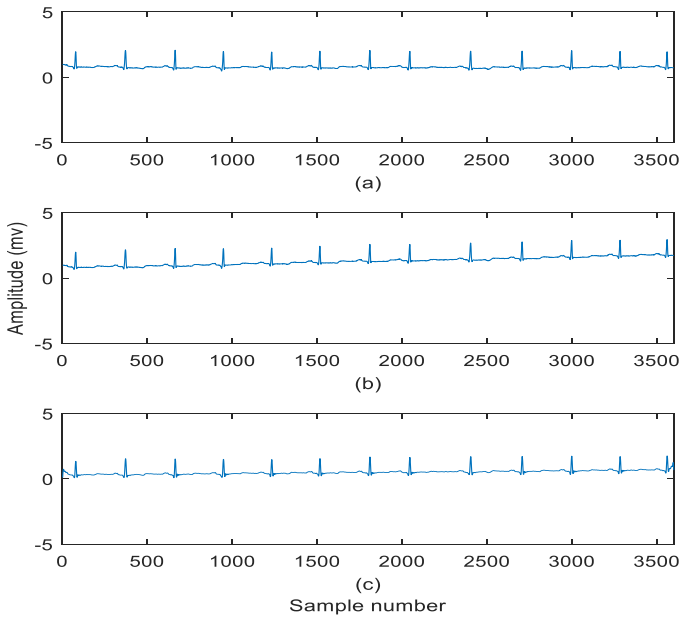

Fig. 3.1 (a) Noise-free original ECG (record MIT-BIH 100) signal, (b) Baseline wander is introduced in the original signal (linearly incremented), (c) Baseline wander is removed completely.

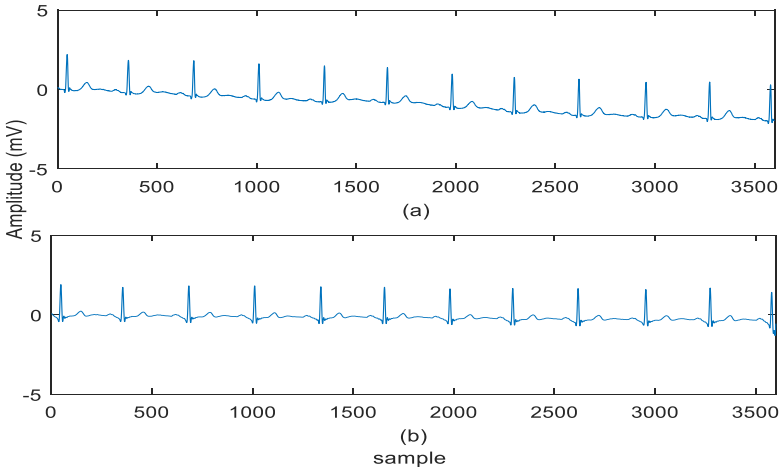

Fig. 3.2 (a) Baseline wander is introduced in the original signal (linearly decremented) and (b) Baseline wander is removed.

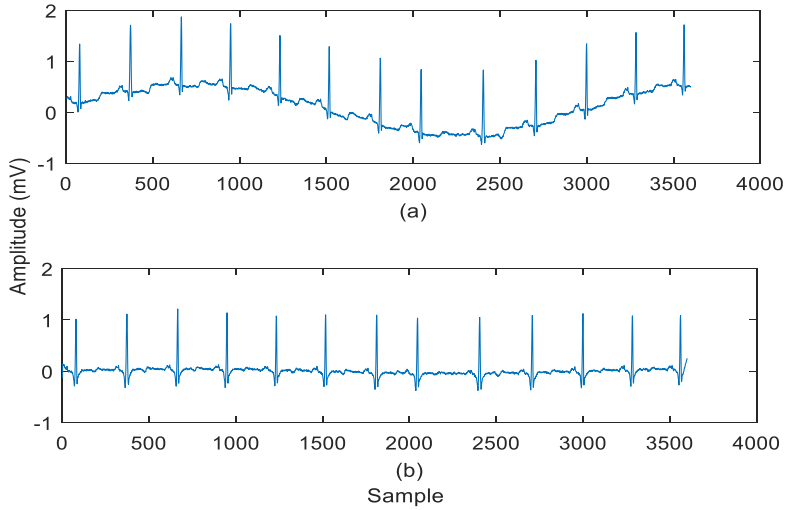

Fig. 3.3 (a) Baseline wander is introduced in the original signal (sine wave 0.57 Hz) and (b) Baseline wander is removed.

Table 3.1 Measured values of correlation coefficient (original and signal after noise elimination).

Sl. no	Dataset	Noise	Correlation coefficient
1.	MIT-BIH record no. 100	Baseline wander(linear decreasing)	0.8727
		Baseline wander(linear increasing)	0.8707
		Baseline wander (sine)	0.7315
		High-frequency noise	0.9855
		Multiple frequency noise	0.9617
2.	MIT-BIH record no. 101	Baseline wander(linear decreasing)	0.9188
		Baseline wander(linear increasing)	0.8593
		Baseline wander(sine)	0.8734
		High-frequency noise	0.9667
		Multiple frequency noise	0.9741
3	MIT-BIH record no. 102	Baseline wander(linear decreasing)	0.9217
		Baseline wander(linear increasing)	0.9624
		Baseline wander(sine)	0.8271
		High-frequency noise	0.9993
		Multiple frequency noise	0.9993
4	MIT-BIH record no. 103	Baseline wander(linear decreasing)	0.9419
		Baseline wander(linear increasing)	0.9435
		Baseline wander(sine)	0.9435
		High-frequency noise	0.9807
		Multiple frequency noise	0.9863
5	MIT-BIH record no. 105	Baseline wander(linear decreasing)	0.9224
		Baseline wander(linear increasing)	0.9458
		Baseline wander(sine)	0.8658
		High-frequency noise	0.9970
		Multiple frequency noise	0.9980
6	MIT-BIH record no. 106	Baseline wander(linear decreasing)	0.9172
		Baseline wander(linear increasing)	0.9205
		Baseline wander (sine)	0.8387
		High-frequency noise	0.9814
		Multiple frequency noise	0.9862

Table 3.2 Computational complexity cost reduction measurement for different design specification.

ω_s	ω_p	A_s	N	L	N_m	N_i	***CRC%***	**(ω_d)**
0.189 0π	0.0353π	100	84	2	42	17	29.76	0.0769
0.179 0π	0.1530π	100	494	3	165	38	58.90	0.0130
0.0890 π	0.0530π	100	357	4	89	36	64.98	0.0180
0.0395 π	0.0053π	100	375	5	75	36	70.40	0.0171
0.0355 π	0.0113π	100	531	6	88	45	74.95	0.0121
0.0355 π	0.0213π	100	904	7	129	56	79.53	0.0071
0.0255 π	0.0113π	100	904	8	113	60	80.86	0.0071
0.0395 π	0.0323π	100	1784	9	198	85	84.13	0.0036
0.059 π	0.0570π	100	6421	10	642	153	87.61	0.0010
0.0389 π	0.0353π	100	3567	11	324	119	87.58	0.0018
0.039 π	0.0370π	100	6421	13	494	494	**89.73**	**0.0010**
0.0155π	0.0113π	100	3058	14	218	111	**89.24**	**0.0021**

Here, three types of baseline wander are added to the original ECG signal, such as a) linear incremented random signal, b) linear decremented random signal and d) low-frequency sinusoidal signal.

The graphical representation of the minimization of these noises is given in Figs. 3.1, 3.2 and 3.3. Here, the sinusoidal noise (0.57Hz), linear signal of having $s_1(n)=n/p+0.06n$ are added, and linear signal having $s_2(n)=n/p-0.06n$ are added. In Fig. 3.1(a), original MIT-BIH record no 100 is depicted. In Figs. 3.1(b), 3.2(a) and 3.3(a), baseline wander with noise with signal $s_1(n)$, noise with signal $s_1(n)$ and sinusoidal noise are presented, respectively. In Figs. 3.1(c), 3.2(b) and 3.3(b) signals after denoising using FRM based filter are presented. After elimination of noise, the correlation measurement between the original signal and signal obtained after denoising is done using Eqn. (2.90) given in Chapter 2. In Table. 3.1, the measured values of CC are presented. Tabular and graphical results show that the baseline wander noise is minimized significantly.

3.2.1. High-Frequency Noise Reduction

In this section, high-frequency noise is removed from the ECG signal using IFIR filter. First of all, IFIR filter is designed using Park-McClellan method, which is described in Chapter 2. The performance of IFIR filter is done using the parameter given below:

A. Computational complexity reduction ($\%CRC$) [15]:

$$\%CRC = \frac{Multi_{FIR} - Multi_{IFIR}}{Multi_{FIR}} \times 100 \tag{3.2}$$

where, $Multi_{FIR}$ and $Multi_{IFIR}$ are the multiplier of FIR and IFIR filter.

This parameters show how much complexity is reduced. In Fig. 3.4, the structure of 5 tap direct form FIR filter is given, here it is seen that 5 multipliers, 4 adders 4 delay elements are needed for realization [40]. A multiplier usually has the highest implementation or computational cost, and thus it is desired to reduce the number of multipliers in different systems, if possible. Branches with directions and nodes are also very important to realize a filter. The number of multipliers, adders and delay are directly dependent to the filter order, usually; the number of the multiplier is equal to the number of filter tap: and hence, equal to filter order. The number of adders and delay elements are less than 1. In case of IFIR filter, two or more filters are connected in cascade form. The order of model filter is L times lesser than an order of FIR filter and order of interpolator filter is very less, since it can be designed by a large transition width (filter order is inversely dependent on

transition width). Therefore, the number of multipliers, adders, and delay elements required to implement an IFIR filter are very less than those required in classical FIR filter. For example: $\omega_s = 0.0001\pi$ and $\omega_p = 0.200\pi$ therefore, $N_{FIR} = 64$, $N_M = 32$ and $N_i = 16$, hence, the number of multipliers for FIR filter = *64*, adders = *63*, delay elements = *63* and in the case of IFIR number of multipliers = *32+16 = 48*, adders = 31+15 = 46, delay elements = *46*, hence power dissipation in the case of an IFIR filter is better than an FIR filter.

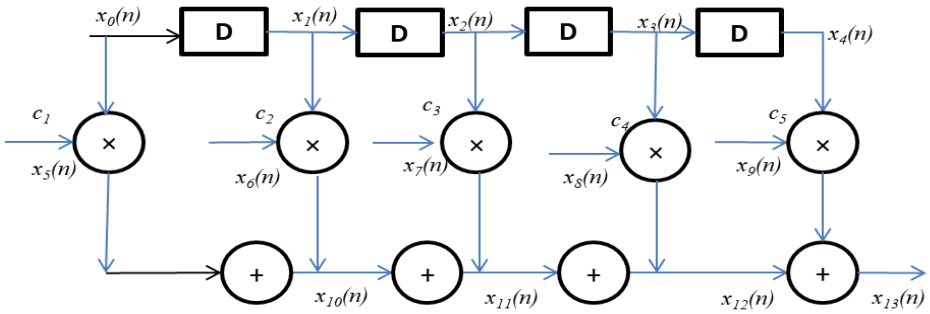

Fig. 3.4 FIR filter structure of 5 tap.

B. Transition width (*TW*) [148]:

$$TW = \frac{1}{2}\left(\omega_s - \omega_p\right) \tag{3.3}$$

The high-frequency noise is removed from the ECG waveform using IFIR filter. An ECG signal is contained wave components of different frequencies. ECG signal has useful diagnostic information within frequency 1 to 100 Hz [170]. However, it is contaminated EMG signal (50-150Hz), other high frequency noise of the range (100 to 400 Hz) in case of telemedicine and telecommunication system other high frequencies are also presented which can current the signal (2,500 to 3,000 Hz) [172, 176, 179]. For this purpose, the high-frequency signal (450 to 1050 Hz) is added in the MIT-BIH database as depicted in Fig. 3.5(b).

The noisy signal is generated by using the expression given below:

$$n(t) = n_1(t) + n_2(t) + n_3(t)... \tag{3.4}$$

In this Eqn, $n_i(t)$ are sine function having different amplitude and different frequencies and *i= 1, 2, 3, 5… n.*

For this purpose, the high-frequency signal (450 to 1050 Hz) is added in the MIT-BIH database as depicted in Fig. 3.5(b). Since, an ECG signal has all significant frequencies within 100Hz, therefore for removing high-frequency noise, a low-pass filter is used which can reject frequency above 100Hz. Here also, the WLS technique is used to design

the sub-filters of IFIR structure given in Chapter 2. Then after, IFIR filter is used to discard the high-frequency components by applying it on the noisy ECG signal. The resulted data, *i.e.*, a noise-free signal is presented in Fig. 3.5(c). In this work, multi-amplitude and multi-frequency signals are also removed which is shown in Fig. 3.6(a). In this figure, MIT-BIH record no. 106 is depicted. This signal is contaminated with noise, which is generated by adding multiple signals having different amplitudes and frequency as depicted in Fig. 3.6(b). This noise is eliminated in Fig. 3.6(c). Other signals are also used to remove the noise; the quantitative results of this work are depicted in Tables. 3.1 and 3.3.

The values of cross correlation and SNR are calculated for the signal before and after the filtration. Table 3.1 shows that the original signal (*ECG*) without addition of noise and the signal after removing noise (generated and contaminated is the signal) are having average value of correlation 0 = 0.9, that shows the IFIR filter can be used to remove Baseline wander, High-frequency noise and Multiple frequency noise. Here, IFIR filter is used to obtain linear filtering, which is important in real time applications. However, the linear filtering methods are not efficient in terms of computational cast, therefore IFIR filter is used. The performance of IFIR filter is obtained in terms of computational complexity reduction cost, which is evaluated by Eqn. (3.2). This table demonstrates that, for the same design specifications, complexity can be reduced by 89.24% without affecting other parameters.

Table 3.3 Computed values of SNR and CC using IFIR filter.

Sl no.	Dataset	Noise	SNR (in dB)	CC
1	MIT-BIH dataset record no. 118e00	Baseline wander record (bwm	75.21	0.8816
		muscle (EMG) artifact (mam)	91.39	0.9771
		electrode motion artifact (emm)	63.5085	0.8461
2	MIT-BIH dataset record no. 118e06	Baseline wander record (bwm)	75.2140	0.8816
		muscle (EMG) artifact (mam)	91.3977	0.9771
		electrode motion artifact (emm)	-30.8505	0.8480
3	MIT-BIH dataset record no. 118e12	Baseline wander record (bwm)	75.21	0.8816
		muscle (EMG) artifact (mam)	91.3977	0.9771
		electrode motion artifact (emm)	63.5085	0.8461
4	MIT-BIH dataset record no. 119e00	Baseline wander record (bwm)	71.7635	0.7848
		muscle (EMG) artifact (mam)	90.8208	0.9888
		electrode motion artifact (emm)	-31.8556	0.9124
5	MIT-BIH dataset record no. 119e06	Baseline wander record (bwm)	71.7635	0.7848
		muscle (EMG) artifact (mam)	90.8208	0.9888
		electrode motion artifact (emm)	62.9316	0.9107
6	MIT-BIH dataset record no. 119e12	Baseline wander record (bwm)	71.7635	0.7848
		muscle (EMG) artifact (mam)	90.8208	0.9888
		electrode motion artifact (emm)	62.9316	0.9107

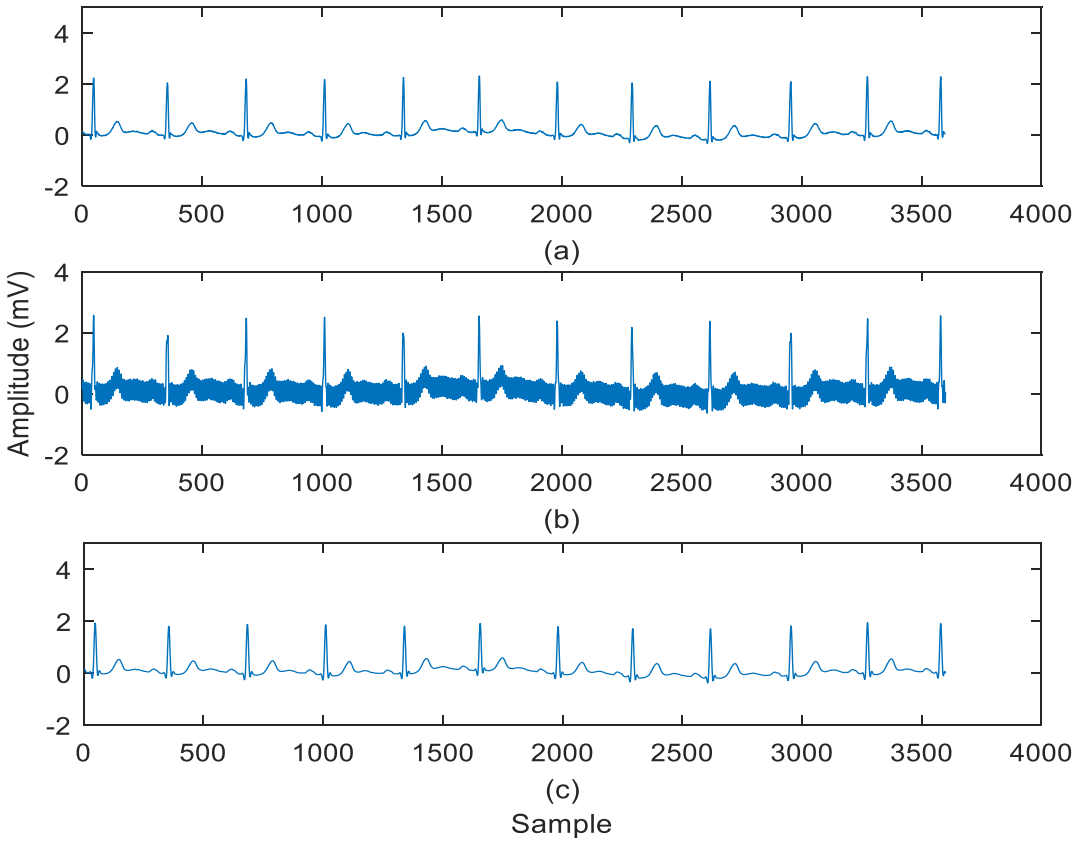

Fig. 3.5 (a) Original signal (MIT-BIH dataset record no. 103), (b) High-frequency noise (450 to 1000 Hz) is present in the signal and (c) Noise is removed.

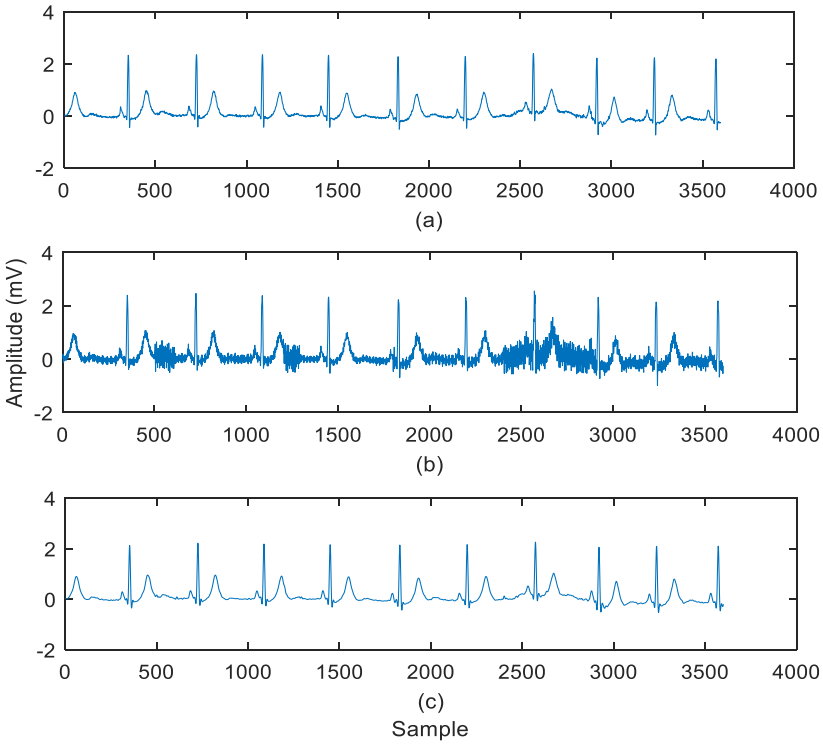

Fig. 3.6 (a) Original signal (MIT-BIH dataset record no. 106), (b) Multiple frequencies with multiple amplitude noise (450 to 1000 Hz) is present in the signal and (c) Noise is removed.

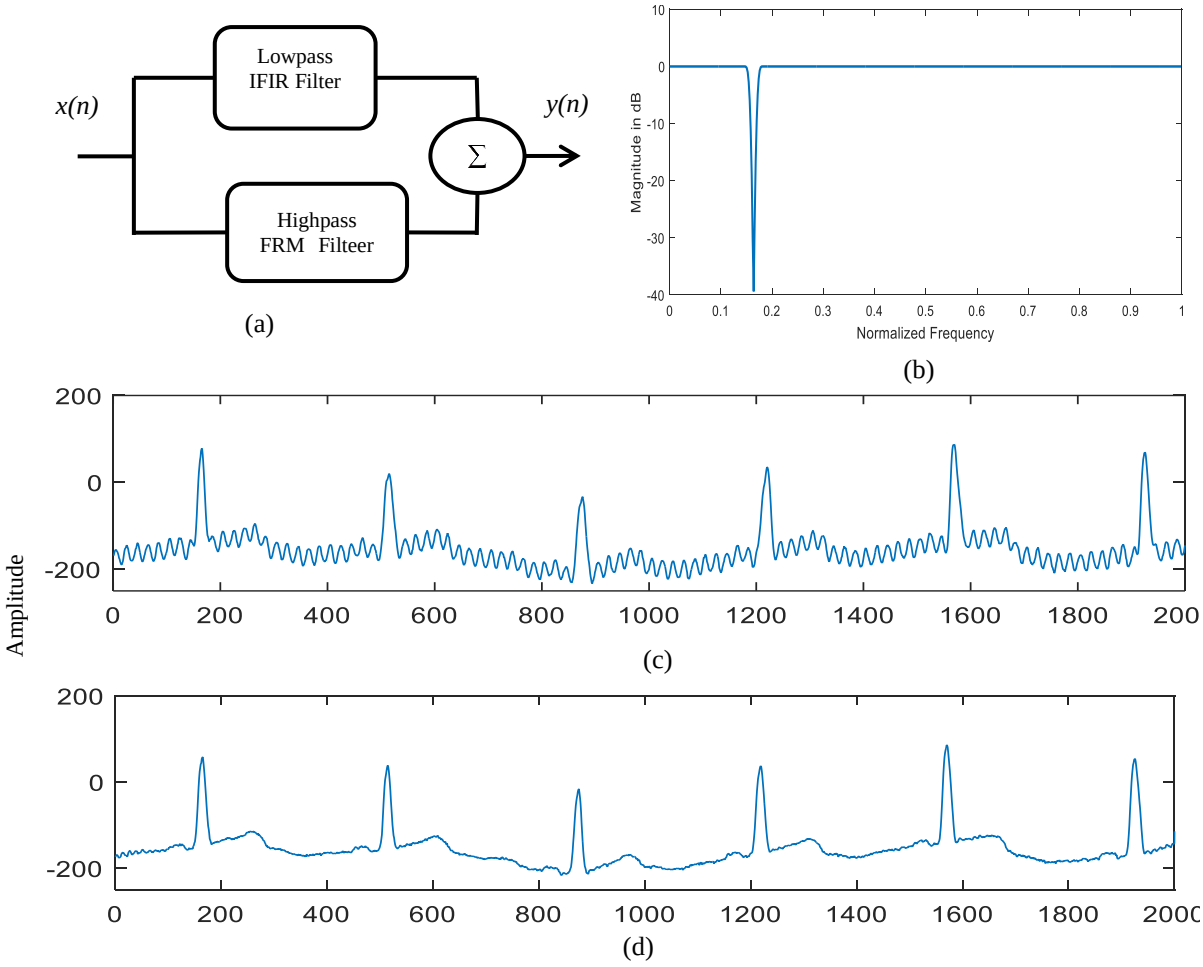

Fig. 3.7 (a) Notch filter structure, (b) Response of notch filter using IFIR technique (c) Power line interferences present in ECG signal (MIT-BIH arrhythmia record no. 121) and (d) Noise is eliminated using notch filter.

3.2.3. Powerline Interference Minimization

For minimization of power line interferences, the notch filter is always preferred. Here also, the 50/60 Hz noise is eliminated using the notch filter. For designing notch filter; first, the lowpass filter is designed using IFIR filter, then highpass is derived using FRM technique. These filters are then added to form the notch filtering. The structure of this filter is shown in Fig. 3.7(a). The specifications of these filters are taken in a way so that the signal of frequency 50/60 Hz can be remove completely. The frequency response of the notch filter is given in Fig 3.7(b). After designing notch filter, it is used to remove the power line interference from the ECG signal. In Fig. 3.7(c), MIT-BIH arrhythmia record no. 121is presented which contaminated by power line interference. This noise is removed using designed notch filter. The PLI free signal is presented in Fig. 3.7(d).

3.3. Proposed IFIR Filter

The designing of an IFIR filter involves up-sampling and convolution of two sub-filters. Because of up-sampling, $L-1$ images are generated which are removed using the interpolator filter. Interpolator filter and up-sampled model filter are convolved to obtain IFIR filter. As a result, large ripples are generated in stop band in the frequency domain at the location of unwanted images as depicted in Fig. 3.8 (convolution of Fig. 3.8(c) with Fig. 3.8(d), generates ripples in stop band that is depicted in Fig. 3.8(e)). To suppress these ripples, the time domain coefficients of IFIR filter are analyzed and some of these eventually removed.

3.3.1. Analysis of The Time Domain Coefficients of FIR and IFIR Filters

The number of coefficients of FIR filter equals the order of filter *i.e.*, N. It can be calculated using Eqns. (2.5) and (2.6). The number of coefficients of model filter is equal to N_m. Hence, the number of coefficients of model filter is L times less than the coefficients of FIR filter $h(n)$. After up-sampling, these coefficients are increased by the factor L (*i.e.*, coefficients of $G(z^L)$ become N). The number of coefficients of the interpolator filter is equal to N_i, therefore after convolution of the up-sampled model filter with interpolation filter ($H(z)=G(z^L)I(z)$) the total coefficients become [306]:

Similarly, in the case of two-stage IFIR filter, the total number of coefficients are [306]:

$$N_{IFIR2} = N + N_{i1} + N_{i2} \tag{3.5}$$

where, N_{IFIR2} is the total number of coefficients of two-stage IFIR filter ($H(z) = G(z^L)I_1(z^{L_1})I_2(z)$), N_{i1} and N_{i2} are the orders of $I_1(z)$ and $I_2(z)$, respectively.

If the time domain filter coefficients of FIR and IFIR filters are compared, then it is observed that many extra zero-valued coefficients are generated in case of IFIR filter that cause ripples in the stopband region. During the analysis of IFIR filter coefficients, it is observed that the locations of these zero-valued coefficients are at the starting and ending of filter taps as illustrated in two experiments carried out. In study one, the results being shown in Table 3.4, filter coefficients of IFIR $h(1)$ to $h(10)$ and $h(90)$ to $h(99)$ are having zero value, while in case of FIR only $h(1)$ to $h(3)$ and $h(82)$ to $h(84)$ are having zero value. In another experiment, a similar behavior of filter coefficients can be observed in Fig. 3.9(a), where IFIR filter has the larger number of coefficients with same shape locations of extra zero values, depicted here once again at the starting and ending filter tap values. It is important to mention here that the selected design specifications of filters in experiment 1, are as follows:

FIR filter: $\omega_s = 0.27\pi$, $\omega_p = 0.17\pi$ and $A_s = 100$.

IFIR filter: *L=2* and other specifications are calculated using Eqns. (2.54) to (2.59).

While the selected design specifications of filters in experiment 2, Fig. 3.9(a) are as follows;

FIR filter: $\omega_s = 0.127\pi$, $\omega_p = 0.056\pi$ and $A_s = 100$.

IFIR filter: here computed value of $L = 4$:

The ripples in the stopband of IFIR filter create distortion that can be minimized by discarding the unwanted zero-valued coefficients. For elimination of these coefficients, a new technique has been proposed. The following steps have been carried out to execute the elimination of zero-valued coefficients, the methodology being the contribution of the present work.

Step 1. The total number of coefficients of IFIR filter (N_{IFIR}) are calculated using Eqn. (3.6):

$$N_{IFIR} = L \times M_m + N_i \tag{3.6}$$

Step 2. Number of extra zero-valued coefficients are calculated

Since $N_{FIR} = N$ is the length of FIR filter, the minimum number of coefficients (M_{zeros}) required to be discarded is equal to [306] ;

$$M_{zeros} \geq N_{IFIR} - N \tag{3.7}$$

Table 3.4 Coefficients representation of FIR and IFIR filter.

Sq. No	Filter Tap (IFIR)	Coefficients of IFIR filter	Filter Tap (FIR)	Coefficients of FIR filter
1.	h(1)=h(99)	0	-	-
2.	h(2)=h(98)	0	-	-
3.	h(3)=h(97)	0	-	-
4.	h(4)=h(96)	0	-	-
5.	h(5)=h(95)	0	-	-
6.	h(6)=h(94)	0	-	-
7.	h(7)=h(93)	0	-	-
8.	h(8)=h(92)	0	-	-
9.	h(9)=h(91)	0	h(1)=h(84)	0
10.	h(10)=h(90)	0	h(2)=h(82)	0
11.	h(11)=h(89)	0.0001	h(3)=h(82)	0
12.	h(12)=h(88)	0.0001	h(4)=h(81)	0.0001
13.	h(13)=h(87)	0.0001	h(5)=h(80)	0.0001
14.	h(14)=h(86)	0.0001	h(6)=h(79)	0.0001
15.	h(15)=h(85)	0	h(7)=h(78)	0.0001
16.	h(16)=h(84)	-0.0001	h(8)=h(77)	0
17.	h(17)=h(83)	-0.0002	h(9)=h(76)	-0.0001
18.	h(18)=h(82)	-0.0004	h(10)=h(75)	-0.0003
19.	h(19)=h(81)	-0.0006	h(11)=h(74)	-0.0005
20.	h(20)=h(80)	-0.0008	h(12)=h(73)	-0.0007
21.	h(21)=h(79)	-0.0009	h(13)=h(72)	-0.0009
22.	h(22)=h(78)	-0.0009	h(14)=h(71)	-0.0009
23.	h(23)=h(77)	-0.0006	h(15)=h(70)	-0.0008
24.	h(24)=h(76)	0	h(16)=h(69)	-0.0004
25.	h(25)=h(75)	0.0008	h(17)=h(68)	0.0003
26.	h(26)=h(74)	0.0019	h(18)=h(67)	0.0013
27.	h(27)=h(73)	0.003	h(19)=h(66)	0.0024
28.	h(28)=h(72)	0.004	h(20)=h(65)	0.0035
29.	h(29)=h(71)	0.0046	h(21)=h(64)	0.0043
30.	h(30)=h(70)	0.0046	h(22)=h(63)	0.0047
31.	h(31)=h(69)	0.0037	h(23)=h(62)	0.0043
32.	h(32)=h(68)	0.0018	h(24)=h(61)	0.0029
33.	h(33)=h(53)	-0.0011	h(25)=h(60)	0.0005
34.	h(34)=h(67)	-0.0048	h(26)=h(59)	-0.0028
35.	h(35)=h(66)	-0.009	h(27)=h(58)	-0.0068
36.	h(36)=h(65)	-0.0129	h(28)=h(57)	-0.0109
37.	h(37)=h(64)	-0.016	h(29)=h(56)	-0.0146
38.	h(38)=h(63)	-0.0172	h(30)=h(55)	-0.0168
39.	h(39)=h(62)	-0.0159	h(31)=h(54)	-0.0169
40.	h(40)=h(61)	-0.0115	h(32)=h(53)	-0.0141
41.	h(41)=h(60)	-0.0034	h(33)=h(52)	-0.0079
42.	h(42)=h(59)	0.0082	h(34)=h(51)	0.0019
43.	h(43)=h(58)	0.0229	h(35)=h(50)	0.0151
44.	h(44)=h(57)	0.04	h(36)=h(49)	0.0312
45.	h(45)=h(56)	0.0581	h(37)=h(48)	0.0489
46.	h(46)=h(55)	0.0759	h(38)=h(47)	0.0671
47.	h(47)=h(54)	0.0918	h(39)=h(46)	0.0842
48.	h(48)=h(53)	0.1044	h(40)=h(45)	0.0986
49.	h(49)=h(52)	0.1125	h(41)=h(44)	0.1091
50.	h(50)=h(51)	0.1153	h(42)=h(43)	0.1146

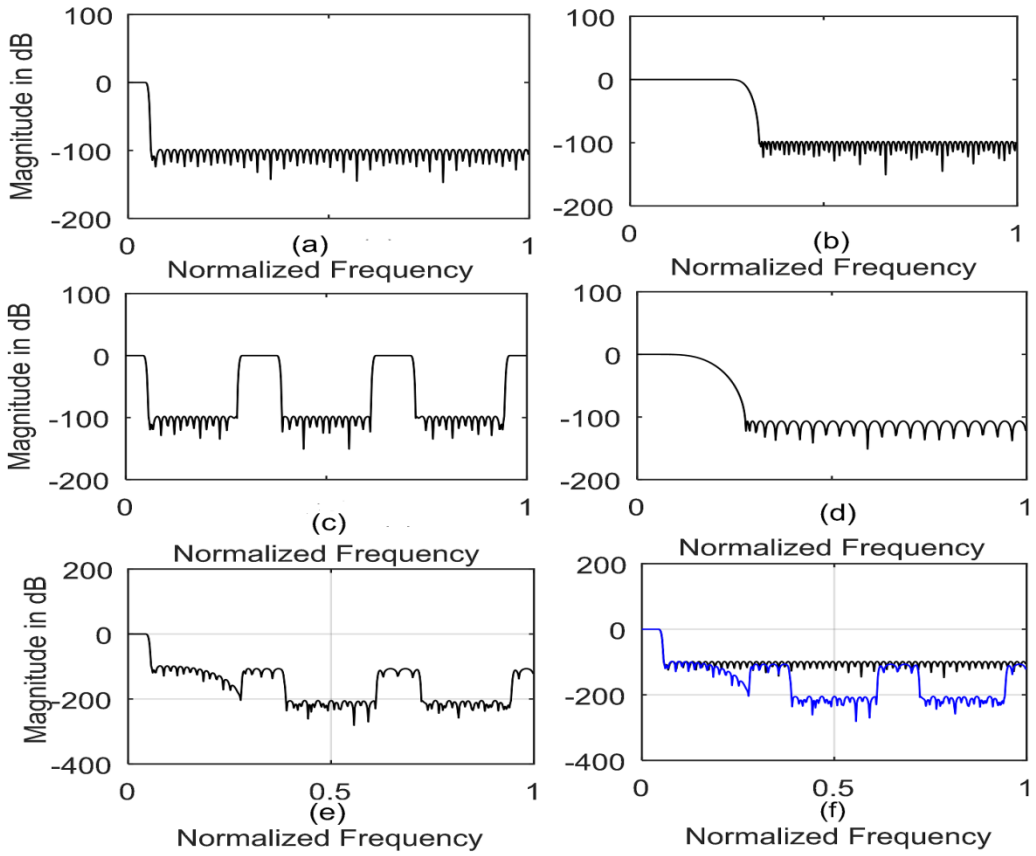

Fig. 3.8 Design of IFIR filter using conventional approach $A_s = 100$ dB, $\omega_{ss} = 0{:}0555\pi$ and $\omega p = 0{:}0413\ \pi$. Magnitude response: (a) FIR model filter, (b) modal filter, (c) up-sampled model $G(z^L)$, (d) Interpolator filter, (e) IFIR filter and (f) Comparison of FIR and IFIR filter.

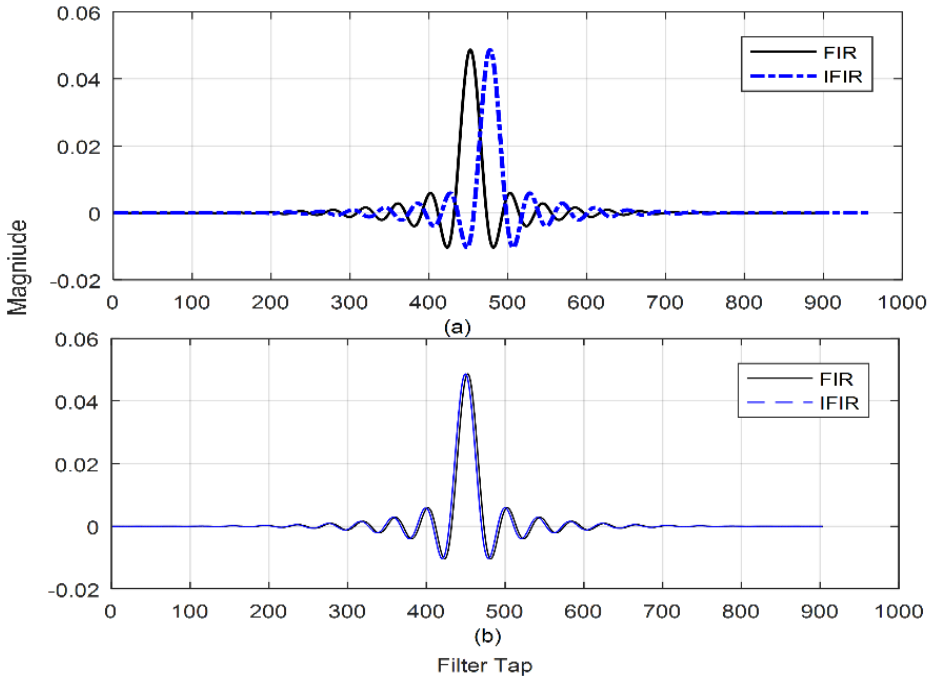

Fig. 3.9 Coefficient plots of FIR and IFIR, using (a) Conventional method and (b) Proposed method.

Step 3. For elimination of M_{zeros} suitable locations /filter tap value will be selected by two means [306]:

a) If M_{zeros} is even:

For starting the filter tap value:

$$1 \text{ to } M_{zeros}/2 \tag{3.8}$$

For ending location of filter tap value:

$$(N_{IFIR} - M_{zeros})/2 \text{ to } N_{IFIR} \tag{3.9}$$

b) If M_{zeros} is odd

For starting the filter tap/indices value:

$$1 \text{ to } M_{zeros} + 0.5 \tag{3.10}$$

For ending filter tap value:

$$N_{IFIR} - M_{zeros} + 1/2 \text{ to } N_{IFIR} \tag{3.11}$$

Step 4. In this step, the coefficients elimination is performed from the extracted locations. Similarly, in case of two-stage IFIR filter, the following points are used:

The total number of coefficients of two staged IFIR filter for finding M_{zeros} are computed by using Eqn. (3.12) is used [306]:

$$M_{zeros} \geq N_{IFIR2} - N \tag{3.12}$$

where, N_{IFIR2} is the number of coefficients of two staged IFIR filter and calculated as:

$$N_{IFIR2} = L \times M_m + L_1 \times N_{i1} + N_{i2} \tag{3.13}$$

In this case also, coefficients are removed from the filter tap location by following ways [306]:

a) For even value of M_{zeros}

For starting filter tap value:

$$1 \text{ to } M_{zeros}/2 \tag{3.14}$$

For ending filter tap value:

$$(N_{IFIR2} - M_{zeros})/2 \quad \text{to} \quad N_{IFIR2} \tag{3.15}$$

b) If M_{zeros} is odd:

For starting filter tap value;

$$1 \text{ to } M_{zeros} + 0.5 \tag{3.16}$$

For ending filter tap value:

and $$(N_{IFIR2} - M_{zeros}) + 0.5 \text{ to } N_{IFIR2} \tag{3.17}$$

After removing the M_{zeros}, the proposed filter response is compared with that of the conventional IFIR filter described in the next section.

3.3.2. Performance Evaluation of the Proposed Technique

In this section, the modified filter for minimization of ripples in the stopband region is given for designing IFIR filters. The performance of proposed algorithm is evaluated in terms of following significant parameter given below:

Distortion in the frequency domain (DFD)

$$DFD = \max \left| \sum_{k=\omega}^{\pi} A_s - p(k) \right| \tag{3.18}$$

where, $p(k)$ represents the frequency domain coefficient of the filter in dB.

Example of Proposed Single Stage IFIR Filter Design:

In this segment, the single stage IFIR filter is designed. Park-Mcclellan algorithm is used for designing of sub filters (model and interpolator filter), because it gives equiripple response. The design specifications of $H(z)$ are: stopband attenuation $(A_s) = 100dB$, passband edge frequency $(\omega_p) = 0.0413\pi$, and stopband edge frequency $(\omega_s) = 0.0555\pi$. The calculated value of L is 6. In this case, computational complexity reduction is 77.32%. The experimental results are shown in Fig. 3.8. Fig. 3.8(a) shows the frequency response of the desired FIR filter $H(z)$ and in Fig. 3.8(b) response of the model filter is shown. Since $L = 6$, 5 unwanted images are generated, which are depicted in Fig. 3.8(c). For removing these images, the interpolator filter $I(z)$ has been used, that is shown in Fig. 3.7(d). The magnitude response of the final IFIR filter is depicted in Fig. 3.7(e). The comparative analysis of the response of FIR and IFIR filter is shown in Fig. 3.8(f). From this figure, it can be observed that both filters have identical passband. However, in case of IFIR filter, there are large ripples in the stopband region (*100-280 dB*). In Fig. 3.10, relations: $\%CR$, N and TW with L are presented. Form this figure, it is observed that value of L should be high for achieving high CR. The frequency response of the proposed IFIR filter is given in Fig. 3.11(a) and comparative analysis of FIR, conventional IFIR and proposed IFIR filter is given in Fig. 3.11(b). The comparison of DFD of FIR, conventional IFIR and proposed IFIR filter is given in Fig. 3.11(c).

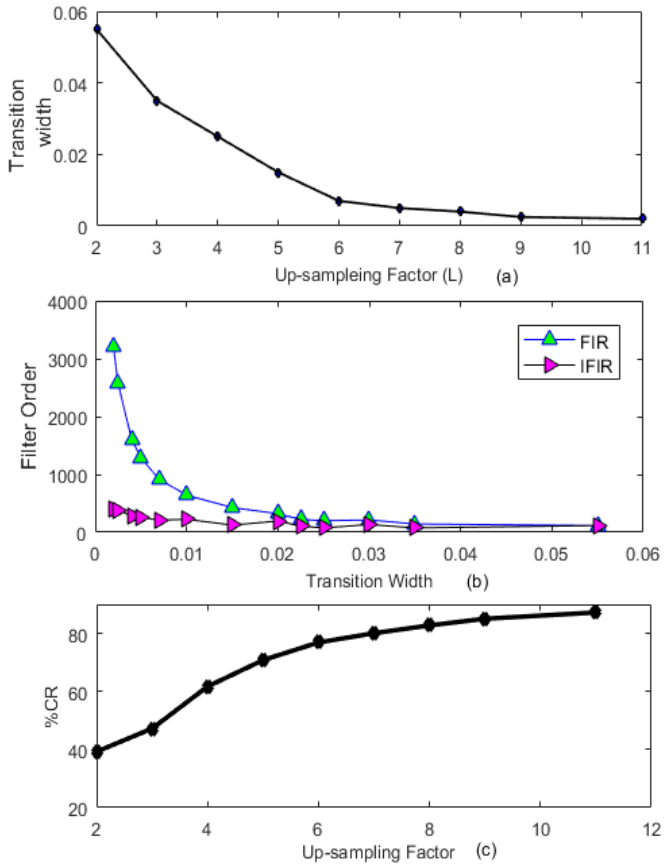

Fig. 3.10 Relationship plot between (a) Up-sampling factor and transition width, (b) Transition width and filter orders of FIR and IFIR filter and (c) Up-sampling factor and computational complexity reduction.

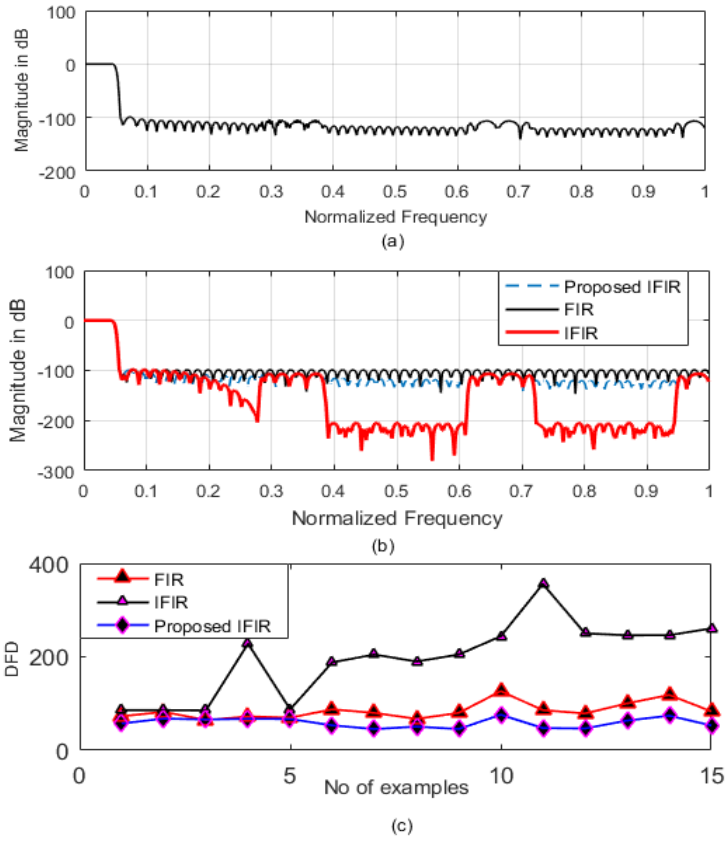

Fig. 3.11 (a) Response of proposed IFIR filter, (b) Comparison of responses of FIR, conventional IFIR and proposed IFIR filter and (c) Comparison of *DFD* of FIR, conventional IFIR and proposed IFIR filter.

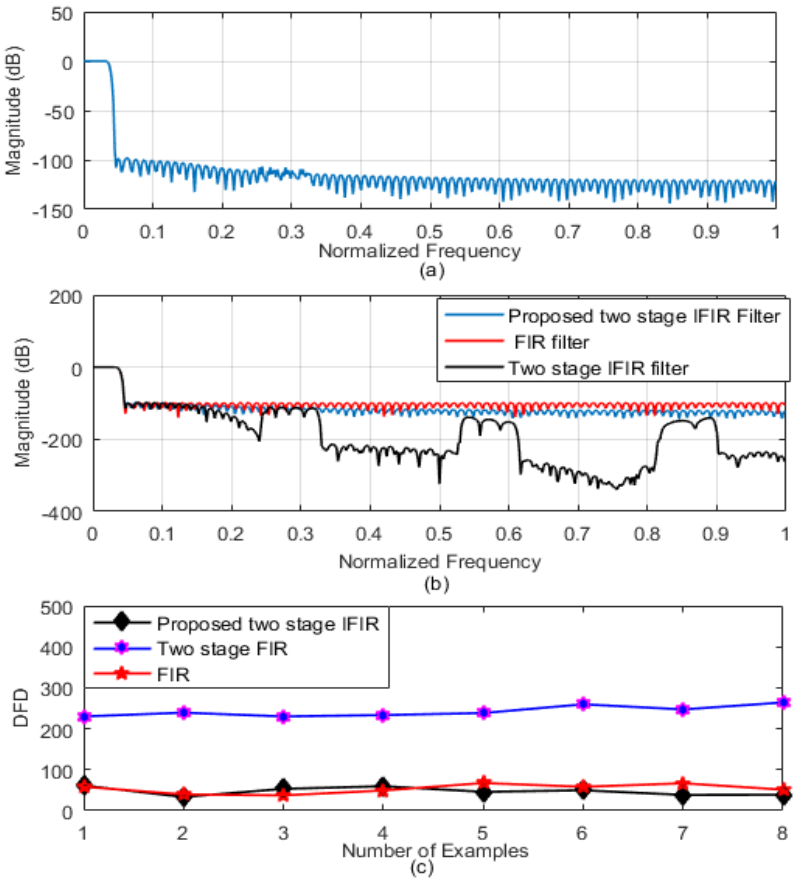

Fig. 3.12 (a) Response of proposed two-stage IFIR filter, (b) Comparison of responses of FIR, conventional two-stage IFIR and proposed two-stage IFIR filter and (c) Comparison of *DFD* of FIR, conventional two-stage IFIR and proposed two stage IFIR filter.

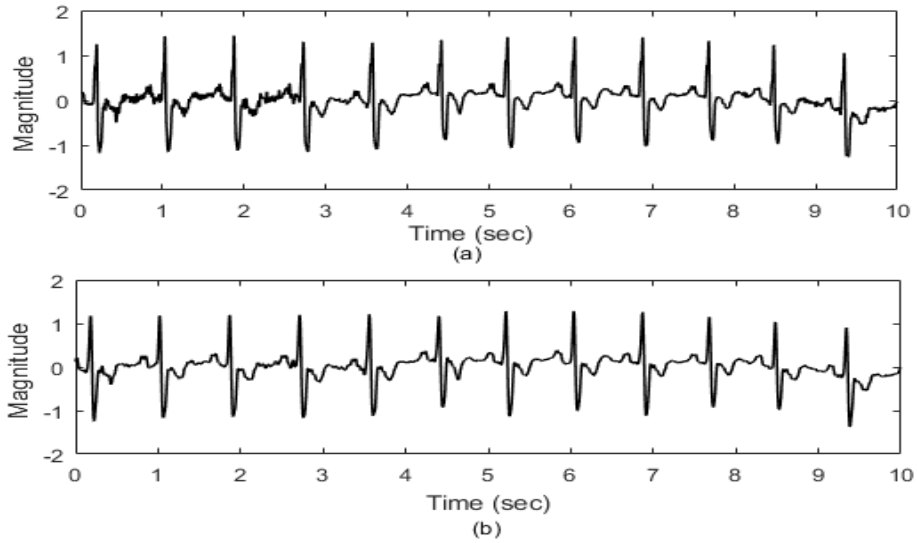

Fig. 3.13 (a) Noisy ECG signal (MIT-BIH-118e00) and (b) Noise is removed using proposed IFIR filter.

Example of Proposed Two Staged IFIR Filter

In this case, the two-stage IFIR filter is designed. Here also, the Park-Mcclellan algorithm is used for designing of sub-filters (*i.e.*, $G(z)$, $I_1(z)$ and $I_2(z)$). The design specifications of $H(z)$ are: $A_s = 100dB$, $\omega_p = 0.030\pi$, and ω_s is 0.0450π. Here, *80.14* % of *CR* is achieved and the calculated values of up-sampling factors are: $L = 7$ and $L_1 = 2$. In this case, the number of coefficients of FIR filter is 856, number of coefficients of two stage IFIR filter is 930, thus $M_{zeros} = 74$. The response of proposed IFIR is given in Fig. 3.12(a), comparative analysis of FIR and proposed IFIR filters is depicted in Fig. 3.12(b) and *DFD* comparison of proposed two-stage IFIR filter, conventional two-stage IFIR filter, and FIR filter is given in Fig. 3.11(c). Different other examples are taken to evaluate the performance of the proposed methodology, which are given in Table 3.5. From Figs. 3.11(b), 3.11(c), 3.12(b), 3.12(c) and Table 3.5, it can be seen that the response of proposed IFIR (single and two-stage) filters are better than the conventional IFIR filters in terms of stopband ripples without affecting any other parameters.

3.4. Noise Elimination using Proposed Filters

IFIR filter can be used for removing the high-frequency noise with less computational complexity. The high-frequency noise is removed using the proposed single stage IFIR filter from an ECG signal. Signal presented in Fig. 3.13(a) represents MIT-BIH record no. 118e00, which is contaminated by high-frequency noise. The noise is removed using the proposed IFIR filter, which is shown in Fig. 3.13(b). PLI and baseline wander are also eliminated using the proposed filter is given in Figs. 3.14 and 3.15, respectively. For minimizing the PLI MIT-BIH record no. 123 is taken and for baseline wander, MIT-BIH record no. 224 is used. From these figures, it can be demonstrated that the proposed filter can remove noise from an ECG signal without affecting the diagnostic information. Other parameters are also used to measure the performance of overall noise reduction methodology. These parameters are presented in Table 3.6. From this table, it is observed that the overall coefficients of the proposed filter are reduced, the delay in filtering is also reduced. Therefore, the method is efficient for both (*i.e.*, designing cost of filter and in filtering).

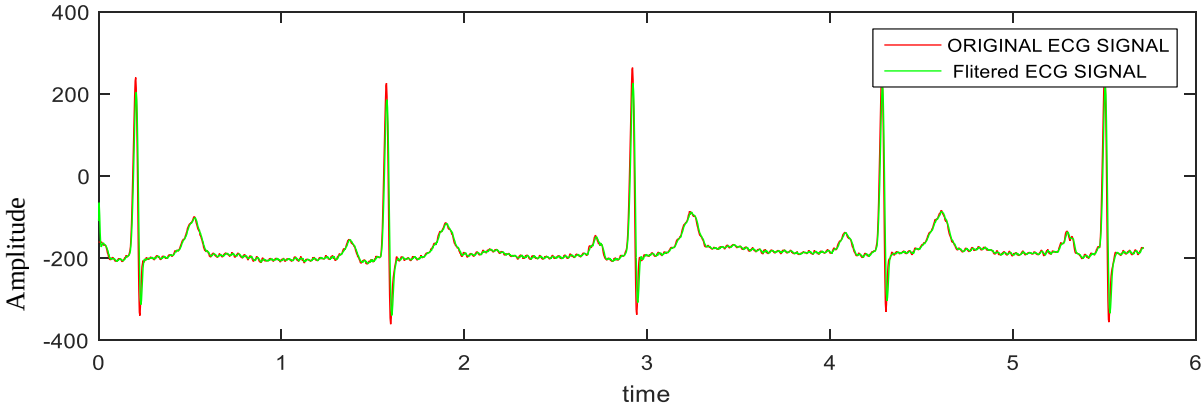

Fig. 3.14 50 Hz noise reduction from MIT-BIH record no. 123 using notch filter designed by proposed.

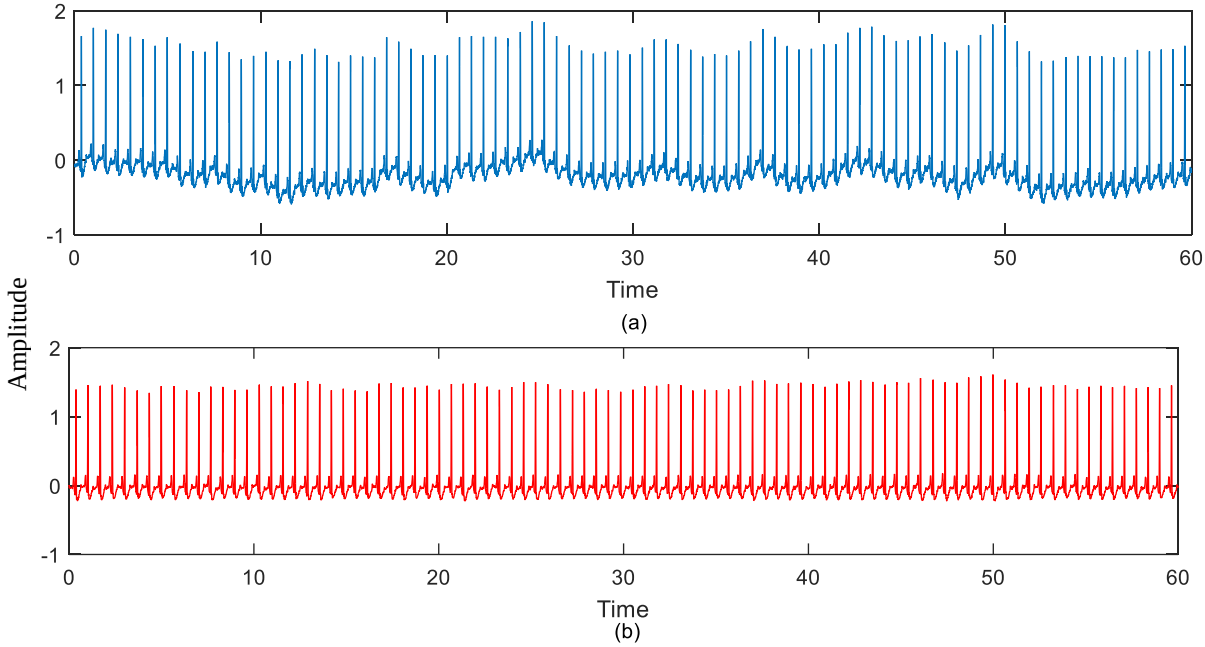

Fig. 3.15 (a) MIT-BIH record no. 224 with Baseline wander reduction and (b) Baseline wander is removed using IFIR filter.

Table 3.6 Delayed coefficients and SNR measurement using designed IFIR filters.

Sq. No	Dataset	FIR		IFIR		Proposed IFIR		Proposed IFIR2	
		SNR	Delayed coefficients	SNR	Delayed coefficients	SNR	Delayed coefficients	SNR	Delayed coefficients
1.	118e24	22.51	= *N*	23.54	*N*+*Ni*	23.86	< *N*	24.51	< *N*
2.	118e18	20.74	= *N*	18.97	*N*+*Ni*	20.71	< *N*	22.78	< *N*
3.	118e12	13.08	= *N*	14.08	*N*+*Ni*	13.08	< *N*	13.08	< *N*
4.	118e06	8.00	= *N*	8.23	*N*+*Ni*	8.42	< *N*	12.31	< *N*
5.	118e00	0.04	= *N*	0.91	*N*+*Ni*	1.74	< *N*	5.00	< *N*
6.	118e_6	-2.46	= *N*	5.43	*N*+*Ni*	5.32	< *N*	10.23	< *N*

Table 3.5. Comparative analysis of FIR, proposed single stage IFIR and Two-Stage IFIR using different fidelity parameters.

ω_s	ω_p	N	L	N_m	N_i	L_1	N_{i1}	N_{i2}	N_{FIR}	N_{IFIR}	M_{zeros}	N_{IFIR2}	$CR\%$	*DFD (FIR)*	*DFD (IFIR) (con.)*	*FDD IFIR-proposed*	*DFD (Two stage IFIR)*	*DFD IFIR2-proposed*
0.300π	$\frac{0.0001}{\pi}$	43	2	21	18	-	-	-	43	59	16	-	**09.30**	89.07	224.32	**48.20**	-	-
0.200π	$\frac{0.0001}{\pi}$	64	2	32	16	-	-	-	64	79	15	-	**25.00**	88.92	227.42	**95.75**	-	-
0.200π	$\frac{0.0051}{\pi}$	66	2	33	16	-	-	-	66	81	15	-	**25.75**	61.82	172.82	**46.15**	-	-
0.240π	$\frac{0.0500}{\pi}$	68	2	34	18	-	-	-	68	85	17	-	**23.52**	59.42	224.14	**50.57**	-	-
0.270π	$\frac{0.1300}{\pi}$	92	2	46	21	-	-	-	92	112	20	-	**27.17**	40.78	224.14	**58.22**	-	-
0.150π	$\frac{0.1000}{\pi}$	257	3	86	31	-	-	-	257	288	31	-	**54.47**	57.72	149.61	**29.23**	-	-
0.070π	$\frac{0.0100}{\pi}$	214	4	54	31	-	-	-	214	246	32	-	**60.28**	67.70	234.70	**54.03**	-	-
0.050π	$\frac{0.0100}{\pi}$	321	5	64	38	-	-	-	321	357	36	-	**68.22**	67.19	200.19	**47.87**	-	-
0.040π	$\frac{0.0100}{\pi}$	428	6	71	45	-	-	-	428	470	42	-	**72.89**	51.14	175.18	**29.37**	-	-
0.090π	$\frac{0.0700}{\pi}$	642	5	128	-	2	27	21	642	-	713	713	**72.58**	58.27	175.61	**53.69**	230.00	**61.20**
0.040π	$\frac{0.0250}{\pi}$	856	7	122	-	2	29	18	856	-	72	928	**80.25**	39.56	163.93	**31.07**	239.22	**33.38**
0.031π	$\frac{0.0200}{\pi}$	1142	8	143	-	2	32	17	1142	-	81	1223	**83.18**	37.34	240.13	**53.45**	230.00	**53.26**
0.040π	$\frac{0.0350}{\pi}$	2568	10	257	-	2	51	16	2568	-	118	2686	**87.38**	49.20	163.07	**36.55**	233.39	**59.60**
0.039π	$\frac{0.0370}{\pi}$	6421	13	494	-	3	55	25	6421	-	189	6610	**91.06**	67.44	163.10	**42.74**	238.31	**45.90**
0.010π	$\frac{0.0050}{\pi}$	2568	14	183	-	3	33	24	2568	-	115	2683	**90.65**	58.18	197.69	**54.30**	259.65	**49.73**
0.005π	$\frac{0.0010}{\pi}$	3210	17	189	-	3	38	23	3210	-	138	3348	**92.21**	66.79	204.36	**41.82**	247.15	**38.41**
0.004π	$\frac{0.0015}{\pi}$	5137	21	245	-	3	48	22	5137	-	172	5309	**93.86**	51.28	196.00	**39.30**	264.10	**38.75**

3.5. Noise Reduction using WT

Wavelet transform has been discussed in Chapter 2. Multi-resolution property of the WT is important for signal processing. WT is also used as an iterative processing tool of signal processing, in which a signal /image is fragmented into finer resolution signals in time and frequency. The first step of WT processing is: designing of two symmetric filters from a mother wavelet and a scaling function. These functions provide an orthogonal basis to decompose the signal in two equal parts in an iterative way. Each level of decomposition included the down-sampling process to reduce the sampling frequency.

3.5.1. High-Frequency Noise Minimization

In this segment, linear filtering is done by MODWT along with universal thresholding. MODWT is good for real-time application, because the computation of noisy coefficients is faster than other filtering approaches [28]. Here, the first step is; decomposition of the signal into different frequency band using MODWT, then after removed of noisy coefficients using universal thresholding. In Fig. 3.16(a), MIT-BIH arrhythmia database (record-232) is presented, which also has high-frequency noise and in Fig. 3.15(b), the noise is minimized.

3.5.2. Baseline Wander Removing

In an ECG signal, the low-frequency components are the source of baseline shifting. Here, baseline wander is removed using deferent mother wavelets (db6 to db8) by decomposing the signal, Therefore, to remove or minimize the BW, the approximation found is needed to be a narrow spectrum to make the interferences pure sinusoids. Further, the variance of resulting signal should be as low as possible, since the approximation must not have high-frequency components (R waves); and therefore, the resulting signal must be moderately flat. As soon as the level is acquired, the wavelet approximation is computed, then after, it is deducted from the original signal. Subsequently, the BW of given signal is significantly eliminated. In Fig. 3.17(a), MIT-BIH noise stress test database record no. 118e24m is depicted, in which the baseline wander is presented, and this is removed using wavelet transform and depicted in Fig. 3.17(b).

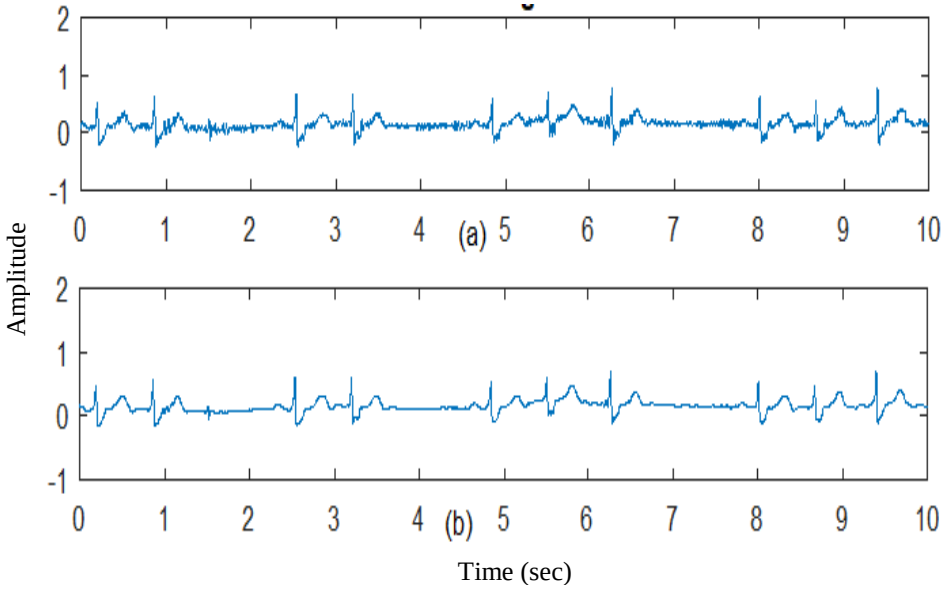

Fig. 3.16 (a) Noise present in the ECG signal (MIT-BIH arrhythmia record no. 232) and (b) Noise is eliminated using MODWT.

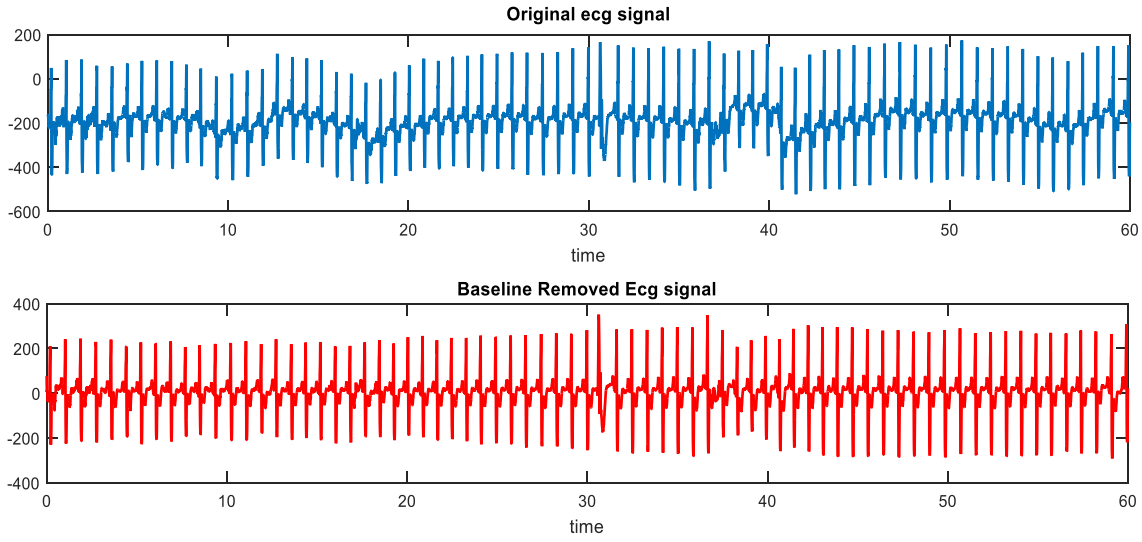

Fig. 3.17 (a) 60 seconds ECG signal (MIT-BIH noise stress test database record no.118e24m) with baseline wander and (b) Signal after baseline wander removal.

3.6. Discussion

In this Chapter, linear filtering is carried out to minimize the noise presented in the ECG signal. In [152] the researchers have used adaptive filtering to minimize baseline wonder. Adaptive filtering is used to minimize the mean square error and can be utilized for real time processing. However, this provides estimated point and also the mean square error is not relevant in all cases. In [159], a modified morphological filtering (MMF) technique is used for signal conditioning in order to accomplish baseline wander correction and noise suppression with minimum signal distortion. By using structuring element pair in closing and opening operations, signal distortion rate in ECG signal can be decreased. However the noise suppression rate will be affecting by using this type of methodology. In 177, the researchers have used FIR and IIR filters to reduce the noise from the ECG signal. IIR filter based filter can provide good results in terms of computational efficiency however; phase distortion may disturb the component of the ECG wave form, especially in real time processing. And FIR filters are not computationally efficient. In 163, the researchers have used Digital Elliptic Filter for noise elimination from the ECG signal the method provide good results; better than Butterworth, chebyshev type I & type II. However, the work does not claim the noise elimination improving parameter. The tabular results of present study *i.e.*, Table 3.1 and 3.2 show that method provides good results in terms of SNR. Table 3.6 shows that the method given in this Chapter, provided better results in terms of delay.

3.7. Summary

In this Chapter, noise elimination of ECG signal is presented. First, baseline wander, high frequency and power line interference noises are removed using a computationally efficient linear phase filter. Then after, new (single and two-stage) IFIR filters are proposed. The experimental results of various examples and comparative analysis clearly indicate that the proposed algorithm demonstrates outstanding performance in terms of stopband ripples and maximum computational complexity reduction. The comparative results show that the IFIR filter response designed by using the proposed algorithm has the same passband and stopband regions as the desired FIR filter. Proposed mathematical relations used to evaluate the zero-valued coefficients are simple and easy to implement for discarding zero-valued coefficients giving an excellent response. The method would render landmark results in telemedicine, audio and image data compression and other areas of signal processing, where power loss /consumption and ease of computational

burden are the major issues.. The technique would find immense applications in the areas like noise removal in bioelectrical signals, *viz.*, the ECG, where any loss of diagnostic information would be highly inappropriate; high-speed transmission of bioelectrical signals, where data compression is an important process during which the power losses incurred would lead to false diagnosis. Several design examples are included to illustrate the performance of proposed method along with its improved response over other existing methods. Designed filters are also used to remove the noise from the MIT-BIH noise stress test database, indicating that the proposed filters can successfully eliminate noise to a great extent with low computational complexity and a lesser amount of delay.

CHAPTER 4

ECG DATA COMPRESSION TECHNIQUES

4.1. Overview

In this chapter, the essential aspects of biomedical signal compression techniques are described. Data compression is one of the important fields of research from the last five decades. Two most important applications of data compression are: storage requirement reduction and transmission cost reduction. This chapter presents the techniques of compression of ECG signals. The need for ECG data compression is already discussed in Chapter 1. In general, Data compression is mainly classified into two types: lossless data compression (LLDC) and lossy data compression (LDC) [17]. In the LLDC schemes, original data can be recovered exactly, however low compression ratio (CR) is achieved. This type of compression is generally applied in the areas, where any difference between the original and reconstructed data cannot be tolerated; for example, text compression and bank records. Huffman and run-length coding are famous examples of LLDC. In contrast, the high compression ratio can be achieved using LDC methods by eliminating the irrelevant coefficients. In numerous data compression applications, exact reconstruction is not mandatory, for example in speech communication or telecommunication and video transmission [29].

In most of the ECG data compression applications, *viz*., telemedicine and e-healthcare, Holter monitor systems and in reducing the storage requirement, the lossless data compression does not provide sufficient value CR; therefore, LDC techniques are more preferred for data compression of ECG rhythms over l LLDC techniques. However, algorithms used for ECG signal compression must be provided with the acceptable fidelity. 1-D ECG data compression methods are classified into three types: a) direct data compression method, b) transformational data compression methods and c) parameter extraction based data compression methods [25].

In direct data compression techniques, estimation of redundancies of the original signal samples is done by direct analysis [36].

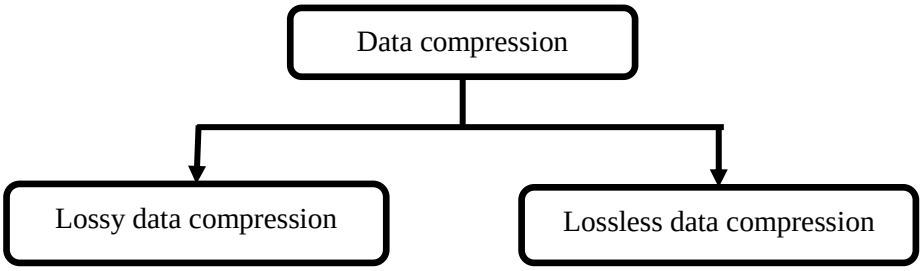

Fig. 4.1 Broad classification of data compression [36].

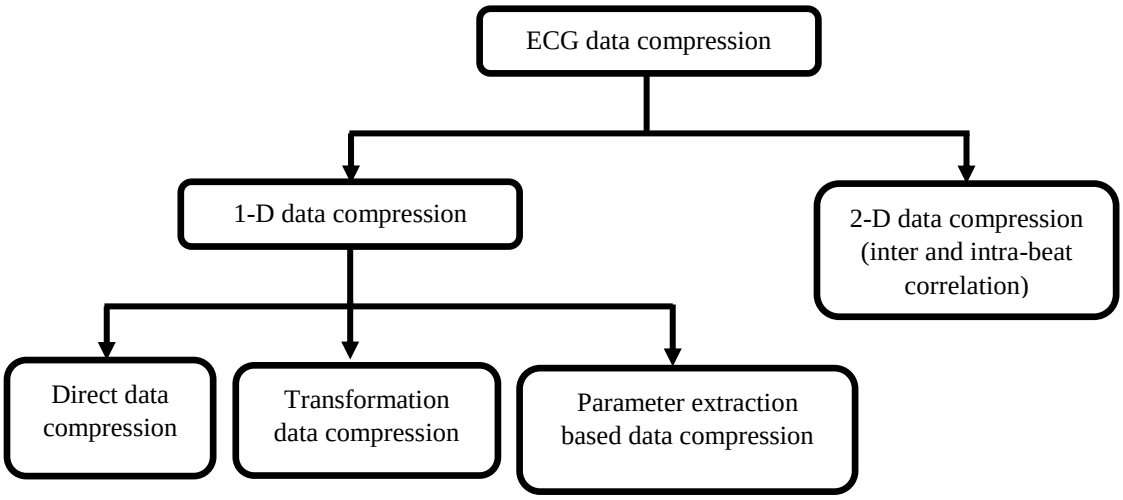

Fig. 4.2 Classification of data compression techniques.

4.2. Direct Data Compression Techniques

In the direct data compression methods, the compression is done by estimation of irrelevant information on direct analysis of samples of the signal. Several direct data compression methods have been used to reduce the data size of ECG signal. This section illustrates the theory of these algorithms [49].

4.2.1. Amplitude Zone Time Epoch Coding (AZTEC)

The amplitude zone time epoch coding (AZTEC) technique, involves the decomposition of input data into horizontal lines and slopes [26]. The horizontal lines are made on the principle of zero order interpolation (ZOI), and the information is put in storage in form of magnitude and sample values. A slope is designated, whenever the number of samples needed to form a horizontal line is less than three. A slope is stored as its duration (the number of samples) and advancement of preceding point. Reconstruction of signal is accomplished by expanding first the horizontal line data and slope into the sets of discrete points. In this case, the reconstructed signal is having significant discontinuities and distortions. Furht and Perez have further modified this method in 1988 named as modified AZTEC [28]. Further improvement has been done in modified AZTEC, where results are validated, and the technique is named as improved modified AZTEC [50].

4.2.2. Turning Point (TP)

The turning point (TP) algorithm was proposed to reduce the sampling frequency of an ECG signal. In this method, the sampling frequency is reduced without shrinking the advancement in the amplitude of QRS segment [30]. Here firstly, the analysis of sampled points is done, and then a single sample of each pair of consecutive points is stored. The term "turning point" derives from the fact that this method preserves turning points of the data (points at which sign of the signal slope changes or turns). Here, three data points (one reference point (X_0) and two consecutive data points (X_1 and X_2) are processed at a time. It is dependent on the point, which preserves the slope of original three points. In the turning point algorithm, either X_1 or X_2 is to be retained according to the conditions given in Eqns. (4.1) and (4.2) [31].

$$if\ (X_2 - X_1)(X_1 - X_0) < 0 \qquad X_0 = X_1 \tag{4.1}$$

$$if\ (X_2 - X_1)(X_1 - X_0) \geq 0 \qquad X_0 = X_2 \tag{4.2}$$

The turning point algorithm produces a fixed compression ratio of *2:1*. It has some advantages, *viz*., it is easy to implement, very fast algorithm and important for real-time processing. This algorithm yields an image that approximately similar to that, to which a physician is familiarized for observing. The major disadvantage of this method is that the saved points do not symbolize equally spaced time interval. Although there is no long-term distortion; however, there is exist short-term distortion [31].

4.2.3. Co-ordinate Reduction Time Encoding System (CORTES)

The co-ordinate reduction time encoding system (CORTES) is the technique of data compression that utilizes the combination of AZTEC and TP methodologies. This technique takes the advantages of strength of both techniques while sidestepping their weakness. In this technique, the AZTEC and TP are applied to isoelectric regions, and clinically significant high-frequency regions of the input signal are processed in a parallel way. Here, for every AZTEC generation, a decision based on the length of line is used to verify that the AZTEC/TP data is saved or not. It is decided by the length of line for example; if it is shorter than the threshold (which is determined empirically), the TP data are saved, otherwise the AZTEC line is saved. The determination of probationary and permanent data is done by two points. The identification of transition between the AZTEC and TP data is done by utilizing a marker. Here, the signal reconstruction can be accomplished by expanding the AZTEC plateaus into discrete data points and interpolating the TP data [32].

4.2.4. Fan Algorithm

Fan algorithm is also a direct data compression method. In this technique, the implementation of first-order interpolation with two degrees of freedom is exploited. Here, storage requirement of all the actual data samples as well as the present data point throughout the execution of the program is not needed. Furthermore, for keeping all the intermediate data points within the defined error tolerance; the longest possible line is drawn, started from the first sample to the last sample. This method is named as fan, because the slope stretched from original specimen to future sample, from a set of radial lines is analogous to a fan [36].

4.2.5. Scan Along Polygonal Approximation (SAPA)

The scan along polygonal approximation (SAPA) technique is an admirable approximation technique used to reduce the data. It is based on the principle of first-order interpolation with two degrees of freedom (FOI-2DF). This technique is accessible from the piecewise linear segments inside the corridor formed by two functions. These functions are less in size than the certain waveform, by a threshold value. Similar to the fan algorithm, here also a straight line sketching is done between the current and last saved sample for maintaining the intermediate data within a specified tolerance of the interpolated value. Storage of each line segment is done in form of data as well as the starting and ending points. Here, the final point is used as the beginning point for the next segment [35,36].

4.2.6. Encoding Methodologies

Encoding methodologies are always needed to improve the data compression efficiency in the reduction of an ECG signal. Three types of encoding methodologies are utilized in this work such as: Run-length, Huffman and LZW encoding. Therse are discussed below.

4.2.6.1. Run-Length Encoding (RLE)

Run-length encoding schemes later employed in the transmission of television signals. It is a simple and lossless data compression technique, in which the data is compressed by representing the consecutive runs of the same value in data as the value followed by the count. For example: aaaabbccccccrrrrrrffff can be represented as 4a2b6c6r4f. It is a fast scheme, however the compression efficiency of this method depends on the data type. It can also be expressed in multiple ways to put up data properties and additional compression methods. RLE is also very useful in image compression [107].

4.2.6.2. Huffman Coding

Huffman coding allocates the variable length code words to a fixed length input data/characters based on their frequencies. The allocation is done in such a manner so that the more repeated characters are allocated by smaller code words, and the less repeated characters are allocated by larger code words. Here, cade digits are assigned to all edges along the path to a character. A tree structure is formed in this compression scheme, in that zero is used for the left side and one for the right side. The leaves contain a letter and its frequency count. In all other nodes, instead of one character, a zero, and the count of

its frequency and its descendants will be eligible. For instance, consider the string *ABRACADABRA*. There are a total of characters in the string. This number should match the count in the ultimately determined root of the tree. Our frequencies are and. The two smallest frequencies are for and, both equal to, so it creates a tree with them. The root node will contain the sum of the counts of its descendants, in this case. The left node will be the first character encountered, and the right will contain [86].

4.2.6.3. LZW Encoding

Lempel ZivWelch (LZW) is also a lossless compression method. This method is a general purpose method, which has some advantages over other coding methodologies such as simplicity and versatility. Generally, this method can compress data using coding way in which the resultant file becomes one-half of the original size. The LZW method provides very good results in terms of compression ratio in some applications such as: tabulated numbers, computer source code, and acquired signals [25].

LZW compression uses a code table, as illustrated in Fig. 4.3. A common choice is to provide 4096 entries in the table. In this case, the LZW encoded data consists of entirely of 12-bit codes, each referring to one of the entries in the code table. The decompression is achieved by taking each code from the compressed file and translates it through the code table to find what character or characters it represents. Codes 0-255 in the code table are always assigned to represent single bytes from the input file. For example, if only these first 256 codes were used, each byte in the original file would be converted into 12 bits in the LZW encoded file, resulting in a 50% larger file size. During the decompression, each 12-bit code would be translated via the code table back into the single bytes [307].

4.3. Transform Based Techniques

Signal processing is one of the fast emergent areas from the last few decades. Different signal processors have been established for implementing the theoretical facts efficiently. Currently, these processors are often utilized in several areas, such as: radio-frequency analysis, transportation system, medicine and production, biomedical engineering, communication systems, *etc*. The most important and widely used methodologies of signal processing are the transform-based techniques. In these techniques, analysis of a signal is done by converting the signal from one domain to another domain. Different transform techniques are used in the field of signal processing; *viz*., Hilbert transform

(HT), Fourier transform (FT), discrete cosine transform, empirical mode decomposition (EMD), wavelet transform, short time Fourier transform (STFT), *etc*., [25].

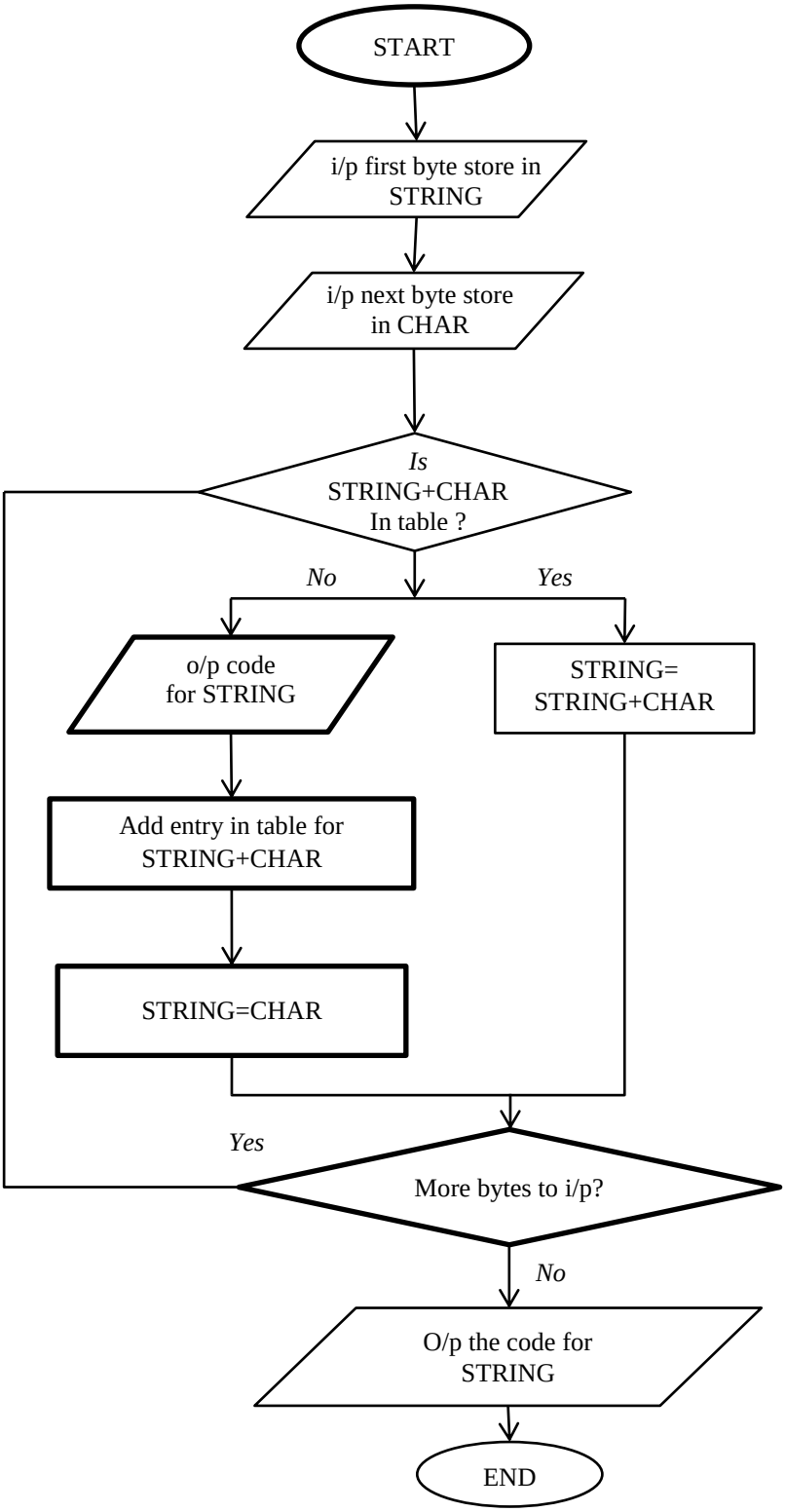

Fig. 4.3 LZW encoding algorithm [307].

4.3.1. Hilbert Transform (HT)

The HT is a linear operative task, which utilizes a function (*f(t)*) of a real variable and yields another function of a real variable, *i.e.*, *H(u)(t)*. In this method, the *f(t)* and its HT (*i.e.*, $\hat{f}(t)$) are correlative and produce strong analytic data. Here, the produced data is a signal, which can be written in form of magnitude (amplitude) and phase. For estimation of phase derivative, instantaneous frequencies are used. If FT is applied to strong analytic signal, a one-sided spectrum is obtained in the frequency domain, and if HT is applied to a function it gives orthogonal relation between the function and its HT. However, due to numerical calculations and truncations, orthogonality is not realized in applications. The energy of a function and its HT are always same; hence, it can be utilized to quantify the accuracy of approximated HT [216].

In the time domain, HT can be defined in the form of convolution of Hilbert transform (*i.e.*, $1/(\pi t)$) and the function *f(t)*, and mathematically can be expressed as [119]:

$$\hat{f}(t) = \frac{1}{\pi} p \int_{-\infty}^{\infty} \frac{f(\tau)}{t-\tau} d\tau \tag{4.3}$$

where, the *P* is the front of integral symbolized by the Cauchy's principal.

Generally, the calculation of HT is not possible as an ordinary improper integral due to the pole presents at $\tau = t$ [20].

4.3.2. Fourier Transform

The FT is an essential part of the signal processing, which converts a time domain signal into the number of frequencies. It can be defined as [1]:

$$F(\omega) = \int_{-\infty}^{\infty} f(t) e^{-i\omega t} dt \tag{4.4}$$

where, $F(\omega)$ is the Fourier transform of the function *f(t)*. This definition makes sense that $f \in L^1(\Re)$. Signal recovery from the FT is needed in several applications. This operation is known as the inverse Fourier transform, which is defined in Eqn. (4.5) [173].

$$\tilde{f}(t) = \frac{1}{2} \int_{-\infty}^{\infty} F(\omega) e^{i\omega t} d\omega \tag{4.5}$$

If *f* and its transform belong to $L^1(\Re)$, then *f(t)* is bounded and continuous for the complete set of real *t* and as a consequence, $\tilde{f}(t) = f(t)$; therefore, Eqn. (4.5) can be written as:

$$f(t) = \frac{1}{2}\int_{-\infty}^{\infty} F(\omega)e^{i\omega t}d\omega \tag{4.6}$$

This expression represents a form of Fourier inversion theorem. According to other variants of the inversion theorem, it can be written as [20]:

$$f(t) = \lim_{T\to\infty}\frac{1}{2\pi}\int_{-T}^{T} F(\omega)e^{i\omega t}d\omega \tag{4.7}$$

Here, the condition is changed that is: if *f* belongs to $L^1(\Re)$, then f is of bounded variation in a neighborhood of *t* and is also continuous at entire range of *t.*

Eqn. (4.7) is to be described as a form of Cauchy principal value. According to another theory, *i.e.*, when $f \in L^2(\Re)$ the Fourier transform is defined as [100]:

$$F(\omega) = \lim_{N\to\infty}\int_{-N}^{N} f(t)e^{-i\omega t}dt \tag{4.8}$$

or

$$F(\omega) = \lim_{N\to\infty} F_N(\omega) \tag{4.9}$$

Therefore, the interpretation of this expression can be done as:

$$\lim_{N\to\infty}\left\|F(\omega) - F_N(\omega)\right\|_2 = 0 \tag{4.10}$$

and the inverse Fourier transform for $F \in L^2(\Re)$ can be stated as:

$$f(t) = \lim_{N\to\infty}\frac{1}{2\pi}\int_{-N}^{N} F(\omega)e^{i\omega t}d\omega \tag{4.11}$$

In many cases, the Fourier transform of a signal is needed to consider as it neither belongs to $f \in L^1(\Re)$ nor to $L^2(\Re)$, for example, delta function [1].

4.3.3. Discrete Cosine Transform

Discrete Cosine Transform (DCT) is used to convert a finite sequence of data points into the summation of a series of cosine functions oscillating at different frequencies. DCTs are simpler to calculate. The applications of DCT are mainly in the areas such as: image processing, audio signal processing, seismic signal processing, biomedical signal compression, *etc*. DCT is analogous to FT; however, it involves the use of just cosine functions and real coefficients, while in case of FT, sine term, cosine term, and complex numbers are involved. Similar to FT, DCT converts data from a spatial-domain into a frequency-domain, and signal can be reconstructed using inverse functions [91].

$$X_k = \frac{1}{2}(x_0 + (-1)^k x_{N-1}) + \sum_{n=1}^{N-2} x_n \cos\left[\frac{\pi}{N-1}nk\right] \quad k = 0,\ldots,N-1 \tag{4.12}$$

where, N is the real numbers, which denotes the number of sequences, *i.e.*, x_0, ..., x_{N-1} and X_k represents the transformed sequence [96].

4.3.4. Empirical Mode Decomposition (EMD)

EMD is the method of decomposing the signal into a specific mode**.** It is a completely different approach of signal processing, which is self-adapting according to the input signal. In this method, decomposition of the input signal is done as a finite sum of *M+1* functions, which are also known as intrinsic mode function (IMF). This method satisfies two conditions, (a) the input signal has the difference of number of extrema, and the number of zero crossings should be either equal to zero or at most by one and (b) the mean value of envelope is defined by the local maxima and the envelope is defined by the local minima and the zero crossing, at any point. It is amplitude modulated- frequency function and can be defined as [164]:

$$f(t)=\sum_{k=0}^{M} f_k(t) \tag{4.13}$$

where, $$f_k(t)=F_k\cos(\varphi_k(t)) \tag{4.14}$$

In this equation, $F_k(t)$ behaves as a harmonic comment and > 0, $\forall t$ and $\varphi'_k(t)$ are slower and also $> 0\ \forall t$.

Mathematically, the following are the steps used in EMD methods [167].

Step 1: Identification of all extrema of the original input signal $f(t)$

Step 2: Interpolation between the minima “envelope”

Step 3: Computation of minima and maxima average.

Step 4: Calculation of difference between signal and average of the signal.

Step 5: Residual iteration of the average

Here, the first four steps are the shifting steps and the fifth step is an iteration operation. A very important fact of this method is that it is highly adaptable and able to extract features of the non-stationary signal, which is a challenging task. However, mathematically it is difficult to model this algorithm. To overcome this problem, Ensemble EMD is used, in which, computation of several EMD decomposing of the input signal is done by artificial noise [157].

4.3.5. Discrete Wavelet Transform (DWT)

The wavelet transform is one of the most popular mathematical tools used to analyze a signal. It is superior to other transform methods of data compression, because of its multiresolution ability. *i.e.*, a signal can be analyzed by different scale or resolutions using the WT, which makes WT more popular and large number of applications in different areas. It is mainly classified into two types such as continuous wavelet transform (CWT) and discrete wavelet transform (DWT). A very important property of WT is that it can be used as a filter bank. In Fig. 2.21, wavelet filter bank structure is shown, where the input signal ($\chi(n)$) is divided into two frequency bands using lowpass *G* and highpass filter *H*, these signals are down-sampled by 2. Further, the low pass band is divided into two bands using lowpass and highpass filter, and then after again down-sampled by 2, d_1, d_2, and d_3 are three decomposition levels. This structure is called the tree-structured filter bank. It is done by a single prototype filter. From this prototype filter, all the analysis filters can be defined mathematically as [10]:

$$h_{a,b}(t) = \frac{1}{\sqrt{a}} h\left(\frac{t-b}{a}\right) \tag{4.15}$$

where, *a* and $b \in R$.

The continuous time WT can be defined for a signal *x(t)*

$$X_W(a,b) = \frac{1}{\sqrt{a}} \int_{-\infty}^{\infty} x(t) h^*\left(\frac{t-b}{a}\right) x(t) dt \tag{4.16}$$

where, the * is used for complex conjugate. A discrete wavelet transform is more compact and only required wavelet coefficients. DWT of a signal *x(t)* can be defined as [137]:

$$DWT_h x(m,n) = \int_{-\infty}^{\infty} x(t) h^*_{(m,n)}(t) dt \tag{4.17}$$

where, $h^*_{(m,n)} = 2^{-m} h(2^m t - n)$, *m* and *n* are the positive set of integers *(Z)*, and *a* and *b* are coefficients that can be calculated using equations given below:

$$a = 2^{-m} \tag{4.18}$$

$$b = n2^{-m} \tag{4.19}$$

scaling function ($\phi_{m,n}(t)$) is used for a finite number of coefficients, which can be obtained as:

$$\phi_{m,n}(t) = 2^{-m} \phi(2^m t - n) \tag{4.20}$$

DWT decomposes input sequence into two new sequences using lowpass $h_1(n)$ and highpass filter $g_1(n)$ at each level of decomposition. [10]

$$\phi(t) = \sum_k h(k)\phi(2t-k) \tag{4.21}$$

4.3.6. Empirical Wavelet Transform (EWT)

Empirical wavelet can be defined as the set of bandpass filters on each belongs to $\wedge_n$. Empirical wavelet is important for non- stationary signal analysis, because it has adaptability property. It is superior to another adaptable method in terms of less complexity and good mathematical corroboration, which can perform a consistent decomposition of a non-stationary signal. In EWT, Fourier point of view is taken for the bandpass filters. Here, IMF functions are used, because these are compact support and concerned with the spectrum of information. Here, the empirical wavelet function is considered which is shown in Eqn. (4.22) [34].

$$\hat{\phi}_n(\omega) = \begin{cases} 1 & \text{if } |\omega| \le \omega_n - \tau_n \\ \cos\left[\frac{\pi}{2}\beta\left[\frac{1}{2\tau_n}\left(|\omega| - \omega_n + \tau_n\right)\right]\right] & \text{if } \omega_n - \tau_n \le |\omega| \le \omega_n + \tau_n \\ 0 & \text{otherwise} \end{cases} \tag{4.22}$$

where, $\beta(x)$ is the function of $C^k([0,1])$ and defined in Eqn. (4.23).

$$\beta(x) = \begin{cases} 0 & \text{if } x \le 0 \text{ and } \beta(x) + \beta(1x) = 1 \ \forall x \in [0,1] \\ 1 & \text{if } x \ge 1 \end{cases} \tag{4.23}$$

and empirical wavelet can be expressed as:

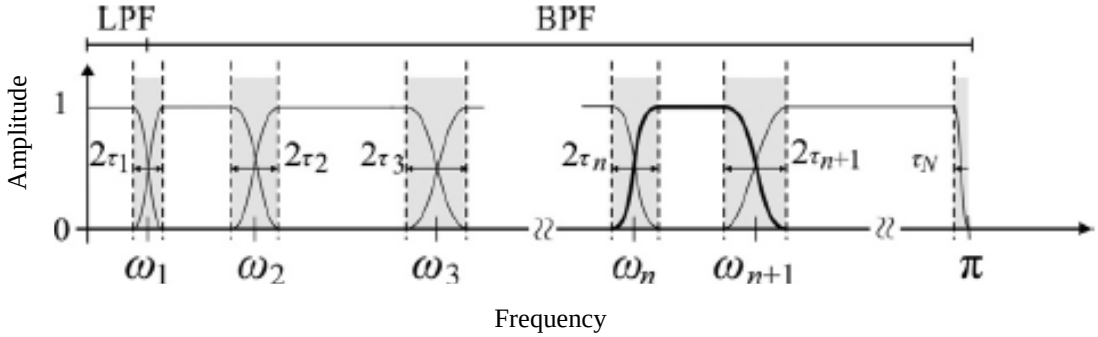

Fig. 4.4 EWT decomposition representation using low pass and band pass filters [18].

$$\hat{\psi}_n(\omega)=\begin{cases}1 & \text{if } \omega_n+\tau_n\le\omega_{n+1}-\tau_{n+1}\\ \cos\left[\frac{\pi}{2}\beta\left(\frac{1}{2\tau_{n+1}}\left(|\omega|-\omega_{n+1}+\tau_{n+1}\right)\right)\right] & \text{if } \omega_n-\tau_n\le\omega_{n+1}+\tau_{n+1}\\ \sin\left[\frac{\pi}{2}\beta\left(\frac{1}{2\tau_n}\left(|\omega|-\omega_n+\tau_n\right)\right)\right] & \text{if } \omega_n-\tau_n\le|\omega|\le\omega_n+\tau_n\\ 0 & \text{otherwise}\end{cases} \tag{4.24}$$

There are several options possible to choose τ_n. In this work, τ_n proportional to ω_n *i.e.*, $0<\gamma<1$, thus $\forall n>0$. On putting these values in Eqns. (4.23) and (4.24):

$$\hat{\phi}_n(\omega)=\begin{cases}1 & \text{if } |\omega|\le(1-\gamma)\omega_n\\ \cos\left[\frac{\pi}{2}\beta\left(\frac{1}{2\gamma\omega_n}\left(|\omega|-(1-\gamma)\omega_n\right)\right)\right] & \text{if } (1-\gamma)\omega_n\le|\omega|\le(1+\gamma)\omega_n\\ 0 & \text{otherwise}\end{cases} \tag{4.25}$$

and

$$\hat{\psi}_n(\omega)=\begin{cases}1 & \text{if } (1+\gamma)\omega_n\le|\omega|\le(1-\gamma)\omega_{n+1}\\ \cos\left[\frac{\pi}{2}\beta\left(\frac{1}{2\gamma\omega_{n+1}}\left(|\omega|-\omega(1-\gamma)\omega_{n+1}\right)\right)\right] & \text{if } (1-\gamma)\omega_{n+1}\le|\omega|\le(1+\gamma)\omega_{n+1}\\ \sin\left[\frac{\pi}{2}\beta\left(\frac{1}{2\gamma\omega_n}\left(|\omega|-(1-\gamma)\omega_n\right)\right)\right] & \text{if } (1-\gamma)\omega_n\le|\omega|\le(1+\gamma)\omega_n\\ 0 & \text{otherwise}\end{cases} \tag{4.26}$$

The most important part of the signal processing is the segmentation of a signal. In WT method, the segmentation of a signal is done, to separate different part of the signal in the frequency domain. EWT is an adaptive wavelet transform capable of extracting individual instantaneous frequencies of a signal. Fig. 4.4 shows the EWT decomposition with lowpass and highpass filters. Here, $\omega_1, \omega_2 \ldots\ldots\ldots \omega_n$ are different cutoff frequencies for these filters. Mathematically, EWT is defined in Eqns. (4.27) to (4.31) [136].

$$W_f^{\varepsilon}(n,t)=\langle f,\psi_n\rangle=\int f(\tau)\overline{\psi_n(\tau-t)}d\tau \tag{4.27}$$

here, $W_f^{\varepsilon}(n,t)$ is EWT,

$$W_f^{\varepsilon}(0,t)=\langle f,\phi_1\rangle=\int f(\tau)\overline{\phi_1(\tau-t)}d\tau \tag{4.28}$$

$$\overline{f(t)}=W_f^{\varepsilon}(0,t)\times\phi_1(t)+\sum W_f^{\varepsilon}(n,t)\times\psi_n(t) \tag{4.29}$$

Consequently, empirical mode f_k , can be written as

$$f_0(t) = w_f^{\varepsilon}(0,t) \times \varphi_1(t) \tag{4.30}$$

$$f_k(t) = w_f^{\varepsilon}(k,t) \times \varphi_k(t) \tag{4.31}$$

4.4. Parameter Extraction Techniques

Another class of compression techniques is parameter extraction compression (PEC) techniques. By utilization of these techniques, high compression can be achieved; however, these methods are irreversible. In these techniques, specific characteristics /features (*i.e.*, amplitude and time index/duration) of a signal are extracted, and then extracted features are employed for classification, based on the basis of prior knowledge of the signal features. Extraction of features can be done using any feature extraction technique, *viz*., artificial neural network, WT, peak detection, slop detection method, *etc*. For reconstruction of the signal, extracted features are used. The main aim of this type of data compression is to quantize a small set of extracted features of the signal, excellently enough to render a precisely unnoticeable distortion. Methods, *viz*., peak-peaking methods, cycle-pool-base compression (CPBC) algorithm, linear prediction methods, and neural network methods are basically utilized for this type of compression [14].

In peak-peaking compression techniques, the sampling rate of continuous data at the peaks (amplitude and location) and other significant points are extracted. This method involves all significant feature extraction of the original signal that can express most of the signal information. Here, the features are: peaks value, zero-crossing intervals, slope changes, and on-set and offset points of the signal. The original signal is replaced by the extracted features. The reconstruction of signal can be done by using a suitable fitting method for example: polynomial fitting techniques, straight lines or parabolic function. In some studies, spline functions are also used for reconstruction of the signal [85]. In CPBC technique, a template-matching algorithm is used. This method is analogous to average beat subtraction and residual differencing (ABSRD) method of compression, in which two distinct template banks are utilized. It is subjected to fiducial point occurrence [66]. Conceptually, CPBC is developed for text compression *i.e.*, analogous to dictionary-based coding.

4.5. 2-Dimensional Compression Techniques

In 1D data compression techniques, sample-to-sample (intra-beat) correlation is employed for compression of the signal. In case of ECG signal, both intra-beat, as well as beat-to-beat (inter-beat) correlations can be used for the compression. Therefore, a 2D representation of ECG data may yield better performance in terms of compression. In several studies, ECG compression is done by considering 1D ECG signal as a 2D image, where exploiting of inter and intra-beat correlations is used by utilizing the suitable encoder technique [84]. In these techniques, preprocessing, QRS detection, ECG segmentation, and transformation are done. The "cut and align beats approach and 2D DCT" and "period normalization and truncated SVD algorithm" are available preprocessing methodologies to acquire the better performance of compression [79,89]. Similar to JPEG2000 preprocessing, these methodologies are also often associated with the use of state-of-the-art image encoders. In a study, 2D ECG signal compression by converting 1D ECG into an image is done, where the researchers have used inter and intra-beat dependencies for compressing irregular ECG signals. And for preprocessing, period sorting technique is used. Given technique is based on the theory that periods with comparable lengths tend to be highly correlated [97]. Another technique of preprocessing consisting of period length normalization, period preprocessing, QRS detector and image transform is also used for 2D ECG compression. The primary aim of the technique is to preprocess the data by minimizing the vertical high-frequency content. The smoothing of t image is accomplished by minimizing the sharp discontinuities along the vertical direction with variance based complexity sorting methodology [134].

4.6. Performance Parameters

This section includes the parameters which are used for estimating the performance data compression and reconstruction [104,105,107].

- Compression ratio (*CR*) [17]:

$$CR = \frac{N_x}{H + N_s + N_v} \tag{4.32}$$

  In this equation, N_x is the number of bits in *x(n)*, N_v is the number of bits used to code the significant coefficients, N_s represents the number of bits in the compressed implication map and *H* is a 64-bit header [32].

- Percent root mean square difference (*PRD*)

$$PRD = \left(\frac{Reconstrutcted\ noise\ energy}{Origional\ signal\ energy}\right)^{1/2} \times 100 \quad (4.33)$$

- Percent root mean square difference normalized (PRDN) [],

$$PRDN(\%) = 100 \times \sqrt{\frac{\sum_{n=1}^{N}(x(n)-y(n))^2}{\sum_{n=1}^{N}(x(n)-\bar{x}(n))^2}} \quad (4.34)$$

where, $\bar{x}(n)$ is the mean value of input signal.

- Correlation coefficient (γ_{xy}) [50].

$$\gamma_{xy} = \frac{\sum_{n=1}^{N}(x(n)-\bar{x}(n))(y(n)-\bar{y}(n))}{\sqrt{\sum_{n=1}^{N}(x(n)-\bar{x}(n))^2(y(n)-\bar{y}(n))^2}} \quad (4.35)$$

where, $\bar{y}(n)$ is the mean value of input signal.

- Signal to noise ratio *(SNR)* [107]

$$SNR = 100log_{10}\left\{\frac{\sum x^2(n)}{\sum |x(n)-y(n)|^2}\right\} \quad (4.36)$$

- Mean Square error (*MSE*)[136]

$$MSE = \frac{1}{2}\sum |x(n) - y(n)|^2 \quad (4.37)$$

- Maximum error (*ME*) [143]

$$ME = \max_n |\, x(n) - y(n) \,| \quad (4.38)$$

- Quality Score (*QS*) [107]

$$QS = \frac{CR}{PRD} \quad (4.39)$$

4.7. Summary

In this chapter, data compression techniques used for ECG signal compression are discussed. Most of the techniques are belongs to the lossy compression technique. These techniques provide high compression performance, which is always needed for high transmission within a limited channel capacity. ECG data compression techniques are broadly classified DDC, transformation compression PEC. However, the 2D data compression technique is also used to compress the ECG data. From the last two decades transformational compression techniques are more preferred than other data compression technique for compression of ECG data. Hybrid methodologies are also used to compress the data compression of ECG rhythms. The choice of algorithms for the compression of ECG rhythms must have tradeoff between the data compression and information content of the signal *i.e.*, the reconstructed data must be within the acceptable fidelity limits.

CHAPTER 5

DATA COMPRESSION OF ECG SIGNAL USING WAVELET FILTER BANK

5.1. Overview

The electrocardiogram (ECG) is one of the most important physiological signals that illustrates the electromechanical activity of human heart. Compression of an ECG signal has given much consideration to researchers, since the ECG's computer-aided analysis has come into being. In some critical cases, *viz*., astronauts, a person under cardiac surveillance and ambulatory patients, continuous ECG data recording and transmitting it from one location to other location is required. However, the size of recorded data becomes so voluminous. Therefore, transmission of data becomes practically impossible. Hence, the compression of ECG data is important before transmission. In several cases, ECG data is used to store for later use, for example: in research in the area of health care. As discussed in Chapters 1 and 3, several data compression schemes are used for ECG signal compression. These schemes are broadly classified into three groups, such as a) direct data compression b) transformation compression, and c) parameter extraction based compression. The primary objective of any ECG data compression scheme is to acquire maximum data reduction without loss of diagnostic information [72]. Theoretically, data compression is the procedure of extracting and removing the unnecessary /redundancy /un-useful information from the data. In direct data compression methods, samples of the signal are directly handled to provide the compression. Parameter extraction based compression provides admirable performance in terms of compression ratio, however exact signal reconstruction is not possible. In transformation compression methods, data is transformed in other domain, and then compress by applying, thresholding /quantization /encoding. These methods are generally preferred for the compression of ECG rhythms over other methods, because of easy implementation and small computational time requirement. In this chapter, ECG data compression using

transformation-based techniques are presented, such that; a) wavelet packet algorithm with RLE, b) quadrature mirror filter (QMF) bank with RLE based, c) wavelet with Huffman encoding, d) wavelet and LZW and e) empirical wavelet transform and RLE. In this work, results have been tested using MIT/BIH (Massachusetts Institute of Technology/Beth Israel Hospital) arrhythmia databases [15]. The performance of these methodologies is examined by quantitative and qualitative manner. For quantitative analysis different fidelity parameters are used which are given in Eqns. (4.32) to (4.39).

5.2. Data Compression using Wavelet Packet Decomposition and RLE

In this section, the wavelet packet (WP) based compression methodology is presented to compress the ECG signals. This mythology employs the WP, level thresholding along with RLE by executing the steps as follows;

Step 1: Acquisition of ECG data

In this work, MIT-BIH arrhythmia database has been chosen for examining the performance of proposed method.

Step 2: Signal decomposition

Wavelet packet decomposition is done to divide the ECG signal into number of frequency bands. Here, level 3/4 decomposition is done. For example, if the total frequency of a signal is 100Hz, by applying 3 level decomposition using WP, produce 8 signals, *viz*., *Aaa* (0-12.5Hz), *Aad* (above 12.50-25Hz), *Ada* (above 25-37.5Hz), *Add* (above 37.5-50Hz), *Daa* (above 50-62.5Hz), *Dad* (above 62.5-75Hz), *Dda* (above 75-87.5Hz), and *Ddd* (above 87.5-100Hz). The lowest frequency signal (*Add*) is also known as approximation subband and reaming signals are known as detail subbands.

Step 3: Application of thresholding

Level thresholding is applied to all decomposed signal, except the lowest frequency signal (*Add*). Here, all the coefficients, which have magnitude less than the threshold value are replaced by zero.

Step 4: Vector '*v*' formation

After obtaining the thresholded coefficients of all bands, these are placed in a vector (*v*), which is illustrated in Eqn. (5.1).

$$v = [Aaa\ thr_7\ thr_6\ thr_5\ thr_4\ thr_3\ thr_2\ thr_1] \tag{5.1}$$

where, thr_1 to thr_7 are the signals obtained after applying thresholding, as depicted in Table 5.1.

Step 5: Application of modified run-length encoding

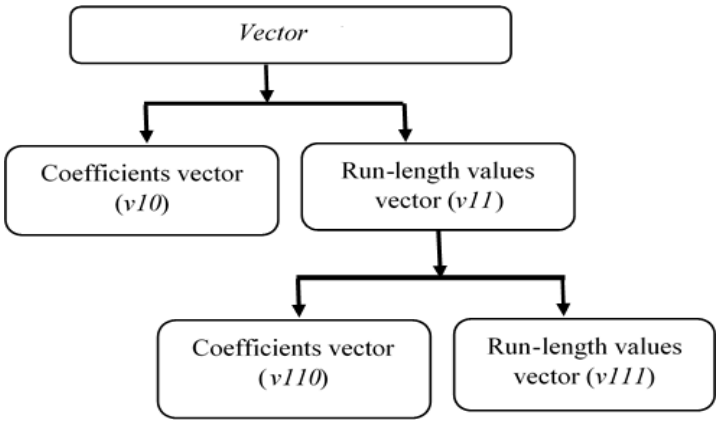

Fig. 5.1 Modified RLE.

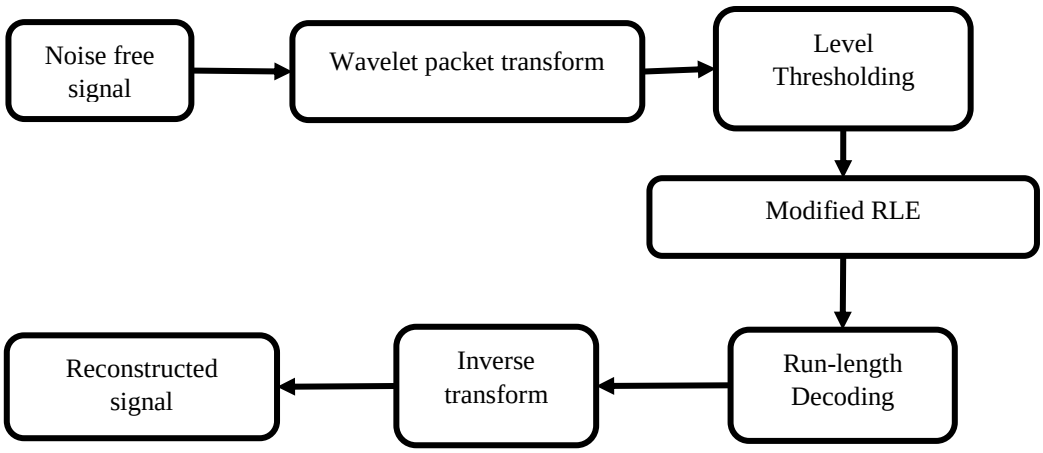

Fig. 5.2 ECG data compression methodology.

In this step, RLE is applied to *v*. RLE is a lossless compression method, therefore it increases the performance of compression without loss of information. In this work, modified RLE is deployed in which, two-stage RLE is used. Therefore, the output of modified RLE is in the form of three vectors (v_{10}, $v_{110,}$ and v_{111}). The modified RLE is presented in Fig. 5.1.

Reconstruction of data is done by following steps:

Step a: Application of run-length decoding

Run-length decoding (RLD) is applied two times *i.e.*, firstly to the vectors v_{110} and v_{111}, which gives one output vector "v_{11}", again RLD is applied to v_{11} and v_{10}, and it provides reconstructed coefficients of vector *v*.

Step b: Coefficient distribution of *v*

The coefficients of *v* are divided into eight groups to reconstruct signals, such as: *Aaa*, thr_7, thr_6, thr_5, thr_4, thr_3, thr_2 and thr_1.

Step c: Inverse transform

The inverse transform is used to reconstruct the signal. These steps are depicted in the block diagram given in Fig. 5.2.

In this section, experimental results of WP and RLE based compression method are described. Here, parameters for evaluating the performance are considered which are given in Chapter 4 Section 4.6. The experiments are done by using different mother wavelets, such as: biorthogonal, Daubechies, symlet and Fejér-Korovkin. And the 3/4level of decomposition is taken. The tabular results of these experiments are presented in Tabls 5.2 (a), (b), (c), (d) and (e).

The methodology illustrated in Fig. 5.2 is based on decomposition of the signal into frequency signals. Here, the signal is decomposed into a number of frequency bands using wavelet packet based algorithm. In Figs. 5.3 and 5.4, decomposed signals are depicted. Next, compression is achieved by truncating the unwanted coefficients by applying level thresholding. To achieve compression without affecting the diagnostic information, RLE is applied in modified form. The compression performance is measured by computing the *CR*. The highest value of *CR* is 10. For recovering the signal, RLD is applied and signal is reconstructed using the inverse transform. It is found that the reconstructed signal is exact replica of the original signal. Both original and reconstructed signals are depicted in Fig. 5.5. The performance of data decompression method is also evaluated by comparing diagnostic information of both signals (original and reconstructed signal).

Table 5.1. Signals naming before and after thresholding

Before thresholding	*Aaa*	*Aad*	*Ada*	*Add*	*Daa*	*Dad*	*Dda*	*Ddd*
After thresholding	-	thr_7	thr_6	thr_5	thr_4	thr_3	thr_2	thr_1

Table 5.2. (a) Fidelity parameters of proposed data compression technique (using bior2.8)

Level	Signal	CR	PRD	SNR	CC	QS
	MIT-BIH-100	5.6774	0.3621	48.8246	0.9942	15.67909
	MIT-BIH-101	6.2301	0.3214	49.8579	0.9965	19.38426
	MIT-BIH-102	4.3909	0.2989	50.4907	0.9999	14.6902
	MIT-BIH-103	5.6021	0.4245	47.4431	0.9979	13.19694
L=3	MIT-BIH-104	5.2932	0.2079	53.6426	0.9989	25.46032
D1=0	MIT-BIH-105	5.0286	0.1605	55.8910	0.9997	31.33084
	MIT-BIH-106	5.8830	0.4715	46.5295	0.9979	12.4772
	MIT-BIH-107	4.6829	0.3824	48.3486	0.9997	12.24608
	MIT-BIH-108	3.4010	0.1085	59.2892	0.9994	31.34562
	MIT-BIH-109	4.4277	0.1938	54.2527	0.9997	22.84675
	MIT-BIH-100	7.000	0.4815	46.3484	0.9897	14.5379
	MIT-BIH-101	7.000	0.3804	48.3950	0.9951	18.40168
	MIT-BIH-102	5.4768	0.4446	47.0414	0.9998	12.31849
	MIT-BIH-103	6.6469	0.6784	43.3699	0.9945	9.797907
L=4	MIT-BIH-104	7.000	0.2653	51.5252	0.9982	26.38522
D1=0, Ad=0	MIT-BIH-105	6.4000	0.2992	50.4813	0.9989	21.39037
	MIT-BIH-106	6.1202	0.5517	45.1657	0.9971	11.09335
	MIT-BIH-107	5.7143	0.5349	45.4348	0.9995	10.68293
	MIT-BIH-108	5.0564	0.1801	54.8895	0.9984	28.07551
	MIT-BIH-109	5.5309	0.4079	47.7883	0.9987	13.55945
	MIT-BIH-100	8.4528	0.5117	45.8200	0.9883	16.51905
	MIT-BIH-101	8.0866	0.4133	47.6742	0.9943	19.56593
	MIT-BIH-102	6.4928	0.6935	43.1787	0.9996	9.362365
	MIT-BIH-103	8.3895	0.7136	42.9313	0.9939	11.75659
L=4	MIT-BIH-104	7.1565	0.4116	47.7097	0.9955	17.38703
D1=0	MIT-BIH-105	6.9565	0.4081	47.7838	0.9980	17.04607
	MIT-BIH-106	7.0662	0.5796	44.7375	0.9968	12.19151
	MIT-BIH-107	6.8085	0.6372	43.9149	43.9149	10.68503
	MIT-BIH-108	5.5309	0.2675	51.4540	0.9965	20.67626
	MIT-BIH-109	7.0000	0.5641	44.9721	0.9975	12.40915

Table 5.2 (b) Fidelity parameters of proposed data compression technique (using bior1.5)

Level	Signal	CR	PRD	SNR	CC	QS
	MIT-BIH-100	5.5568	0.8460	41.4531	0.9691	6.5687
	MIT-BIH-101	5.8743	0.7846	42.1069	0.9797	7.4869
	MIT-BIH-102	3.8216	1.0871	39.2743	0.9989	3.5153
	MIT-BIH-103	4.5286	1.2883	37.7994	0.9807	3.5151
L=3	MIT-BIH-104	4.0314	0.4452	47.0286	0.9948	9.0549
D1=0	MIT-BIH-105	4.5689	0.7517	42.4793	0.9934	6.0782
	MIT-BIH-106	3.5633	1.0191	39.8359	0.9903	3.4966
	MIT-BIH-107	3.5085	1.2267	38.2249	0.9974	2.8600
	MIT-BIH-108	3.3215	0.2663	51.4923	0.9966	12.4723
	MIT-BIH-109	3.2480	0.5909	44.5691	0.9973	5.4963
	MIT-BIH-100	6.2041	2.6543	31.5209	0.6975	2.3373
	MIT-BIH-101	5.7826	2.4567	32.1929	0.8016	2.3538
	MIT-BIH-102	4.4895	4.5388	26.8611	0.9815	0.9891
	MIT-BIH-103	5.2673	4.3616	27.2071	0.7795	1.2077
L=4	MIT-BIH-104	6.1503	1.3528	37.3756	0.9523	4.5465
D1=0, Ad=0	MIT-BIH-105	5.4845	2.6798	31.4378	0.9161	2.0466
	MIT-BIH-106	4.7713	4.3176	27.2951	0.8275	1.1051
	MIT-BIH-107	5.1401	4.4471	27.0384	0.9660	1.1558
	MIT-BIH-108	5.1776	0.9673	40.2889	0.9548	5.3527
	MIT-BIH-109	5.3200	2.2966	32.7782	0.9596	2.3164
	MIT-BIH-100	7.5730	2.6818	31.4316	0.6924	2.8239
	MIT-BIH-101	6.2222	2.4605	32.1795	0.8012	2.5288
	MIT-BIH-102	4.9145	4.5566	26.8272	0.9814	1.0786
	MIT-BIH-103	6.0974	4.3658	27.1987	0.7795	1.3966
L=4	MIT-BIH-104	7.1171	1.4414	36.8244	0.9463	4.9377
D1=0	MIT-BIH-105	5.6446	2.6867	31.4156	0.9157	2.1009
	MIT-BIH-106	5.6000	4.3519	27.2265	0.8254	1.2868
	MIT-BIH-107	5.5707	4.4892	26.9567	0.9654	1.2409
	MIT-BIH-108	5.8947	1.0095	39.9178	0.9510	5.8392
	MIT-BIH-109	5.8301	2.4420	32.2451	0.9543	2.3874

Table 5.2 (c) Fidelity parameters of proposed data compression technique (using bior3.5)

Level	Signal	CR	PRD	SNR	CC	QS
	MIT-BIH-100	5.8039	0.2659	51.5054	0.9969	21.82738
	MIT-BIH-101	6.6624	0.2119	53.4758	0.9985	31.44125
	MIT-BIH-102	5.7080	0.2393	52.4223	0.9999	23.8529
	MIT-BIH-103	6.4750	0.2507	52.0183	0.9993	25.82768
L=3	MIT-BIH-104	6.1667	0.2290	52.8043	0.9986	26.92882
D1=0	MIT-BIH-105	5.1160	0.1134	58.9098	0.9998	45.11464
	MIT-BIH-106	6.6410	0.3324	49.5678	0.9990	19.97894
	MIT-BIH-107	5.8039	0.3310	49.6028	0.9998	17.53444
	MIT-BIH-108	3.7000	0.1138	58.8769	0.9994	32.51318
	MIT-BIH-109	4.8411	0.1829	54.7540	0.9997	26.46856
	MIT-BIH-100	8.8163	0.5418	45.3232	0.9869	16.27224
	MIT-BIH-101	8.5714	0.4788	46.3976	0.9923	17.90184
	MIT-BIH-102	7.8261	0.5611	45.0199	0.9997	13.94778
	MIT-BIH-103	9.1525	0.8756	41.1538	0.9909	10.45283
L=4	MIT-BIH-104	8.5714	0.4730	46.5032	0.9941	18.12135
D1=0, Ad=0 yes	MIT-BIH-105	8.1509	0.3074	50.2449	0.9989	26.51561
	MIT-BIH-106	8.4375	0.8490	41.4222	0.9932	9.938163
	MIT-BIH-107	8.2443	0.9272	40.6566	0.9985	8.891609
	MIT-BIH-108	6.9903	0.2413	52.3499	0.9972	28.96933
	MIT-BIH-109	8.8889	0.5605	45.0289	0.9976	15.85888
	MIT-BIH-100	9.0011	0.6644	43.5510	0.9810	13.54606
	MIT-BIH-101	8.9256	0.5241	45.6110	0.9907	17.03034
	MIT-BIH-102	8.3077	1.1152	39.0533	0.9989	7.449516
	MIT-BIH-103	9.2704	0.8915	40.9971	0.9905	10.39865
L=4	MIT-BIH-104	9.9083	0.7536	42.4569	0.9850	13.14796
D1=0 yes	MIT-BIH-105	8.5039	0.3826	48.3442	0.9983	22.22661
	MIT-BIH-106	9.1915	0.9075	40.8427	0.9922	10.12837
	MIT-BIH-107	8.3398	1.0231	39.8020	0.9982	8.1515
	MIT-BIH-108	8.0297	0.3547	49.0034	0.9939	22.638
	MIT-BIH-109	9.7297	0.8164	41.7625	0.9949	11.91781

Table 5.2 (d) Fidelity parameters of proposed data compression technique (using bior6.8)

Level	Signal	CR	PRD	SNR	CC	QS
	MIT-BIH-100	9.2562	0.7149	42.9154	0.9770	12.94755
	MIT-BIH-101	8.7843	0.5851	44.6559	0.9884	15.01333
	MIT-BIH-102	7.6976	0.5924	44.5481	0.9997	12.99392
	MIT-BIH-103	8.5824	0.7271	42.7680	0.9937	11.8036
L=4	MIT-BIH-104	7.6190	0.4276	47.3785	0.9952	17.81805
D1=0	MIT-BIH-105	9.2181	0.7501	42.4976	0.9933	12.28916
	MIT-BIH-106	8.4528	0.4696	46.5655	0.9979	18
	MIT-BIH-107	7.2492	0.9921	40.0686	0.9983	7.306925
	MIT-BIH-108	6.4368	0.2641	51.5646	0.9966	24.37259
	MIT-BIH-109	7.9715	0.5807	44.7213	0.9974	13.7274
	MIT-BIH-100	9.2946	0.7551	42.4398	0.9744	12.3091
	MIT-BIH-101	8.9600	0.9569	40.3831	0.9687	9.36357
	MIT-BIH-102	8.4528	0.9126	40.7941	0.9993	9.262327
	MIT-BIH-103	5.6281	0.7440	42.5687	0.9934	7.564651
L=4	MIT-BIH-104	9.4515	0.7015	43.0789	0.9870	13.47327
D1=0 yes	MIT-BIH-105	9.4118	1.0000	40.0002	0.9881	9.4118
	MIT-BIH-106	8.9960	0.5751	44.8055	0.9969	15.6425
	MIT-BIH-107	8.1752	1.3453	37.4238	0.9969	6.07686
	MIT-BIH-108	7.2258	0.4372	47.1861	0.9907	16.52745
	MIT-BIH-109	8.6154	0.8892	41.0196	0.9939	9.688934

Table 5.2 (e) Fidelity parameters of proposed data compression technique (sym)

Level	Signal	CR	PRD	SNR	CC	QS
Sym2	MIT-BIH-100	8.3967	0.7039	43.0493	0.9777	11.9281
L=4	MIT-BIH-101	8.4667	0.6279	44.0420	0.9867	13.4838
D1=0 yes	MIT-BIH-102	5.7892	0.9102	40.8174	0.9993	6.3604
	MIT-BIH-103	6.7508	0.9079	40.8390	0.9901	7.4354
	MIT-BIH-104	6.5338	0.4516	46.9046	0.9946	14.4675
	MIT-BIH-105	7.0311	0.7173	42.8855	0.9939	9.8017
	MIT-BIH-106	6.5128	0.7388	42.6295	0.9948	8.8154
	MIT-BIH-107	6.2331	0.9062	40.8556	0.9986	6.8784
	MIT-BIH-108	5.6602	0.3217	49.8507	0.9950	17.5941
	MIT-BIH-109	5.7401	0.5443	45.2838	0.9977	10.5465
Fk4 L=4	MIT-BIH-100	9.0131	2.1807	33.2283	0.7979	4.1332
D1=0 yes	MIT-BIH-101	9.6449	2.1446	33.3731	0.8466	4.4973
	MIT-BIH-102	5.5335	3.3561	29.483	0.9898	1.6488
	MIT-BIH-103	6.8344	3.2072	29.8775	0.8808	2.1310
	MIT-BIH-104	7.7594	1.2705	37.9206	0.9579	6.1074
	MIT-BIH-105	9.3818	2.1601	33.3106	0.9444	4.3433
	MIT-BIH-106	8.1905	3.2210	29.8401	0.9035	2.5428
	MIT-BIH-107	4.8112	3.3675	29.4538	0.9809	1.4287
	MIT-BIH-108	9.0526	0.8991	40.9242	0.9606	10.0690
	MIT-BIH-109	7.6729	1.8788	34.5224	0.9731	4.0839
Db10	MIT-BIH-100	7.4492	0.6154	44.2168	0.9830	12.1045
L=4	MIT-BIH-101	7.9164	0.5339	45.4509	0.9904	14.8276
D1=0 yes	MIT-BIH-102	6.7219	0.4458	47.0179	0.9998	15.0796
	MIT-BIH-103	6.2590	0.4030	47.8939	0.9981	15.5309
	MIT-BIH-104	6.2762	0.3488	49.1473	0.9968	17.9914
	MIT-BIH-105	7.2821	0.5685	44.9056	0.9962	12.8096
	MIT-BIH-106	8.1434	0.5622	45.0021	0.9970	14.4847
	MIT-BIH-107	7.0779	0.8569	41.3416	0.9987	8.2601
	MIT-BIH-108	5.0265	0.2073	53.6673	0.9979	24.2458
	MIT-BIH-109	5.3585	0.4765	46.4386	0.9983	11.2453

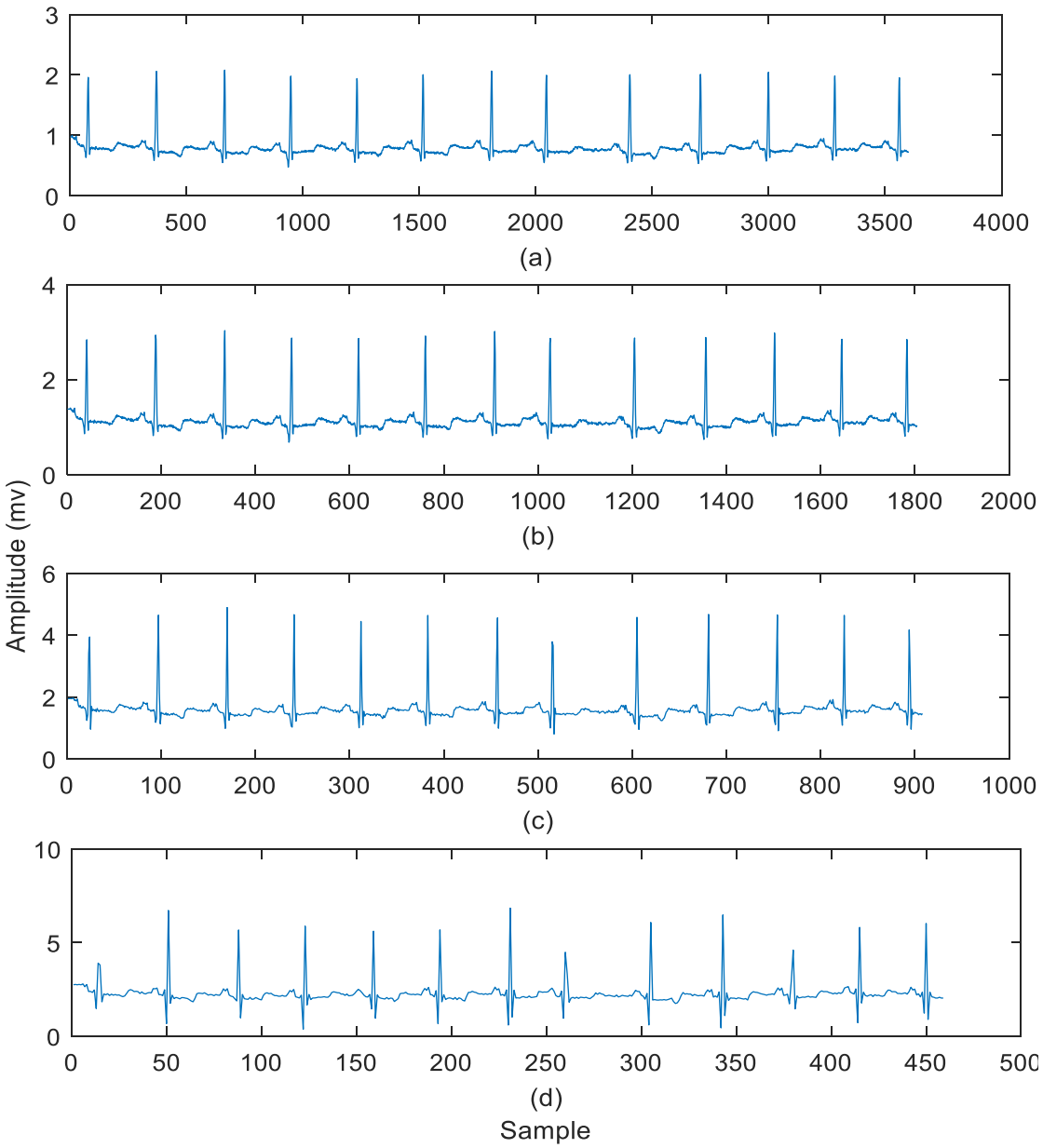

Fig. 5.3 Signal decomposition of lower frequency bands.

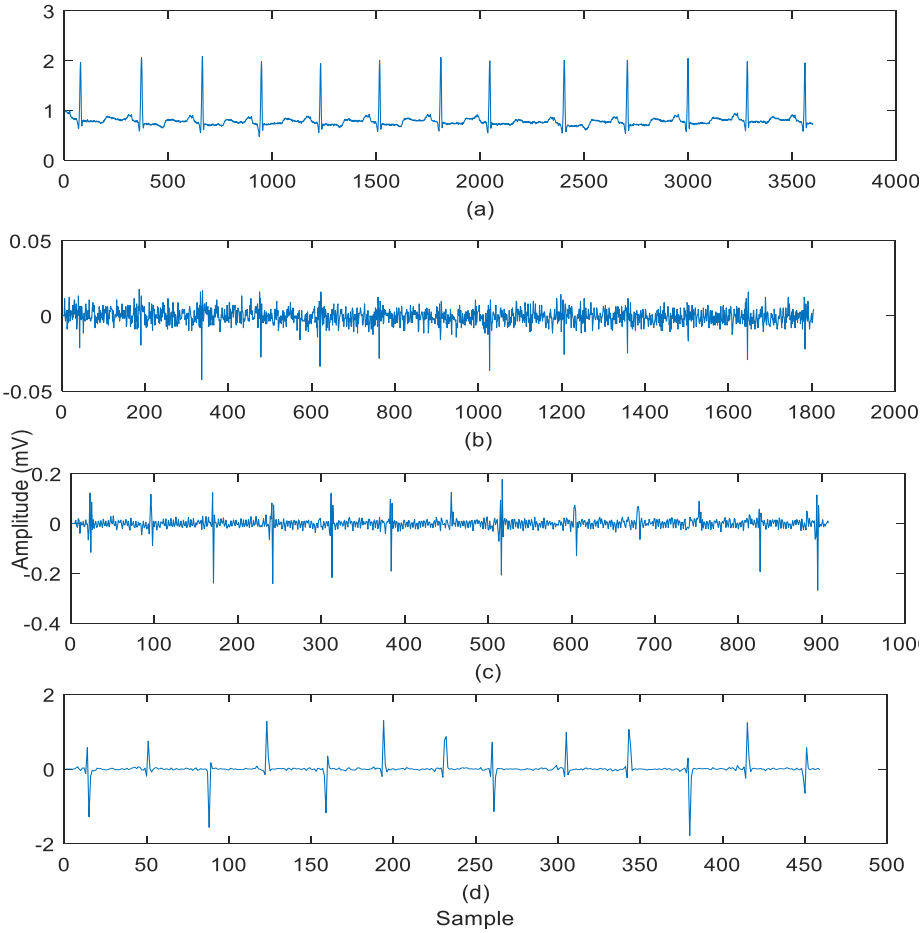

Fig. 5.4 Signal decomposition of higher frequency.

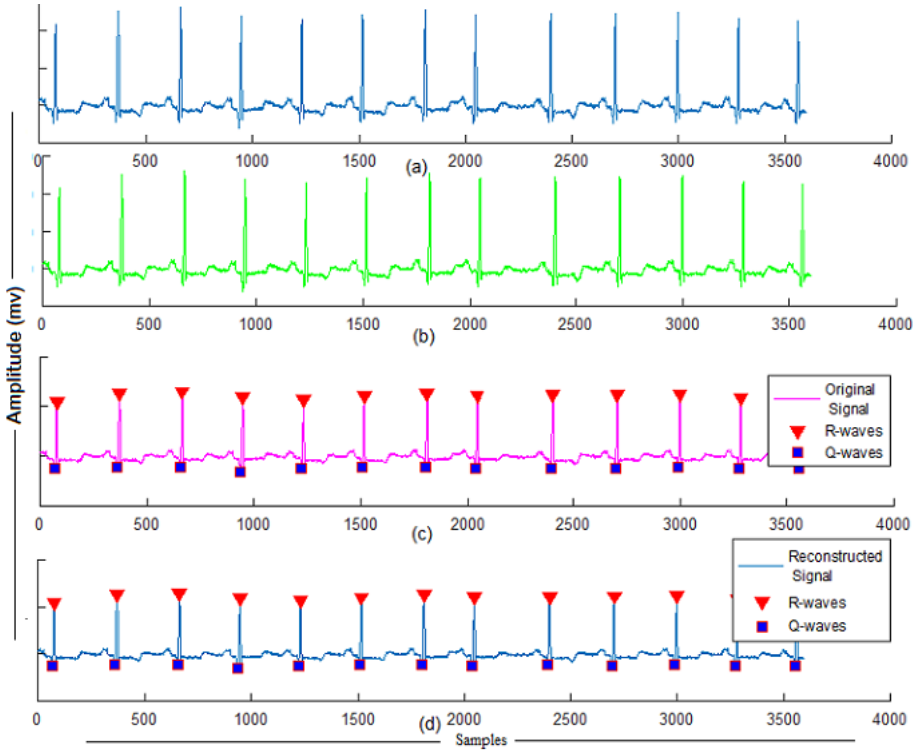

Fig. 5.5 (a) Original signal, (b) Reconstructed signal after decompression, (c) Beat detection in the original signal and d) Beat detection in the reconstructed signal.

The beat detection is accomplished by applying amplitude and time thresholding, and extracting the maxima for R peak, which is depicted in Fig. 5.5 (c) and (d). It has been demonstrated that beats of the original and reconstructed signal are identical.

5.3. Data Compression using Two-Channel Filter Bank

In this section, data compression is carried out using a two-channel QMF filter bank and RLE. The data compression is done by using the following steps;

Step 1: ECG signal acquisition

Here also, the ECG signal is taken from physionet (MIT-BIH database lead II data).

Step 2: Noise elimination

Noise elimination is done using the methodology given in chapter 3

Step 3: Decomposition of Signal

ECG signal is decomposed into five frequency bands (four level decomposition) using analysis QMF bank. QMF bank is designed using FIR filter. Here, first analysis lowpass filter ($H_0(z)$) is designed, and then other filters are drieved using the following expressions;

$$H_1(z) = H_0(-z) \ , \tag{5.2}$$

$$F_0(z) = H_0(z) \tag{5.3}$$

and,

$$F_1(z) = -H_1(z) \tag{5.4}$$

Step 4: Thresholding

Thresholding is used to truncate the irrelevant coefficients. Here, adaptive thresholding is done by using Stein's principle given in [304].

Step 5: Coefficients vector formation

$$v = [A5\ thr4\ thr3\ thr2] \tag{5.5}$$

Coefficients of D_1 are not considered, because this signal is having high-frequency low amplitude signal.

Step 6: Run-length encoding

Here, also modified RLE is used.

Data reconstruction is done using the following steps;

Step a: Run-length decoding

Step b: Coefficient partition

After **Step a**, vector "*v*" is reconstructed, in **Step b**, the coefficients of *v* are divided into four signals: *A5 thr4 thr3 thr2*

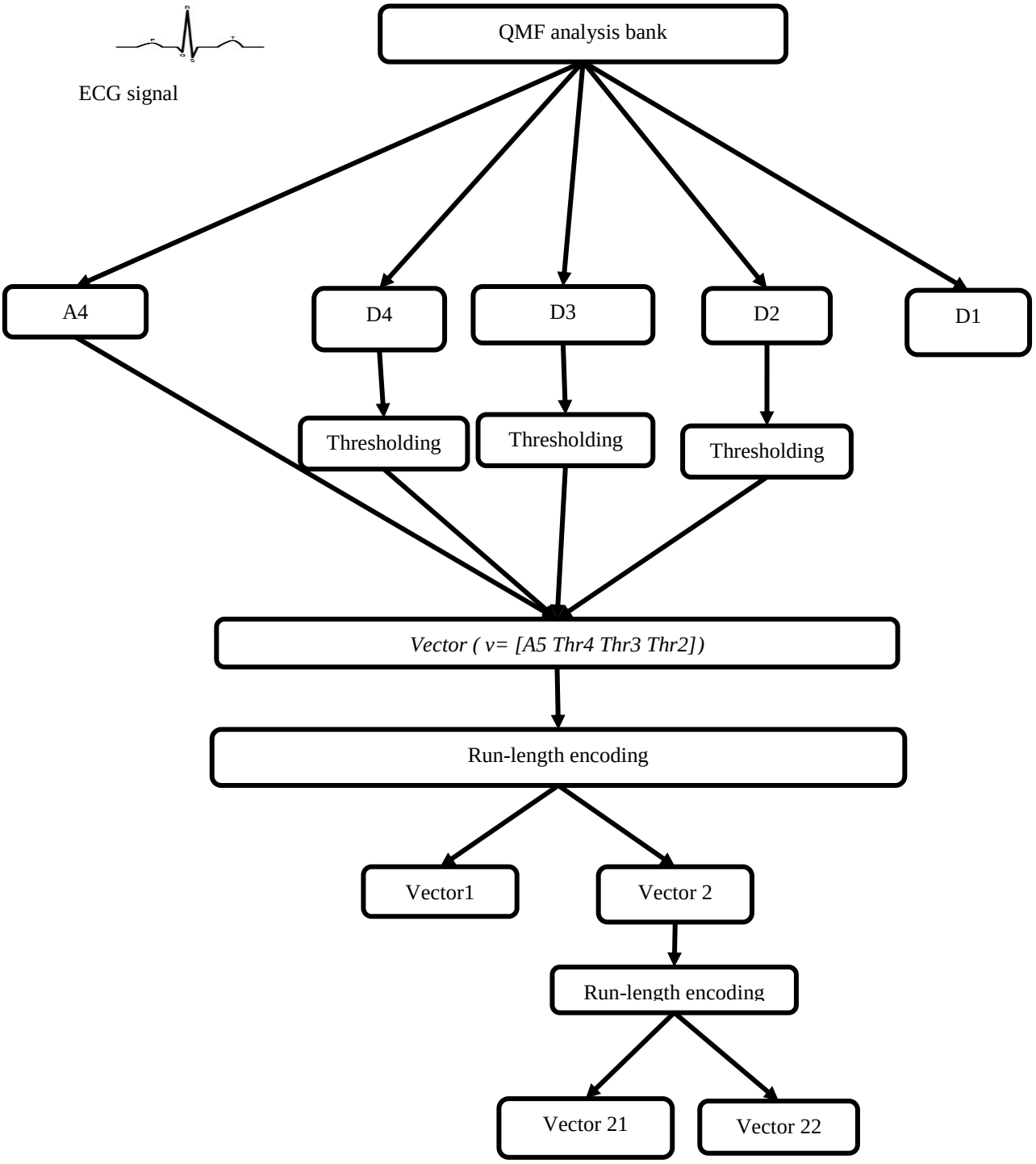

Fig. 5.6 Proposed data compression technique.

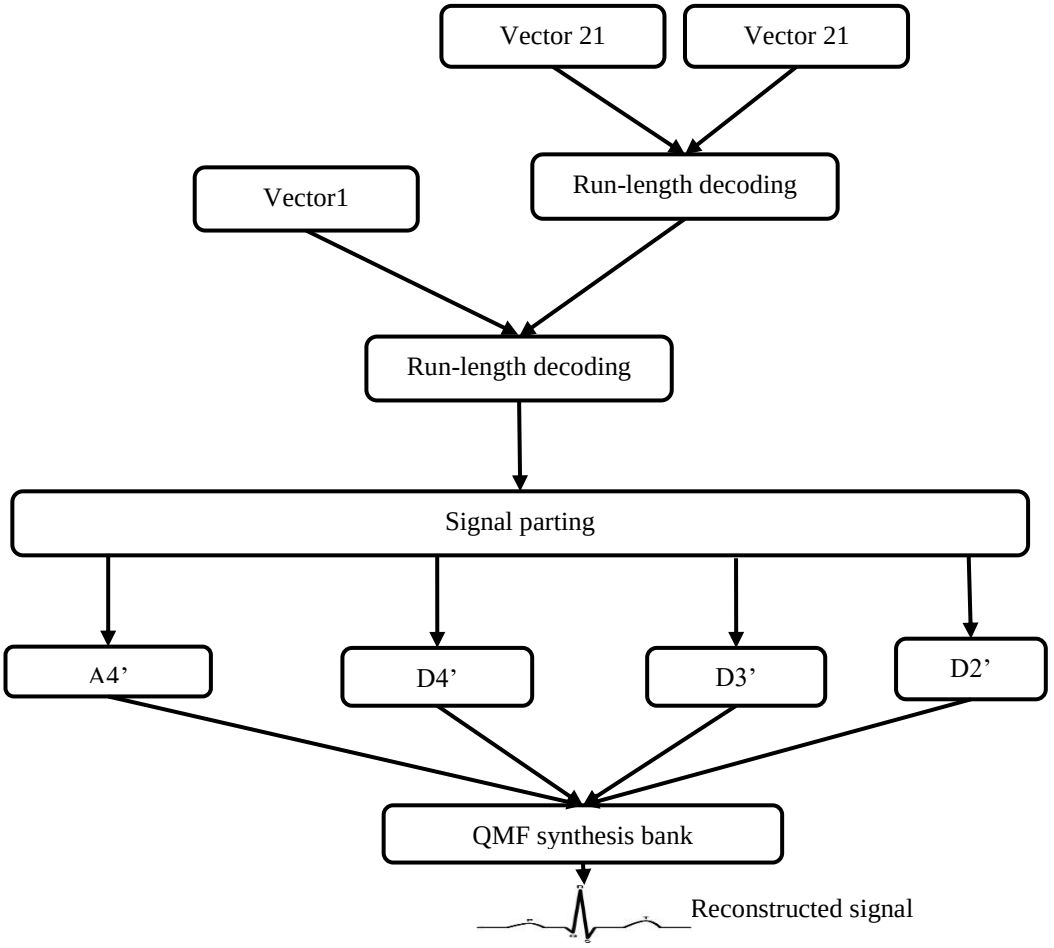

Fig. 5.7 Signal reconstruction steps.

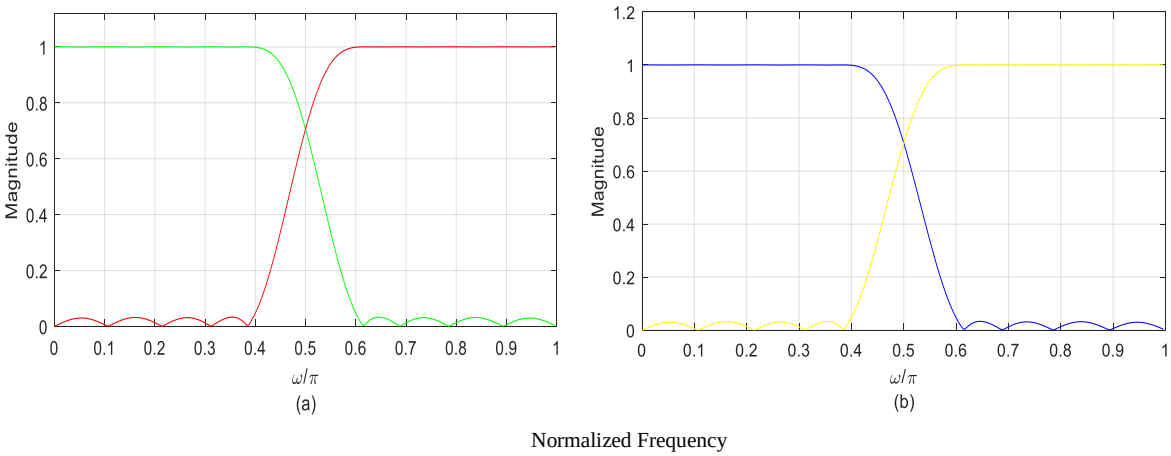

Fig. 5.8 (a) Analysis filter bank response and (b) Synthesis filter bank.

Step c: Reconstruction of signal

Reconstruction of the signal is done to recombine the signals using synthesis filter bank. The process of compression and reconstruction is given in Figs. 5.6 and 5.7, respectively. The linear phase FIR filter is designed using Parks-McClellan method. The design specifications of FIR filter are: $\omega_p = 0.395\pi$, $\omega_s = 0.605\ \pi$, $A_s = 60$ and calculated value of filter order is, N =35. After designing of prototype filter, analysis and synthesis bank is designed using Eqns. 5.2 to 5.4. The response of analysis and synthesis filter bank is depicted in Fig. 5.8 respectively. The ECG signal is applied to analysis bank to decompose it into a number of frequency bands. Here four level decomposition is carried out, therefore five frequency bands are formed. These signals are presented in Fig. 5.9. Further, RLE is applied to improve compression. This method yields up to 10.0 *CR*. The reconstructed signal is obtained by applying RLD followed by synthesis bank of QMF bank. Different fidelity parameters are measured which are presented in Table 5.3.

The reconstructed and original input signals are compared in Fig. 5.10, which shows that both the signals are identical. Further, the R-peaks of both the signals (locations and amplitudes) are also compared, which are depicted in Fig. 5.11. Tabular results (Table 5.4) demonstrate that these signals have some diagnostic information. The performance of proposed ECG data compression method is compared with other existing methods in Table 5.5, which demonstrates that the proposed method provides better CR and PRD, ultimately the QS.

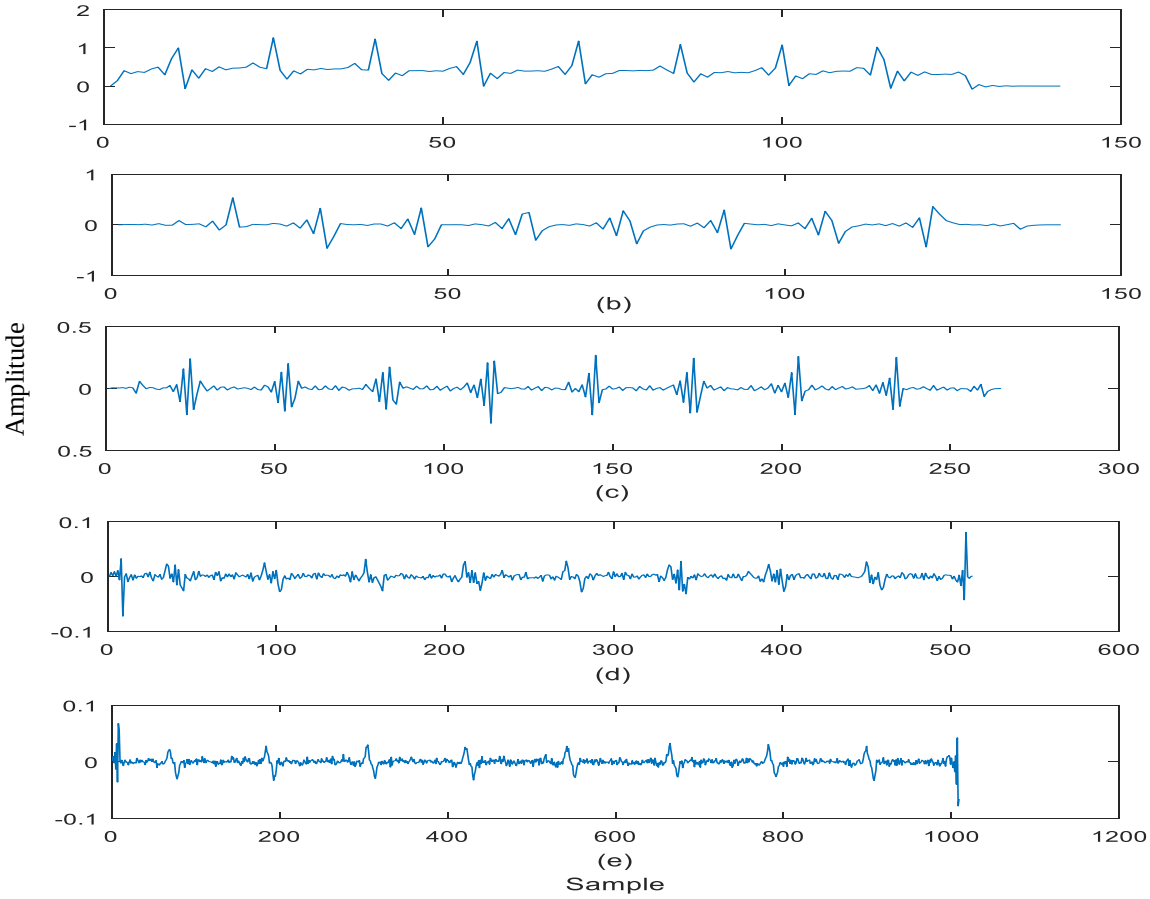

Fig. 5.9 Decomposition of signal.

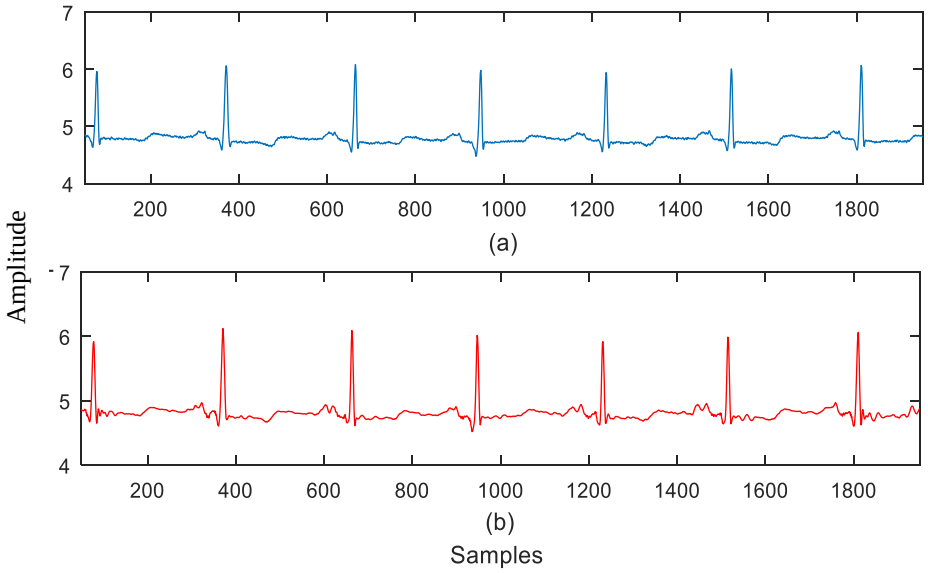

Fig. 5.10 Original and reconstructed signal.

Table 5.3 Various performance indices of the QMF and RLE based method

Signal	CR	PRD	SNR	CC	QS
MIT-BIH-100	8.8419	0.98149	20.1600	0.9934	9.008650
MIT-BIH-101	9.6233	0.81518	21.7750	0.9957	11.80512
MIT-BIH-102	6.5268	0.33544	29.4878	0.9994	19.45743
MIT-BIH-103	8.9567	0.70157	23.0786	0.9969	12.76665
MIT-BIH-104	8.0194	0.61077	24.2824	0.9925	13.12998
MIT-BIH-105	8.5144	0.50883	25.8685	0.9983	16.73329
MIT-BIH-106	10.449	0.85875	21.3226	0.9946	12.16827
MIT-BIH-107	7.5788	0.48738	26.2427	0.9988	15.55008
MIT-BIH-108	7.4693	0.72539	22.7886	0.9955	10.29694
MIT-BIH-109	6.8738	0.50989	25.8505	0.9986	13.48095
MIT-BIH-111	9.1145	0.49891	26.0396	0.9960	18.26883
MIT-BIH-112	8.3765	0.26756	31.4517	0.9972	31.30700
MIT-BIH-113	10.345	0.79353	22.0087	0.9964	13.03668
MIT-BIH-114	9.6233	0.45911	26.7617	0.9961	20.96077
MIT-BIH.115	9.3198	0.74824	22.5192	0.9970	12.45563
MIT-BIH.116	8.8043	0.55214	25.1590	0.9971	15.94577
MIT-BIH.117	9.5787	0.35196	29.0701	0.9975	27.21531
MIT-BIH.118	7.6066	0.37884	28.4309	0.9974	20.07866
MIT-BIH.119	9.4045	0.42128	27.5086	0.9983	22.32363
MIT-BIH.121	8.4106	0.28099	31.0261	0.9986	29.93203
MIT-BIH.122	8.1137	0.44019	27.1271	0.9979	18.43227
MIT-BIH.123	10.0927	0.44273	27.0772	0.9967	22.79651
MIT-BIH.124	10.2935	0.40103	27.9365	0.9987	25.66766
MIT-BIH.200	8.2760	0.50963	25.8549	25.854	16.23923
MIT-BIH.201	8.3765	0.48663	26.2560	0.9970	17.21328
MIT-BIH.202	9.8057	0.33031	29.6215	0.9970	29.68636
MIT-BIH.203	7.6066	0.4785	26.4023	0.9987	15.89676
MIT-BIH.205	8.9957	0.79162	22.029	0.9968	11.36366
MIT-BIH.207	9.1956	0.43275	27.2752	0.9987	21.24922
MIT-BIH.208	8.3765	0.49278	26.1469	0.9984	16.99846
MIT-BIH.209	7.8371	0.77604	22.2023	0.9932	10.09884
MIT-BIH.210	7.5511	0.42394	27.4540	0.9978	17.81172
MIT-BIH.212	8.3765	0.59091	24.5696	0.9968	14.17559
MIT-BIH.213	7.8669	0.54836	25.2186	0.9985	14.34623
MIT-BIH.214	8.4106	0.42823	27.3664	0.9987	19.64038
MIT-BIH.215	7.5236	0.69826	23.1197	0.9940	10.77478
MIT-BIH.217	7.8371	0.51189	25.8164	0.9982	15.31013
MIT-BIH.219	8.9567	0.62733	24.0501	0.9977	14.27749
MIT-BIH.220	9.1145	0.74955	22.5040	0.9960	12.15996
MIT-BIH.221	8.2760	0.46431	26.6639	0.9981	17.82430
MIT-BIH.222	8.5851	0.54642	25.2495	0.9894	15.71154
MIT-BIH.223	8.4449	0.48564	26.2736	0.9987	17.38922
MIT-BIH.228	7.5236	0.76155	22.3660	0.9946	9.879325
MIT-BIH.230	8.4106	0.63255	23.9781	0.9978	13.29634
MIT-BIH.231	9.4908	0.54994	25.1936	0.9970	17.25788
MIT-BIH.232	7.9577	0.55247	25.1539	0.9927	14.40386
MIT-BIH.233	8.1137	0.40428	27.8664	0.9990	20.06951
MIT-BIH.234	8.2760	0.38974	28.1846	0.9976	21.23467

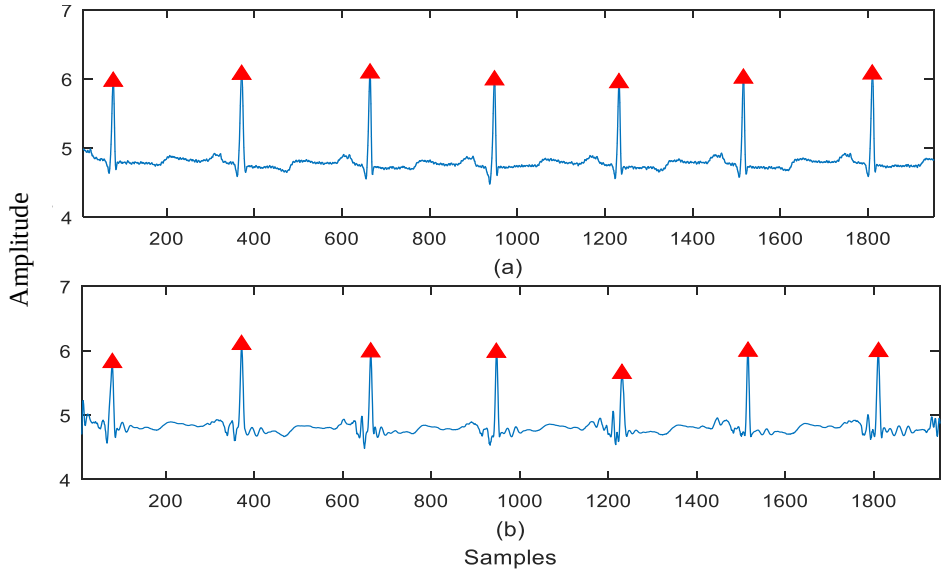

Fig. 5.11 R-peaks detection in the original and reconstructed signal.

Table 5.4 Comparison of diagnostic features of original and reconstruction signal

	Dataset	P (mA)	R (mA)	T (mA)	R-R interval	HR
100	Original	0.19	1.29	-0.21	0.82	78
	Reconstructed	0.17	1.25	-0.21	0.79	78
106	Original	0.46	2.42	0.94	1.02	61
	Reconstructed	0.43	2.39	0.90	1.07	61
116	Original	0.45	3.45	0.95	0.76	84
	Reconstructed	0.45	3.47	0.93	0.75	84
117	Original	0.12	0.95	0.06	1.22	54
	Reconstructed	0.15	0.95	0.05	1.21	54
118	Original	0.095	1.4	-0.17	0.83	72
	Reconstructed	0.094	1.1	-0.19	0.80	72
209	Original	0.15	1.4	0.43	0.62	90
	Reconstructed	0.13	1.7	0.45	0.67	90
215	Original	0.12	0.91	0.49	0.52	108
	Original	0.15	0.97	0.49	0.57	108

Table 5.5 Various ECG compression methods and their reported performance

Methods	Signal	CR	PRD
	MIT-BIH arrhythmia database (using QMF)	10.09	4.4273
Proposed method	MIT-BIH arrhythmia database (using QMF)	10.29	4.0103
	MIT-BIH arrhythmia database (using WP)	8.4528	0.5117
Method [107] (2013)	MIT-BIH arrhythmia database	5.73	0. 321
Method [8](2015)	MIT-BIH arrhythmia database	8.4	0.84
Method [137](2009)	MIT-BIH arrhythmia database	15.02	0.23
Method [78](2005)	MIT-BIH arrhythmia database.	7.18	25.5
Method [28](1988)	MIT-BIH arrhythmia database.	2.9	9.25

Table 5.6 WT decomposition

Level 3 decomposition	Level 4 decmposition	Level 5 decomposition
a_3	a_4	a_5
d_3	d_4	d_5
d_2	d_3	d_4
d_1	d_2	d_3
-	d_1	d_2
-	-	d_1

Table 5.7 Performance of compression ratio using wavelet transform and RLE

Level	Signal	CR	PRD	SNR	CC	QS
Sym2	MIT-BIH-100	11.0385	1.3839	37.1779	0.9110	7.9764
L=4	MIT-BIH-101	11.4800	1.2916	37.7776	0.9422	8.8884
	MIT-BIH-102	9.9950	1.4794	36.5986	0.9980	6.7564
	MIT-BIH-103	8.9289	2.1442	33.3745	0.9437	4.1641
	MIT-BIH-104	10.4635	0.7161	42.9010	0.9865	14.6126
	MIT-BIH-105	10.6862	1.1601	38.7104	0.9839	9.2118
	MIT-BIH-106	8.4059	1.9279	34.2981	0.9642	4.3600
	MIT-BIH-107	9.3442	1.7280	35.2491	0.9949	5.4075
	MIT-BIH-108	10.0450	0.4728	46.5066	0.9891	21.246
	MIT-BIH-109	9.7053	0.8682	41.2281	0.9942	11.1792
Bior5.5	MIT-BIH-100	11.0978	1.4563	36.7352	0.9009	7.6208
D1=0 yes	MIT-BIH-101	11.1585	1.0190	39.8368	0.9645	10.9507
	MIT-BIH-102	9.7238	0.7237	42.8089	0.9995	13.4363
	MIT-BIH-103	10.1089	2.0955	33.5741	0.9464	4.8240
	MIT-BIH-104	10.1089	0.5875	44.6198	0.9909	17.2066
	MIT-BIH-105	10.3655	0.9412	40.5263	0.9894	11.0130
	MIT-BIH-106	10.2613	1.4954	36.5049	0.9786	6.8619
	MIT-BIH-107	9.6777	1.5067	36.4396	0.9961	6.4232
	MIT-BIH-108	9.5421	0.3472	49.1887	0.9941	27.4839
	MIT-BIH-109	9.2398	0.5858	44.644	0.997	15.7728
Db10 L=4	MIT-BIH-100	10.1122	1.3842	37.1758	0.9110	7.3052
D1=0 yes	MIT-BIH-101	10.5765	1.0481	39.5920	0.9623	10.0912
	MIT-BIH-102	8.9740	0.7281	42.7567	0.9995	0.9995
	MIT-BIH-103	8.8970	1.9778	34.0763	0.9523	4.4984
	MIT-BIH-104	8.6375	0.5858	44.645	0.9910	14.7450
	MIT-BIH-105	9.3801	0.8197	41.7265	0.9920	11.4427
	MIT-BIH-106	10.3650	1.6260	35.7775	0.9747	6.3745
	MIT-BIH-107	9.8714	1.4617	36.7029	0.9963	6.7534
	MIT-BIH-108	9.0130	0.2979	50.5187	0.9957	30.2558
	MIT-BIH-109	8.9740	0.6277	44.0443	0.9970	14.2956

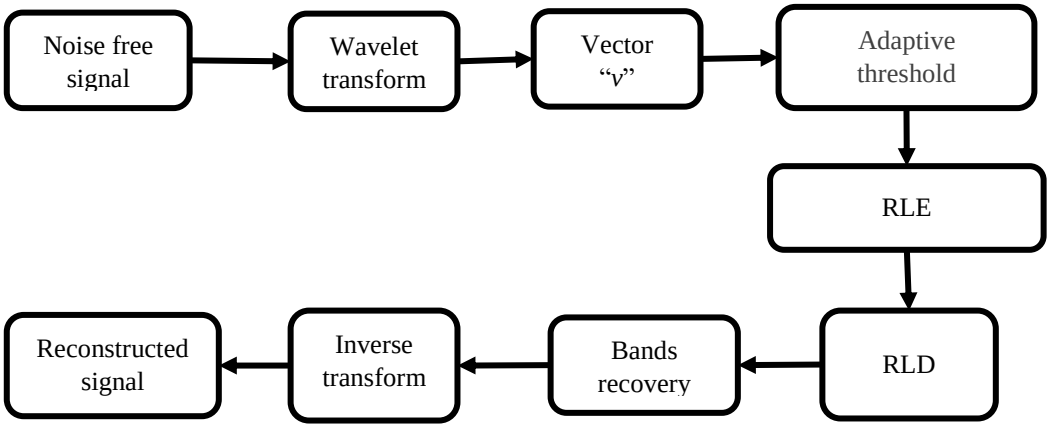

Fig. 5.12 ECG compression using wavelet and RLE.

5.4. ECG Data Compression using Wavelet Transform and RLE

ECG compression based on wavelet transform and RLE is presented. The steps used to compress the signal are depicted in Fig. 5.12. Here, first the wavelet transform decomposition is done, that splits the signal into different frequency bands (level 4 is used to decompose the signal into approximation (*a*) and detail bands (*d*)). This distribution is presented in Table 5.6. Then after the resultant coefficients are subjected by threshold (Adaptive threshold) using the principle of Stein's unbiased risk estimate. The coefficients below the threshold value are replaced by zero, while remaining coefficients are having the same magnitude. These coefficients are kept in vector "*v*". Next, the RLE is applied which is a lossless coding. The performance of this method is given in Table 5.7.

5.5. ECG Data Compression using Wavelet Transform and Huffman Coding

In this section, ECG compression based on wavelet transform and Huffman's coding is presented. The steps used to compress the signal are depicted in Fig. 5.13. Here, also the first step is the decomposition of signal into different frequency bands (level 4). Then, vector quantization is performed to the coefficient of vector "*v*". The steps of the quantization are evaluated using Eqn. given below:

$$step = floor\left(N \frac{\log(v / v\min)}{\log(vMax / vMin)} \right) \tag{5.6}$$

Next, the Huffman's coding is applied. The performance of this method is given in Table 5.8.

5.6. ECG Data Compression using Wavelet Transform and LZW

In this section, ECG data compression is done using WT and LZW coding. LZW is lossless "dictionary-based" compression algorithm [51]. LZW encoding is chosen as the entropy encoder for simplicity. The steps taken to compress ECG signal are given in Fig. 5.14. These steps are same as in the previous methodologies except coding method. The quantitative results of this methodology are presented in Table 5.9. Here, symlet, bi-orthogonal, Daubechies and Fejér-Korovkin wavelet filters are used, and 5-level decomposition is done.

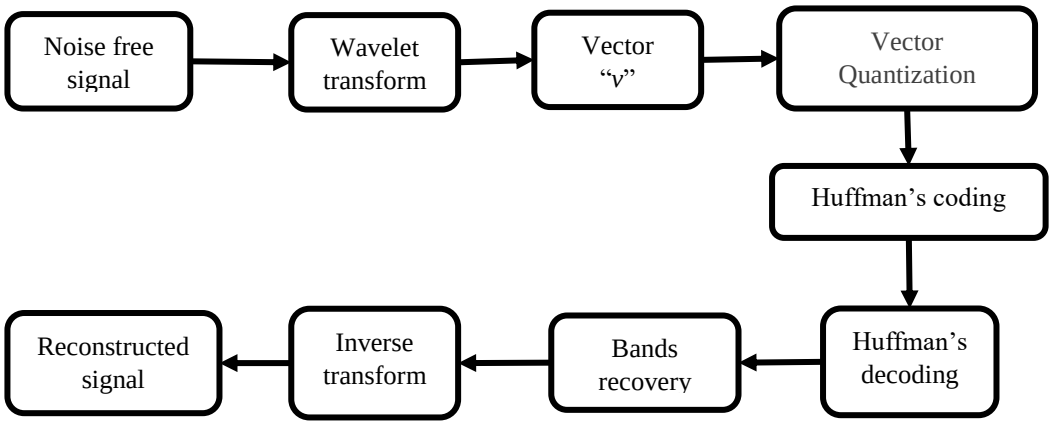

Fig. 5.13 ECG compression using wavelet and Huffman's coding.

Table 5.8 Performance comparison of different wavelet and Huffman's coding base algorithm.

Level	Signal	CR	PRD	SNR	CC	QS
Sym2	MIT-BIH-100	13.1062	0.0765	56.3084	0.9990	171.3666
L=4	MIT-BIH-101	12.8970	0.0665	57.5235	0.9994	193.9524
D1=0 yes	MIT-BIH-102	10.9058	0.0575	58.7797	1.0000	189.5283
	MIT-BIH-103	11.7271	0.1063	53.4491	0.9995	110.0065
	MIT-BIH-104	12.4788	0.0432	61.2679	0.9998	288.798
	MIT-BIH-105	11.9350	0.0429	61.3291	0.9999	278.1698
	MIT-BIH-106	12.8662	0.1084	53.2791	0.9996	118.0277
	MIT-BIH-107	9.8297	0.0805	55.8680	1.0000	122.1716
	MIT-BIH-108	13.3223	0.0220	67.1402	0.9999	606.2051
	MIT-BIH-109	11.0609	0.0352	63.0368	1.0000	313.8049
Fk4 L=4	MIT-BIH-100	12.9695	0.1683	49.4595	0.9950	77.07760
D1=0 yes	MIT-BIH-101	12.8356	0.1532	50.2764	0.9968	83.80430
	MIT-BIH-102	10.5208	0.2598	51.4491	0.9998	40.49590
	MIT-BIH-103	11.4854	0.2655	45.4972	0.9966	43.25530
	MIT-BIH-104	12.5857	0.0882	55.0661	0.9992	142.6309
	MIT-BIH-105	11.6510	0.1544	50.2044	0.9989	75.44270
	MIT-BIH-106	13.0980	0.2643	45.5361	0.9974	49.54920
	MIT-BIH-107	9.2607	0.2592	45.7068	0.9995	35.72860
	MIT-BIH-108	13.2242	0.0580	58.7163	0.9993	228.1475
	MIT-BIH-109	10.9115	0.1312	51.6198	0.9995	83.15870
Db10 L=4	MIT-BIH-100	11.3563	0.0020	88.0265	1.0000	5.7226e+03
D1=0 yes	MIT-BIH-101	11.3007	0.0018	88.6740	1.0000	6.1353e+03
	MIT-BIH-102	10.4724	0.0034	83.4032	1.0000	3.0991e+03
	MIT-BIH-103	9.9020	0.0019	88.1814	1.0000	5.0795e+03
	MIT-BIH-104	11.4529	0.0034	83.4378	1.0000	3.4028e+03
	MIT-BIH-105	10.3457	0.0016	89.7840	1.0000	6.3825e+03
	MIT-BIH-106	11.6315	0.0039	82.1375	1.0000	2.9754e+03
	MIT-BIH-107	8.6742	0.0040	81.9599	1.0000	2.1705e+03
	MIT-BIH-108	8.6742	0.0019	88.4014	1.0000	6.2610e+03
	MIT-BIH-109	10.3723	0.00468	80.7925	1.0000	2.2726e+03

Table. 5.9 Performance of compression ratio using wavelet transform and LZW encoding.

Level	Signal	CR	PRD	SNR	CC	QS
Sym6 L=5 D1=0 yes	MIT-BIH-100	27.8974	0.6331	43.9705	0.9838	44.0646
	MIT-BIH-101	25.9048	0.7368	42.6535	0.9826	35.1606
	MIT-BIH-102	20.5283	0.7657	42.3192	0.9995	26.8109
	MIT-BIH-103	21.9798	0.5572	45.0799	0.9965	39.4476
	MIT-BIH-104	23.6522	0.7141	42.9247	0.9869	33.1211
	MIT-BIH-105	23.3978	0.7231	42.8160	0.9939	32.3576
	MIT-BIH-106	23.6522	0.8150	41.7767	0.9940	29.0204
	MIT-BIH-107	18.2857	1.0776	39.3510	0.9981	16.9693
	MIT-BIH-108	25.9048	0.4919	46.1624	0.9884	52.6625
	MIT-BIH-109	18.9217	0.6491	43.7533	0.9968	29.1493
Fk4 L=5 D1=0 yes	MIT-BIH-100	30.8060	1.7270	29.2335	0.9036	17.8378
	MIT-BIH-101	25.1707	1.5992	29.9015	0.9692	15.7398
	MIT-BIH-102	19.6571	2.8617	24.8470	0.9704	6.86910
	MIT-BIH-103	22.4348	2.7785	25.1032	0.8461	8.07440
	MIT-BIH-104	23.4545	0.925	34.6490	0.9110	25.3341
	MIT-BIH-105	22.9333	1.6685	29.5328	0.8691	13.7448
	MIT-BIH-106	22.4348	2.7697	25.1306	0.8187	8.10000
	MIT-BIH-107	18.2655	2.8114	25.0008	0.9467	6.49690
	MIT-BIH-108	25.1707	0.6542	37.6648	0.9177	38.4740
Db22 L=5 D1=0 yes	MIT-BIH-100	25.0566	0.7750	42.2144	0.9806	32.0304
	MIT-BIH-101	32.0304	0.7750	42.2144	0.9806	32.0304
	MIT-BIH-102	19.6741	0.8170	41.7551	0.9994	24.0795
	MIT-BIH-103	20.7500	1.2514	38.0519	0.9820	16.5810
	MIT-BIH-104	23.5044	0.7499	42.4995	0.9855	31.3418
	MIT-BIH-105	24.1455	0.7214	42.8364	0.9939	33.4700
	MIT-BIH-106	22.3193	0.7557	42.4335	0.9948	29.5363
	MIT-BIH-107	16.9172	0.9964	40.0316	0.9983	16.9789
	MIT-BIH-108	23.7143	0.4756	46.4560	0.9891	49.8666
	MIT-BIH-109	19.9699	0.5797	44.7361	0.9975	34.4493
L=5 Bior3.5	MIT-BIH-100	24.4494	0.5490	45.2080	0.9877	44.5314
	MIT-BIH-101	24.1778	0.5043	45.9460	0.9919	47.9419
	MIT-BIH-102	19.0877	0.7403	42.6117	0.9995	25.7833
	MIT-BIH-103	21.3333	0.6648	43.5459	0.9950	32.0888
	MIT-BIH-104	23.3978	0.7020	43.0729	0.9873	33.3287
	MIT-BIH-105	22.2041	0.5148	45.7671	0.9969	43.1310
	MIT-BIH-106	22.4330	0.8178	41.7470	0.9939	27.4307
	MIT-BIH-107	17.5484	0.8073	41.8598	0.9989	21.7385
	MIT-BIH-108	24.7273	0.4079	47.7891	0.9921	60.6218
	MIT-BIH-109	18.4407	0.5285	45.5386	0.9979	34.8905

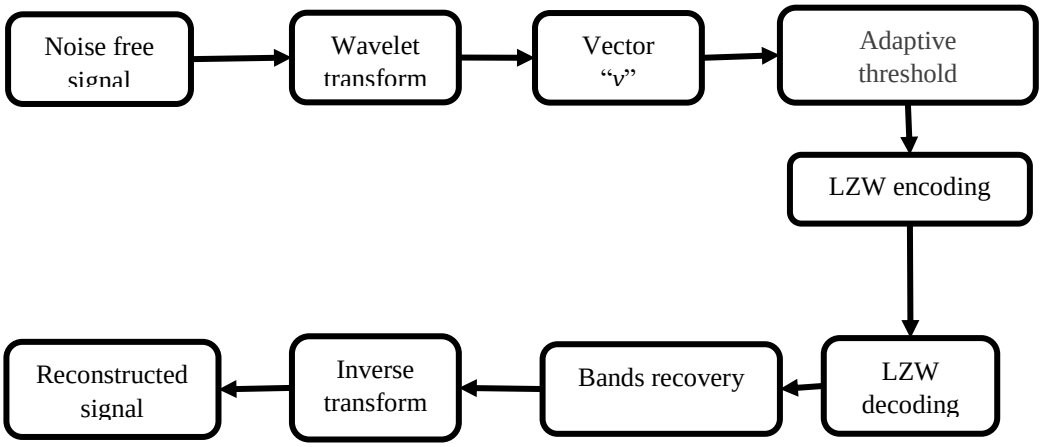

Fig. 5.14 ECG compression using wavelet and LZW encoding.

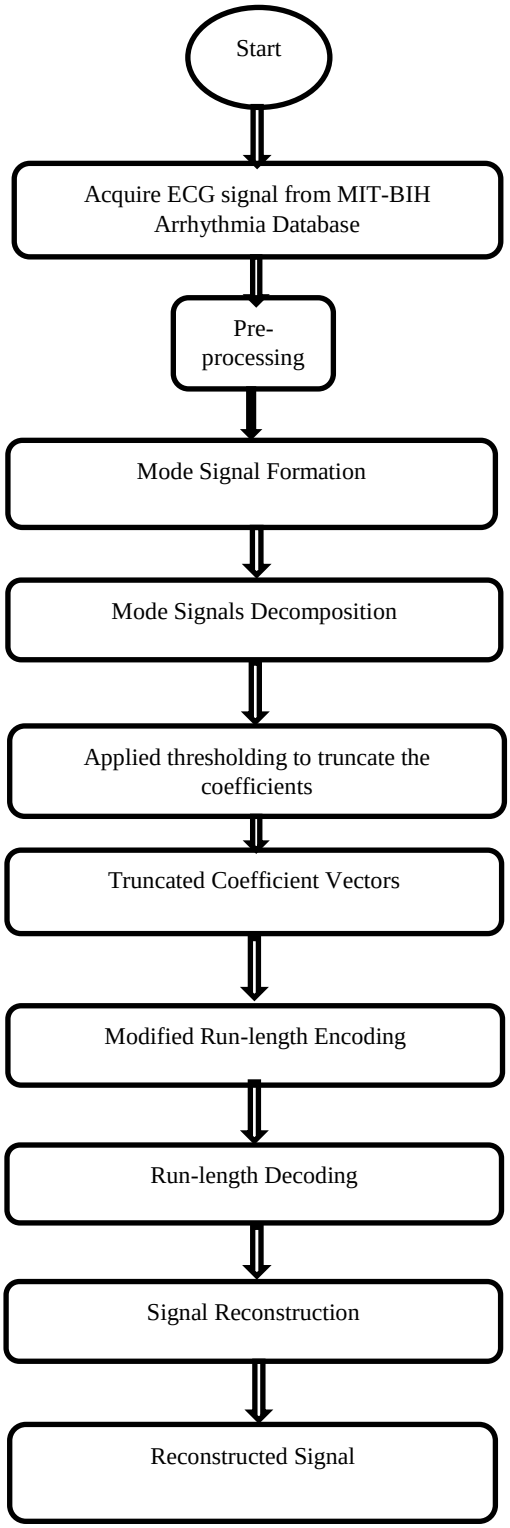

Fig. 5.15 Steps used in data compression methodology.

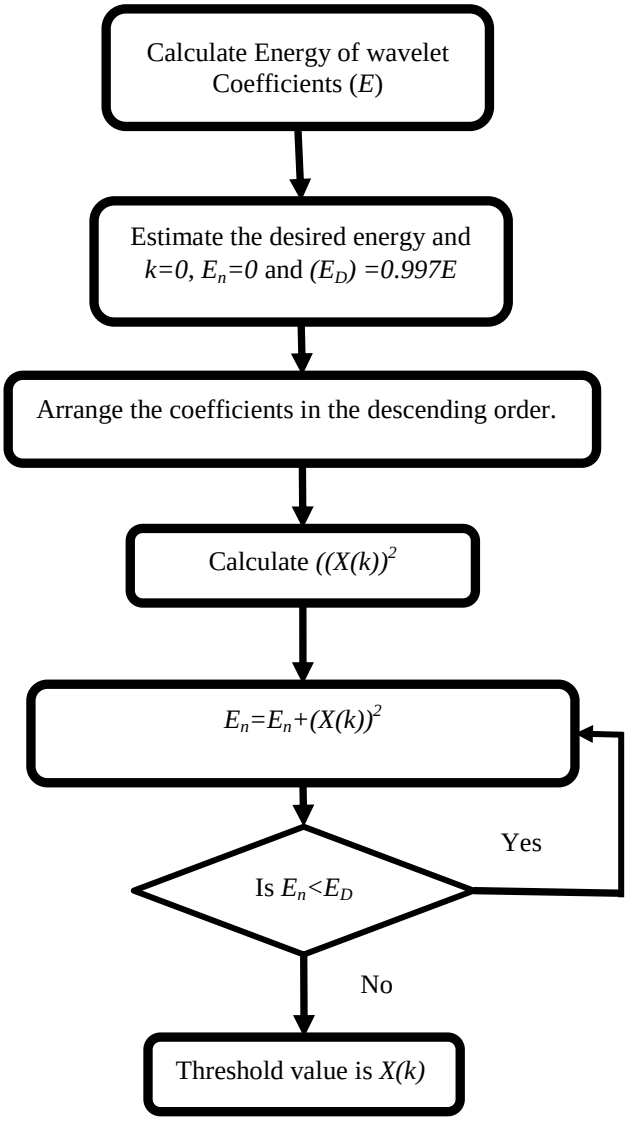

Fig. 5.16 Threshold value measurement.

5.7. ECG Data Compression using Empirical Wavelet Transform

In this section, ECG signal compression is done using EWT and RLE. The methodology of data compression is done by using the steps given in the flow chart of Fig. 5.15 and described as follows:

Step 1: ECG signal acquisition

Step 2: Signal decomposition

EWT divides the ECG signal into three modes (frequency modes). Three mode decomposition is chosen, to divide frequency efficiently. Two modes signals (such as mode2 and mode3 are selected, because most of the significant information is presented in these modes) are decomposed into different bands using DWT. Selection of decomposition level must be done in such a way so that all the relevant frequency components are separated from the most irrelevant frequency components, and signal reconstruction can be done efficiently at the synthesis section. Therefore, in this work, 5 levels of decomposition are applied.

Step 4: Thresholding

In this method, the selection of thresholding is done by the evaluation of energy packing efficiency (EPE) of the decomposed signals. EPE is defined in Eqn. (5.7).

$$EPE_{Di} = \frac{\overline{ECD_i}}{ECD_i} \times 100\% \tag{5.7}$$

where, $\overline{ECD}_i$ and ECD_i are representing the total energy in the detail bands after and before applying the threshold value, respectively. Selection of thresholding values should be done in such a way so that maximum energy remains the same. Since, most of the energy is presented in the approximation band (99.9%) and lower detail band, therefore coefficients of approximation band are not truncated. While the coefficients of lowest detail band (*d5*) are truncated in such a way so that the energy remains (99-97%). For the remaining detail bands, energy will be 85 to 99%. The steps used for detection of thresholding values are depicted in Fig. 5.16. After measuring the threshold values, thresholding is done to all bands. Then, significant coefficients of all the bands are used to form two vectors, such as;

$$vector_1 = [a_{51}\ b_{51}\ b_{41}\ b_{31}\ b_{21}\ b_{11}] \tag{5.4}$$

$$vector_2 = [a_{52}\ b_{52}\ b_{42}\ b_{32}\ b_{22}\ b_{12}] \tag{5.5}$$

Here, *a* represents the approximation band and *b* detailed band.

Step 5: Modified RLE application

Modified RLE (given in Fig. 5.1) is applied. Here, vector coefficient values are used up to 3 decimal points. In this work, 5-bit representation is used to represent the data: first bit is used to sign, and remaining four for the magnitude representation. At the receiver end, signal is reconstructed using the following steps:

Step i: Application of Run-length decoding

Step ii: Reconstruction of signal

The signal reconstruction is done using inverse transforms. First, the vector coefficients are divided into 5 signals, and then recombine all by taking inverse transform.

The noise-free signal is divided into 3 modes (Mode1, Mode2, and Mode3) using EWT, which is depicted in Fig. 5.17. Mode3 and Mode2 signals are applied to wavelet decomposition of the signal. In this work, bi-orthogonal (bior6.8) wavelet is used to decompose Mode2 and Mode3 signal into five frequency bands.

In this work, for approximation band (a_5) EPE is taken 99.99% and for lowest detail band (d_5), if is 95% to compute the threshold value. The threshold value is estimated by using steps given in Fig. 5.16. The value of *CR* and *PRD* for different *EPE* are shown in Fig. 5.18 and 5.19, respectively. In Fig. 5.19 (a) and (b), original input and reconstructed signal are presented. In this case, the measured values of performance parameters are: *CR 29.9, PRD* is *= 0.78, SNR = 31.45* and *RE = 99.96*. The performance of this method is presented in Table 5.10, and the comparative analysis of the performance of proposed method with other existing methods is depicted in Table 5.11, from this table, it can be observed that the proposed algorithm provides better results as compared to other methods in terms of *CR* and *PRD* both, *i.e*., overall *QS* is improved.

5.8. Discussion

In this chapter, transformation-based methodologies are used to compress the ECG rhythms. Here, the noise elimination is done before compression, *i.e*., as given in Chapter 3. Methodologies such as; a) wavelet packet algorithm, b) QMF filter bank, c) wavelet transform and d) EWT are employed for ECG data compression. In these methods, the thresholding /quantization and coding is used after decomposition of the signal. Here, the level and adaptive thresholding is applied, to truncate irrelevant coefficients of the signal. Then coding, such as: modified RLE/Huffman's/ LZW coding are used to compress the data. The compression performance is examined by calculating the compression ratio, and signal reconstruction analysis is done using different fidelity parameters and the visual depiction of comparison of beats present in both the signals.

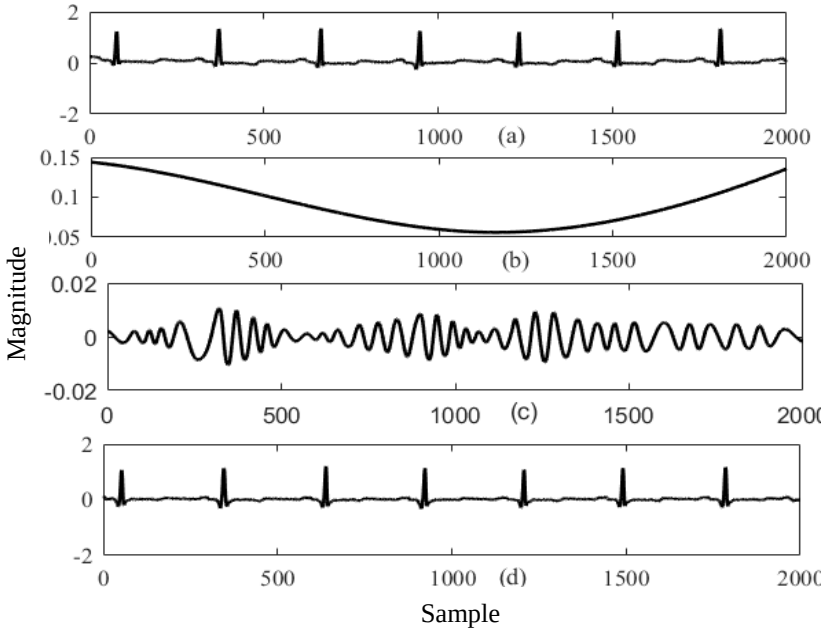

Fig. 5.17 MIT-BIH arrhythmia database (100m signal) and 3 mode signals.

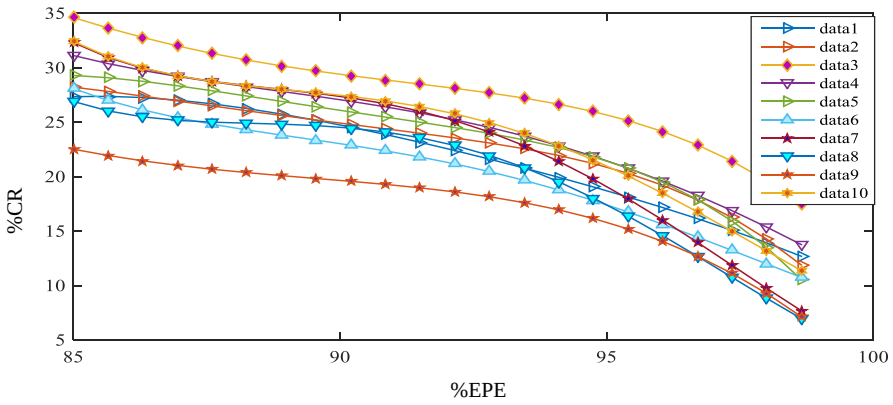

Fig. 5.18 Compression ratio on different detailed energy packing efficiencies.

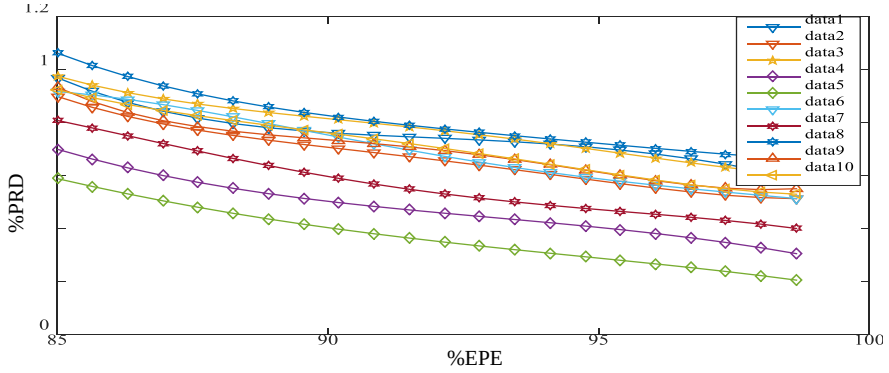

Fig. 5.19 PRD on different detailed energy packing efficiencies.

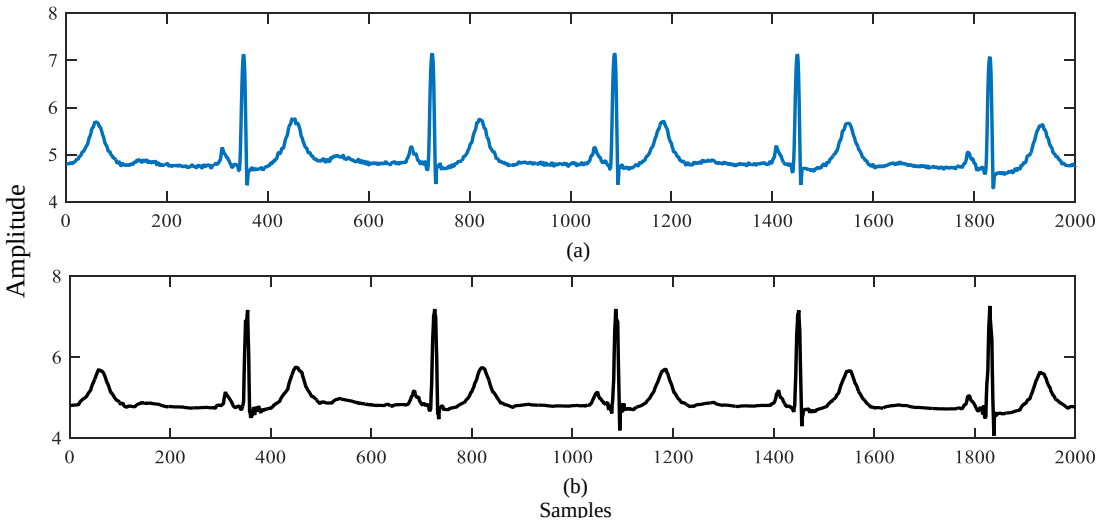

Fig. 5.20 (a) Original and (b) Reconstructed signal.

Table 5.10 Fidelity assessment parameters in the EWT and RLE based method

Signal	CR	PRD	QS	SNR	RE
MIT-BIH-100	29.2	0.254	114	31.44	99.76
MIT-BIH-101	28.7	0.184	155	28.99	99.94
MIT-BIH-102	29.1	0.178	163	41.23	99.95
MIT-BIH-103	28.9	0.282	102	21.45	99.96
MIT-BIH-104	29.7	0.121	245	23.76	99.98
MIT-BIH-105	31.1	0.075	414	23.76	99.89
MIT-BIH-106	30.3	0.178	170	34.90	99.49
MIT-BIH-107	30.4	0.277	109	41.43	99.88
MIT-BIH-108	29.0	0.083	349	47.23	99.94
MIT-BIH-109	30.9	0.058	532	21.70	99.92
MIT-BIH-111	28.4	0.191	148	22.24	99.67
MIT-BIH-112	30.8	0.259	118	34.76	99.83
MIT-BIH-113	29.3	0.198	147	24.84	99.75
MIT-BIH-114	28.9	0.193	149	20.82	99.56
MIT-BIH-115	28.3	0.078	362	39.26	99.65

Table 5.11 Comparative analysis of the performance of the proposed method with other methods

Methods	Signal	CR	PRD
Proposed method	100	29.2	0.254
	103	28.9	0.282
	105	31.1	0.075
Beta wavelet based and lossless encoding (Kumar et al., 2013)	100	5.73	3.210
Uniform scalar dead-zone quantization & entropy coding. (Chen et al., 2008)	100	14.29	2.980
EWT and RLE (Kumar and Saini, 2014)	100	34	2.1
Singular value decomposition and embedded zero tree wavelet (Kumar et al., 2016)	100	16.87	1.000
Daubechies mother wavelet (Motinath et al., 2016)	100	19.76	0.220
Mother wavelet parameterization (Abo-Zahhad et al., 2013)	117	23.0	1.600
EP-based wavelet coecient quantization (Hung et al., 2014)	100	22.94	-
ontext modeling Arithmetic coding with dynamic learning VSQ (Huang et al., 2013)	119	25.0	2.260
Quad level vector (Kim et al., 2010)	231	16.9	0.640

Tabular results (Table 5.2 (a), (b), (c), (d), (e)) show that methodologies provide good performance of signal compression and reconstruction. In Table 5.3, these parameters are evaluated using QMF and RLE technique. In Tables 5.7, 7.8 and 5.9, the performances of wavelet and encoding based methodologies are given. The data compression is also done by the highly adaptable technique "EWT". The performance of algorithm is depicted in Table 5.10. Different fidelity parameters are used to evaluate the performance of proposed method. Simulated results demonstrate that this algorithm can be used to reconstruct the compressed signal without loss of diagnostic information. Table 5.10 shows that proposed method gives up to *31.1* of *CR* and 0.075 PRD, which is highly recommended. Figs. 5.5, 5.10, 5.11 and 5.20 show that both the signals have some visual and beats (location and amplitude). Tabular comparison given in Table 5.4 and 5.11, indicate that the methodologies used in this work are superior to several existing methods. Therefore, it can be observed that the limited bandwidth problem can be overcome by minimizing the number of bits in transmission of compressed ECG data. The applications of these methodologies include the real-time hospital environment that is estimated to give proficient solutions to ECG data storage and transmission difficulties.

5.9. Summary

In this chapter, data compression of ECG signal is presented. Presented data compression algorithms provide higher compression performance with low signal quality degradation at the decomposition than several other algorithms. Another advantage of these methods is that all the information of the signal is hidden, because the signal is encoded. Therefore, these methodologies can be used at the transmission. These are protected, because transmitted data are encoded with decomposed coefficients. Hence, the method is applicable to 1-D signal compression with more security. Several signals taken from the MIT-BIH database are used to obtain the results of the methodologies. From the tabular and graphical results, it can be observed that these compression algorithms are capable of achieving good compression ratio values and good reconstruction quality. These methods can be used to compress all kinds of ECG rhythms in an efficient way. Using these methodologies, truncation of a bit stream at any point can be done, and a good quality of reconstruction can be obtained.

CHAPTER 6

DATA COMPRESSION OF ECG SIGNAL USING COSINE MODULATED FILTER BANK

6.1. Overview

Filter bank (FB) is one of the most significant tools of multirate signal processing (MSP), which is used to divide a signal into a number of frequency bands to process each band independently [259]. Initially, the two-channel quadrature mirror filter (QMF) bank was designed, which divides an input signal into two bands: successively, it was extended to multi-channel/*M*-channel filter banks (MFBs), where the input signal is decomposed into M number of frequency bands. *M*-channel filter banks are also classified into two types: a) uniform filter banks (UFBs) and b) non-uniform filter banks (NUFBs). UFBs decompose an input signal into M number of uniformly distributed frequency bands. On the contrary, in the case of NUFBs, signal decomposition is performed in M number of unequally distributed frequency bands [264]. A NUFB is extensively used in various signal processing applications as a consequence of its flexibility in dividing subbands [252].

Nearly perfect reconstruction (NPR) filter banks suffer from three types of distortions, i) aliasing distortion, ii) phase distortion and iii) amplitude distortion. These distortions can be minimized or completely eliminated by considering the following points; a) filters used to design a filter bank should have linear phase (*i.e*. finite impulse response (FIR)) to remove the phase distortion, b) aliasing distortion function should be equal to zero, to remove aliasing distortion and c) amplitude distortion is minimized by using suitable computer-aided technique [265]. For narrowband filtering and sharp transition width, filter order of an FIR filter is high. Therefore, a large number of multipliers and adders are required, and computational complexity become high [21].

In this chapter, the design of nearly perfect reconstructed uniform M-channel cosine modulated filter bank using three approaches a) a simple and proficient linear iterative technique b) Schittkowski algorithm and c) passband edge iteration to minimize the cost function. In technique (a), the cut-off frequency of the model filter is optimized to satisfy

the perfect reconstruction condition in CMFB. Different fixed /adjustable window functions are used for designing the linear phase IFIR prototype filter for the CMFB. In approach (b), the prototype filter is constrained to be a linear-phase spectral-factor of a *2M*th band filter and in (c), linear iteration process is done to optimum filter response by changing the value of passband edge frequency of model filter. In a CMFB, all the analysis and synthesis filters are implemented by applying the cosine modulation technique on the prototype filter. Here, several examples have been taken using various methodologies for filter design, filter optimization and for different channel filter bank design. This study is made to examine, weather the IFIR filter based filter bank design is possible or not using these techniques, and also to verify the performance of the designed filter bank. The tabular results demonstrates that the IFIR filter based filter bank provides improved results in terms of *%CRC*, and in some cases other performance indices are also improved.

Here, CMFB is also used for ECG data compression. The non-uniform CMFB is used for ECG data compression by decomposing ECG signal into various frequency bands. Subsequently, thresholding is applied for truncating the insignificant coefficients. The estimation of threshold value is done by examining the significant energy of each band. RLE is utilized for the compression. Here also, the MIT-BIH arrhythmia database is taken for performance analysis of the proposed work. The experimental observations demonstrate that the proposed method has accomplished a high compression ratio with the admirable quality of signal reconstruction with low percentage root mean square difference.

6.2. Near-Perfect-Reconstruction Pseudo-QMF Banks using IFIR Filter

Perfect-Reconstruction reconstruction filter banks are very important in numerous applications, for example*:* designing of wavelet. Nevertheless, in most of the applications, a near perfect reconstruction (NPR) is sufficient [297]. In this section, an approach to design the Multi-channel filter banks using IFIR prototype is presented. In this section, filter design is done by using the Parks–McClellan algorithm. Here, the prototype filter is constrained to be a linear-phase spectral-factor of a 2*M*th band filter. Therefore, the overall transfer function of the filter bank system is a delay. The PR cosine-modulated filter banks widely used as the analysis and synthesis filters are modulated versions of a prototype filter. In these types of filter banks, overlapping between the nonadjacent filters is negligible for the reason that the desired analysis and synthesis filters have narrow

transition bands and high stopband attenuation. Designing a filter bank with small aliasing (e_a*-100 dB*), high stopband attenuation (~-100 dB) and small overall distortion is a difficult task. It can be solved using the given method with low computational complexity.

For high stopband attenuation and low computational complexity, the IFIR filter is used as the prototype filter. In this method, minimization of the weighted objective function is done, which consists of stopband attenuation and total magnitude distortion. The analysis and synthesis banks design is performed by applying the modulation term given in Eqns. (2.76) and (2.77).

Furthermore, the aliasing terms are also canceled. Subsequently, the aliasing level at the output is analogous to stopband attenuation of the prototype filter. Therefore, it can be observed that only aliasing error is generated in this FB at the output of analysis-synthesis system, which is at the level of stopband attenuation. This type of optimization problem can be solved very accurately by the nonlinearity constrained minimization algorithm of Schittkowski.

For evaluation of the performance of filter, the following parameters are used are used

Step 1: Specify the number of bands (M), m, m_1, ω_s and ω_p

Step 2: Compute the value of N using Eqn. 6.1

$$N = 2(mM + m_1) \quad \text{for Even } N \tag{6.1a}$$

$$N = 2(mM + m_1) + 1 \quad \text{for odd } N \tag{6.1b}$$

$$\text{where, } 0 \le m_1 \le M - 1$$

Step 3: Compute the specifications of model and interpolation filter using Eqns. (2.54) to (2.59)

Step 4: Design the prototype filter. Initialization of low-pass filter ($H(z)$) is done using steps given in Section 2.2.3. Here, Parks–McClellan algorithm is used to design model and interpolation prototype filter.

Step 5: Compute the quadratic condition. In this step, the computation of quadratic condition and their gradients is done using mathematical expressions given in Eqns. (6.2) to (6.8).

$$\begin{cases} h^t S_n h = 0 & \begin{cases} \left\lfloor \frac{m+1}{2} \right\rfloor \le l \le (m-1), \quad m_1 = 0 \\ \left\lfloor \frac{m+1}{2} \right\rfloor \le l \le m, \quad m_1 \ne 0 \end{cases} \\ h^t (S_n + JS_{n-mM-m_1} + S_{n-mM-m_1} J)h = 0 & 1 \le l \le \left\lfloor \frac{m+1}{2} \right\rfloor - 1 \\ h^t (JS_{mM+m_1-1} + S_{mM+m_1-1} J)h = \frac{1}{2M} & \end{cases} \tag{6.2}$$

here, $h = \left[h(0) \;\; h(1) \;\; ... \;\; h(mM + m_1 - 1)\right]^t$ and S_n is the constant matrixes, which have the elements of magnitude either *0* or *1* that can be calculated using the expressions given below:

$$\left[S_n\right]_{k,l} = \begin{cases} 1, & k + l = n \\ 0, & otherwise \end{cases} \tag{6.3}$$

J is also the matrix given in Eqn. (6.4).

$$J_k = \begin{pmatrix} 0 & . & . & . & 0 & 1 \\ 0 & . & . & . & 1 & 0 \\ . & . & & & . & . \\ . & & . & & . & . \\ . & & & . & . & . \\ 1 & . & . & . & 0 & 0 \end{pmatrix}_{M \times M} \tag{6.4}$$

$$\begin{cases} h^t V S_n V h = 0 & \left\lfloor \frac{m}{2} + 1 \right\rfloor \le l \le m, \\ h^t V (S_n + JS_{n-mM-m_1} + S_{n-mM-m_1} J) V h = 0; & l \le l \le \left\lfloor \frac{m}{2} \right\rfloor \\ h^t (S_{2mM+2m_1-1} + JS_{mM+m_1-1} + S_{mM+m_1} J + S_0 J) V h = \frac{1}{2M} & \end{cases} \tag{6.5}$$

where,

$$V = \begin{pmatrix} I_{mM+m_1} & 0 \\ 0 & \frac{1}{2} \end{pmatrix} \tag{6.6}$$

Step 6: Calculate the stopband error

Stopband error is calculated using the following Eqn.

$$\int_{\omega_s}^{\pi} \left| H(e^{j\omega}) \right|^2 d\omega = h^t P h \tag{6.7}$$

where, $[P]_{k,l} = 2\sum_{i=1}^{K} \beta_i \int_{\omega_i,1}^{\omega_i,2} [\cos(k-l) + \cos\omega(N-1-k-l)] d\omega$,for $, 0 \le k, l \le mM + m_1 - 1$

(6.8)

in this Eqn. β_i, represents the relative weights and $\omega_{i,1}$ & $\omega_{i,2}$ are the band edges frequencies of the stopbands.

Step 7: Minimize the quadratic constrained problem, *i.e.*, find *h* that minimizes h^tPh and satisfies (6.5)

Step 8: Derive all the analysis and synthesis filters using Eqns. (2.76) and (2.77).

For evaluation of the performance of the filter bank, the following parameters are used are used

- Amplitude distortion (e_{am})

$$e_{am} = \max\left(1 - \left|T_0\left(e^{j\omega}\right)\right|\right) \tag{6.9}$$

- The worst case aliasing distortion (e_a)

$$e_a = \max\left(T_l\left(e^{j\omega}\right)\right) \text{ for } \omega \in [0, \pi],\ 1 \le l \le M-1 \tag{6.10}$$

- Computational reduction cost (*% CRC*).

$$\%(CRC) = \frac{(Multi(FIR) - Multi(IFIR))}{Multi(FIR)} \times 100 \tag{6.11}$$

  where, *Multi(FIR)* and *Multi(IFIR)* represent the multiplier of FIR and IFIR filter, respectively.

- Peak reconstruction error (*PRE*)

$$PRE = \max\left\{\sum_{k=0}^{M-1}\left|H_k\left(e^{j\omega}\right)\right|^2\right\} - \min\left\{\sum_{k=0}^{M-1}\left|H_k\left(e^{j\omega}\right)\right|^2\right\} \tag{6.12}$$

- Computational time (*CPU time*)

  The CPU time is the time required to execute the program for designing the CMFBs.

Example 6.1. In this example, four channel FB is designed using the steps given above, Here, the value of *M=4, m=13, K = 1,* β_i = 1, $\omega_s = 0.675\pi/(2\text{M})$ and $\omega_p = 0.35\pi/(2\text{M})$. The uniform CMFB is designed by using a single stage IFIR prototype filter. Parks–McClellan algorithm is used to design *F(z)* and *I(z)*. The stopband attenuation (A_s) = *100dB*. Fidelity parameters have magnitude: *PRE =3.7322e-06,* e_{am} *= 9.5479e-15* and e_a *=100dB*. In Fig. 6.1(a), the response of analysis bank is depicted, and the peak reconstruction error plot is shown in Fig. 6.1(b).

Example 6.2. In this case, an 8-channel pseudo-QMF bank is designed using the same methodology. Here, *M=8, m=13 K =1,* β_i = 1, $\omega_s = 0.675\pi/(2M)$ and $\omega_p = 0.35\pi/(2M)$. Here also, the uniform CMFB is designed by using the single stage IFIR prototype filter. Parks–McClellan algorithm is used to design *F(z)* and *I(z)*. In this case, the aliasing error is also about *-142dB*. *PRE* =5.8025×10^{-5}, e_{am} = 4.129×10^{-5}. The responses of the the analysis bank and reconstruction error are given in Fig. 6.2(a) and 6.2(b) respectively.

6.3. CMFB Design using Window Function

The researchers have developed methodologies, based on direct minimization of error function either in the time or frequency domain [284]. However, for the larger filter bank, these methodologies are not suitable due to the high degree of nonlinearity. CMFB have emerged as an attractive choice of filter banks with respect to implementation cost and design saving. Numerous algorithms [261-285] have been proposed for designing CMFB. However, these approaches need more iterations, as a result, a large computation time is required. Consequently, an efficient algorithm is used which can minimize the reconstruction error, aliasing error, computational time, and the number of iterations. Therefore, this chapter presents a simple and computationally efficient iterative algorithm for the design of NPR -uniform and non-uniform CMFB.

This methodology uses different window functions for designing the prototype filter for NPR banks. The techniques also employed for optimizing the cut off edge frequency to improve the performance of filter banks comparative to other existing algorithms. Optimization is very important to reduce the reconstructed noise. One of the major advantages of CMFBs is: if the prototype filter is optimized, then remaining all the filters get optimized, because all filters are derived from the single prototype filter only.

In this section, IFIR (single stage and two stages) filters are used as a prototype filter for CMFBs. Here, the coefficients of prototype filter are optimized using linear iterative algorithm given in [268]. Here, the cutoff edge frequency of model filter is varied to satisfy the nearly perfect condition.

PR filter banks produce the reconstructed signal, which is exact replica of the input signal without any distortion, *i.e.,* the reconstructed signal is a delayed version of the input signal. The PR filter bank must satisfy Eqn. (6.14) [260].

$$\left|H_0(e^{j\omega})\right|^2 + \left|H_0(e^{j(\omega-\pi/M)})\right|^2 = 1 \qquad for\ 0 < \omega < \pi/M \tag{6.13}$$

This condition changes at $\omega = \pi/M$, and the new PR condition becomes [265]:

$$\left|H_0(e^{j\omega/2M})\right| = 0.707 \tag{6.14}$$

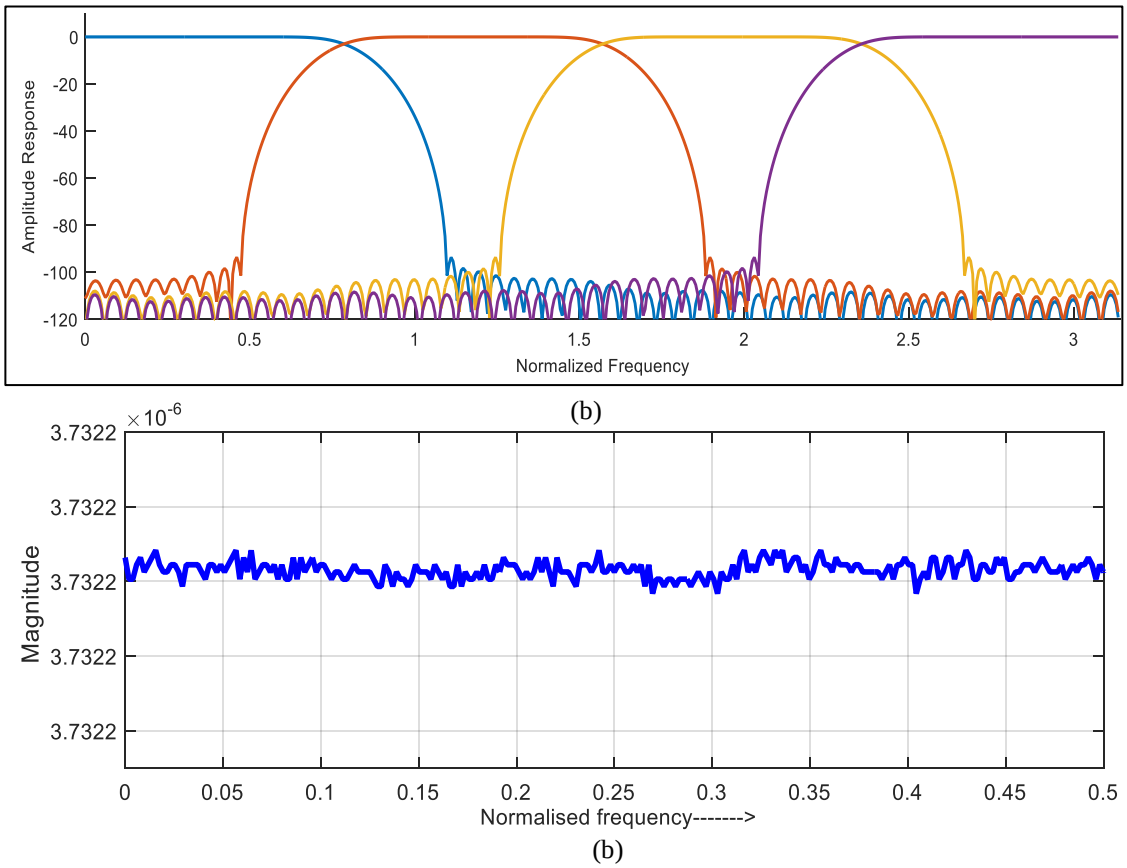

Fig. 6.1 (a) Frequency response of analysis filters and (b) Reconstruction error in dB.

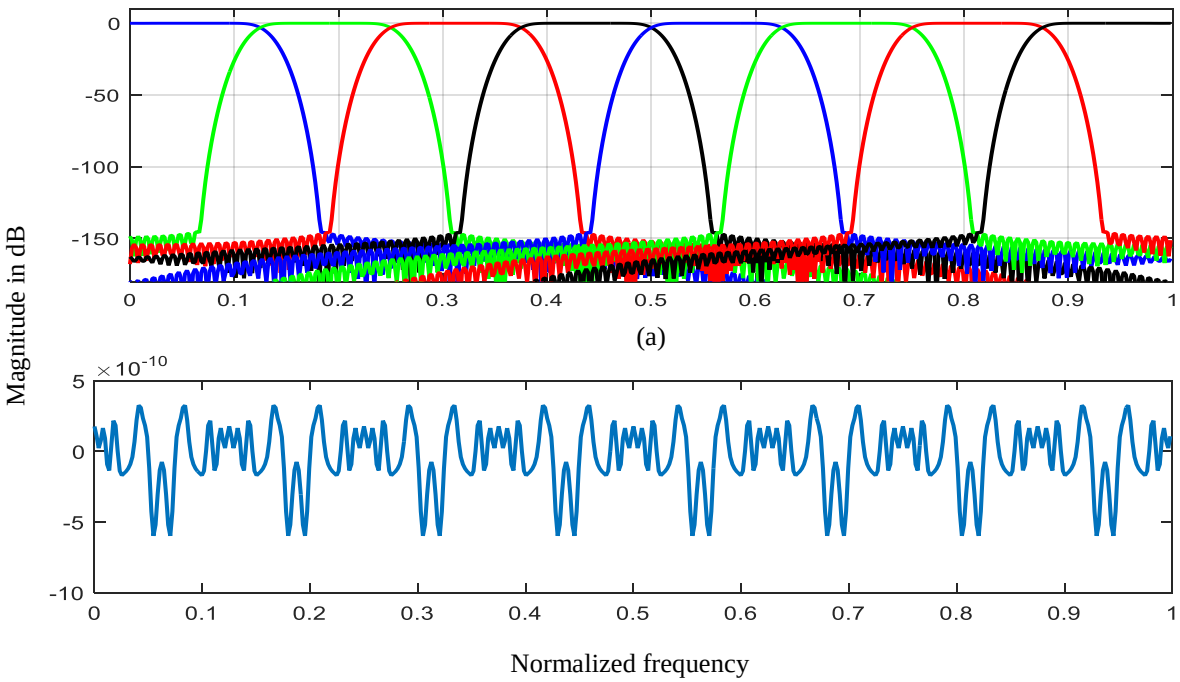

Fig. 6.2 (a) Frequency response of analysis filters and (b) Reconstruction error in dB.

In this work, this condition is utilized to get an optimized prototype filter. To obtain this condition, cutoff edge frequency is changed iteratively using the steps given below.

Step 1. Specifications of *H(z)*, such as; ω_p / π , ω_s / π and A_s are identified

Step 2. Step size (*step*), tolerance value (*Tol* =± *0.0001*), counter (*C= 0*) and ideal magnitude response (*MR*=0.707) are specified.

Step 3. The value of L is estimated using Eqn. (2. 42)

Step 4. Specifications of *F(z)* and *I(z)* are computed.

Step 5. *I(z)* is designed using the windowing method. A windowing method uses filter order, cutoff edge frequency, and stopband attenuation to design the filter response. The cutoff frequency is measured.

Step 6. *F(z)* is designed.

Step 7. Up-sampling of *F(z)* by *L* is done, (*i.e.* $F(z^L)$)

Step 8. Convolution of up-sampled model filter and interpolator filter is done ((*i.e.* $F(z^L)I(z)$).

Step 9. Calculation of magnitude response (*MRD*) of the prototype filter at $(\omega) = \pi/2M$ and *Err* (*Err=MRD* - *MR*) is done.

Step 10. *Err* value is verified:

Err must be within the *Tol* value. In this work, the *Tol=0.0001*. If the *Err* is not in the *Tol* level, then linear iteration is started by changing the value of ω_{cm} in two ways:

1) If *MR* is greater than *MRD*, ω_{cm} is increased using $\omega_{cm} = \omega_{cm}$ + *step* and go to **Step 11**

2) Otherwise, ω_{cm} is decreased using $\omega_{cm} = \omega_{cm}$ - *step* and go to **Step 11**

Step 11. The counter value is increased by 1 and *step=step /2.*

Step 12. Redesigning of *F(z)* using new ω_{cm} is done with the same filter order and follow **Step 7** till the tolerance level is achieved.

The same steps are used for optimizing the two-stage IFIR prototype filter, the only difference is in designing of *I(z)* (**Step 5**), *i.e.*, first $I_1(z)$ and $I_2(z)$ are designed, then after up-sampling of $I_1(z)$ is done by factor L_1, and then convolution of $I_1(z^{Li})$ and $I_2(z)$ is also done.

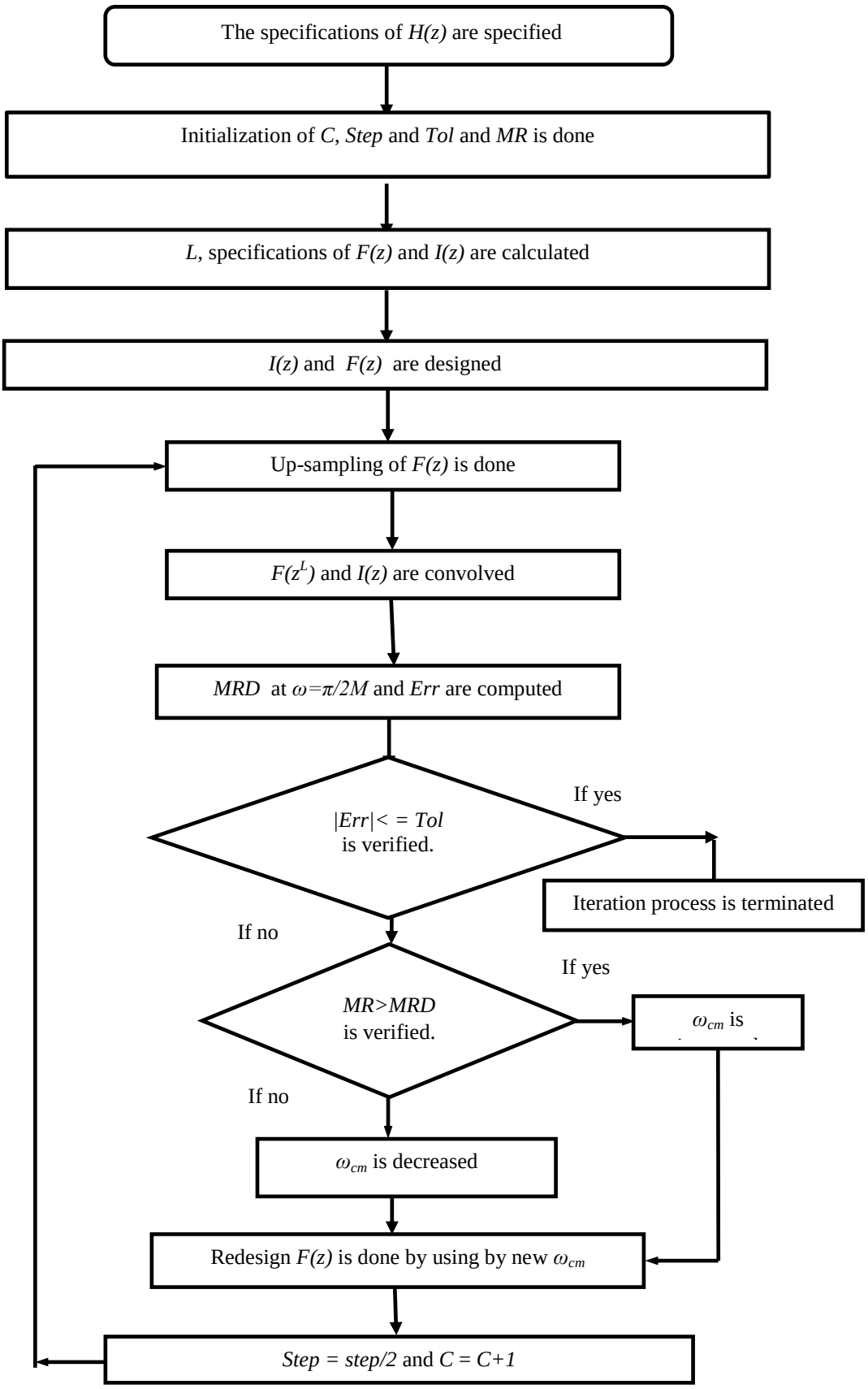

Fig. 6.3 Block diagram of optimization of prototype filter.

After the optimization of prototype filter, cosine modulated technique is used to derive all the analysis and synthesis filters using cosine modulated expressions given in Chapter 2. This methodology is employed to design 4, 8, 16 and 32 bands filter banks using single and two-stage IFIR prototype filters. Further, the NUFB is also derived using methodology given in [254]. Here, 3-channel, 4-channel, and 5-channel NUFBs are designed using 4-channel, 8-channel, 16-channel, and 32-channel UFB.

Several design examples have been included to illustrate the proposed algorithm and its improved performances over other existing methods. The proposed methodology has been extended for designing *M*-channel cosine-modulated filter banks. Finally, the application of these methodologies is considered in the area of subband coding of the ECG signals.

6.3.1. CMFB Design using Fixed Window Function

In a fixed window function, only one controlling factor is used to adjust the side lobe and main lobe (width and height). In this section, Blackman, rectangular, Bartlett, Hanning, and Hamming window functions are used for designing of model and interpolator filter.

Example 6.3*:* 8-channel uniform CMFB is designed using single stage IFIR prototype filter. Blackman window function is utilized to design *F(z)* and *I(z)*. The design specifications of prototype filter are: $\omega_s = 0.125\pi$, $\omega_p = 0.0312\pi$ and $A_s = 80dB$. Designing of the prototype filter is done by following steps given in Fig. 6.3. After obtaining the optimized prototype filter, other analysis and synthesis filters are derived using cosine modulated functions.

The frequency responses of prototype filter, analysis filter bank and reconstruction error are given in Fig. 6.4. This methodology is applied to obtain 8 and 16 channel filter bank using different fixed window functions given in Chapter 2. The performances of these fixed window functions are presented in Table 6.1.

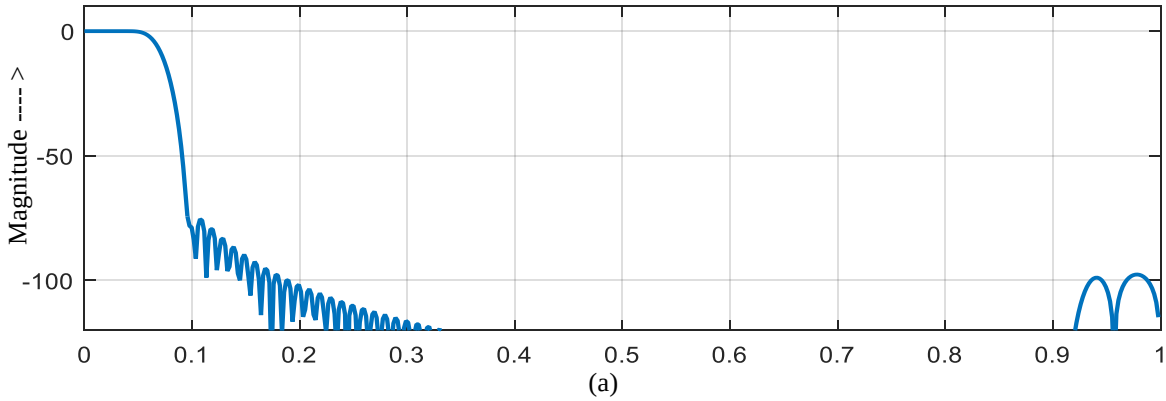

(a)

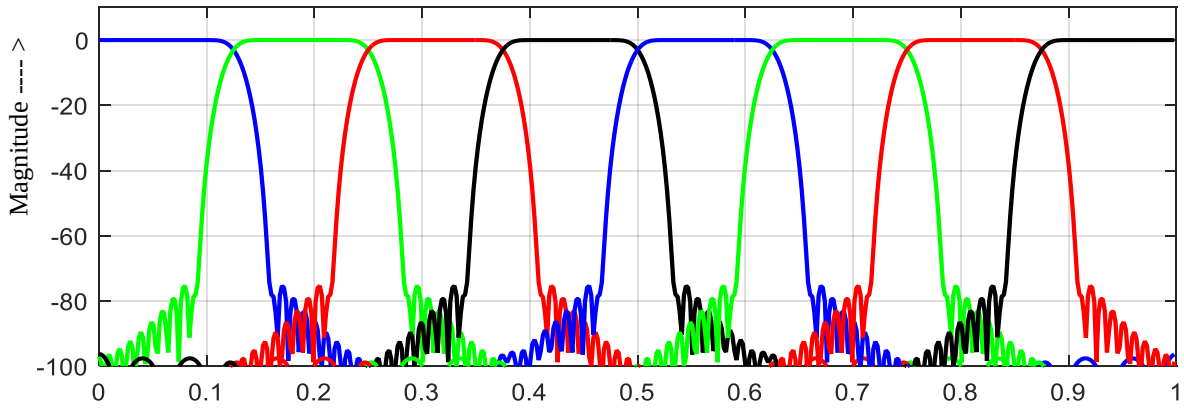

(b)

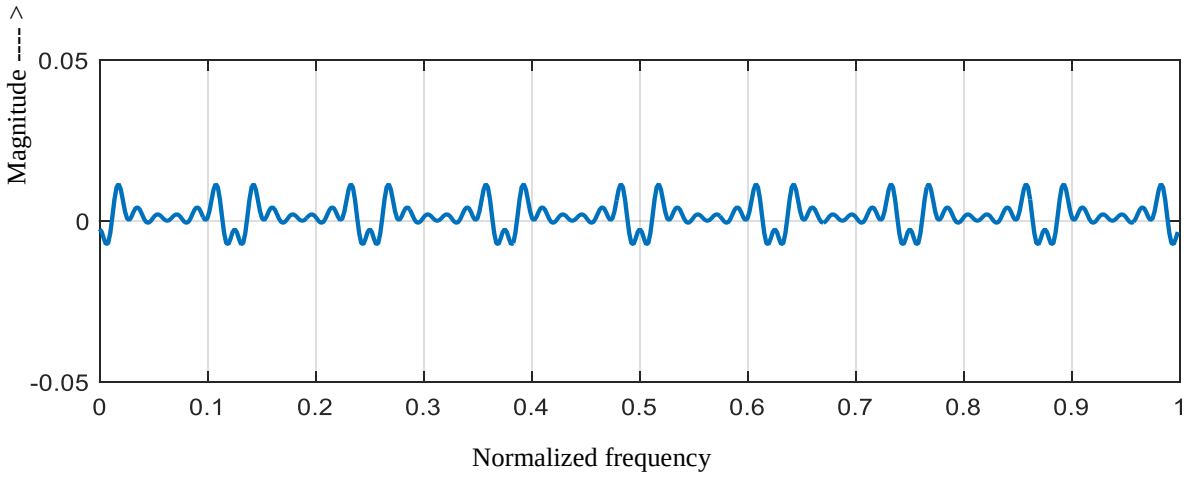

(c)

Fig. 6.4 (a) Magnitude response of prototype filter, (b) Analysis filters response, and (c) Reconstruction error in dB using the iterative algorithm by utilizing fixed window function.

Table 6.1. Performance measurement of cosine modulated filter bank using fixed window function.

Window function	**Filter**	e_{am}	e_a	***PRE***	***CPU Time***	***Noe***	***%CRC***
Blackman	FIR(*M=8*)	0.0021	4.2093e-05	0.0103	0.706230	21	-
	IFIR (*M=8*)	0.0040	3.5317e-05	0.0072	0.614688	10	57.2165
	$IFIR_2$(*M=8*)	0.0017	1.5637e-05	0.0041	0.675604	15	67.4058
	IFIR (*M=16*)	0.0011	1.0707e-04	0.0098	0.875355	17	68.7339
	$IFIR_2$(*M=16*)	2.2743e-04	5.2455e-06	0.0020	0.788495	19	77.0308
Rectangular	FIR(*M=8*)	0.2747	0.0091	1.0271	0.659506	23	-
	IFIR(*M=8*)	0.3365	0.0221	2.5228	0.557402	12	57.2165
	$IFIR_2$(*M=8*)	0.3792	0.0026	2.3592	0.557402	19	67.4058
	IFIR (*M=16*)	0.1332	0.0131	1.0863	0.959513	21	68.7339
	$IFIR_2$(*M=16*)	0.0014	0.0235	0.0122	0.588910	17	77.0308
Bartlett window	FIR(*M=8*)	0.0483	0.0178	0.0057	0.627344	19	-
	IFIR(*M=8*)	0.0585	0.0116	0.0421	0.688154	11	57.2165
	$IFIR_2$(*M=8*)	0.2836	2.1608e-04	1.0998	0.588910	14	67.4058
	IFIR (*M=16*)	0.1332	0.0131	1.0863	0.959513	21	68.7339
	$IFIR_2$(*M=16*)	0.0014	0.0235	0.0122	0.588910	17	77.0308
Hanning window	FIR(*M=8*)	0.0246	5.4605e-05	0.1865	0.694581	21	-
	IFIR(*M=8*)	0.0245	1.6817e-04	0.1761	0.442073	11	57.2165
	$IFIR_2$(*M=8*)	0.0248	4.1301e-05	0.1372	0.429859	17	67.4058
	IFIR (*M=16*)	0.0197	9.4879e-05	0.1698	1.000708	20	68.7339
	$IFIR_2$(*M=16*)	0.0234	7.2255e-04	0.2008	0.734366	17	77.0308
Hamming window	FIR(*M=8*)	0.0041	2.4379e-04	0.0755	0.931441	22	-
	IFIR(*M=8*)	0.0158	0.00014	0.1073	0.788471	11	57.2165
	$IFIR_2$(*M=8*)	0.0170	4.9486e-04	0.1068	0.555456	15	67.4058
	$IFIR_2$(*M=16*)	0.00007	0.0012	5.5371e-05	0.882155	17	77.0308

6.3.2. CMFB Design using Adjustable Window Function

By utilizing the fixed window function, controlling of the main lobe width is achieved using only one independent parameter *i.e.*, length of the window function. However, in some multirate signal processing applications, such as speech signal processing and ECG signal processing, additional spectral parameter, called side lobe roll-off ratio is needed. Consequently, numerous window functions have been developed to improve the spectral characteristics, which have one or more additional controlling parameters. Kaiser, Modified Kaiser-Bessel window, Dolph-Chebyshev, Saramaki, ultraspherical, symmetric hyperbolic cosine window, exponential, symmetric Nuttall window, extended Norton-Beer window, Gaussian window and Taylor window are used in this work to design the filters (mathematical description of these windows is presented in Chapter 2).

Example 6.4*:* In this example, 4-channel uniform CMFB is designed using a single stage IFIR prototype filter. Kaiser window is used to design *F(z)* and *I(z)*. The design specifications of prototype filter are: $\omega_s = 0.195\,\pi$, $\omega_p = 0.0628\pi$ and $A_s = 100dB$. In this case, the calculated value of $L = 3$, therefore, calculated passband and stopband edge frequency of model filter are $(\omega_{pm}) = 0.188\pi$, and $(\omega_{sm}) = 0.585\pi$, respectively and passband and stopband edge frequency of interpolator filter are $(\omega_{pi}) = 0.0628\pi$ and $\omega_{si} = 0.471\pi$.

After designing of prototype filter, a filter bank is designed. In this case, *8* iterations are used to optimize the cutoff frequency at 3 dB. After obtaining the optimum prototype filter, cosine modulation technique is applied to obtain the analysis and synthesis filter banks, using Eqns. (2.76) and (2.77), respectively. Performance of the proposed filter bank is evaluated using parameters given in Eqns. (6.9) to (6.12).

The quantitative values of resulted parameters of CMFB are: $e_{am} = 4.1\times10^{-3}$, $e_a = 3.1\times10^{-6}$, $PRE = 5.1\times10^{-3}$, $NOE = 8$, $CPU\ Time = 4.06\times10^{2}$, this and $CRC = 57.21\%$. In Fig. 6.5(a), the response of the prototype filter is represented. Fig. 6.5(b) shows the analysis bank of CMFB and in Fig 6.5(c), the reconstruction noise is depicted.

Table 6.2. Performance of cosine modulated filter bank using adjustable window functions

Window	Filter	e_{am}	e_a	*PRE*	*Noe*
Kaiser	FIR	0.0025	5.4112e-06	0.0102	18
	IFIR	0.0034	3.3808e-07	0.0043	11
	$IFIR_2$	0.0037	3.1351e-07	4.9338e-04	13
Dolph-Chebyshev Window	FIR	0.0053	1.7916e-07	2.8840e-04	19
	IFIR	0.0058	4.9751e-07	0.0103	11
	$IFIR_2$	0.0051	1.9120e-06	1.6666e-04	17
Saramaki window function	FIR	0.0028	4.0773e-05	0.0195	21
	IFIR	0.0078	2.3179e-05	0.0559	11
	$IFIR_2$	0.0051	1.9120e-06	1.6666e-04	17
Ultraspherical polynomials	FIR	0.0090	1.3349e-04	0.0028	11
	IFIR	0.0089	8.5300e-08	3.6507e-05	11
	$IFIR_2$	0.0077	5.5410e-08	2.8347e-05	12
Symmetric exponential window	FIR	0.0028	1.6112e-05	0.0160	18
	IFIR	0.0019	1.4341e-05	0.0139	9
	$IFIR_2$	0.0051	1.9120e-06	1.6666e-04	17
Symmetric hyperbolic cosine window	FIR	0.0029	1.8692e-05	0.0161	22
	IFIR	0.0150	1.3412e-05	0.1308	11
	$IFIR_2$	0.0140	5.5201e-08	0.1182	17
Symmetric Nuttall window	FIR	0.0055	4.2298e-07	1.6626e-04	20
	IFIR	0.0060	8.5186e-07	1.4468e-04	11
	$IFIR_2$	0.0053	1.6304e-06	2.0734e-04	15
Extended Norton-Beer window	FIR	0.0174	5.2121e-04	0.1432	22
	IFIR	0.0251	8.2668e-04	0.2114	12
	$IFIR_2$	0.0181	1.5329e-04	0.1530	18
Modified Kaiser-Bessel window	FIR	0.0055	4.9169e-06	1.5090e-04	22
	IFIR	0.0072	7.9773e-08	0.0079	10
	$IFIR_2$	0.0067	4.2238e-07	7.3928e-07	17
Gaussian window	FIR	0.0138	5.8067e-05	2.3759e-04	14
	IFIR	0.0138	2.4703e-06	0.0010	9
	$IFIR_2$	0.0140	5.1257e-06	4.5905e-10	15
Taylor window	FIR	0.0039	1.4846e-05	0.0034	21
	IFIR	0.0047	4.8153e-05	0.0165	10
	$IFIR_2$	0.0037	5.3420e-05	2.8647e-05	16

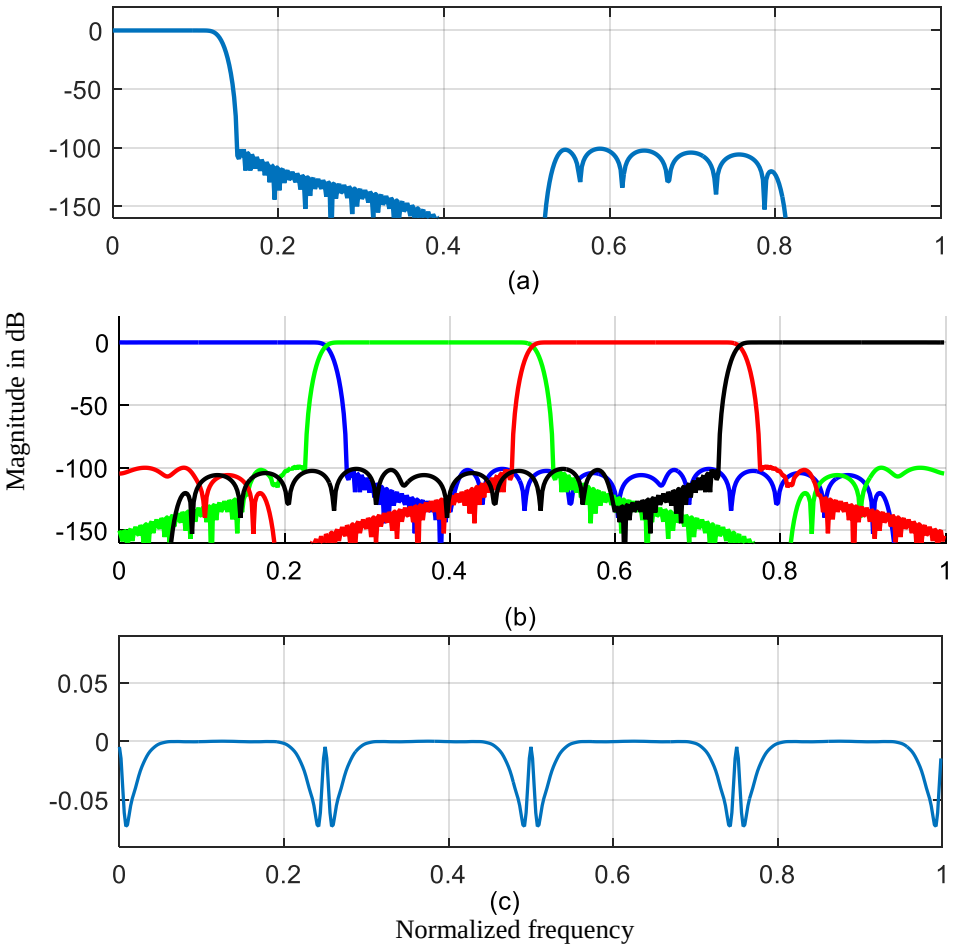

Fig. 6.5 Response of (a) Prototype low pass filter, (b) 4-band analysis filter bank and (c) Reconstruction.

Example 6.5: In this example, 8-channel uniform CMFB is designed using design specifications; $\omega_s = 0.0595\pi$, $\omega_p = 0.0262\pi$ and $A_s = 100dB$. Similar to *Example 6.4*, here also filters are designed by windowing method. The resulted parameters of CMFB using single stage IFIR filter are: $L=5$, $e_{am}= 5.1\times10^3$ $e_a= 1.5\times10^6$, $PRE=5.4\times10^3$, $NOE =11$, $CPU\ Time = 7.99\times10^3$ *ms*, and $CRC = 74.34\%$ and using two-stage IFIR prototype filter; $L= 5$, $L_1=2$, $e_{am}=3.6\times10^3$, $e_a = 1.05\times10^6$, $PRE=5.3\times10^4$, $NOE =18$, CPU Time $=8.237\times10^3$ms and $CRC = 79.09\%$. The resultant response of prototype filter, analysis bank, and reconstruction noise are shown in Fig. 6.6. These results are obtained using a two-stage IFIR filter. Other window functions are also used to design CMFB using single and two-stages IFIR filters. The performance using fidelity parameters are presented in Table 6.2 for *8*-channel FBs. The same procedure is followed to design the 16 and 32-channel filter banks using different design specifications. Obtained fidelity parameters of these examples are given in Table 6.3.

Further, NUFB is also derived using the methodology given in [23]. Here, *3*-channel, *4*-channel, and *5*-channel NUFBs are designed using *4*-channel, *8*-channel, *16*-channel, and *32*-channel UFB,

Example 6.6: The non-uniform CMFBs are designed using design specifications of the prototype filter; $\omega_s =0.0625\pi$,v $\omega_p =0.0312\pi$ and $A_s = 100dB$. First, 16-channel UFB is designed, then after *3* and *5*-channel NUFBs are derived by merging bands of UFB in such a way:

For 3-channel non-uniform CMFB, $B_1= b_1$, $B_2= b_2 + b_3+ b_4$ and $B_3 =b_5+b_6+b_7+ b_8$.

For 5–channel non-uniform CMFBs, $B_1= b_1$, $B_2= b_2$, $B_3 =b_3+b_4$, $B_4= b_5$, $B_5= b_6+ b_7+ b_8$.

In this case, $L=4$, $L_1= 2$, $e_{am}=3.70\times10^3$, $e_a =1.70\times10^6$, $PRE=4.20\times10^3$, $NOE =16$, $CPU\ Time =3.070\times10^3$ *msec* and $CR = 83.01\%$ are obtained. The prototype filter response and analysis bank are presented in Fig. 6.7(a) and(b), respectively. Several other examples are also used to examine the performance of NUFBs using single stage and two stage IFIR prototype filter, which are depicted in Table 6.4. Performance of designed uniform and non-uniform NPR filter banks are compared with the performance of several other filter banks which is depicted in Table 6.5. This table shows that the proposed work has reduced the computational complexity significantly.

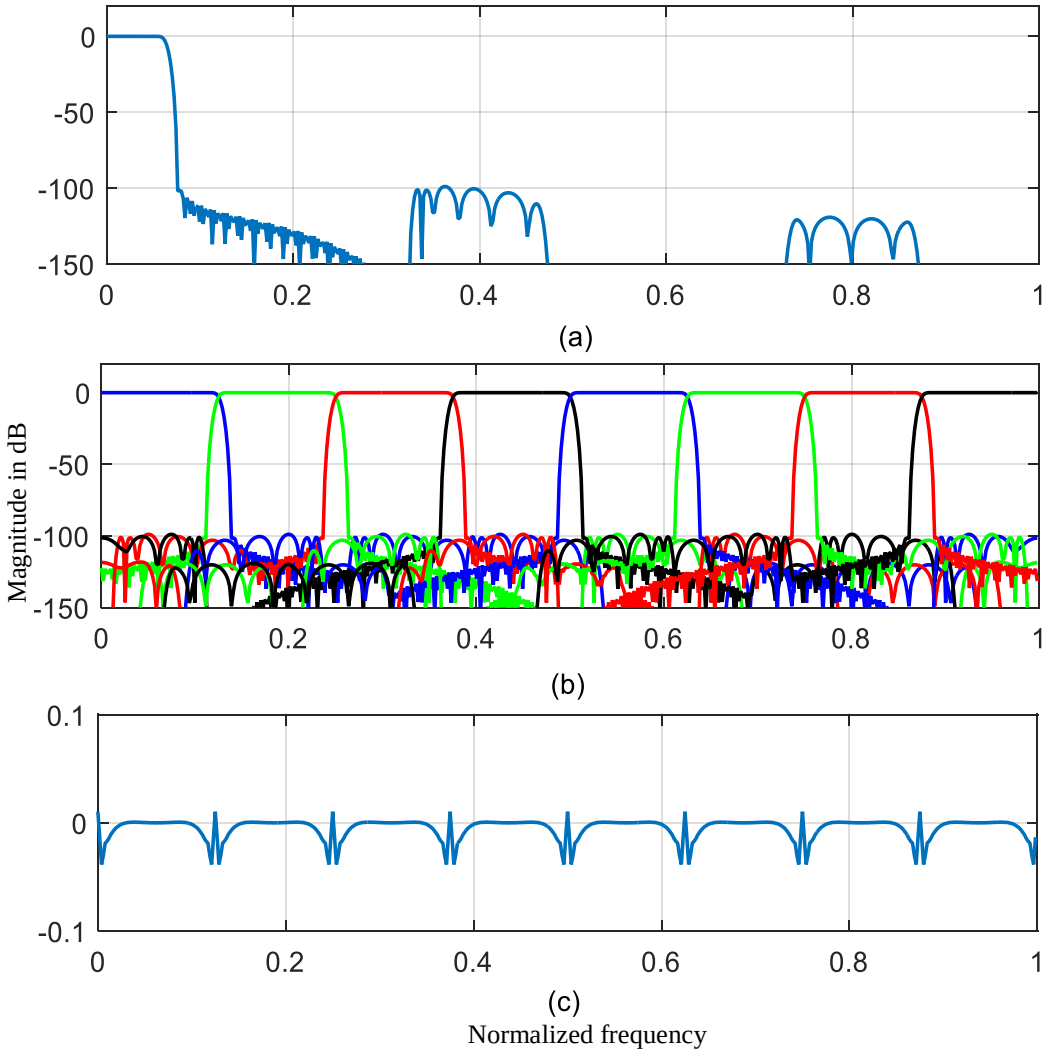

Fig. 6.6 Response of (a) Prototype low pass filter, (b) 8-band analysis filter bank and (c) Reconstruction error.

Table 6.3 Performance parameters of IFIRs filter for UFBs.

M	Filter	ω_s/π	ω_p/π	*N*	N_m	N_i	N_{1i}	N_{i2}	e_{am}	e_a	*PRE*	*CPU Time*	*Noe*	*CRC (%)*
4	FIR	0.250	0.083	100	-	-	-	-	0.0037	7.58×10^{-6}	0.0030	137.37	10	-
	IFIR	0.125	0.083	-	80	23	-	-	0.0036	2.92×10^{-7}	0.0030	116.855	14	60.05
8	FIR	0.062	0.031	416	-	-	-	-	0.0024	1.03×10^{-6}	0.0093	3.07×10^{2}	18	-
	IFIR	0.062	0.031	-	105	32	-	-	0.0039	1.30×10^{-6}	2.87×10^{-4}	3.06×10^{2}	10	69.62
	$IFIR_2$	0.062	0.031	-	102	-	25	12	0.0031	8.25×10^{-7}	5.36×10^{-4}	1.42×10^{2}	16	70.29
16	FIR	0.031	0.015	288	-	-	-	-	0.0020	5.24×10^{-6}	0.0020	3.61×10^{2}	19	-
	IFIR	0.065	0.015	-	89	32	-	-	0.0024	5.73×10^{-6}	0.0024	4.76×10^{2}	17	68.73
	$IFIR_2$	0.062	0.015	-	56	-	25	29	0.0027	1.08×10^{-6}	0.0027	4.765×10^{2}	17	77.03
32	FIR	0.031	0.007	576	-	-	-	-	0.0011	5.05×10^{-6}	0.0011	6.53×10^{2}	20	-
	IFIR	0.031	0.007	-	85	52	-	-	1.65×10^{-6}	3.16×10^{-6}	1.65×10^{-4}	6.33×10^{2}	17	78.79
	$IFIR_2$	0.031	0.007	-	73	-	28	18	0.0023	1.02×10^{-6}	0.0023	7.32×10^{2}	17	83.01

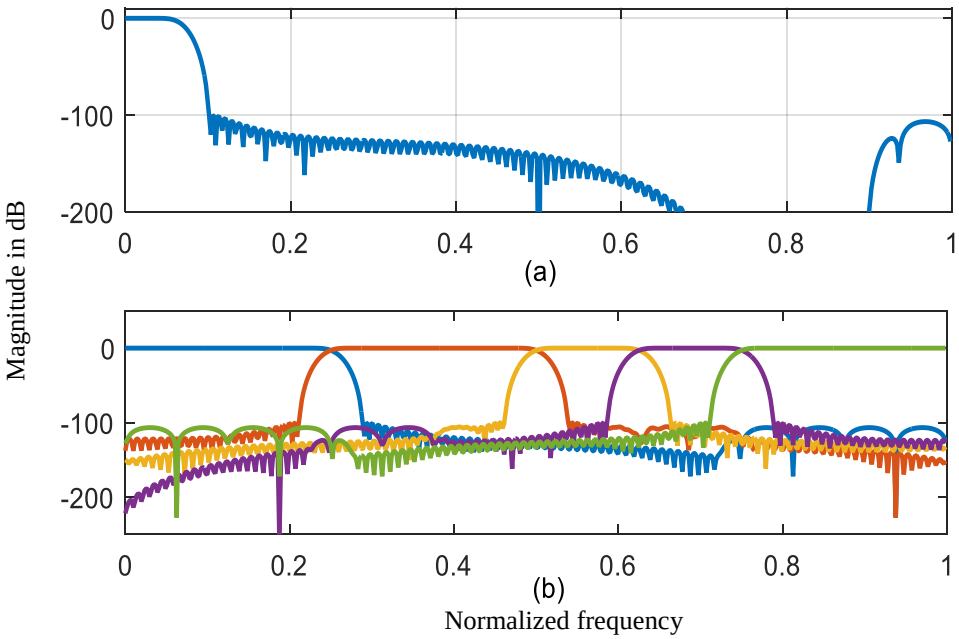

Fig. 6.7 Response of (a) Prototype low pass filter, (b) 5-band non-uniform analysis filter.

Table 6.4. Performance parameters of IFIRs filter for NUFBs

M	Filter	ω_s/π	ω_p/π	*N*	N_m	N_i	N_{1i}	N_{2i}	e_{am}	e_a	*PRE*	*CPU Time*	*Noe*	*%CRC*
3	FIR	0.1250	0.0833	312	-	-	-	-	0.0036	1.62×10^{-7}	0.0028	8.91×10^{3}	14	-
	IFIR	0.0625	0.0312	-	102	33	-	-	0.0036	2.92×10^{-7}	0.0030	8.92×10^{3}	14	60.05
4	FIR	0.0892	0.0290	384	-	-	-	-	0.0026	1.18×10^{-5}	0.0112	9.17×10^{3}	18	-
	IFIR	0.0625	0.0156	-	89	32	-	-	0.0024	5.73×10^{-6}	0.0024	4.76×10^{3}	17	68.73
	$IFIR_2$	0.0625	0.0156	-	56	-	25	29	0.0027	1.08×10^{-5}	0.0027	4.76×10^{3}	17	77.03
5	FIR	0.0694	0.0304	400	-	-	-	-	0.0025	1.89×10^{-7}	0.0011	9.02×10^{3}	20	-
	IFIR	0.0694	0.0304	-	108	26	-	-	0.0035	4.69×10^{-6}	0.0027	6.33×10^{3}	11	78.79
	$IFIR_2$	0.0694	0.0304	-		-	28	18	0.0038	1.28×10^{-7}	0.0023	7.32×10^{3}	17	67.90

Table 6.5. Comparisons of proposed work with other methods

Approach	**Filter**	e_{am}	A_s	e_a	*PRE*	*%CRC*
LP-NPR [297]	Parks-McClellan algorithm	7.803×10^{-3}	110	1.013×10^{-3}	-	-
NUFB [290]	constrained equiripple FIR technique	-	80	-	3.72×10^{-3}	-
CMFB [281]	CS optimized fractional derivative constraints	$1.4\times10-3$	30	$8.08\times10-8$	2.2×10^{-3}	-
Uniform CMFB [305]	IFIR filter	-	85	5.43e-07	0.0069	43.03
	Two stage IFIR filter	-	85	1.15e-06	0.0099	60.30
CMFB. [299]	Parks McClellan Algorithm	-	45	$2.62\times10-4$	4.35×10^{-3}	22
Proposed uniform CMFB	IFIR filter	0.0039	100	**1.3013e-06**	**2.8750e-04**	**69.62**
	Two stage IFIR	0.0314	100	**8.2502e-07**	**5.3622e-04**	**70.29**
Proposed non-uniform CMFB	IFIR filter	0.0035	100	**4.6909e-06**	**0.0027**	**72**
	Two stage IFIR	0.0038	100	**1.2814e-06**	**0.0023**	**84**

6.3.3. CMFB Design using Other Optimum Convex Method of Equiripple Filter

In this Section, designing the IFIR prototype filters essential is presented to contrivance the *M*-band pseudo QMF banks. In this method, optimization of a single parameter on a convex error surface is done, consistently delivering the best equiripple filter possible while minimizing the overlapped passband distortion using Eqn, (6.15). Steps used to design the prototype filter are given below [260].

$$\phi = \max_{\omega}\left\{\left|H(\omega)\right|^2 + \left|H\left(\omega - \frac{\pi}{M}\right)\right|^2 - \right\}, \quad 0 < \omega < \frac{\pi}{M} \tag{6.15}$$

Step 1. Specifications of *H(z),* such as: ω_p / π , ω_s / π and stopband ripple and passband are defined.

Step 2. Initial values of some parameters such as: step size (*step*), tolerance value (*Tol=±0.000001*), *Err = 10* and counter (*C= 0*) are specified.

Step 3. The value of *L* is estimated.

Step 4. Specifications of *F(z)* and *I(z)* are computed.

Step 5. *I(z)* is designed.

Step 6. *F(z)* is designed.

Step 7. Up-sampling of *F(z)*

Step 8. Convolution of up-sampled model filter and interpolator filter is done.

Step 9. Calculation of *Err* is done using Eqn. (6.15).

Step 10. Tolerance range is value is verified using Eqn. (6.16)

$$\left|Err - previous\ Err\right| < tol \tag{6.16}$$

a) If tolerance range is achieved then **Step 11** is executed.

b) If tolerance range is not achieved then greater than value ω_{pm} is changed according to $Err - previous\ Err$ value *i.e.*,

I). The ω_{pm} is increased using $\omega_{pm} = \omega_{pm}$ + *step* and go to **Step 11**

II). Otherwise, the value of ω_{pm} is decreased using $\omega_{pm} = \omega_{pm}$ - *step* and go to **Step 11**

Step 11. The counter value is increased by 1 and *step=step /2.*

Step 12. Redesigning of *F(z)* using new ω_{pm} is done with the same filter order and follow **Step 7** till the tolerance level is achieved.

The same steps are used for optimizing the two-stage IFIR prototype filter. The only difference is in designing of *I(z)* (**Step 5**), *i.e.,* first $I_1(z)$ and $I_2(z)$ are designed, then after up-sampling of $I_1(z)$ is done by factor L_1. After that the convolution of $I_1(z^{Li})$ and $I_2(z)$ is also done.

Example 6.7: In this example, 16-channel uniform CMFB is designed using design specifications; $\omega_s = 0.0625\pi$, $\omega_p = 0.0156\pi$ and $A_s = 100dB$ using methodology given above. Here, for model and interpolator filter design Parks–McClellan algorithm is used. The resulted parameters of CMFB using single stage IFIR filter are: $L=2$ $e_{am}= 5.1\times10^3$ $e_a= 1.5\times10^6$, $PRE=5.4\times10^3$, $NOE =11$, $CPU\ Time = 7.99\times10^3$ *ms*, and $CRC = 74.34\%$ and using two-stage IFIR prototype filter; $L= 5$, $L_1=2$, $e_{am}=1.0\times10^3$, $e_a = 2.9287\times10^6$, $PRE=8.4\times10^3$, $NOE = 98$, CPU Time = 0.295594 sec and $CRC = 49.19\%$. The resultant response of prototype filter, analysis bank, and reconstruction noise are shown in Fig. 6.8. The performance of this method with other optimization methods, are presented in Table 6.6 for 8-channel FBs. In this table, FIR, single staged IFIR and two-staged IFIR filter's fidelity parameters are presented.

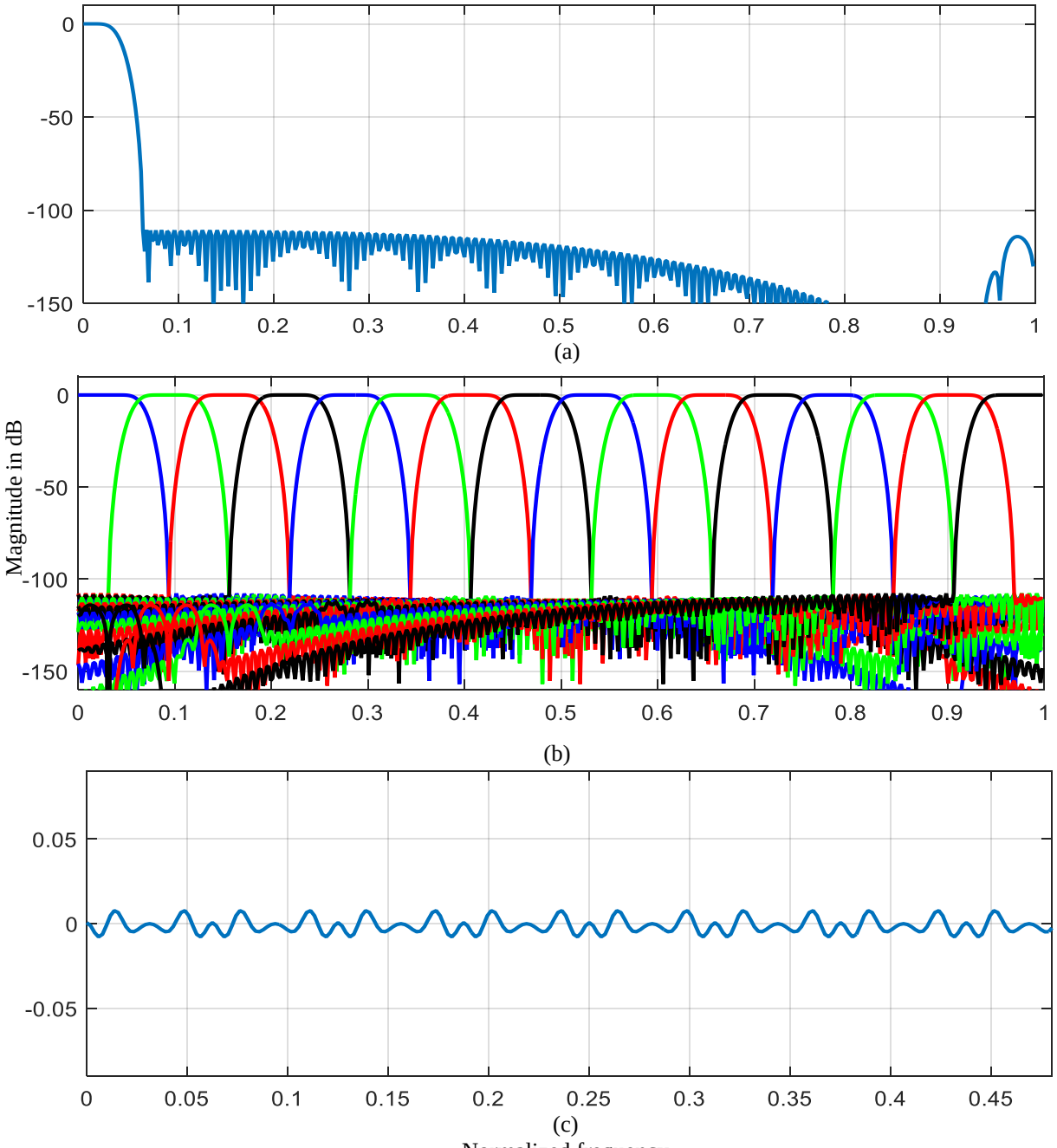

Fig. 6.8 Response of a) Prototype low pass filter, b) 8-band analysis filter bank and c) Reconstruction error.

Table 6.6. Performance of cosine modulated filter bank with other optimization

Approaches	Filter	e_{am}	e_a	PRE	Noe
Parks–McClellan algorithm,	FIR	0.0020	2.4084e-06	0.0088	60
	IFIR	0.0026	3.4765e-06	0.0057	206
	$IFIR_2$	0.0031	9.7823e-08	0.0134	98
Complex and nonlinear-phase equiripple FIR filter design	FIR	0.0055	2.4024e-09	0.0240	45
	IFIR	0.0026	3.4812e-06	0.0057	60
	$IFIR_2$	0.0031	9.9306e-08	0.0135	102
Constrained-least-squares FIR multiband filter design	FIR	0.0320	7.9828e-05	0.1365	50
	IFIR	0.0339	9.1136e-05	0.0729	71
	$IFIR_2$	0.0428	5.9976e-05	0.2854	71
Constrained-least-squares linear-phase FIR lowpass	FIR	0.0832	3.8292e-06	0.3522	57
	IFIR	0.0732	3.0956e-06	0.1561	91
	$IFIR_2$	0.2784	9.5383e-06	1.7263	70
Least-squares linear-phase FIR filter design	FIR	0.0012	3.2134e-07	0.0052	42
	IFIR	0.0031	3.8566e-06	0.0059	38
	$IFIR_2$	0.0035	2.4843e-07	0.0152	135

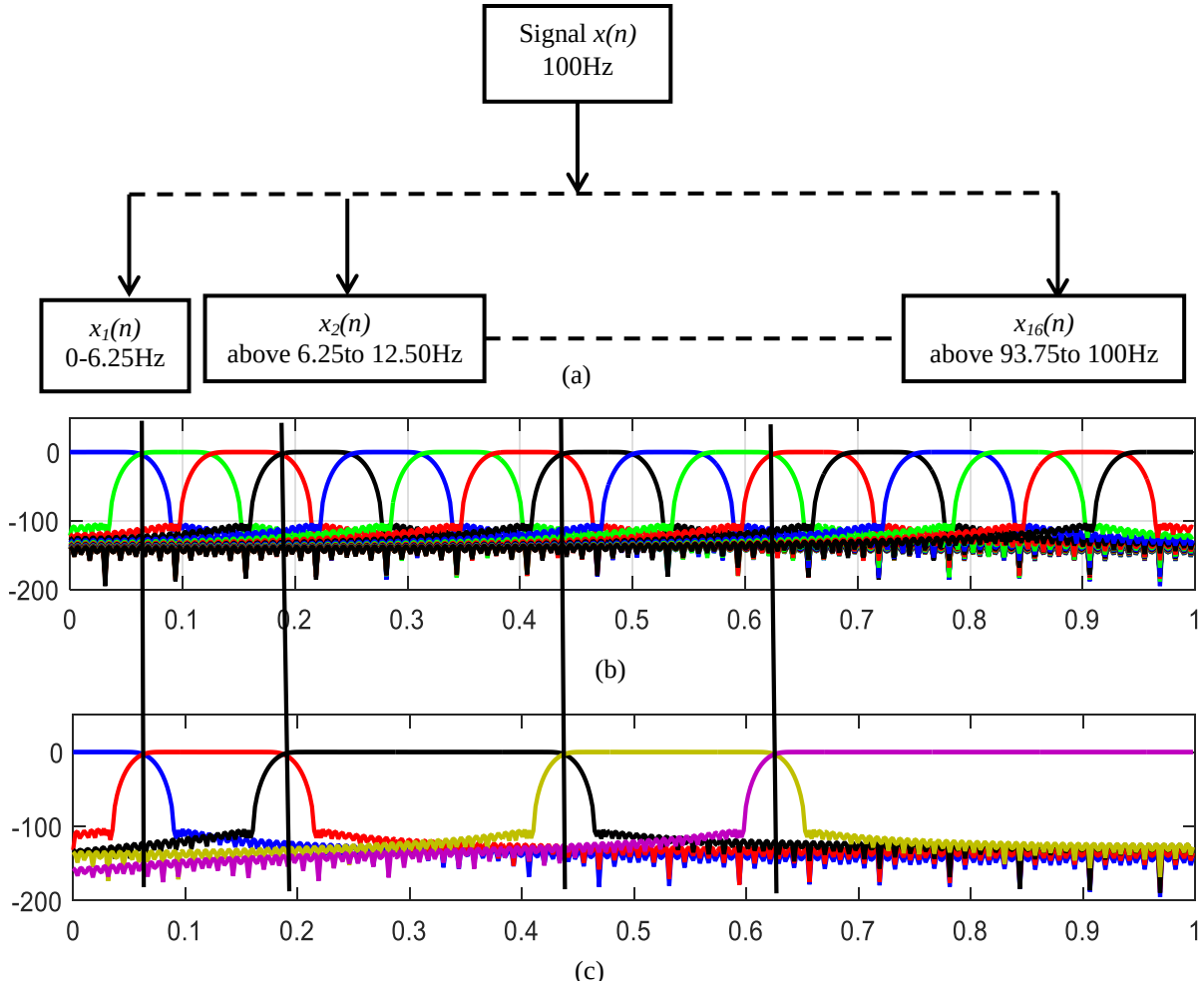

Fig. 6.9 a) Uniformly distribution of the signal, b) 16-channel UFB and c) 5-channel NUFB.

6.4. **Compression of ECG Rhythms using CMFB**

This section includes data compression and data decompression methodologies.

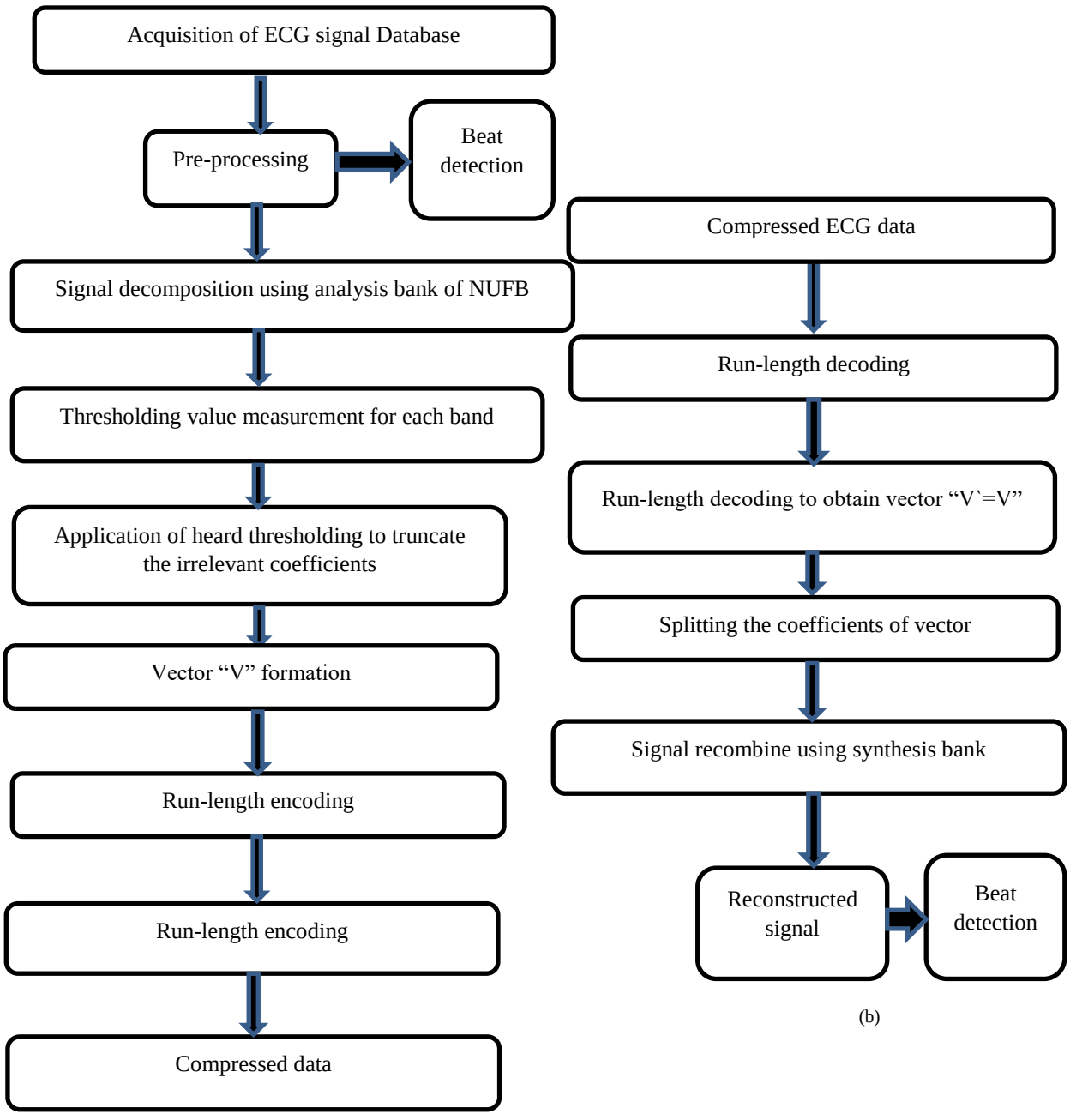

Fig. 6.10 Steps of (a) Proposed data compression technique and (b) Data reconstruction.

6.4. Compression of ECG Rhythms using CMFB and RLE

The data compression methodology is described as follows:

Step 1: Acquisition of the ECG signal

Here, the ECG database is taken from physionet. MIT-BIH arrhythmia database (lead MLII/V1/V2 and V5) is chosen to examine the performance of proposed method.

Step 2: Decomposition of the signal

Computationally efficient NUFB is used for the decomposition of signal. First, the *16*-channel uniform filter bank is designed using the steps given in Section 6.3. Each band of this FB has 6.25% frequency of total frequency, as depicted in Fig. 6.9(a). Then after, 5-channel NUFB is designed from 16-channel UFB by merging the bands, such as; $B_1= b_1$, $B_2= b_2+ b_3$, $B_3 = b_4+b_5+b_6+ b_7$, $B_4=b_8+b_9+ b_{10}$ and $B_5= b_{11}+ b_{12}+ b_{13} +b_{14}+ b_{15}+ b_{16}$, here, B and b represent bands of non-uniform and uniform CMFBs, respectively, it is shown in Fig 6.9(b) and (c). Therefore, the derived FB decomposes the signal into 5 bands, *i.e.*, one approximation band ($A_{5,}$ 0 to 6.25Hz) and four dilation bands (D_4 (above 6.25 to18.75 Hz), D_3 (above 18.75 to 43.75 Hz), D_2 (above 18.75 to 62.5 Hz) and D_1 (above 62.5to 100 Hz)).

Step 3: Estimation of the threshold value.

Selection of threshold value is a very important part of ECG signal compression. It should be done in such a way so that the maximum insignificant coefficient is removed without affecting the diagnostic information. More coefficients truncation will provide better compression ratio; however, a large value of threshold may affect the reconstruction quality of signal. Therefore, this study uses the following steps to estimate the value of threshold level. This method utilizes the most significant energy content in the signal. The energy distribution is represented in Table 6.7. Most of the significant energy is presented in A_5 (*i.e.*, 99%). Up to 0.8-1 % of energy is presented in D_4 and D_3. Remaining bands are having insignificant energy. Therefore, coefficients of D_2 and D_0 are not considered in this work. To estimate the value of thresholding for A_5, D_4 and D_3 following steps are used. To find the thresholding value, iteration methodology (Fig. 5.16) is used given below.

Table 6.7. Energy distribution in the bands of MIT-BIH record no- 100

Band	Energy present	Percentage
Total	28.337	100%
A_5	28.055	99.0050%
D_4	0.250	0.8842%
D_3	0.009	0.0341%
D_2	0.007	0.0279%
D_1	0.013	0.0089%

Step i: Coefficients are arranged in the ascending order

Step ii: The value of $k = 1$, $E_n = 0$ and desired energy E_d are specified (0.9978% of total energy for A_5, 0.0978 of total energy for D_4 and 0.0378 of total energy for D_3).

Step iii: The threshold value $= |X(k)|$ is applied in the signal, and the energy $E_n = E_n + |X(k)|^2$ is measured. The same steps are taken for obtaining, the threshold value for band D_4 and D_3.

Step 4: Computed threshold values are applied to their respective bands.

In this step, the extracted values of threshold (obtained by following Step 3) are applied to the respective signals. As a result, the coefficients that have a magnitude equal or less then the threshold value are replaced by zero.

Step 5: Vector formation

After application of thresholding, all the coefficients of signals A_5 D_4 and D_3 are put in a vector, such as:

$$V = [A_5\ D_4\ D_3] \tag{6.17}$$

Step 6: Run-length encoding is applied to V

Step 7: Run-length encoding

Further, the improvement in compression performance is obtained by applying run-length encoding on the vector, which has values of run-length coefficients.

Data reconstruction

At the receiver site, reconstruction of the signal is done using the following steps.

Step i: Compressed ECG signal is taken

Application of RLE compressed signal is given in three vectors, one is consisting of actual coefficients signal value and the other two are consisting of the run-length digits.

Step ii: Run-length decoding is applied

Run-length decoding is applied to two vectors, it converts the output into one vector.

Step iii: Further Run-length decoding is applied

Run-length decoding is applied to two vectors; *i.e*., one is obtained from the output of previous step (run-length decoding) and another consists of the original coefficient value (*i.e*, an output of Step 7). After this step, all the coefficients are kept in one vector *V`*.

Step iv: Dividing the coefficients of vector *V`* is performed.

Divide the coefficients of vector *V`* to obtain the coefficients of three groups, such as A_5, D_4, and D_3.

Step v: Reconstruction of the signal is done by using the synthesis filter bank.

Signal reconstruction steps are given in Fig. 6.10(b).

Example 6.8: MIT-BIH database record no. 103 is chosen for the compression. First, the decomposition of this signal is done by using 5-channel CMFB. Most of the informational energy is presented in A_5, D_4, and D_3 and remaining bands have approximate irrelevant coefficients. Thresholding values for each band are measured by following the steps given in Section 6.4, Step 3. The obtained values of threshold for band A_5, D_4, and D_3 are 0.102mv, 0.03mv and 0.02mv, respectively. Extracted threshold values are applied to corresponding signals. And then coefficients are truncated. Then after using these coefficients, a vector *V* is formed as given in Step 5. After this, RLE is applied to *V*, for improving the results in terms of CR. It provides two vectors one for information valued coefficients and other for frequency of the information valued coefficients. The second vector is again decomposed into two vectors for further improvement in the compression. The compression ratio is measured by using expression given in Eqn. (4.32).

6.4.1. Data Reconstruction

Signal reconstruction is obtained by following the steps given in Fig. 6.10(b). Here, also MIT-BIH database record no. 103 is chosen. The compressed signal is obtained after run-length encoding (last step of Fig 6.10(a)). Vector *V`* is obtained by applying the run-length decoding two times. Coefficients of vector V`= coefficients of V. After obtaining these coefficients, distribution of these coefficients is done for extracting A_5, D_4, and D_3. Then after, these signals are applied to the synthesis bank of CMFB to recombine the result. Finally, the reconstructed signal is obtained. Fidelity parameters of reconstruction signal analysis can be obtained by using Eqns. (4.33) to (4.39). The resultant values of these parameters are: *PRD*=1.2744%, *PRDN*=1.3062%, *CC=99*, *SNR*=37.89, *MSE* = 0.0325 and *ME*=0.0234. The graphical comparison of original and reconstructed signal is

illustrated in Fig. 6.11, which depicts that the reconstructed signal is a delayed version of the input signal. This methodology is applied to both the database of MIT-BIH arrhythmia database for all 48 records. The performance indices for other signals are given in Table 6.8 and Table 6.9.

Form the above experimental consequences, it can be seen that the proposed method can be used for biomedical signals in terms of signal compression. It has been examined on the MIT-BIH arrhythmia database. Table 6.8 and 6.9 illustrate the resulting values of CR and PRD, PRDN, CC SNR, MSE, ME and QS performance measures for the considered compression methods. Fig. 13 depicts the visual comparison of the original and reconstructed signal. The average value of CR is *23.99* for a dataset I and for dataset II, it is *23.73*. For the same signals, this method provides excellent performance in terms of CR, such as; record no 100, 203 and 207 of the dataset I and record no 107, 116 and 220 of dataset II. The average value of PRD is *1.308* for a dataset I and for dataset II, it is *1.503*. In Table 6.10, performance comparison of the proposed work with several existing methods is done which shows that the proposed work compresses ECG signals better than the existing methods.

Table 6.8 Performance parameters of compression using MIT-BIH arrhythmia dataset I

Sl.no	Signal	CR	PRD	PRDN	CC	SNR	MSE	ME	QS
1.	100	**30.35**	2.4701	2.5748	0.9997	32.14	0.0346	0.5730	12.28695
2.	101	29.19	2.1089	2.1964	0.9998	33.51	0.0344	0.0198	13.84134
3.	102	21.30	0.4838	0.5070	1	46.30	0.0674	0.0570	44.02646
4.	103	27.30	1.2744	1.3062	0.9999	37.89	0.0325	0.0234	21.42185
5.	104	21.65	1.6745	3.0150	0.9995	35.52	0.0840	0.1385	12.92923
6.	105	27.22	1.3022	1.4004	0.9999	37.70	0.0320	0.0643	20.90309
7.	106	25.94	1.5888	1.7605	0.9998	35.97	0.0831	0.0848	16.32679
8.	107	22.38	1.1148	1.1174	0.9999	39.05	0.1673	0.4308	20.07535
9.	108	22.38	1.1148	1.1174	0.9999	39.05	0.1673	0.4308	20.07535
10.	109	27.81	2.7790	2.9411	0.9996	31.12	0.0412	0.0834	10.00720
11.	111	24.06	1.5668	2.3600	0.9997	36.09	0.0384	0.0862	15.35614
12.	112	21.88	0.7870	2.1816	0.9998	42.08	0.0353	0.0984	27.80178
13.	113	25.71	1.6913	1.7568	0.9998	35.43	0.0989	0.1205	15.20132
14.	114	21.39	0.9124	1.6296	0.9999	40.79	0.0393	0.0993	23.44367
15.	115	24.98	1.4842	1.5866	0.9999	36.57	0.0401	0.0541	16.83062
16.	116	21.40	1.0421	1.4768	0.9999	39.64	0.1416	0.1312	20.53546
17.	117	22.27	1.0970	2.4995	0.9997	39.19	0.0606	0.1414	20.30082
18.	118	21.19	0.8361	1.7210	0.9999	41.55	0.0664	0.1613	25.34386
19.	119	21.76	0.9404	1.3311	0.9999	40.53	0.0735	0.1610	23.13909
20.	121	17.96	1.1599	2.3428	0.9997	38.71	0.0495	0.1553	15.48409
21.	122	21.73	1.0315	1.6811	0.9999	39.73	0.0621	0.1592	21.06641
22.	123	22.97	0.9220	1.8195	0.9998	40.70	0.0499	0.1121	24.91323
23.	124	22.93	0.9901	1.4866	0.9999	40.08	0.0548	0.1613	23.15928
24.	200	22.98	1.2001	1.3507	0.9999	38.41	0.0645	0.1890	19.14840
25.	201	25.17	1.2689	1.7460	0.9998	37.93	0.0214	0.0348	19.83608
26.	202	21.88	1.1012	2.1335	0.9998	39.16	0.0421	0.0947	19.86923
27.	203	**33.42**	0.9126	0.9657	1.0000	40.79	0.0466	0.0491	37.05895
28.	205	21.09	1.9729	1.9729	0.9998	34.09	0.0239	0.0392	10.68985
29.	207	**32.42**	1.2654	1.4347	0.9999	37.95	0.0340	0.0614	25.62036
30.	208	23.69	1.4365	1.5973	0.9999	36.85	0.1278	0.3867	16.49147
31.	209	22.77	1.4921	2.0933	0.9998	36.52	0.0459	0.0899	15.26037
32.	210	23.86	1.2886	1.8363	0.9998	37.79	0.0353	0.0776	18.51622
33.	212	23.38	1.2175	1.4371	0.9999	38.29	0.0409	0.0926	19.20329
34.	213	23.32	1.2657	1.2819	0.9999	37.95	0.0940	0.3184	18.42459
35.	214	23.27	0.8783	1.0039	1.0000	41.12	0.0415	0.0703	26.49436
36.	215	23.69	1.7116	2.3699	0.9997	35.33	0.0553	0.1515	13.84085
37.	217	23.17	0.8950	0.9653	1.0000	40.96	0.0584	0.1210	25.88827
38.	219	21.75	0.8112	0.9222	1.0000	41.81	0.0327	0.0835	26.81213
39.	220	22.07	1.6687	2.0574	0.9998	35.55	0.0740	0.0819	13.22586
40.	221	23.80	1.2960	1.5842	0.9999	33.40	0.0402	0.0543	18.36420
41.	222	22.88	1.6578	3.1543	0.9995	35.60	0.0425	0.0844	13.80142
42.	223	22.57	1.1371	1.2686	0.9999	38.88	0.0448	0.1443	19.84874
43.	228	26.25	2.3370	2.7636	0.9996	32.62	0.0438	0.0541	11.23235
44.	230	28.65	1.0960	1.1230	0.9999	39.20	0.0299	0.0373	26.14051
45.	231	22.44	1.0340	1.4309	0.9999	39.70	0.0309	0.0691	21.70213
46.	232	23.61	1.8287	3.2990	0.9995	34.75	0.0270	0.0380	12.91081
47.	233	23.72	0.6915	0.7096	1.0000	43.20	0.0323	0.0752	34.30224
48.	234	23.82	0.9797	1.3510	0.9999	40.17	0.0297	0.0743	24.31357

Table 6.9 Performance parameters of compression using MIT/ BIH arrhythmia dataset II

Sl no.	Signal	CR	PRD	PRDN	CC	SNR	MSE	ME	QS
1.	100	22.82	2.1438	3.621	0.9993	33.37	0.0354	0.0785	10.6446
2.	101	21.88	1.8428	9.648	0.9953	34.69	0.0307	0.0693	11.8732
3.	102	25.27	1.8840	2.568	0.9997	34.49	0.0365	0.0429	13.4129
4.	103	21.92	1.2673	2.140	0.9998	37.94	0.0419	0.1082	17.2966
5.	104	21.53	1.2728	2.622	0.9997	37.9	0.0832	0.1446	16.9154
6.	105	21.90	1.1218	5.141	0.9987	39.00	0.0564	0.1623	19.5222
7.	106	21.59	1.1955	9.408	0.9956	38.44	0.051	0.1452	18.0593
8.	107	**31.65**	1.0599	1.176	0.9999	39.49	0.0995	0.2283	29.8613
9.	108	22.28	0.6576	0.907	1.0000	43.64	0.0365	0.1044	33.8807
10.	109	23.76	1.2557	1.380	0.9999	38.02	0.0797	0.2576	18.9217
11.	111	22.02	1.0163	2.050	0.9998	39.85	0.0549	0.1763	21.6668
12.	112	22.05	1.5151	6.183	0.9981	36.39	0.0332	0.0639	14.5534
13.	113	21.73	0.9294	2.256	0.9997	40.63	0.0516	0.1401	23.3806
14.	114	23.30	2.3242	4.572	0.9990	32.67	0.0416	0.0844	10.0249
15.	115	26.03	2.8224	4.904	0.9988	30.98	0.0306	0.0513	9.22264
16.	116	**35.84**	2.4352	3.347	0.9994	32.26	0.0860	0.2248	14.7174
17.	117	23.25	1.7626	1.964	0.9998	35.07	0.0549	0.0303	13.1907
18.	118	23.14	1.5690	2.247	0.9997	36.08	0.0577	0.0764	14.7482
19.	119	23.14	1.5690	2.247	0.9997	36.08	0.0577	0.0764	14.7482
20.	121	27.55	1.8127	1.934	0.9998	34.83	0.0552	0.0613	15.1983
21.	122	22.21	1.3336	2.360	0.9997	37.49	0.0314	0.0712	16.6541
22.	123	17.39	2.4444	4.193	0.9991	32.23	0.0600	0.0929	7.11422
23.	124	24.14	1.5687	2.629	0.9997	36.08	0.0350	0.0800	15.3885
24.	200	21.75	1.2092	14.46	0.9895	38.34	0.0592	0.1189	17.9871
25.	201	23.31	2.0761	2.939	0.9996	33.65	0.0273	0.0419	11.2277
26.	202	21.88	1.0677	3.399	0.9994	39.43	0.0461	0.1278	20.4926
27.	203	21.68	1.2916	2.823	0.9996	37.77	0.0543	0.1107	16.7853
28.	205	26.60	3.0190	7.367	0.9973	30.40	0.0263	0.0446	8.81086
29.	207	22.00	0.8597	1.047	0.9999	41.31	0.0418	0.1186	25.5903
30.	208	22.10	0.9659	1.625	0.9999	40.30	0.0551	0.1444	22.8802
31.	209	21.52	1.1776	7.235	0.9974	38.57	0.0541	0.1364	18.2744
32.	210	21.82	1.1404	4.787	0.9989	38.85	0.0465	0.1288	19.1336
33.	212	22.56	0.8244	1.209	0.9999	41.67	0.0504	0.1077	27.36536
34.	213	25.06	1.8192	2.077	0.9998	34.8	0.2402	0.5888	13.77529
35.	214	22.06	0.8452	1.158	0.9999	41.46	0.0573	0.1156	26.10033
36.	215	21.6	1.0764	2.765	0.9996	39.36	0.0589	0.1434	20.06689
37.	217	21.63	0.8334	1.065	0.9999	41.58	0.0421	0.1012	25.95392
38.	219	26.78	1.5827	1.643	0.9999	36.01	0.0469	0.1504	16.92045
39.	220	**32.27**	4.0672	4.074	0.9992	27.81	0.0374	0.0208	7.934205
40.	221	21.72	0.9392	2.421	0.9997	40.54	0.0435	0.1081	23.12606
41.	222	**35.82**	2.2937	2.684	0.9996	32.78	0.0341	0.0635	15.61669
42.	223	27.55	1.7336	1.734	0.9998	35.22	0.0349	0.0544	15.89179
43.	228	21.06	1.1434	1.269	0.9999	38.83	0.0715	0.1004	18.41875
44.	230	24.22	1.3032	1.776	0.9998	37.69	0.0344	0.0703	18.58502
45.	231	21.84	0.9819	2.901	0.9996	40.15	0.0468	0.1319	22.24259
46.	232	21.88	1.0473	3.929	0.9992	39.59	0.0576	0.1489	20.89182
47.	233	22.22	0.9109	1.147	0.9999	40.81	0.0495	0.1523	24.39346
48.	234	21.78	1.1412	4.407	0.999	38.85	0.0454	0.1295	19.08517

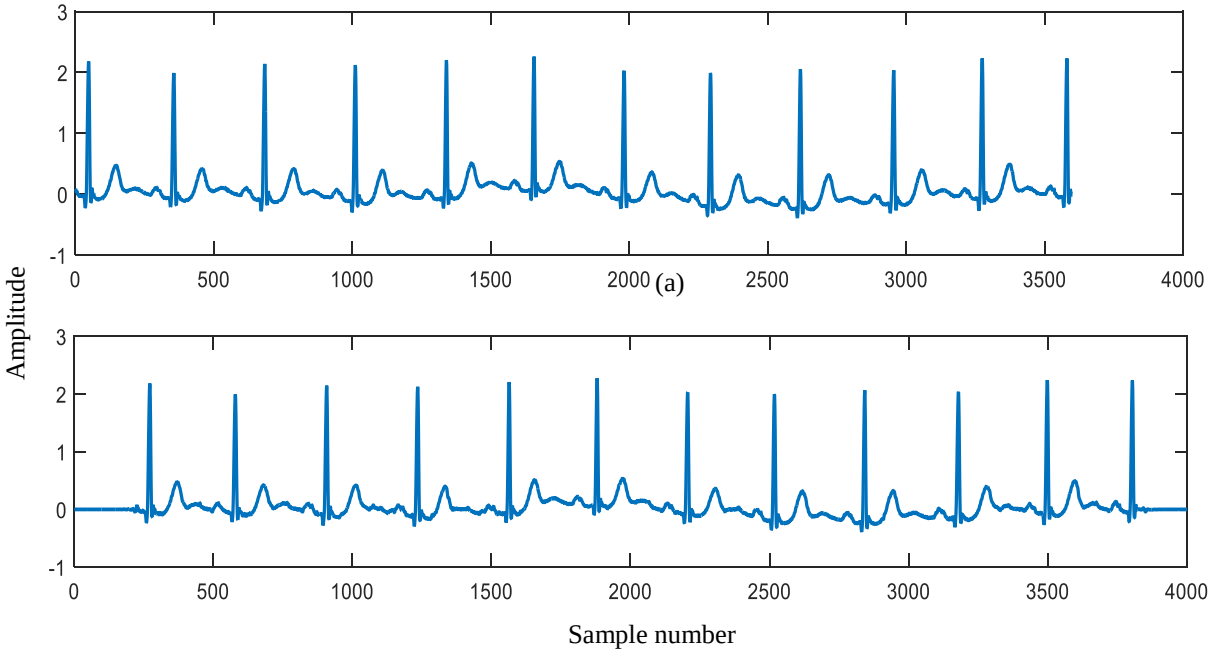

Fig. 6.11 (a) Original and (b) reconstruction signal.

Table 6.10 Performance comparison of proposed data compression method with several existing methods

Approach	Year	Dataset	PRD	CR
Proposed	2018	**MIT/ BIH arrhythmia dataset I 100**	**2.4701**	**30.35**
		MIT/ BIH arrhythmia dataset I 207	**1.2654**	**32.42**
		MIT/ BIH arrhythmia dataset II 107	**1.059**	**31.65**
		MIT/ BIH arrhythmia dataset II 116	**2.4352**	**35.84**
		MIT/ BIH arrhythmia dataset I average	**1.308**	**23.99**
		MIT/ BIH arrhythmia dataset II average	**1.503**	**23.73**
[135]	2017	Recorded case #1	4.30	5.12
		Recorded case #2	5.66	5.50
		Recorded case #3	4.93	5.10
[126]	2016	MIT/ BIH arrhythmia dataset 100	1.00	16.83
		MIT/ BIH arrhythmia dataset 207	1.03	31.12
[136]	2014	MITBIH record no.215, M 81	1.07	31.39
[156]	2002	MIT/ BIH arrhythmia dataset 117	1.06	22.19
		MIT/ BIH arrhythmia dataset 119	1.98	23.1
[138]	2013	MIT/ BIH arrhythmia dataset 124	1.11	6.06
		MIT/ BIH arrhythmia dataset 117	2.5	5.95
[132]	2015	MIT/ BIH arrhythmia dataset 117	0.31	7.24
		MIT/ BIH arrhythmia dataset 117	1.05	19.44
[182]	2017	MIT/ BIH dataset average	3.43	11.49

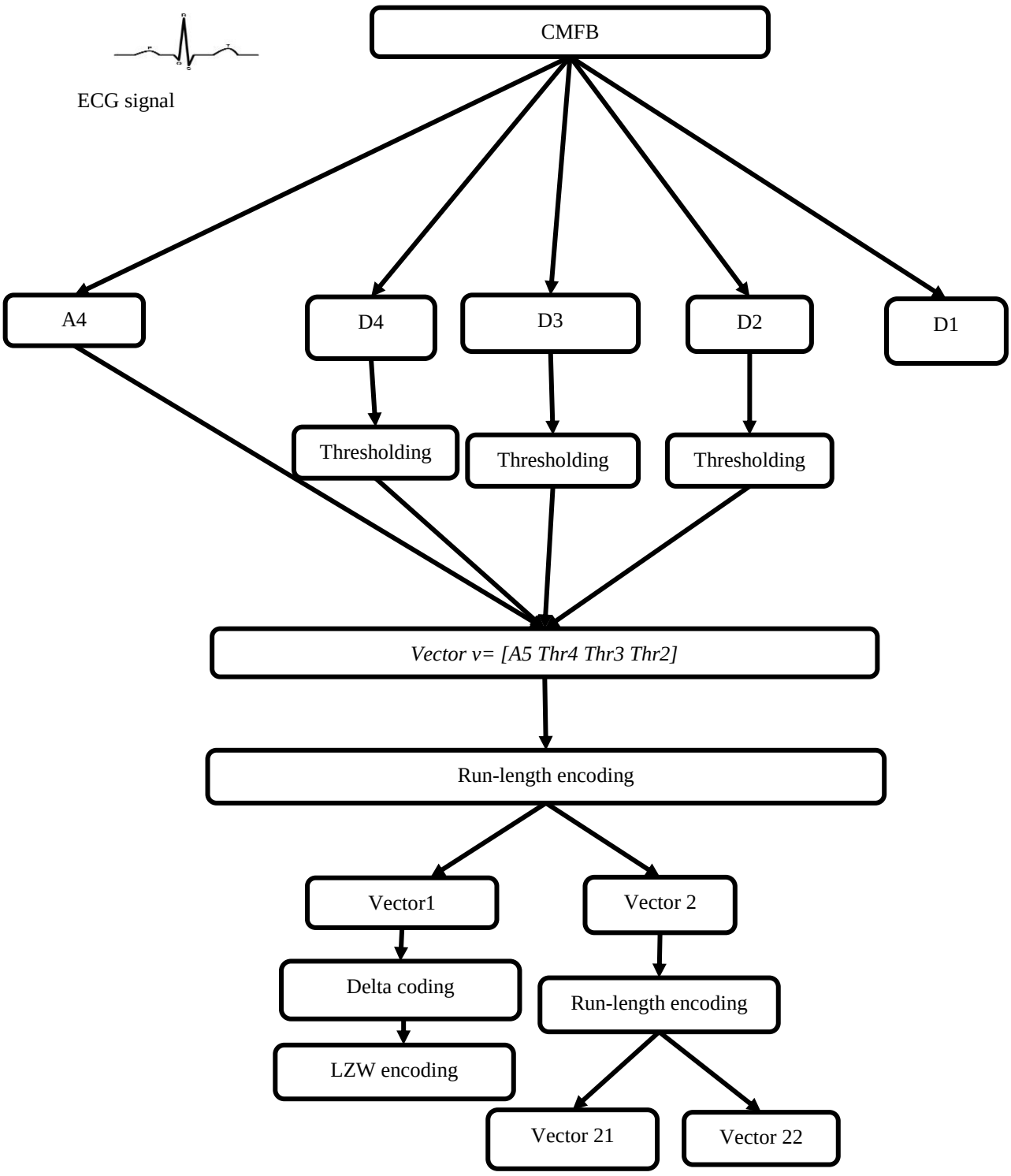

Fig. 6.12 Data compression technique using LZW and RLE.

6.4.2. Compression of ECG Rhythms using CMFB and LZW Encoding

In this section, data compression is performed by utilizing CMFB with RLE and LZW based hybrid coding. The steps of this methodology are presented in Fig. 6.12. Here, the CMFB is designed using Remez exchange algorithm: illustrated in Section 6.3.3. In this methodology, two steps are added in the previous methodology, *i.e.* coefficients of vector *v1* are delta encoded, and then preceded by LZW coding. LZW coding is used to increase the compression performance without affecting the reconstruction quality. The LZW coding is a "dictionary-based" lossless compression method, which looks for repetitive sequences of data that are used to build a dictionary. The reconstruction of ECG signal from its compressed version begins with the LZW. Remaining steps are same as the prior methodologies. The reconstruction steps are shown in Fig. 6.13. The original and reconstructed signals are depicted in Fig. 6.14, which shows that the reconstructed signal is the delayed form of original signal. The comparison of CRs obtained by different coding and CMFB based methodologies is presented in Table 6.10 and Fig. 6.15.

CMFBs are popular among all other types of FB due to ease and efficient implementation. Several approaches have been used to design this type of CMFBs as discussed in the introduction section. Linear search optimization techniques are used to optimize the coefficients of the filter because it is simple and easy in implementing. Window technique is used to design the prototype filter, because it provides high stopband attenuation with low computational complexity. IFIR filter has been used, because it provides very less computational complexity in order to reduce the filter order. Further, improvement in reduction in computational complexity is done using multistage IFIR prototype filter. From Table 6.1, 6.2, 6.3, 6.3, 6.4 and 6.5, it can be ascertained that IFIR prototype based CMFBs are more efficient than the FIR for both the cases (*i.e.*, uniform and non-uniform filter bank). In order to authenticate the effectiveness of proposed FBs for ECG signal compression application, it is tested for numerous ECG signal (MIT/BIH arrhythmia database dataset I and II) available in the Physionet. ECG signal is a non-stationary signal, therefore to process this type of signals; time–frequency signal processing is always desired.

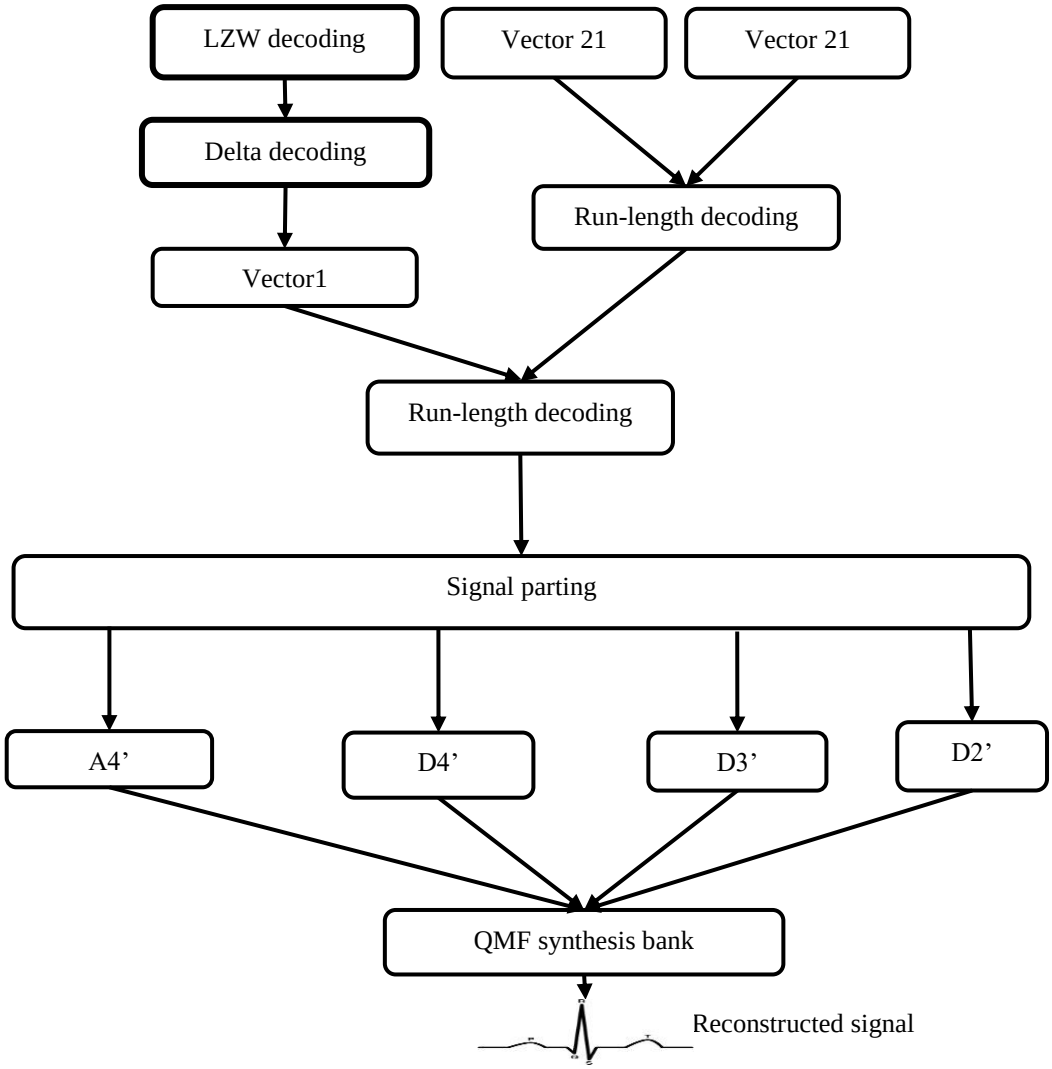

Fig. 6.13 Signal Reconstruction Steps.

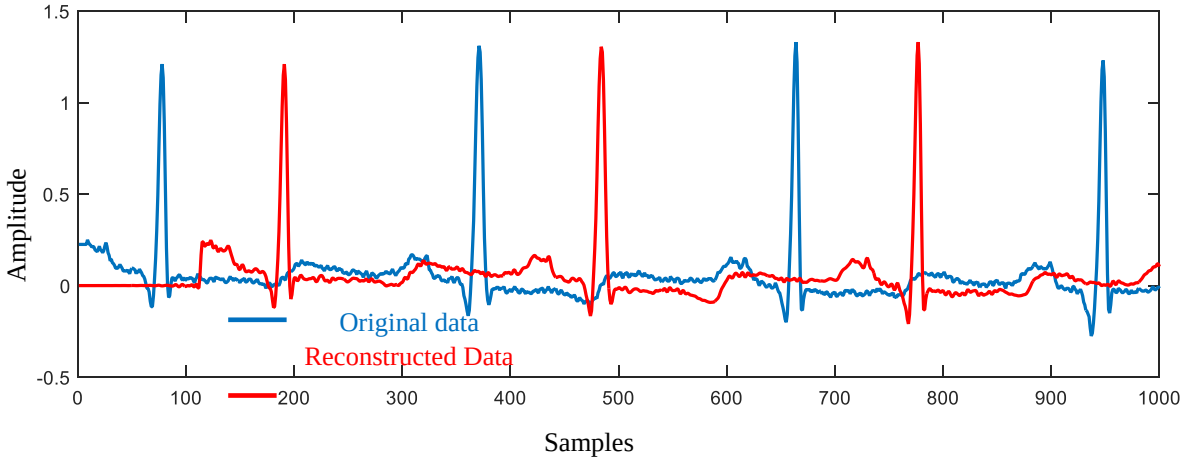

Fig. 6.14 Original and reconstructed MIT/BIH record.

Table 6.11 Performance comparison of proposed data compression method with several existing methods

Dataset	CR (RLE)	CR (RLE+RLE)	CR (lzw)	CR (lzw+RLE)	CR (RLE +RLE) With iterative thresholding	CR (Huffman coding) With quantization
100	12.6205	15.1746	16.341	18.7053	**30.35**	17.9682
101	10.3073	11.9500	16.272	16.5117	29.19	17.2756
102	6.7324	11.7121	10.036	14.6389	21.3	11.46821
103	8.4508	9.7613	14.3221	15.2742	27.3	15.39626
104	7.1947	12.6101	10.7416	18.6602	21.65	12.01415
105	10.9101	14.4986	12.7255	15.3956	27.22	13.98963
106	12.6833	17.6018	12.6413	15.3043	25.94	13.78793
107	10.7718	16.6261	11.4663	13.2830	22.38	12.6044
108	8.1797	12.6518	11.3810	16.8348	22.38	12.38205
109	9.2479	13.6938	10.0105	14.0290	27.81	10.97948

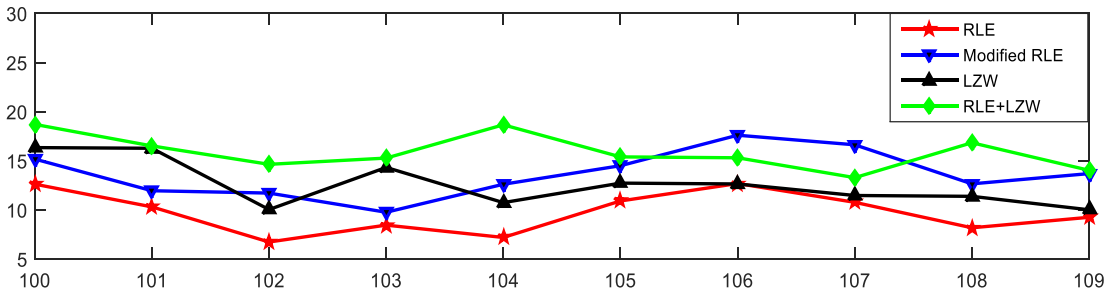

Fig. 6.15 Data compression performance of different encoding with CMFB.

Filter bank based approaches are always preferred than other methods, because these types of methods provide better localization of the signal components in time–frequency space unlike other methods, *viz*., Fourier transform and short-time Fourier transform. From Tables. 6.8 and 6.9, it is observed that the proposed methodology provides a very good performance in terms of CR, PRD and several parameters. The proposed methodology provides better results in comparison to numerous existing methods of data compression of ECG signal as shown in Table. 6.10.

6.4. Summary

In this chapter, computationally efficient uniform and non-uniform CMBs have been designed using different filter design techniques. The performance of the proposed filter banks is better than the performance of other filter banks in terms of computational complexity, as depicted in Table 6.5. Proposed NUFB is used to compress the ECG signal by decomposing it into different bands. Threshold values for each band are obtained using the iterative method based on energy coefficients. Different coding methods, *viz*., RLE/modified RLE/LZW/ LZW+RLE have been used to improve the performance of compression. Several results show that the proposed data compression method is superior to several existing methods in terms of CR and PRD (Table 6.10). Therefore, it is concluded that the proposed method can be used very effectively and efficiently for data compression of ECG signals. The proposed CMFBs can also be used to compress the multi-lead ECG dataset and to detect other features of ECG signal.

CHAPTER 7

PERFORMANCE EVALUATION

7.1. Overview

The main objective of data compression of ECG signal is to eliminate the irrelevant information (*i.e.*, diagnostic information remains same). However, achieving high compression without affecting the diagnostic information is a difficult task. Therefore, numerous studies are given for the data compression of ECG signal for last 3-4 decades, in which different methodologies are used [18]. In most of the studies, the data reconstruction performance is estimated using mathematical parameter *i.e.*, percentage root mean square difference (PRD). In some studies, performance is evaluated using, correlation coefficient (CC), percentage root mean square difference normalized (PRDN), and several other parameters given in Chapter 4. However, for measurement of signal reconstruction quality of a biological data, such measurement parameters are almost irrelevant. According to the physiologists, original and reconstructed data must have the same diagnostic information. Thus, the data reconstruction quality must be examined by analyzing both signals (*i.e.*, feature to feature comparison). Therefore, the weighted diagnostic distortion (WDD) parameter is introduced, which show the feature to the comparison of both signals. In this chapter, feature extraction using wavelet and CMFB is done. The extraction of other features, *viz.*, Q waves, S waves, P waves, T waves, P wave onset & offset points, T wave onset & offset points, QRS onset and offset points are identified using some rule-based algorithms. The performance of data compression and decompression is measured using a comparison of extracted features. In this chapter, WDD is also used to measure the performance of signal reconstruction. Two new features are used to measure the WDD.

7.2. Beat Detection using WT

The WT provides the depiction of signal in time-frequency scale, allowing the illustration of time-based features of a non-stationary signal at various resolutions. Hence, it is an appropriate mathematical tool to examine an ECG signal [70]. Several researchers have

proposed techniques based on wavelet transform for beat detection, arrhythmia classification and ECG data compression [273]. In this section, R-peaks are detected using WT, for which Bi-orthogonal wavelet is used, because it is more flexible and allows more degree of freedom.

The following steps are used for R-peak detection:

Step 1: Acquisition of EGG signals: In this study, the MIT-BIH arrhythmia database is taken as the input signal.

Step 2: Elimination of different kinds of noise: Elimination of noise is done using MODWT (described in Sections 2.3.3.3 and 3.5.1) and universal thresholding. The expression used to find the thresholding is presented by Eqn. (7.1) for *n* number of signal coefficients.

$$Tuv = \sqrt{2 \times \log n\hat{\sigma}} \tag{7.1}$$

where, $\hat{\sigma}$ is an estimate of the noise level [29].

Step 3: Decomposition of signal: Decomposition of the signal into number of frequency bands is done by using DWT. Bi-orthogonal wavelet is used for decomposition, and 3 levels of decomposition is done.

Step 4: Peaks detection: Peak detection is done using thresholding.

Step 5: R-peak detection: R-peaks detection is performed using Eqn. (7.2).

$$R_i = P_i \times 2^j \tag{7.2}$$

where, R_i is the i^{th} R-peak location, P_i, i^{th} peak location detected by **Step 4**, $i = 1, 2, ..., K$ and K is the total number of peaks present in the signal of 30 minutes duration. Actual R-peak location is obtained by detecting the peak location of signal between the samples from $R_i - 16$ *to* $R_i + 16$. This window segment of 33 samples has been decided on the basis of extensive testing and detailed observation of the MIT-BIH dataset. After detection of R-peaks, R-R intervals and heart rate are measured.

Detection of heart rate is not the complete study of an ECG signal. A normal heart rate signal may include different abnormal rhythms or arrhythmias. These arrhythmias are classified as: supra-ventricular arrhythmias, atrial fibrillation, atrial utter, paroxysmal supraventricular tachycardia, ventricular arrhythmias, ventricular tachycardia, ventricular fibrillation, etc. These arrhythmias are analyzed by observing all the components of ECG signal (a complete study includes the amplitude and duration of ECG wave components).

Therefore, estimating ECG rhythms as normal or abnormal, extraction of other features besides the heart rate is equally important. This work presents the extraction of all such diagnostic features using different algorithms.

7.3. R-Peaks Detection using CMFB

In this section, R-peaks detection is done using uniform CMFB and thresholding by following the steps given below:

Step 1: ECG signal acquisition

Step 2: Signal decomposition

Signal decomposition is done using the 8-channel uniform analysis bank of CMFB. Here, computationally efficient CMFB is used, which is given in Chapter 6.

Step 3: Detection of the peak points

Detection of these peaks can be done using time and amplitude thresholding.

Step 4: Detection of R-peaks in the original signal.

Since, 8-band decomposition followed by the down-sampling factor 8 is done, therefore in the original signal, R-peaks come at $R_i=8\times r_i$ sample locations. Here, R is the approximate R-peaks location in original signal and r_i is the peak locations on decomposed signal and $i=1,2,3,\ldots\ldots\ldots\ldots n$, n is the number of R-peaks present in the signal. Actual R-peak locations are determined by extraction of peak amplitude, location between the sample's value R_i-4 *to* R_i+4. Detection of R-peaks is done for both the signals (original and reconstructed signal). After detecting R-peaks, a comparative study is done for the detected R peaks locations and amplitude of original and reconstructed.

7.4. Feature Extraction

In this section, feature detection techniques are described.

Q and S-Waves Detection

Detection of Q-waves includes the following steps

Step 1: Take ECG signal: for detection of Q wave, also 3rd level decomposed ECG signal is chosen (achieved by wavelet decomposition).

Step 2: Define a counter: it is assumed that the number of R-waves is equal to the number of Q waves, thus set the counter equal to the total number of R-waves, also set $b=1$.

Step 3: Select the time interval: Q-wave occurs just before the R wave, so the time interval is 0.2 seconds before the corresponding R wave. So, for detection of Q-wave, the time interval is chosen = 0.025 sec *i.e.*, 9 samples of 3rd level decomposed signal before the respective peak.

Step 4: Find the minimum amplitude location: Q-wave is the minimum amplitude point before R-wave, so by finding minima of the selected interval, Q wave can be detected.

Step 5: Increment the value of *b* by 1

Step 6: Repeat for all R-waves: Detect all minima locations by repeating **Step 3** to **Step 5** until the value of *b* becomes equal to the value of total number of R-peaks.

Step 7: Evaluate actual Q-waves: Actual Q wave can be evaluated by using Eqn. (7.3)

$$Q_i = q_i \times 2^j \tag{7.3}$$

where, Q_i is the i^{th} Q wave location, q_i, i^{th} minima, which is detected by **Step 4.** Steps of detecting S waves are same as steps of detection of Q wave, and the only difference is the selection of time interval *i.e.* Step 2. In detection of S wave, the time interval is taken from R-peak to 0.2 seconds after the corresponding R waves.

Onset Points of QRS Complex

The following steps are used to extract onset points of the QRS complex:

Step 1: Take ECG signal: Similar to Q, R and S-wave detection, for onset points of QRS complex detection, 3rd level decomposed signal is taken.

Step 2: Set counter value: Equal to the number of R-waves/peaks and set $i = 1$.

Step 3: Choose the time interval: The time interval is of 0.2 second duration after the P-peak (for decomposed signal only five samples is taken before Q-wave)

Step 4: Calculate moving slope of a selected portion of the signal: The slope of ECG signal changes on different parts of the signal. From onset point to Q wave/peak, it is negative and before that, it is 0 or approximately 0. Thus, the point at which the slope is changed is the onset point of QRS complex.

Step 5: Calculate the onset point of i^{th} QRS complex using Eqn. (7.4)

$$Q_{oni} = q_{oni} \times 2^j \tag{7.4}$$

where, Q_{oni} is the i^{th} onset point of QRS complex and q_{oni}, i^{th} onset point of QRS complex location of the decomposed signal detected by **Step 4**.

Step 6: Increment in the value of *i* by 1

Step 7: Repeat Step 3 to Step 7 for the detection of all onset points of the QRS complexes wave, until i = *counter*.

Offset Points of QRS Complex

For detection of offset points of QRS complexes, the following steps are used:

Step 1: Take ECG signal

Step 2: Define counter, $i = 1$ and the threshold value

Step 3: Select the time interval: Select five samples after S-wave of the decomposed signal

Step 4: Calculate the moving slope of a selected portion of the signal and identify points at which the slope changes from positive to 0 or approximately 0

Step 5: Calculate offset point of i^{th} QRS complex using Eqn. (7.5)

$$Q_{offi} = q_{offi} \times 2^{j} \tag{7.5}$$

where, Q_{offi} is the i^{th} offset point of QRS complex, q_{offi}, i^{th} onset point of QRS complex location of the decomposed signal detected by Step 4.

Step 6: Increment the value of i by 1.

Step 7: Detect all the offset points of QRS complex by repeating Step 2 to Step 4, *i.e.*, until $i = C$.

P and T-Waves/peaks Detection

Steps of detection of P-waves/peaks are:

Step 1: Take ECG signal.

Step 2: Set a counter value, $i = 1$ and threshold value:

Step 3: Define the time interval: P-waves/peaks occur before the Q-waves/peaks, so the time interval is of 0.3 seconds starting from before the Q-wave/peak.

Step 4: Find the maxima of the selected portion of the signal to find maximum amplitude of the P-wave.

Step 5: Increment the value of i by 1

Step 6: Repeat for all P-waves: Detect all P-waves/peaks by repeating Step 3 to 5, $i = counter$

Steps for detecting the T-waves are same as the steps of detection of P-wave except Step 2. Here, the time interval is taken from S-point to 0.1 seconds after it.

Onset Points of P-Wave

The following are the steps for detecting the onset points of P-wave.

Step 1: Take ECG signal.

Step 2: Set counter = number of R-waves/peaks and $b = 1$

Step 3: Choose the time interval: 0.1sec interval is chosen *i.e.*, started before the P-peak to the P-peak.

Step 4: Estimate the moving slope of selected portion of the signal: Changing point in slope from 0 to some positive value is the onset point of P-wave.

Step 5: Increment in the value of *b* by 1

Step 6: Repeat for all the P-waves/peaks

Offset Points of P Wave

Here, extraction of offset points of P-wave is done by following the steps:

Step 1: Take ECG signal

Step 2: Define counter

Step 3: Choose the time interval: 0.3 sec after the P-peak point

Step 4: Calculate moving slope of selected portion of the signal: Changing point in slope from negative to approximate zero is the onset point of the corresponding P-wave.

Step 5: Decrement the counter value by 1.

Step 6: Repeat Steps 3, 4 and 5 for obtaining all offset points of the P-waves.

Onset and Offset Points of T Wave

The extraction of onset and offset points of T-waves is the same as the steps carried out for detecting onset and offset points of P-waves. The only difference is the selection of time duration, *i.e.,* Step 3. For extraction of onset point of T-waves, the selected time interval is started from the offset point of QRS complex to T-peak. The time interval for extracting offset of T-wave is 0.3 sec duration started from the T-peak. Other features (shown in Fig. 1.6) are also calculated, that are given below:

PR segment = Duration started from the offset point of P-wave to the onset point of the QRS complex.

ST segment = Duration started from the offset point of the S-wave to the onset point of T-wave.

ISO segment = Duration initiated from offset point of T-wave to onset point of the consecutive P-wave.

After extracting these features, these are then grouped into normal or abnormal ranges. If these features are not inthe normal range, then this leads to arrhythmias.

7.5. Experiments and Results

The performance evaluation of beat detection is done by measuring the following parameters [215]:

Sensitivity (S_e)

$$S_e = \frac{TP}{TF + FN} \tag{7.6}$$

where, *FN* is false negative and *TP* is True positive.

Positive Predictivity ($+P$)

$$+P = \frac{TP}{TP + FP} \tag{7.7}$$

here, *FP* is false positive

Error (E_r)

$$E_r = \frac{FP + FN}{TB} \tag{7.8}$$

where, *TB* is the total number of beats present in the signal as indicated in MIT-BIH datasets.

Summarizing the results of this study, the first step of this work is to remove different kinds of noises, which are presented in the signal to accomplish accurate feature extraction. Elimination of noise is presented in Chapters 2 and 3. The second step is R-peaks detection as illustrated in Section 7.2. For detection of R-peaks, bi-orthogonal wavelet is used along with amplitude and time thresholding. For this also, MIT-BIH arrhythmia database is used, since for lead II, R-wave has the maximum amplitude in the signal. ECG signal is decomposed into three frequency bands. A 0.08 mV amplitude and time thresholding are applied for peak detection, which is represented in Fig. 7.1. Fig. 7.1(a) represents the noise free ECG signal, Figs. 7.1(b) and 7.1(c) include the first level decomposed signals. In Figs. 7.1(d) and 7.1(e), second level decomposed signals are depicted, Figs. 7.1(f) and 7.1(g) present the 3rd level decomposed signals and in Fig. 7.1(h), peaks are detected in 3rd level decomposed signal. (Estimated R-peak locations are determined using Eqn. 7.2).

Table 7.1 Tabular results of beat detection using bi-orthogonal WT

Sq. No	Dataset	TB	TP	FP	FN	$+P$	S_e	E_r
1.	100	2273	2273	0	0	100.00	100.00	00.00
2.	101	1865	1865	0	0	100.00	100.00	00.00
3.	102	2187	2187	0	0	100.00	100.00	00.00
4.	103	2084	2081	0	3	100.00	99.85	0.0014
5.	104	2230	2230	0	0	100.00	100.00	0.00
6.	105	2572	2572	0	0	100.00	100.00	0.00
7.	106	2027	2029	2	0	99.90	100.00	0.009
8.	107	2037	2039	2	0	99.90	100.00	0.0009
9.	108	1763	1770	8	1	99.55	99.94	0.0051
10.	109	2532	2531	0	1	100.00	99.96	0.0003
11.	111	2124	2124	0	0	100.00	100.00	0.00
12.	112	2539	2538	0	1	100.00	99.96	0.0003
13.	113	1795	1795	1	1	99.94	99.94	0.0011
14.	114	1879	1879	0	0	100.00	100.00	0.00
15.	115	1953	1953	0	0	100.00	100.00	0.00
16.	116	2412	2412	0	0	100.00	100.00	0.00
17.	117	1535	1535	0	0	100.00	100.00	0.00
18.	118	2275	2275	0	0	100.00	100.00	0.00
19.	119	1987	1989	2	0	99.89	100.00	0.0010
20.	121	1863	1863	0	0	100.00	100.00	0.00
21.	122	2476	2476	0	0	100.00	100.00	0.00
22.	123	1518	1518	0	0	100. 00	100.00	0.00
23.	124	1619	1619	0	0	100.00	100.00	0.00
24.	200	2601	2601	0	0	100.00	100.00	0.00
25.	201	1963	1960	0	0	100.00	100.00	0.00
26.	202	2136	2136	0	0	100.00	100.00	0.00
27.	203	2982	2979	0	3	100.00	99.89	0.0010
28.	205	2656	2656	0	0	100.00	100.00	0.00
29.	207	1862	1862	0	0	100.00	100.00	0.00
30.	208	2956	2956	0	1	100.00	99.96	0.0003
31.	209	3004	3004	0	0	100.00	100.00	0.00
32.	210	2647	2647	0	0	100.00	100.00	0.00
33.	212	2748	2748	0	0	100.00	100.00	0.00
34.	213	3251	3251	2	2	99.93	99.93	0.0012
35.	214	2262	2262	0	0	100.00	100.00	0.00
36.	215	3363	3363	0	0	100.00	100.00	0.00
37.	217	2208	2208	0	0	100.00	100.00	0.00
38.	219	2154	2154	0	0	100.00	100.00	0.00
39.	220	2048	2048	0	0	100.00	100.00	0.00
40.	221	2427	2427	0	0	100.00	100.00	0.00
41.	222	2484	2484	0	0	100.00	100.00	0.00
42.	223	2605	2605	0	0	100.00	100.00	0.00
43.	228	2053	2056	4	1	99.80	99.95	0.0024
44.	230	2256	2256	0	0	100.00	100.00	0.00
45.	231	1886	1886	0	0	100.00	100.00	0.00
46.	232	1780	1783	4	1	99.77	99.94	0.0028
47.	233	3079	3079	0	0	100.00	100.00	0.00
48.	234	2753	2753	0	0	100.00	100.00	0.00

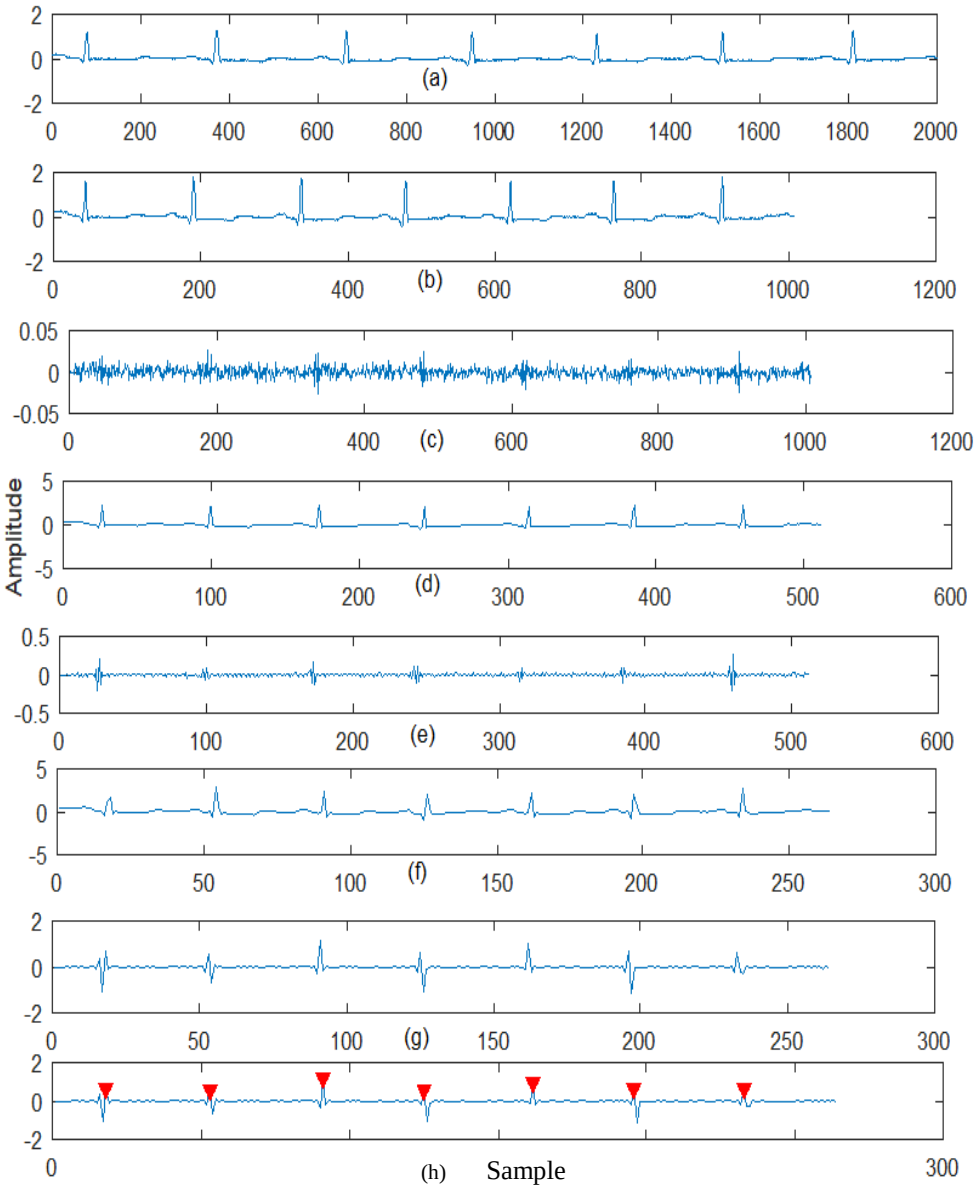

Fig. 7.1 Wavelet decomposition of MIT-BIH record no. 100.

In this work, 33 samples are used to detect R-peak. Locations of these samples are: R_i*-16* to R_i*+16*, here R_i is the location of R-peak. For example: while determining the R-peak location of signal (MIT-BIH record no. 222), extracted peak locations, as sample numbers, of decomposed signal are: 37, 72, 109, 143, 180, 211, 253, 293, 331, 367, 405, 437…, and the sample locations in respective original signal are: 242, 522, 818, 1090, 1386, 1634, 1970, 2290, 2594, 2882, 3186, 3442,..,. For finding actual R-peak location of respective R_1*=242*, selected 33 samples are: from 226 to 258. A peak of this segment (constituted by 33 samples) is 0.5050mV at the location of 233 sample number. Therefore, R-peak amplitude (original signal) of 0.505mV at the time instant *0.64sec* is verified. The performance of beat detection is presented in Table 7.1. Referring to this table, it can be demonstrated that this work is very effective in detecting R-peaks. After R-peak detection, full beat detection is performed.

The performance of proposed beat detection method has been compared with other existing methods and results are given in Table 7.2. This table shows that the proposed method is superior to other methods. After R-peak detection, other features are also detected. The average R-R interval is measured by detected R peaks using Eqn. (7.9).

$$R - R_{\text{int}} = \frac{\sum_{i=1}^{N-1}(R_i - R_{i+1})}{N} \tag{7.9}$$

where, N is the total number of R waves /peaks and R is the time index at R-peak.
Heart rate is the total number of heartbeats present in one minute. All the other features are detected using the given steps. The results of these algorithms are presented in Table 7.3, where, P (amp) is the average of highest amplitudes of P waves, T amp is average of highest amplitudes of T waves, $Pdur$ is average P-wave durations calculated by Eqn. (7.10), $Tdur$ the average is T-wave duration calculated using Eqn. (7.11) and $QRSdur$ is the average of QRS complexes calculated by Eqn. (7.12).

$$Pdur = \frac{\sum_{i=1}^{N-1}(P_{off(i)} - P_{on(i)})}{N} \tag{7.10}$$

where, P_{off} is the offset point of P-wave and P_{on} is the onset point of P-wave:

$$Tdur = \frac{\sum_{i=1}^{N-1}(T_{off(i)} - T_{on(i)})}{N} \tag{7.11}$$

where, T_{off} is the offset point of T wave and T_{on} is the onset point of T wave.

$$QRSdur = \frac{\sum_{i=1}^{N-1}(QRS_{off\,(i)} - QRS_{on(i)})}{N} \tag{7.12}$$

where, QRS_{off} is the offset point of QRS complex and QRS_{on} is the onset point of QRS complex.

The results of these algorithms are depicted in Fig 7.2. Here, in Fig. 7.2(a), (b), (c) and (d), input signal, beat detection, P-wave detection and T-wave detection are presented, respectively. For an ECG rhythm to be NSR, the addition of all segments of ECG signal should be equal to corresponding R-R interval *i.e.*,

$$Pdur + PR\ segment + QRSdur + ST\ segment + Tdur + ISO\ segment = R - R\,interval.$$

Two examples are used to illustrate the performance of this work for arrhythmia detection that would lead to identifying the methodology as a potential diagnostic tool. In Table 7.3, different features of ECG signal is presented.

Example 2: In this case, MIT-BIH record no. 232 is analyzed to extract the features. The extracted values of features are: R-peak point = 0.512mv, average R-R interval = 1.23sec, heart rate (HR) = 48 b/m, P-peak value for first R-peak =0.131mv and T-peak point =0.42 mv. It can be observed that if only HR is considered, then the signal is not an NSR rhythm, but a condition called bradycardia is indicated.

7.6. Performance Measurement of Data Decompression

In this section, signal reconstruction performance is measured. For measurement of signal reconstruction performance, features of the original and reconstructed signal are extracted using the methodology given in this chapter (Section 7.4). After feature extraction, a comparative analysis of these features is done, that is depicted in Tables 7.4(a) and 7.4(b). The R-peaks comparison of both the signals is presented in Fig. 7.3. From, tabular and graphical results, it can be concluded that both the signals have the same diagnostic information.

Example 1: In this example, MIT-BIH record no. 212 is analyzed by extracting the R-peaks using the proposed methodology given in in this work. The measured value of heart rate is 110 beats/ min, which indicates that tachycardia is present in the signal.

Table 7.2 Beat detection performance comparison with other methods.

Approach (Reference)	TB	TP	FP	FN	Error (avg%)	Se (avg%)	+P (avg%)
Proposed	109709	109717	**25**	**15**	**0.05**	**99.98**	**99.97**
CWT	110159	109837	322	120	-	99.91	99.72
Hilbert transform	-	-	-	-	0.39	99.88	99.73
Bandpass filter, derivative Shannon energy and Smoothing	-	-	140	79	-	99.93	99.86
Least square support vector machine	-	-	-	-	-	99.17	96.66
K-Nearest Neighbor algorithm (KNN)		109,759	151	207	99.81	99.81	-
Haar wavelet transform	109,494	109,101	193	393	0.54	99.64	99.82
Wavelet-based beat-detection mechanism	104363	-	223	208	0.41	-	-
Hilbert and Wavelet Transforms based hybrid method	109,495	108,568	856	928	1.69	99.15	99.18
Wavelet bases and adaptive threshold technique	109494	107808	1073	1686	2.57	98.47	98.96

Table 7.3 Tabular results of feature detection.

Data	R (amp)	R-R (interval)	HR	P (amp)	*Pdur*	T (amp)	*Tdur*	*QRSdur*	PR segment	ST segment	ISO segment
101	1.50	0.86	71	0.15	0.06	0.25	0.16	0.06	0.06	0.16	0.32
103	1.50	0.88	70	0.05	0.01	0.40	0.16	0.51	0.04	0.02	0.36
105	1.40	0.76	88	0.02	0.06	0.10	0.10	0.06	0.08	0.12	0.25
106	2.25	0.97	66	0.25	0.05	1.40	0.18	1.04	0.03	0.03	0.42
111	1.00	0.82	72	0.05	0.10	0.25	0.16	0.12	0.08	0.08	0.23
113	2.35	1.04	60	0.02	0.04	1.25	0.21	0.06	0.03	0.06	0.44
114	2.20	1.12	55	0.05	0.04	0.25	0.64	0.05	0.06	0.21	0.34
115	2.10	0.99	63	1.53	0.06	1.50	1.21	0.12	0.04	0.14	0.24
116	2.60	0.75	78	0.25	0.06	0.85	0.24	0.61	0.03	0.05	0.23
117	0.80	1.17	50	1.35	1.20	0.60	0.23	0.06	0.08	0.08	0.56

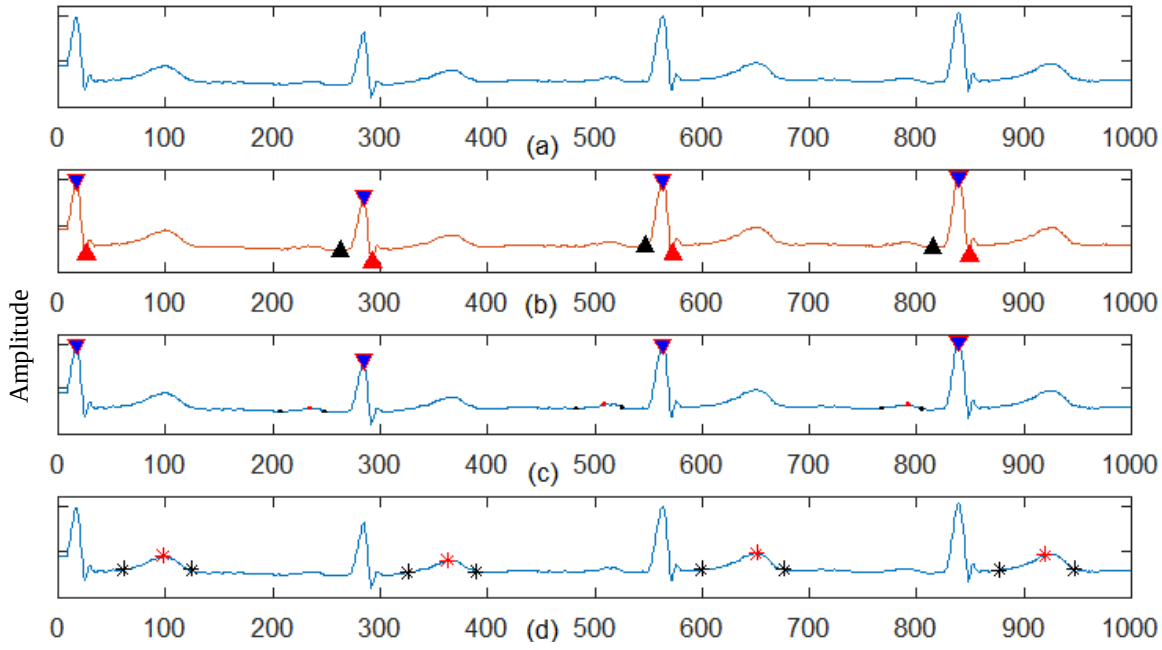

Fig. 7.2 Feature detection in ECG signal.

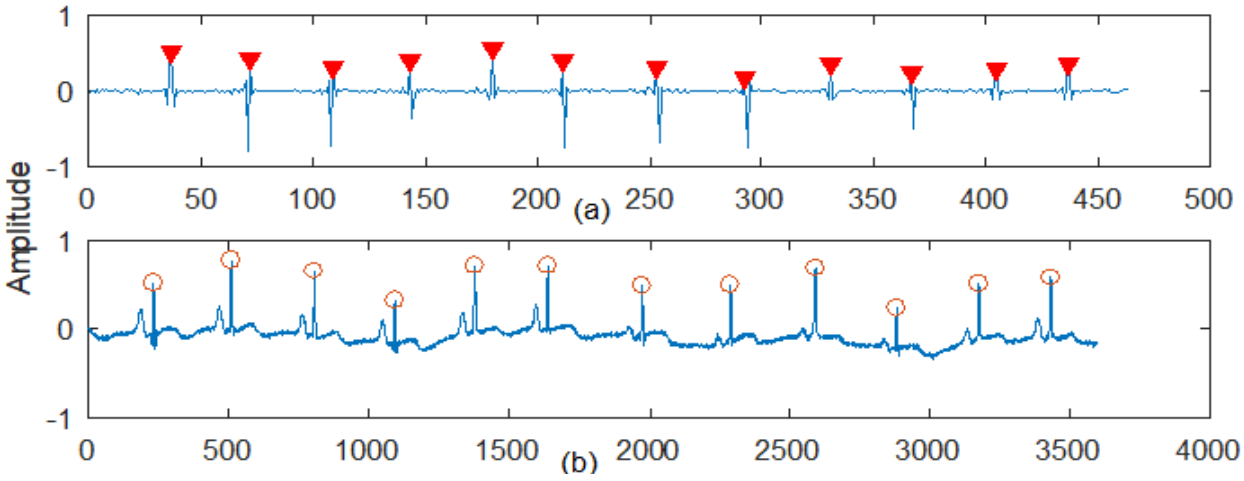

Fig. 7.3 (a) Peak detection of decomposed ECG signal (MIT-BIH record no. 222) and (b) Actual R peak detection of signal.

Table 7.4 (a) Performance measurement of data decompression using features comparison

Record no.	R ori. amp	R recon.	Deviation	Q original amp	Q reconstructed amp	deviation	S original amp	S recon. amp	No. of QRS ori.	No QRS recon.
100	0.818	0.818	0.000	-0.5804	-0.5818	0.0014	-8.420×10^{-4}	-4.37×10^{-6}	73	73
101	0.896	0.896	0.000	-0.3375	-0.3379	0.0004	00	00	71	71
102	0.725	0.725	0.000	-0.3375	-0.3391	0.0016	-0.0052	-0.0052	67	67
103	0.951	0.951	0.0001	-5.163×10^{-4}	-2.245×10^{-4}	2.247	-8.420×10^{-4}	-7.518×10^{-4}	81	61
104	0.489	0.489	0.0001	-6.049×10^{-5}	-0.263×10^{-5}	0.2629	-0.000	-0.0015	92	92
105	0.739	0.739	0.000	-2.347×10^{-4}	-1.025×10^{-4}	1.020	-9.700×10^{-4}	-9.800×10^{-4}	83	83
106	0.962	0.962	0.000	-2.861×10^{-4}	-1.244×10^{-4}	1.243801	-9.771×10^{-4}	-7.577×10^{-4}	67	67
107	0.888	0.888	0.000	0.0014	6.086×10^{-4}	6.085557	-0.0039	-0.0039	70	70
108	0.560	0.560	0.0001	-4.015×10^{-4}	-1.745×10^{-4}	-1.745×10^{-4}	-6.698×10^{-4}	-7.188×10^{-4}	114	114
109	0.840	0.840	0.000	-9.310×10^{-4}	-4.047×10^{-4}	4.046895	-0.0025	-0.0025	91	91
111	0.857	0.857	0.000	-6.599×10^{-4}	-2.869×10^{-4}	2.868557	-7.692×10^{-4}	-7.706×10^{-4}	68	68
112	0.884	0.884	0.000	-5.533×10^{-4}	-0.240×10^{-4}	0.24054	6.084×10^{-4}	6.527×10^{-4}	85	85
113	0.905	0.905	0.000	-4.799×10^{-4}	-2.086×10^{-4}	2.085564	-6.084×10^{-4}	-6.837×10^{-4}	58	58
114	0.952	0.952	0.000	-3.431×10^{-4}	-1.491×10^{-4}	1.491526	-4.792×10^{-4}	-4.865×10^{-4}	14	14
115	0.841	0.837	0.000	-2.402×10^{-4}	-1.044×10^{-4}	1.044108	-6.885×10^{-4}	-6.897×10^{-4}	63	63
116	0.854	0.854	0.000	-1.2431	-1.2431	0.000-	-	-8.855×10^{-4}	79	79
117	0.925	0.925	0.000	-1.108×10^{-4}	-0.482×10^{-4}	0.481889	-0.0010	-0.0010	50	50
118	0.824	0.820	0.004	-5.887×10^{-4}	-2.559×10^{-4}	2.559194	-9.969×10^{-4}	-0.0011	73	73

Table 7.4 (b) Performance measurement of data decompression using features comparison

Record no.	Pon original amp and sample	Pon reconstructed amp and sample	Deviation	Ton original amp and sample	Ton reconstructed amp and sample	deviation
101	-	-	0	0.1625	-	0.1625
103	-0.0183	-0.0079	0.0104	0.2393	0.2378	0.0015
105	-0.1126	-0.107	0.0056	0.2687	0.2003	0.0684
106	-0.0173	-0.0169	0.0004	0.3543	0.3542	1E-04
111	-0.1645	-0.1629	0.0016	0.293	0.2947	0.0017
113	-0.2682	-0.2745	0.0063	0.932	0.9326	0.0006
114	0.0329	0.0324	0.0005	0.1616	0.1622	0.0006
115	-0.5358	-0.5395	0.0037	0.1373	0.1377	0.0004
116	-1.0783	-1.0767	0.0016	0.5531	0.5548	0.0017
117	-0.7421	-0.7344	0.0077	-	-	0
121	-0.2682	-0.2745	0.0063	0.932	0.9326	0.0006
122	0.0329	0.0324	0.0005	0.1616	0.1622	0.0006
123	-0.5358	-0.5395	0.0037	0.1373	0.1377	0.0004

Table 7.5 Diagnostic parameters for WDD measurement

Feature's indices	Symbol	Description	Unit
1.	R-R_{int}	The time duration between two consecutive R peaks	msec
2.	QRS $_{dur}$	Time duration between the onset and QRS offset point	msec
3.	QT_{int}	The time duration between QRS onset and Toffset point	msec
4.	QTP_{int}	The time duration between onset point of P-wave and peak point of T wave	msec
5.	Pdur	The time duration between onset and offset point of P wave	msec
6.	PRint	The time duration between onset point of P-wave and onset point of QRS complex	msec
7.	QRS-peaks	The number of peaks and notches in the QRS complex	(≥1)
8.	QRS sign	The sign of the first peak in the QRS complex	(1 or -1)
9.	Δwave	The existence of the delta wave	0 or 1
10.	Tshape	Morphology of the T wave	
11.	P shape	Morphology of the T wave	
12.	ST shape	Shape of ST segment	
13.	QRS^{+} amp	The maxima of QRS complex	mm
14.	QRS^{-} amp	The minima of the QRS complex	mm
15.	Pamp	The amplitude of P wave	mm
16.	Tamp	The amplitude of T wave	mm
17.	STelevation	The ST elevation	mm
18.	STslop	The slop of ST element	mm/sec
19.	**Ppeaks**	**The total number of peaks**	**≥1**
20.	**VLP presented**	**Ventricular late potential present**	**0 or 1**

7.6.1. Performance Evaluation using Function WDD.

In this section, the WDD parameter is described in detail. This parameter is based on PQRST complex comparison. For example: features of both the signal (the original ECG signal and reconstructed one), *viz*., QRS complex, QRS complex morphology, P-wave shape, P-wave amplitude, P-wave duration, QT duration, T-wave shape, ST elevation, *etc*., are compared. The mathematical expressions used to measure the WDD are presented in Eqn. (7.13) to Eqn. (7.19).

$$WDD(\beta,\hat{\beta}) = \Delta\beta^T . \frac{\Lambda}{tr[\Lambda]} . \Delta\beta \times 100 \tag{7.13}$$

where, term β, $\hat{\beta}$, $\Delta\beta$ and Λ are original features signal vector, reconstructed signal features vector, normalized difference vector and diagonal matrix of weights, respectively. These terms are defined in Eqns. (7.14), (7.15), (7.16) and (7.17), respectively.

$$\beta^T = [\beta_1, \beta_2, ..., \beta_p] \tag{7.14}$$

$$\hat{\beta}^T = [\hat{\beta}_1, \hat{\beta}_2, ..., \hat{\beta}_p] \tag{7.15}$$

$$\Delta\beta^T = [\Delta\beta_1, \Delta\beta_2, ..., \Delta\beta_p] \tag{7.16}$$

$$\Lambda = \text{diag}[2\ \ 1\ \ 1\ \ 1\ \ 1\ \ 1\ \ 1\ \ 0.25\ \ 0.25\ \ 1\ \ 1\ \ 1\ \ 2\ \ 2\ \ 1\ \ 1\ \ 1\ \ 1] \tag{7.17}$$

Every scalar in vector $\Delta\beta$ provides distance between the original signal feature and reconstructed signal feature. For amplitude and duration features, for example, P-peak, PR segment, QRS complex, *etc*., it can be computed as:

$$\Delta\beta_i = \frac{\left|\beta_i - \hat{\beta}_i\right|}{\max\left\{|\beta_i|, |\hat{\beta}_i|\right\}} \tag{7.18}$$

and for shape features, such as: P_{shape}, $T_{shape,}$ these vectors are determined by fixed penalty matrices ($W^i = \left\{ w^i_{\beta_i,\hat{\beta}_i} \right\}$) given in [132]:

$$W^i = \begin{bmatrix} w^i_{11} & w^i_{12} & . & . & . & w^i_{1Z_i} \\ w^i_{21} & w^i_{22} & . & . & . & w^i_{2Z_i} \\ . & . & . & & & . \\ . & . & & . & & . \\ . & . & & & . & . \\ w^i_{Z_i1} & w^i_{Z_i1} & . & . & . & w^i_{Z_iZ_i} \end{bmatrix} \tag{7.19}$$

Table 7.6 Morphologies of features for WDD extraction

code Shape feature	1	2	3	4	6	7	8	9
Pshape	Biphasic II	Notch negative	Negative	Flat	Positive	pulmonale positive	Notch Positive	Biphasic I
Tshape	Negative	Flat	Positive					
STshape	Straight positive	concave	Flat	convex	Straight positive			

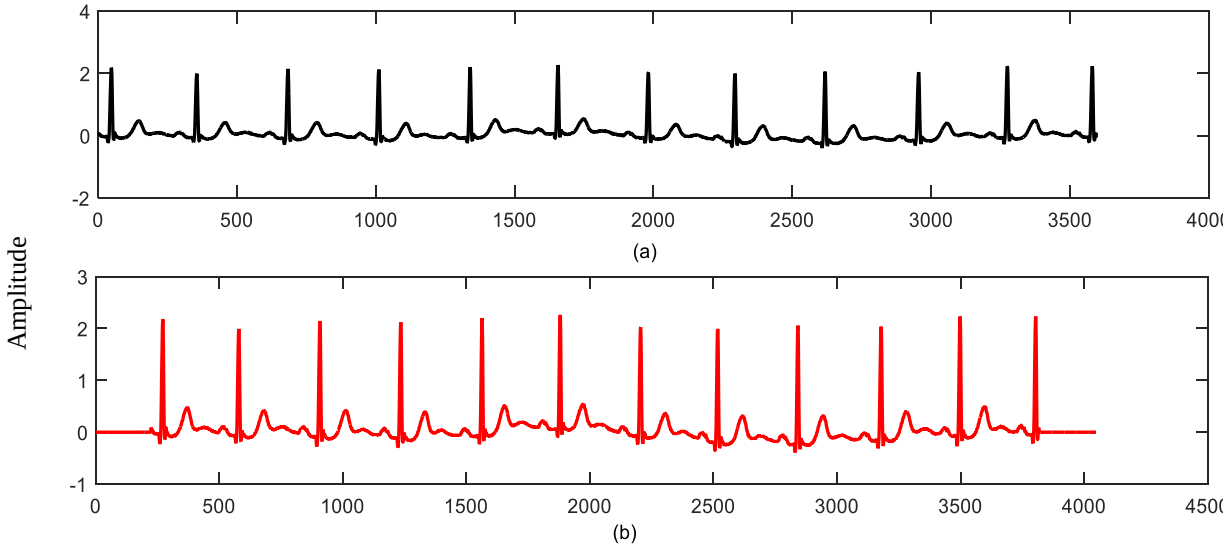

Fig. 7.4 (a) Original data and (b) Reconstruction signal.

Table.7.7 Measured values of WDDs

Record no.	WDD_1	WDD_2	WDD_3	WDD_4	WDD_5	WDD_6	WDD_6	WDD_8	WDD_9	WDD_{10}
100	1.862	2.935	1.585	1.053	2.748	1.932	0.216	2.051	2.583	3.226
101	2.619	2.663	1.760	3.683	1.877	0.998	1.399	1.559	1.419	4.327
102	1.992	1.649	2.451	1.8507	1.853	1.444	1.395	1.151	1.438	2.414
103	3.107	3.619	1.010	3.394	0.445	0.648	1.048	1.759	0.444	2.211
104	1.814	1.949	2.150	2.461	0.527	2.364	2.092	2.602	3.100	2.613
105	0.878	1.187	0.134	1.836	0.238	1.547	0.835	0.483	2.175	1.472
106	2.245	1.561	1.621	3.182	0.455	2.783	0.373	1.931	3.003	3.241
107	3.561	2.858	0.758	3.082	1.544	3.237	1.476	2.782	3.511	1.842
108	0.803	2.195	1.047	1.988	0.085	3.077	1.659	0.579	0.862	0.626
109	1.757	2.888	1.982	3.395	3.946	1.965	0.982	2.669	2.643	2.870
111	3.004	2.069	0.574	3.881	2.439	1.496	1.996	2.683	1.987	0.431
112	0.079	4.486	0.711	2.034	0.367	0.775	0.318	1.117	2.914	0.155
113	2.625	0.334	0.184	1.844	0.545	2.118	0.125	0.495	3.107	2.288
114	2.752	1.584	0.528	2.504	1.592	2.959	1.872	2.433	2.820	1.049
115	2.213	1.915	1.548	2.451	0.012	1.659	1.721	2.808	1.182	1.089
116	1.229	2.089	2.862	2.907	1.240	1.826	0.208	2.578	1.873	1.838
117	1.992	3.456	1.518	1.844	2.791	2.616	0.946	2.762	2.264	1.511
118	2.093	2.219	1.466	2.815	1.536	2.863	2.209	0.817	5.158	1.777

The following steps are used to calculate the value of WDD;

Step 1. Denoised ECG signal is taken.

In this case also MIT-BIH arhhythmia database is taken. The noise is removed using methodologies given in Chapter 3.

Step 2. Feature extraction.

All the features mentioned in Table 7.5 and Table 7.6. are extracted from the denoised ECG data (*i.e.*, data obtained in **Step 1**).

Step 3. Compression.

Denoised signal obtained in **Step 1** is compressed using steps given in Section 6.4.

Step 4. Decompression.

Compressed signal is decompressed by following steps given in 6.4.1.

Step 5. Feature extraction.

All the features mentioned in Table 7.5 and Table 7.6. are extracted from the decompressed ECG data obtained after **Step 4**.

Step 6. Vector β^T formation.

Formation of vector β is done using extracted features given in Table 7.5 and Eqn. (7.14).

Step 7. Vector $\widehat{\beta}^T$ formation.

Formation of vector $\hat{\beta}$ is done using extracted features given in Table 7.5 and Eqn. (7.15).

Step 8. $\Delta\widehat{\beta}^T$ vector is computed by using Eqn. 7.15

Step 9. WDD is calculated using Eqns. 7.13 and 7.17.

In [132], 18 features are considered to measure the WDD. In this work, two more parameters are used to calculate the value of WDD, *i.e*, number of multiple P-wave and ventricle late potential. All the 20 features are listed in Table 7.5 and 7.6. These features are important in disease identification, for example, number of P-waves becomes more in case of atrial fibrillation arrhythmia.

Example 7.3. In this example, the MIT/BIH record no.103 is taken. The signal is first compressed and then decompressed using the methodology given in Chapter 6.

Here, the distortion values for this signal having 10-sec duration. 10 beats are considered to the values for the WDD for different beats are presented in Table 7.7.

7.7. Discussions

Wavelet is a powerful tool to analyze the non-stationary signal due to its multiresolution property. Therefore, in this work, WT and CMFB based filter bank is used to detect the R-peak locations. The beat detection performance of the proposed method is examined by *Se, +P* and *Er,* using the MIT-BIH arrhythmia database. The performance of the proposed rule based algorithms is evaluated using Matlab 2016b. Table 7.1 & Table 7.2 and Fig. 7.2 demonstrate that the algorithm can detect features of ECG significantly. The comparative study of Table 7.2 shows that the proposed work provides better performance in terms of S_e, *+P*, and E_r than several other existing methods. Example 1 and 2 clearly demonstrate that this work is very impactful in cardiac disorders' interpretation.

In this work, different features of ECG signal have been extracted in frequency and time domain. All other useful diagnostic features are extracted using some rule based algorithms. The resulting waveforms and tabular results demonstrate that the proposed method successfully extracts the features from ECG signals. Hence, this work can be used for employing the extracted diagnostic features, in the time domain, to interpret different cardiac problems and providing a potential diagnostic tool in future studies. The methodology provides a technique that is well understood and appreciated by cardiologists who accept only time domain data. Extracted features are used to determine the performance of data compression. WDD is also evaluating the performance of data compression, in which two more features are added, that are important for the diagnosis of a cardiac patient. On observing Tables 7.4(a), 7.4(b) and (7.7), it is seen that the data compression method present in this work can reconstruct the signal, which has almost the same diagnostic information.

7.8. Summary

In this chapter, different features of the ECG signal have been extracted in the frequency and time domain. First, R waves have been detected using bi-orthogonal wavelet transform. In another case CMFB is utilized to detect the R waves locations. After that, all the useful diagnostic features are extracted using some rule-based algorithms. The resulting waveforms and tabular results demonstrate that the proposed method successfully extracts features from ECG signals. After extracting features, these are used to evaluate the performance of reconstructed of the ECG signal. These features are also utilized to measure the WDD. On the basis of the results reported in this work, it is concluded that the WDD based measure is considerably more appropriate for evaluating the ECG reconstructed signals than the popular PRD measure. Tables 7.3(a), 7.3(b) and (7.6) show that the methodology given in this thesis can reconstruct a signal with some diagnostic information as it is presented in the original signal.

CHAPTER 8

CONCLUSIONS AND FUTURE SCOPE

8.1. Overview

This study provides an efficient design of the digital systems, which is used for noise elimination, data compression and feature extraction of the ECG rhythms. Time-frequency analysis preserves time and frequency information for non-stationary signals. This growth was driven by the wide range of applications in telemedicine and e-health care system, Holter monitor system and reducing the storage requirements. Due to the increasing number of applications involving digital filter banks digital filtering, the variety of requirements that have to be met by the digital filter banks has increased as well. Thus, there is a strong need for flexible methods that can design the filter banks satisfying the sophisticated specifications.

8.2. Main Findings

This work includes two major parts, *viz*., filter and filter bank design and data compression. These are discribed in the next section briefly.

8.2.1. Methodologies used for the Design of Filter and Filter Bank

a) Linear-phase IFIR lowpass filter is designed.

b) Linear-phase FRM filters are designed.

c) The notch filter is formulated using a combination of IFIR and FRM technique.

d) For obtaining equiripple nature of the filter, coefficient reduction method is used for single and two staged IFIR filters. After designing of filters, these are utilized for noise reducuion from the ECG signals. In the following way;

I). For removing the baseline wander, high pass FRM filter is used.

II). For removing the high-frequency noise, IFIR lowpass filter is used.

III). For eliminating the power line interfacing, notch filter is used.

For efficient decomposition and to minimize the computational complexity, some methodologies are proposed to design a filterbank using cosine modulation technique. The following methods are proposed to design the filterbank.

a) An iterative method for the design of M-channel linear-phase uniform CMFB modulated based on optimum cut-off frequency of model filter of IFIR filter.
b) An iterative scheme for M-channel uniform CMFB to reduce the objective function of stopband error minimization, optimum passband edge frequency of model filter of IFIR filter.
c) Schittkowski algorithm is used to obtain the optimum filter bank response.
d) Non-uniform filter banks are derived using band merger method.

The following conclusions are made from the filter and filter design methodologies.

- The designing of ripple free single and two staged IFIR filters is done, which has an identical filter response to the FIR filter, which provides less computational complexity, stable nature and linear phase.
- Design and development of computationally efficient uniform and non-uniform CMFBs using single and two staged IFIR filter are done, which would provide optimum performance in terms of computational complexity, aliasing error and peak reconstruction error. To minimize the amplitude error, linear iteration optimization technique is utilized.

8.2.2. ECG Data Compression

ECG data compression is done by the decomposition of signal into the number of frequency bands, which is a primary work of the data compression. Here, decomposition of the signal is done by the following filterbank;

a) QMF with Park-McClellen
b) Wavelet packet filter bank
c) Wavelet transform filter bank
d) Empirical wavelet transform filter bank
e) Non-uniform CMFB

After the decomposition process, thresholding /quantitation is applied to compress the signal. To gain a high compression ratio without affecting the diagnostic information,

lossless methods are used. In this work, for encoding the decomposed signals, the following methods have been used:

a) Run-length encoding
b) Huffman encoding
c) LZW encoding with delta coding

The features are extracted using WT /CMFB with rule base methodologies. The extracted features are used to measure the performance of data reconstruction.

The following conclusions are made from data compression methodologies:

- Compression of ECG rhythms using efficient filter bank(s) is done along with encoding (RLE, modified RLE/Huffman coding/Lempel–Ziv–Welch). The methodologies provide efficient results in terms of computional complexity, compression ratio with out loss of diagnostic information.
- Features are extracted from the denoised original ECG signal and decompressed ECG signal, and then the comparative analysis is performed. WDD is measured to examine the performance of data reconstruction quality. Evaluated values of WDD and comparative analysis shows that both the signals have same diagnostic information

8.3. Future Scope

The methodology used here for data compression can be utilized to multi-lead ECG Data simultaneously. Hybrid methodologies can improve the performance of data compression and decompression, while preserving the diagnostic information. The method developed in this work can be implemented in the DSP processor, chip design that would benchmark the high-speed and efficiency of ECG rhythm compression. Application of this work can be carried out in several e-health-care organizations.

List of Publications

Based on the present research work, three papers are published in SCI expended journals. Two papers are published in refereed journal. Additionally, three papers are presented/accepted in international conferences. The papers are listed as follows:

Journals

Published

1. **S. Chandra**, A. Sharma and G. K. Singh, "Computationally Efficient Cosine Modulated Filter Bank for ECG Signal Compression," Innovation and Research in BioMedical engineering, (online, doi.org/10.1016/j.irbm.2019.06.002). (SCI Expended)
2. **S. Chandra**, A. Sharma and G. K. Singh, "Minimization of Stopband Ripple of IFIR Filter," IETE journal of research, (online, doi.org/10.1080/03772063.2019.1622460) (SCI Expended)
3. **S. Chandra**, A. Sharma and G. K. Singh, "Feature Extraction of ECG Signal," Journal of Medical Engineering & Technology, vol. 42, no.2, pp. 306-316, May 2018.
4. **S. Chandra**, A. Sharma and G. K. Singh, "Denoising ECG Signal: A Review," Asian Journal of Convergence in Technology, 3. 2 pp. 1-5, 2017.
5. **S. Chandra**, A. Sharma and G. K. Singh, "Use of Empirical Wavelet Transform to Compress Electrocardiographic Data for Telemedicine", Advances in Science, Technology and Engineering Systems Journal (ASTESJ), (Accepted), (September, 2019).

Under Review

1. **S. Chandra,** A. Sharma and G. K. Singh, "Comparative Analysis of Various Wavelet based ECG Data Compression Techniques." Innovation and Research in BioMedical engineering, **(Acceptable with minor revisions).**
2. **S. Chandra**, A. Sharma and G. K. Singh, "Comparative Analysis of Various Wavelet based ECG Data Compression Techniques." Innovation and Research in BioMedical engineering.
3. **S. Chandra**, A. Sharma and G. K. Singh, "ECG Data Compression: A Review," IETE journal of Review.

Conference

1. **S. Chandra** and A. Sharma, "A Computationally Efficient Approach for ECG Signal Denoising and Data Compression," IEEE 8th Control and System Graduate Research Colloquium (ICSGRC 2017), **Malaysia**, pp. 22-27 August 2017 (presented).
2. **S. Chandra** and A. Sharma, "Optimum QMF Bank Based ECG Data Compression," IEEE 4th UPCON, GLA University, Mathura, pp. 118-12, October 2017 (presented).
3. **S. Chandra**, A. Sharma and G. K. Singh, "Denoising of ECG Signal using Computationally Efficient Linear Phase Filtering," 10th International conference on computing, communication and networking technologies (ICCCNT), to be held in IIT Kanpur, 6-8 July 2019 (presented).

BIBLIOGRAPHY

[1] J. G. Proakis, "Digital signal processing: principles algorithms and applications", Pearson Education India, 2001.

[2] L. Cromwell, F. J, Weibell, E. A. Pfeiffer, L. B. and Usselman, "Biomedical instrumentation and measurements", Englewood Cliffs, N. J., Prentice-Hall, Inc., 1973. Pp.457

[3] A. Gacek, W. Pedrycz, "ECG signal processing, classification and interpretation: a comprehensive framework of computational intelligence", Springer Science & Business Media, 2011 Sep 18.

[4] R. Wootton and J. Craig, "Introduction to Telemedicine", The Royal Society of Medicine Press Ltd., London, UK, 1999.

[5] P. Stamford, T. Bickford, H. Hsiao and W. Mattern, "The significance of telemedicine in a rural emergency department", IEEE Engineering in Medicine and Biology, 1999 August, vol. 18, no. 4, pp. 45-52.

[6] M. Sareen, P. Prakash and S. Anand, "Wavelet decomposition and feature extraction from pulse signals of the radial artery", In 2008 International Conference on Advanced Computer Theory and Engineering, 2008 Dec 20, pp. 551-555, IEEE.

[7] V. Mahadevan, "Anatomy of the heart," Surgery (Oxford), 2018 Feb 1, vol. 36, no. 2, pp. 43-47.

[8] A. M. Al-Busaidi, L. Khriji, F. Touati, M. F. Rasid, A. B. Mnaouer, "Real-time DWT-based compression for wearable Electrocardiogram monitoring system", In 2015 IEEE 8th GCC Conference & Exhibition, 2015 Feb 1, pp. 1-6. IEEE.

[9] A. Sengur, "Support vector machine ensembles for intelligent diagnosis of valvular heart disease," Journal of medical systems, 2012 Aug 1, vol. 36, no. 4, pp. 2649-2655.

[10] M. Yochum, C. Renaud and S. Jacquir, "Automatic detection of P, QRS and T patterns in 12 leads ECG signal based on CWT", Biomedical Signal Processing and Control, 2016 Mar 1, vol. 25, pp. 46-52.

[11] M. Bahaz and R. Benzid R, "Efficient algorithm for baseline wander and powerline noise removal from ECG signals based on discrete Fourier series", Australasian physical & engineering sciences in medicine, 2018 Mar 1, vol. 41, no. 1, pp. 143-60.

[12] Y. N. Singh and S. K Singh, "Human identification using heartbeat interval features and ECG morphology", In Proceedings of Seventh International Conference on Bio-

Inspired Computing: Theories and Applications (BIC-TA 2012), Springer, India, 2012, pp. 87-98.

[13] P. Swami, T. K. Gandhi, B. K. Panigrahi, M. Bhatia, J. Santhosh and S. Anand, "A comparative account of modelling seizure detection system using wavelet techniques," International Journal of Systems Science, Operations & Logistics, 2017 Jan, vol, 4, no. 1, pp. 41-52.

[14] R. J. Martis, U. R. Acharya, A. K. Ray, C. Chakraborty, "Application of higher order cumulants to ECG signals for the cardiac health diagnosis," In 2011 Annual International Conference of the IEEE Engineering in Medicine and Biology Society, 2011 Aug 30, pp. 1697-1700.

[15] A. L. Goldberger, "Components of a new research resource for complex physiologic signals, physiobank, physiotoolkit, and physionet, american heart association journals," Circulation, 2000, vol. 101, no. 23, pp.1-9.

[16] S. D. Greenwald, "The development and analysis of a ventricular fibrillation detector", Doctoral dissertation, Massachusetts Institute of Technology, 1986.

[17] C. K. Jha, M. H. Kolekar, "ECG data compression algorithm for tele-monitoring of cardiac patients", International Journal of Telemedicine and Clinical Practices, 2017, vol. 2, no. 1, pp. 31-41.

[18] W. K. Seng, R. B. Besar and F. S. Abas, "Collaborative support for medical data mining in telemedicine", In 2006 2nd International Conference on Information & Communication Technologies, 2006, vol. 1, pp. 1894-1899.

[19] E. Castelli and D. Istrate, "Everyday Life Sounds and Speech Analysis for a Medical Telemonitoring System", In Seventh European Conference on Speech Communication and Technology, 2001.

[20] D. Sundararajan, "Discrete wavelet transform: a signal processing approach", John Wiley & Sons, 2016 Mar 7.

[21] Y. Neuvo, D. Cheng-Yu and S. Mitra, "Interpolated finite impulse response filters," IEEE Transactions on Acoustics, Speech, and Signal Processing, 1984 Jun, vol. 32, no. 3, pp. 563-570.

[22] A. Mehrnia, A. N. Willson, "Optimally Factored IFIR Filters", Circuits, Systems, and Signal Processing, 2019 Jan 15, vol. 38, no. 1, pp. 259-86.

[23] F. J. Harris, "Multirate signal processing for communication systems", Prentice Hall PTR; 2004 May 1.

[24] P. P. Vaidyanathan, "Multirate systems and filter banks", Pearson Education India, 1993.

[25] A. M. Al-Busaidi, L. Khriji, F. Touati, M. F. Rasid, A. B. Mnaouer, "Wavelet-based Encoding Scheme for Controlling Size of Compressed ECG Segments in

Telecardiology Systems", Journal of medical systems, 2017 Oct 1, vol. 41, no. 10, pp. 166.

[26] J. R. Cox, F. M. Nolle, H. A. Fozzard and G. C. Oliver, "AZTEC, a preprocessing program for real-time ECG rhythm analysis", IEEE Trans, on BME, April 1968, pp. 128-129.

[27] J. P. Abenstein, "Algorithm for real time ambulatory ECG monitoring", Biomed. Sci. Intrument, 1978, vol. 14, pp. 73-79.

[28] B. Furht and A Perez A, "An adaptive real-time ECG compression algorithm with variable threshold", IEEE Trans, on BME, vol. 35, no. 6, pp. 498-494, June, 1988.

[29] S. M. S. Jalaleddine, C. G. Hutchens, W. A. Coberly and R. D. Strattan R.D, "Compression ofHolter ECG data," Biomec. Sci. Intrument, vol. 24, pp. 35-45, 1988.

[30] W. C. Mueller, "Arrhymia detection program for an ambulatory ECG monitor", Biomed. Sci. Instrument, vol. 14, pp. 81-85, 1978.

[31] J. P. Abenstein and W. J. Tompkins, "New data-reduction algorithm for real time ECG analysis", IEEE Trans, on BME, vol. 29, pp. 43-48, January 1982.

[32] W. J. Tompkins and E. Webster, "Design of microcomputer-based medical instrumentation", Englewood Cliffs, NJ: Prentice-Hall, 1981

[33] L. W. Gardenhire, "Data compression for biomedical telemetry in Biomedical Telemetry", CA. Caceres, Ed., New York: Academic, ch-11, 1965.

[34] L. W. Gardenhire , "Redundancy reduction the key to adaptive telemetry", in Proc. 1964 Nat. Telemetry Conf, pp. 1-16, 1964.

[35] M. Ishijima, S. B. Shin, G. H. Hostetter and J. Sklansky, "Scan along polygon approximation for data compression of electrocardiograms", IEEE Trans, on BME, vol. 30, no. 11, pp. 723-729, November 1983.

[36] V. Kumar, S. C. Saxena, and V. K. Giri, "Direct data compression of ECG signal for telemedicine," International journal of systems science, vol. 37, no. 1, 2006, pp. 45-63.

[37] M. Bertrand, R. Guardo, G. Mathieu, P. Blondeau and R. Leblanc, "A microprocessor based system for ECG encoding and transmission", in Proc. 28l Annu. Conf. Eng. Med. Biol, 1975, pp. 435.

[38] H. K. Wolf, J. Sherwood and P. M. Rautaharu, "Digital in transmission of electrocardiogram-A new approach", in Proc. 4th Can. Med. Biol. Conf., 1972, pp. 39a-39b.

[39] D. Stewart, G, E. Dower and O. Suranyi, "An ECG compression code", Journal of Electrocardiology, 1973, vol. 6, no. 2, pp. 175-176.

[40] U. Ruttiman and H. V. Pipberger, “Compression of the ECG by prediction or interpolation and entropy encoding”, IEEE Trans, on BME, November 1979, vol. 26, no.11, pp. 613- 623.

[41] U. E. Ruttiman, A. S. Berson and H. V. Pipberger, “ECG compression by linear prediction”, Computers in cardiology, 1976, pp. 313-315.

[42] L. Sornmo, O. Pahlm, N. Mats-Erik and O. B. Per, “A mathematical approach to QRS detection”, IEEE Computers in Cardiology, 1980, pp. 205-208.

[43] J. Whitman and H. K. Wolf, “An encoder for electrocardiogram data with wide range of applicability”, In Optimization of Computer ECG Processing, MacFarlane, New York, North-Holland, 1980, pp. 87-90.

[44] O. Pahlm O., Borjesson P. O. and O. Werner, “Compact digital storage of ECGs”, Computer Programs Biomed, 1979, vol. 9, pp. 292-300.

[45] H. O. Burton and D. D. Sullivan, “Error and error control”, Proc. IEEE, November 1972, vol. 60, pp. 1263-1301.

[46] S. C. Tai, “Slope-a real-time ECG data compressor”, Medical & Biological Engineering & Computing, March 1991, vol. 29, pp. 175-179.

[47] S. C. Tai, “ECG data compression by corner detection”, Medical & Biological Engineering & Computing, November 1992, vol. 30, pp. 584-590.

[48] N. J. Holter, “New method for heart studies”, Science, 1961, vol. 134, pp. 1214-1220.

[49] S. C. Saxena and V. K Giri, “ECG data compression using SAPA-CTC techniques”, Proceedings of International Conf. on Computer Applications in electrical engineering -Recent Advances CERA-97, UOR, September 1997, Roorkee, pp. 26-31.

[50] P. K. Kulkami, V. Kumar and H. K. Verma , “Direct data compression techniques for ECG signals effect of sampling frequency on performance”, International Journal of Systems Science, March 1997, vol. 28, no. 3, pp. 217-228.

[51] S. C. Saxena, A. Sharma and S. C. Chaudhary, “Data compression and feature extraction ofECG signals”, International Journal of Systems Science, May 1997, vol. 28, no. 5, pp. 483-498.

[52] Y. Zigel, A. Cohen and A. Katz, “ECG compression using analysis by synthesis coding”, IEEE Trans, on BME, October 2000, November 2000, vol. 47, no. 10, pp. 1308-1314.

[53] Y. Zigel, Cohen A. and Katz A, “The weighted diagnostic distortion (WDD) measure for ECG signal compression”, IEEE Trans, on BME, vol. 47, no. ll, pp. 1422-1430,

[54] E. C. Lowenberg, “Signal theory applied to the analysis of electrocardiogram”, IRE Trans, on Medical electronics, January 1960, vol. ME-7, pp. 7-12.

[55] M. E. Womble, J. S. Halliday, S. K. Mitter, M. C. Lancaster and J. H. Triebwasser, “Data compression for storing and transmitting ECG's/VCG's”, Proc. of IEEE, May 1977, vol. 65, no. 5.

[56] W. S. Kuklinski, “Fast Walsh transform data compression algorithm: ECG applications”, Medical & Biological Engineering & Computing, July 1983, pp. 465-472.

[57] B. R. S. Reddy and I. S. N. Murthy, “ECG data compression using Fourier descriptors”, Trans, on BME, April 1986, vol. 33, no. 4, pp. 428-434.

[58] A. E. Cetin, H. Koymen and M. C. Aydin, “Multichannel ECG data compression by multirate signal processing and transformation domain coding techniques”, Trans, on BME, May 1993, vol. 40, no. 5 pp. 495-499.

[59] W. Philips and C. D. Jonghe, “Data compression of ECG's by high degree polynomial approximation”, Trans, on BME, April, 1992, vol. 39, no. 4, pp. 330-336.

[60] W. Philips, “ECG Data compression with time warped polynomials”, Trans, on BME, November 1993, vol. 40, no. 11 pp. 1095-1101.

[61] R. Jane, S. Olmos, P. Laguna and P. Chaminal, “Adaptive Hermite models for ECG data compression: performance and evaluation with automatic wave detection”, Computers in Cardiology, Los Alamitos, CA, USA, IEEE Computer Society Press, 1993, pp. 389-392.

[62] K. Anant, F. Dowla and G. Rodrigue, “Vector quantization of ECG wavelet coefficients”, IEEE signal processing letters, July 1995, vol.2, no. 2.

[63] A. G. Ramakrishnan and S. Saha, “ECG coding by wavelet-based linear prediction”, IEEE Trans. On BME, , December 1997, vol. 44, no. 12, pp.1253-1261.

[64] C. K. Jha and M. H. Kolekar, “Performance analysis of ECG data compression using wavelet based hybrid transform method”, In 2015 International Conference on Microwave, Optical and Communication Engineering (ICMOCE) 2015 Dec 18, pp. 138-141. IEEE.

[65] B. Bradie, “Wavelet packet-based compression of single lead ECG”, IEEE Trans, on BME, May 1996, vol. 43, no. 5, pp. 493-501.

[66] J. Chen and S. Itoh, “A wavelet transform based ECG compression method guaranteeing desired signal quality”, Trans, on BME, December 1998, vol. 45, no. 12, pp. 1414-1419.

[67] H. Lee and K. M. Buckley, “ECG data compression using cut and align beats approach and 2-D transforms”, Trans, on BME, May 1999. vol. 46, no. 5, pp. 556-564.

[68] Z. Lu, D. Y. Kim and A. Pearlman, “Wavelet compression of ECG signals by the set partitioning in hierarchical trees algorithm”, Trans, on BME, July 2000, vol. 47, no. 7, pp. 849- 855.

[69] R. Besar, C. Eswaran, S. Sahib, R. J. Simpson, “On the choice of the wavelets for ECG data compression,” In 2000 IEEE International Conference on Acoustics, Speech, and Signal Processing. Proceedings, Cat. No. 00CH37100, 2000, vol. 6, pp. 3614-3617.

[70] R. S. H. Istepanian, L. J. Hadjileontiadis and S. M. Panas, “ECG data compression using wavelets and higher order statistics methods”, Trans, on Information Technology in Biomedicine, June 2001, vol. 5, no. 2, pp. 108-115.

[71] B. A. Rajoub, “An efficient coded algorithms for the compression of ECG signals using the wavelet transform”, Trans, on BME, April 2002, vol. 49, no. 4, pp. 355-362.

[72] P. K. Kulkami, V. Kumar and H. K. Verma, “Diagnostic acceptability of FFT- based ECG data compression”, Journal ofMedical Engineering and Technology, Sept-Oct, 1997,vol. 21, no. 5, pp. 185-189,

[73] P. K. Kulkami, V. Kumar and H. K. Verma, “ECG data compression using fast Walsh transform and its clinical acceptability”, International Journal of Systems Science, vol. 28, no. 8, pp. 831-836, August 1997.

[74] A. V. Chagas, E. A. Da Silva and J. Nadal, “ECG data compression using wavelets”, In Computers in Cardiology, 2000, pp. 423-426.

[75] R. Benzid, F. Marir, A. Boussaad, M. Benyoucef and D Arar, “Fixed percentage of wavelet coefficients to be zeroed for ECG compression”, Electronics Letters, 2003 May 29, vol. 39, no. 11. pp. 830-831.

[76] W. J. Hwang, C. F. Chine, K. J. Li, “Scalable medical data compression and transmission using wavelet transform for telemedicine applications”, IEEE transactions on information technology in biomedicine, 2003 Mar, vol. 7, no. 1, pp. 54-63.

[77] Z. Xiong, X. Wu, S. Cheng and J. Hua, “Lossy-to-lossless compression of medical volumetric data using three-dimensional integer wavelet transforms”, IEEE transactions on medical imaging, 2003 Mar, vol. 22, no. 3, pp. 459-470.

[78] S. G. Miaou and S. N. Chao, “Wavelet-based lossy-to-lossless ECG compression in a unified vector quantization framework”, IEEE Transactions on Biomedical Engineering, 2005 Mar, vol. 52, no. 3, pp. 539-43.

[79] S. C. Tai, Sun C, W. C. Yan, “A 2-D ECG compression method based on wavelet transform and modified SPIHT”, IEEE Transactions on Biomedical Engineering, 2005 Jun, vol. 52, no. 6, pp. 999-1008.

[80] I. M. Rezazadeh, M. H. Moradi and A. M. Nasrabadi, “Implementing of SPIHT and sub-band energy compression (SEC) method on two-dimensional ECG compression: a novel approach”, In Engineering in Medicine and Biology Society, 2005, IEEE-EMBS 2005. 27th Annual International Conference of the 2006 Jan 17, pp. 3763-3766.

[81] M. Blanco-Velasco, F. Cruz-Roldán, J. I. Godino-Llorente, J. Blanco-Velasco, C. Armiens-Aparicio and F. López-Ferreras, “On the use of PRD and CR parameters for ECG compression,” Medical engineering & physics, 2005 Nov 1, vol. 27, no. 9, pp. 798-802.

[82] M. Moazami-Goudarzi and M. H. Moradi, “Electrocardiogram signal compression using multiwavelet transform. signal processing, 2005 Jun, vol. 4, no. 12.

[83] M. S. Manikandan and S. Dandapat, “ECG signal compression using discrete sinc interpolation”, In Intelligent Sensing and Information Processing, 2005. ICISIP 2005, Third International Conference on 2005 Dec 14, pp. 14-19. IEEE.

[84] A. S. Al-Fahoum, “Quality assessment of ECG compression techniques using a wavelet-based diagnostic measure”, IEEE Transactions on Information Technology in Biomedicine, 2006 Jan, vol. 10, no. 1, pp. 182-191.

[85] C. T. Ku, H. S. Wang, K. C. Hung, Y. S. Hung, “A novel ECG data compression method based on nonrecursive discrete periodized wavelet transform,” IEEE Transactions on Biomedical Engineering, 2006 Dec, vol. 53, no. 12, pp. 2577-2583.

[86] M. S. Manikandan, S. Dandapat, “Wavelet threshold based ECG compression using USZZQ and Huffman coding of DSM”, Biomedical Signal Processing and Control, 2006 Oct 1, vol. 1, no. 4, pp. 261-270.

[87] G. Tohumoglu and K. E. Sezgin, “ECG signal compression by multi-iteration EZW coding for different wavelets and thresholds”, Computers in Biology and Medicine, 2007 Feb 1, vol. 37, no. 2 pp. 173-82.

[88] L. Brechet, M. F. Lucas, C. Doncarli and D. Farina, “Compression of biomedical signals with mother wavelet optimization and best-basis wavelet packet selection”, IEEE Transactions on Biomedical Engineering, 2007 Dec, vol. 54, no.12, pp. 2186-2192.

[89] S. M. Sahraeian and E. Fatemizadeh, “Wavelet-based 2-D ECG data compression method using SPIHT and VQ coding”, In EUROCON, 2007. The International Conference on" Computer as a Tool, 2007 Sep 9, pp. 133-137. IEEE.

[90] Z. Arnavut, “ECG signal compression based on Burrows-Wheeler transformation and inversion ranks of linear prediction”, IEEE transactions on biomedical engineering. 2007 Mar, vol. 54, no. 3, pp. 410-418.

[91] R. Benzid, A. Messaoudi and A. Boussaad, “Constrained ECG compression algorithm using the block-based discrete cosine transform”, Digital Signal Processing, 2008 Jan 1, vol. 18, no. 1, pp. 56-64.

[92] E. Sharifahmadian, “Wavelet compression of multichannel ECG data by enhanced set partitioning in hierarchical trees algorithm”, In Engineering in Medicine and Biology Society, 2006. EMBS'06 28th Annual International Conference of the IEEE, 2006 Aug 30, pp. 5238-5243.

[93] J. Chen, F. Wang, Y. Zhang and X. Shi, “ECG compression using uniform scalar dead-zone quantization and conditional entropy coding”, Medical Engineering & Physics, 2008 May 1, vol. 30, no. 4, pp. 523-530.

[94] S. Lee and M. Lee M, “A real-time ECG data compression algorithm for a digital holter system”, In Engineering in Medicine and Biology Society, 2008. EMBS 2008. 30th Annual International Conference of the IEEE 2008 Aug 20, pp. 4736-4739. IEEE.

[95] X. Wang and J. Meng, “A 2-D ECG compression algorithm based on wavelet transform and vector quantization”, Digital Signal Processing, 2008 Mar 1, vol. 18, no. 2, pp. 179-88.

[96] V. Aggarwal and M. S. Patterh, “Quality controlled ECG compression using Discrete Cosine transform (DCT) and Laplacian Pyramid (LP)”, Multimedia, Signal Processing and Communication Technology, IMPACT. 2009 Mar 14, 2009, pp. 12-15.

[97] R. Lee and H. King-Chu, “New Modified SPIHT Algorithm for Data Compression System”, Journal of Medical and Biological Engineering, 2019, vol. 39, no. 1, pp.18-26

[98] C. K. Jha, M. H. Kolekar, “Electrocardiogram data compression using DCT based discrete orthogonal Stockwell transform”, Biomedical Signal Processing and Control, 2018 Sep, vol. 1, no. 46, pp. 174-81.

[99] L. Wu ,K, Yu, D. Cao, Y. Hu and Z. Wang, “Efficient sparse signal transmission over a lossy link using compressive sensing”, Sensors, 2015 Aug, vol. 15, no. 8, pp. 19880-911.

[100] A. A. Shinde and P. Kanjalkar, “The comparison of different transform based methods for ECG data compression”, In Signal Processing, Communication, Computing and Networking Technologies (ICSCCN), 2011 International Conference on 2011 Jul 21, pp. 332-335, IEEE.

[101] A. Bendifallah, R. Benzid and M. Boulemden, “Improved ECG compression method using discrete cosine transform”, Electronics letters, 2011 Jan, vol. 47, no. 2, pp. 87-109.

[102] L. F. Polania and Carrillo, M. Blanco-Velasco, K. E. Barner, “Compressed sensing based method for ECG compression”, In Acoustics, Speech and Signal Processing (ICASSP), 2011 IEEE International Conference on, 2011 May 22 pp. 761-764. IEEE.

[103] S. Lee, J. Kim and M. Lee, “A real-time ECG data compression and transmission algorithm for an e-health device”, IEEE Transactions on Biomedical Engineering, 2011 Sep, vol. 58, no. 9 pp. 2448-55.

[104] L. N. Sharma, S. Dandapat and A. Mahanta, “Multichannel ECG data compression based on multiscale principal component analysis”, IEEE Transactions on Information technology in Biomedicine, 2012 Jul 1, vol. 16, no. 4, pp. 730-736.

[105] K, Ranjeet, A. Kuamr, R. K. Pandey, “ECG signal compression using optimum wavelet filter bank based on Kaiser window”, Procedia engineering, 2012 Jan 1, vol. 38, pp. 2889-2902.

[106] B. Huang, Y. Wang and J. Chen, “ECG compression using the context modeling arithmetic coding with dynamic learning vector–scalar quantization”, Biomedical Signal Processing and Control, 2013 Jan 1, vol. 8, no.1, pp. 59-65.

[107] R. Kumar, A. Kumar and R. K. Pandey, “Beta wavelet based ECG signal compression using lossless encoding with modified thresholding”, Computers & Electrical Engineering. 2013 Jan 1, vol. 39, no.1, pp. 130-40.

[108] K. C. Hung, T. C. Wu, H. W. Lee and T. K. Liu, “EP-based wavelet coefficient quantization for linear distortion ECG data compression”, Medical engineering & physics, 2014 Jul 1, vol. 36, no.7, pp. 809-821.

[109] J. Ma, T. Zhang and M. A. Dong, “A novel ECG data compression method using adaptive Fourier decomposition with security guarantee in e-health applications”, IEEE journal of biomedical and health informatics, 2015 May, vol. 19, no. 3, pp. 986-994.

[110] S. Padhy, L. N. Sharma and S. Dandapat, “Multilead ECG data compression using SVD in multiresolution domain”, Biomedical signal processing and control, 2016 Jan 1, vol. 23, pp.10-18.

[111] M. M. Abo-Zahhad, A. M. Mohamed and A. I. Hussein. “A hybrid ECG compression technique based on DWT and removal of interbeats and intrabeats correlations”, In 2015 Tenth International Conference on Computer Engineering & Systems (ICCES) 2015, Dec 23, pp. 416-421, IEEE.

[112] A. Al-Shrouf, M. Abo-Zahhad and S. M. Ahmed, “A novel compression algorithm for electrocardiogram signals based on the linear prediction of the wavelet coefficients”, Digital Signal Processing, 2003 Oct 1, vol. 13, no. 4, pp. 604-22.

[113] R. Besar, “Study of Wavelet Transforms For Data Compression And Decompression of Audio And ECG Signals”, Doctoral dissertation, Multimedia University.

[114] T. Tekeste, H. Saleh, B. Mohammad and M. Ismail, “Ultra-Low Power QRS Detection and ECG Compression Architecture for IoT Healthcare Devices”, IEEE Transactions on Circuits and Systems I: Regular Papers, 2019 Feb, vol. 66, no. 2, pp. 669-679.

[115] A. Cohen, P. M. Poluta and R. S. Millar, “Compression of ECG signals using vector quantization", in Proc. of IEEE-90, COMSIG-90, Johannesburg, South Africa, pp. 45-54, 1990.

[116] H. Imai, N. Kimura and Y. Yoshida, “An efficient coding method for electrocardiography using spline functions”, Syst. Comput. Japan, vol. 16, no. 3, pp. 85-94, 1985.

[117] U. Ruttiman and H. V. Pipberger, “Compression of the ECG by prediction or interpolation and entropy encoding”, IEEE Trans, on BME, vol. 26, no.11, pp. 613- 623, November 1979.

[118] J. Makhoul, “Linear prediction: Atutorial review”, Proc. of IEEE, April 1975, vol. 63, no. 4, pp. 561-580.

[119] R. W. Schafer and L. R. Rabiner, “A digital signal processing approach to interpolation", Proc. of IEEE, June 1973, vol. 61, no. 6, pp. 692-703.

[120] P. D. Souza, “Statistical tests and distance measures for LPC coefficients”, IEEE Trans, on Acoustics, Speech and signal processing, December 1977, vol. ASSP-25, no. 6, pp. 554-559.

[121] P. S. Hamilton and W. J. Tompkins, “Compression of ambulatory ECG by average beat subtraction and residual differencing”, Trans, on BME, March 1991, vol. 38, no. 3, pp. 253- 259.

[122] G. Nave and A. Cohen A, “ECG compression using long term prediction”, IEEE Trans, on BME, September 1993, vol. 40, no. 9, pp. 877-885.

[123] A. Cohen and Y. Zigel, “Compression of multichannel ECG through multichannel long term prediction”, IEEE Engineering in Medical and Biology, January/February 1998, pp. 109-115.

[124] G. D. Barlas and E. S. Skordalakis, “A novel family of compression algorithms for ECG and other semiperiodical, one-dimensional, biomedical signals”, IEEE Trans, on BME, August 1996, vol. 43, no. 8, pp. 820-828.

[125] A. Iwata, Y. Nagasaka and N. Suzumura, “Compression of the ECG using neural network for digital Holter monitor”, IEEE Engineering in Medical and Biology Magazine, 1990, vol. 9, no. 3, pp. 53-57.

[126] Y. Nagasaka and A. Iwata, “Data compression oflong time ECG recording using BP and PCA neural network”, IEICE Trans, on Information and Systems, 1993, E 76-D, 12, pp. H34.1442.

[127] G. D. Barlas and E. S. Skordalakis, “A novel family of compression algorithms for ECG and other semiperiodical, one-dimensional, biomedical signals”, IEEE Trans, on BME, August 1996, vol. 43, no. 8, pp. 820-828.

[128] S. C. Saxena, A. Sharma, and S. C. Chaudhary, "Data compression and feature extraction of ECG signals", International Journal of Systems Science, May 1997, vol. 28, no. 5, pp. 483-498.

[129] M. Cassen and M. J. English, “Computationally efficient ECG compression scheme using a non-linear quantizer”, Computers in Cardiology (Lund), IEEE Computer Society Press, 1997, pp. 283-286.

[130] S. K. Mukhopadhyay, S. Mitra and M. Mitra, “An ECG signal compression technique using ASCII character encoding”, Measurement, 2012 Jul 1, vol. 45, no. 6, pp. 1651-60.

[131] A. Adamo, G. Grossi, R. Lanzarotti and J. Lin, “ECG compression retaining the best natural basis k-coefficients via sparse decomposition”, Biomedical Signal Processing and Control, 2015 Jan, vol. 1, no. 15, pp. 11-17.

[132] G. Y. Cho, S. J. Lee and T. R. Lee, “An optimized compression algorithm for real-time ECG data transmission in wireless network of medical information systems”, Journal of medical systems, 2015 Jan 1, vol. 39, no. 1, pp. 161.

[133] T. Y. Liu, K. J. Lin and H. C. Wu, “ECG Data Encryption Then Compression Using Singular Value Decomposition”, IEEE journal of biomedical and health informatics, 2018 May, vol. 22, no. 3, pp. 707-713.

[134] J. H. Hsieh, R. C. Lee, K. C. Hung and M. J. Shih, “Rapid and coding-efficient SPIHT algorithm for wavelet-based ECG data compression”, Integration the VLSI Journal, 2018 Jan, vol. 1, no. 60, pp. 248-256.

[135] C. J. Deepu, C. H. Heng and Y. Lian, “A Hybrid Data Compression Scheme for Power Reduction in Wireless Sensors for IoT”, IEEE transactions on biomedical circuits and systems, 2017, vol.11, no.2, pp. 245-254.

[136] R. Kumar and I. Saini, “Empirical wavelet transform based ECG signal compression”, IETE journal of research, vol.60, no.6, pp .423-431.

[137] V. A. Motinath, C. K. Jha and M. H. Kolekar, “A novel ECG data compression algorithm using best mother wavelet selection”, In Advances in Computing, Communications and Informatics (ICACCI), 2016 International Conference on 2016 Sep 21, pp. 682-686.

[138] M. Abo-Zahhad, A. F. Al-Ajlouni, S. M. Ahmed and R. J. Schilling, “A new algorithm for the compression of ECG signals based on mother wavelet parameterization and best-threshold levels selection”, Digital Signal Processing, 2013 May 1, vol. 23, no. 3, pp. 1002-1011.

[139] S. Chandra and A. Sharma, “Optimum QMF bank based ECG data compression”, In Electrical, Computer and Electronics (UPCON), 2017 4th IEEE Uttar Pradesh Section International Conference on 2017 Oct 26, pp. 118-123,

[140] S. Chandra and A. Sharma, “A computationally efficient approach for ECG signal denoising and data compression”, In Control and System Graduate Research Colloquium (ICSGRC), 2017 IEEE 8th 2017, Aug 4, pp. 22-27.

[141] A. Pandey , B. Singh, B. S. Saini and N. Sood, “A joint application of optimal threshold based discrete cosine transform and ASCII encoding for ECG data compression with its inherent encryption”, Australasian physical & engineering sciences in medicine, 2016 Dec 1, vol. 39, no. 4, pp. 833-855.

[142] A. Singh , L. N. Sharma and S. Dandapat, “Multi-channel ECG data compression using compressed sensing in eigenspace”, Computers in biology and medicine, 2016 Jun 1, vol. 73, pp. 24-37.

[143] R. Kumar and A. Kumar, “Compressed sensing based ECG signal compression for telemedicine”, In Bombay Section Symposium (IBSS), 2015 IEEE 2015 Sep 10, pp. 1-4.

[144] S. Padhy and S. Dandapat, “A new multilead ECG data compression method using higher-order singular value decomposition’, In Communications (NCC), 2014 Twentieth National Conference on 2014 Feb 28, pp. 1-4

[145] L. N. Sharma, S. Dandapat and A. Mahanta, “Multichannel ECG data compression based on multiscale principal component analysis”, IEEE Transactions on Information technology in Biomedicine, 2012 Jul 1, vol. 16, no. 4, pp. 730-736.

[146] C. Hernando-Ramiro, M. Blanco-Velasco, F. Cruz-Roldán and F. Pedroviejo-Benito, “Efficient thresholding-based ECG compressors for high quality applications using cosine modulated filter banks”, In Engineering in Medicine and Biology Society, EMBC, 2011 Annual International Conference of the IEEE 2011 Aug 30, pp. 7079-7082.

[147] M. Blanco-Velasco, B. Weng and K. E. Barner, “ECG signal denoising and baseline wander correction based on the empirical mode decomposition”, Computers in biology and medicine, 2008 Jan 1, vol. 38, no. 1, pp. 1-3.

[148] M. L. Ahlstrom and W. J. Tompkins, “Digital filters for real-time ECG signal processing using microprocessors”, IEEE Transactions on Biomedical Engineering, vol. 9, 1985, pp.708-713.

[149] A. A. Van. W. Jan, E. Van E and O. E. Herrmann, “ECG baseline wander reduction using linear phase filters” ,Computers and Biomedical Research, vol. 19, no. 5, 1986, pp. 417-427.

[150] C. Chu, and J. D. Edward, “Impulsive noise suppression and background normalization of electrocardiogram signals using morphological operators”, IEEE Transactions on Biomedical Engineering, vol. 36, no. 2, 1989, pp. 262-273.

[151] N. V. Thakor and Y. S. Zhu, “Applications of adaptive filtering to ECG analysis: noise cancellation and arrhythmia detection”, IEEE transactions on biomedical engineering, vol. 38, no. 8, 1991, pp.785-794.

[152] R. Jané, P. Laguna, N. V. Thakor and C. P. Caminal, “Adaptive baseline wander removal in the ECG: Comparative analysis with cubic spline technique”, In Proceedings Computers in Cardiology, pp. 143-146. IEEE, 1992.

[153] S. Pei, and T. Chien-Cheng, “Elimination of AC interference in electrocardiogram using IIR notch filter with transient suppression”, IEEE transactions on biomedical engineering, vol. 42, no. 11, 1995, pp. 1128-1132.

[154] P. S. Hamilton, “A comparison of adaptive and nonadaptive filters for reduction of power line interference in the ECG”, IEEE Transactions on Biomedical Engineering, vol. 43, no. 1 1996, pp. 105-109.

[155] M. Üstündağ, A. Şengür, M. Gökbulut and F. Ata, “Performance comparison of wavelet thresholding techniques on weak ECG signals denoising”, Przegląd Elektrotechniczny, 2013, vol. 89, no.5, pp. 63-76.

[156] P. E. Tikkanen, “Nonlinear wavelet and wavelet packet denoising of electrocardiogram signal”, Biological cybernetics, vol. 80, no. 4 1999, pp. 259-267.

[157] P. M. Agante and J. P. Marques D. Sá, “ECG noise filtering using wavelets with soft-thresholding methods”, In Computers in Cardiology, 1999, vol. 26, Cat. No. 99CH37004, pp. 535-538. IEEE.

[158] D. Raya, D. M. Anne and L. G. Sison. “Adaptive noise cancelling of motion artifact in stress ECG signals using accelerometer”, In Proceedings of the Second Joint 24th Annual Conference and the Annual Fall Meeting of the Biomedical Engineering Society, Engineering in Medicine and Biology, 2002, vol. 2, pp. 1756-1757, IEEE.

[159] S. Yan, L. C. Kap and S. M. Krishnan, “ECG signal conditioning by morphological filtering”, Computers in biology and medicine, 2002, vol. 32, no. 6, pp. 465-479.

[160] Y. Bai, C. Wen-Yang, C. Chien-Yu, L. Yi-Ting, T. Yi-Ching and T. Cheng-Hung, “Adjustable 60Hz noise reduction by a notch filter for ECG signals”, In Proceedings of the 21st IEEE Instrumentation and Measurement Technology Conference EEE Cat. no. 04CH37510, vol. 3, pp. 1706-1711, IEEE.

[161] J. Zhang and B. Donghui, “Wavelet approach for ECG baseline wander correction and noise reduction”, In 2005 IEEE Engineering in Medicine and Biology 27th Annual Conference, pp. 1212-1215. IEEE.

[162] J. M. Łęski and N. Henzel, “ECG baseline wander and powerline interference reduction using nonlinear filter bank”, Signal processing, 2005, vol. 85, no. 4, pp.781-793.

[163] S. Chavan, S. Mahesh, R. A. Agarwala and M. D. Uplane, “Digital elliptic filter application for noise reduction in ECG signal”, WSEAS transactions on Electronics, 2006, vol. 3, no. 1, pp. 65-70.

[164] M. Blanco-Velasco, W. Binwei and E. B. Kenneth, “ECG signal denoising and baseline wander correction based on the empirical mode decomposition”, Computers in biology and medicine, 2008, vol. 38, no. 1, pp. 1-13.

[165] W. Yunfeng, M. Rangaraj. Y. Zhou and N. Sin-Chun, “Filtering electrocardiographic signals using an unbiased and normalized adaptive noise reduction system”, Medical Engineering & Physics, 2009, vol. 31, no. 1, pp. 17-26.

[166] I. Romero, “PCA and ICA applied to noise reduction in multi-lead ECG”, In 2011 Computing in Cardiology, pp. 613-616, IEEE.

[167] K. Chang, and L. Shing-Hong, “Gaussian noise filtering from ECG by Wiener filter and ensemble empirical mode decomposition”, Journal of Signal Processing Systems, 2011, vol. 64, no. 2, pp. 249-264.

[168] El-Dahshan and A. El-Sayed, “Genetic algorithm and wavelet hybrid scheme for ECG signal denoising”, Telecommunication Systems, 2011, vol. 46, no. 3, pp. 209-215.

[169] M. Kaur and B. Singh, “Comparison of different approaches for removal of baseline wander from ECG signal”, In Proceedings of the International Conference & Workshop on Emerging Trends in Technology, 2011, pp. 1290-1294, ACM.

[170] M. A. Kabir and C. Shahnaz, “Denoising of ECG signals based on noise reduction algorithms in EMD and wavelet domains”, Biomedical Signal Processing and Contro, 2012, vol. l7, no. 5, pp. 481-489.

[171] A. Jukka Lipponen and Mika P. Tarvainen, “Advanced maternal ECG removal and noise reduction for application of fetal QRS detection”, In Computing in Cardiology 2013, pp. 161-164, IEEE.

[172] P. Suranai and Y. Xiao-Hua, “An adaptive filtering approach for electrocardiogram (ECG) signal noise reduction using neural networks”, Neurocomputing, 2013, vol. 117, pp. 206-213.

[173] D. Sadhukhan and M. Mitra, “ECG noise reduction using Fourier coefficient suppression”, In Proceedings of the 2014 International Conference on Control, Instrumentation, Energy and Communication (CIEC), pp. 142-146, IEEE.

[174] G. Liu and Y. Luan, “An adaptive integrated algorithm for noninvasive fetal ECG separation and noise reduction based on ICA-EEMD-WS”, Medical & biological engineering & computing, 2015, vol. 53, no. 11, pp. 1113-1127.

[175] A. Mirza, S. M. Kabir, and S. Ayub, “Impulsive Noise Cancellation of ECG signal based on SSRLS”, Procedia Computer Science, 2015, vol. 62, pp. 196-202.

[176] S. Goel, G. Kaur, and P. Tomar, “Performance analysis of Welch and Blackman Nuttall window for noise reduction of ECG”, In 2015 International Conference on Signal Processing, Computing and Control (ISPCC), pp. 87-91, IEEE.

[177] A. K. Belchandan, K. Deshmukh and J. Kumar, “Removal of noises in ECG signal by using a digital FIR-IIR filter in VHDL”, Digit. Signal Process, 2016, vol. 8, pp. 135-139.

[178] S. K. Bashar, A. J. Walkey, D. D. McManus and Chon KH. VERB, “VFCDM-Based Electrocardiogram Reconstruction and Beat Detection Algorithm”, 2019 Jan 21, IEEE.

[179] F. Liu, C. Liu , X. Jiang, L. Zhao, J. Li, C. Song and S. Wei, “A Decision-Making Fusion Method for Accurately Locating QRS Complexes from the Multiple QRS

Detectors", In World Congress on Medical Physics and Biomedical Engineering, 2018 Singapore, pp. 351-355, Springer.

[180] A. Sharma, S. Patidar, A. Upadhyay and U. R. Acharya, "Accurate tunable-Q wavelet transform based method for QRS complex detection", Computers & Electrical Engineering, 2019 May 1, vol. 75, pp. 101-111.

[181] Y. N. Singh and S. K. Singh, "Identifying individuals using eigenbeat features of electrocardiogram", Journal of Engineering. 2013.

[182] S. Jain, M. K. Ahirwal, A. Kumar, V. Bajaj and G. K. Singh, "QRS detection using adaptive filters A comparative study", ISA transactions, 2017 Jan 1, vol. 66, pp. 362-375.

[183] J. Pan and W. J. Tompkins, "A real - time QRS detection algorithm", IEEE Trans, on BME, March 1985, vol. 32, no. 3, pp. 230-236.

[184] P. Trahanias and E. Skordalakis, "Bottom-up approach to the ECG pattern-recognition problem", Medical & Biological Engineering & Computing, May 1989, vol. 27, no. 5, pp. 221-229.

[185] S. S. Mehta, S. C. Saxena and H. K. Verma, "Computer-aided interpretation of ECG for diagnostics", International Journal of Systems Science, January 1996, vol. 27, no. l, pp. 43-58.

[186] F. N. Abdullah, F. S. Abas and R. Besar, "ECG classification using wavelet transform and discriminant analysis", In 2012 International Conference on Biomedical Engineering (ICoBE) 2012 Feb 27, pp. 191-196. IEEE.

[187] P. Trahanias and E. Skordalakis, "Bottom-up approach to the ECG pattern-recognition problem", Medical & Biological Engineering & Computing, May 1989, vol. 27, no. 5, pp. 221-229,

[188] M. Okada, "A digital filter for the QRS complex detection", IEEE Trans, on BME, December 1979, vol. 26, no. 12, pp. 700-703.

[189] N. V. Thakor, J. G. Webster and W. J. Tompkins, "Estimation of QRS complex power spectra for design of a QRS filter", IEEE Trans on BME, November 1984, vol. 31, no. 11, pp. 702- 706.

[190] J. Pan and W. J. Tompkins, "A real - time QRS detection algorithm", IEEE Trans, on BME, March 1985, vol. 32, no. 3, pp. 230-236.

[191] P. S. Hamilton and W. J. Tompkins, "Quantitative investigation of QRS detection rules using the MIT/BIH Arrhythmia database", IEEE Trans, on BME, December 1986, vol. 33, no. 12, pp. 1157-1165.

[192] P. Laguna, D. Vigo, R. Jane and P. Caminal, "Automatic wave onset and offset determination in ECG signals: validation with the CSE database", Computers in

Cardiology, Los Alamitos, CA, USA, IEEE Computer Society Press, 1992. pp. 167-170.

[193] R. J. Martis, C. Chakraborty and A. K. Ray, "Wavelet-based machine learning techniques for ECG signal analysis", In Machine learning in healthcare informatics 2014, pp. 25-45, Springer, Berlin, Heidelberg.

[194] S. Z. Mahmoodabadi, A. Ahmadian, M. Abolhasani, P. Babyn and J. Alirezaie, "A fast expert system for electrocardiogram arrhythmia detection", Expert Systems, 2010 Jul, vol. 27, no. 3, pp. 180-200.

[195] S. Dandapat and G. C. Ray, "Spike detection in biomedical signals using midprediction filter", Medical & Biological Engineering & Computing, pp. 354-360, July 1997.

[196] V. X. Afonso, W. J. Tompkins, N. Q. Nguyen and S. Luo, "ECG beat detection using filter banks", IEEE Trans, on BME, February 1999, vol. 46, no. 2, pp. 192-202.

[197] L. T. Jan, A. K. Jan and H. V. B. Jan, "Algorithms for the detection of events in electrocardiograms", Computer methods and programs in Biomedicine, 1986 pp. 149-161.

[198] L. Sornmo, O. Pahlm, N. Mats-Erik and O. B. Per, "A mathematical approach to QRS detection", IEEE Computers in Cardiology, 1980, pp. 205-208.

[199] M. Üstündağ,M. Gökbulut, A. Şengür and F. Ata,"Denoising of weak ECG signals by using wavelet analysis and fuzzy thresholding", Network Modeling Analysis in Health Informatics and Bioinformatics, 2012 Dec 1, vol. 1, no. 4, pp. 135-140.

[200] P. E. Trahanias, "An approach to QRS complex detection using mathematical morphology", IEEE Trans, on BME, February 1993, vol. 40, no. 2, pp. 201-205,

[201] R. Maheshwari, G. Vijaya, V. Kumar and H. K. Verma, "Signal-analysis and a heuro-logistic interpretation of multi-lead electrocardiograms", International Journal of Systems Science, March 1998, vol. 29, no. 3, pp. 323-334.

[202] R. J. Oweis and B. O. Al-Tabbaa, "QRS detection and heart rate variability analysis: A survey", Biomedical science and engineering, 2014, vol. 2, no. 1, pp. 13-34.

[203] Y. H. Hu, W. J. Tompkins and Q. Xue, "Artificial neural network for ECG arryhthmia monitoring", In Neural Networks for Signal Processing II Proceedings of the 1992 IEEE Workshop, 1992 Aug 31, pp. 350-359, IEEE.

[204] Q. Qin, J. Li, Y. Yue and C. Liu, "An adaptive and time-efficient ECG R-Peak detection algorithm", Journal of healthcare engineering, 2017.

[205] S. Yazdani and J. M. Vesin, "Extraction of QRS fiducial points from the ECG using adaptive mathematical morphology, "Digital Signal Processing, 2016 Sep 1, vol. 56, pp. 100-109.

[206] Y. Zhao, Z. Shang and Y. Lian, “User Adaptive QRS Detection Based on One Target Clustering and Correlation Coefficient”, In 2018 IEEE Biomedical Circuits and Systems Conference BioCAS, 2018 Oct 17, pp. 1-4, IEEE.

[207] G. Smaoui, A. Young and M. Abid, “Single scale CWT algorithm for ECG beat detection for a portable monitoring system”, Journal of Medical and Biological Engineering, 2017 Feb 1, vol. 37, no. 1, pp. 132-9.

[208] W. Jenkal, R. Latif, A. Toumanari, A. Dliou, O. El B’charri and F. M. Maoulainine, “QRS detection based on an advanced multilevel algorithm”, International Journal of Advanced Computer Science and Applications, 2016, vol. 1, no. 7, pp. 253-60.

[209] R. J. Martis, U. R. Acharya, C. M. Lim, K. M. Mandana, A. K. Ray and C. Chakraborty, “Application of higher order cumulant features for cardiac health diagnosis using ECG signals”, International journal of neural systems, 2013 Aug 30, vol. 23, no. 04, pp. 1350014.

[210] P. Laguna, R. Jane, S. Olmos, N. V. Thakor, H. Rix and P. Caminal, “Adaptive estimation of QRS complex wave features of ECG signal by the Hermite Model”, Medical & Biological Engineering & Computing, January 1996, pp. 58-68.

[211] S. Z. Mahmoodabadi, A. Ahmadian and M. D. Abolhasani, “ECG feature extraction using Daubechies wavelets”, In Proceedings of the fifth IASTED International conference on Visualization, Imaging and Image Processing 2005 Sep 7, pp. 343-348.

[212] M. S. Nambakhsh, A. Ahmadian, M. Ghavami, R. S. Dilmaghani and S. Karimi-Fard, “A novel blind watermarking of ECG signals on medical images using EZW algorithm”, In 2006 International Conference of the IEEE Engineering in Medicine and Biology Society 2006 Aug 30, pp. 3274-3277, IEEE.

[213] S. Sahoo, B. Kanungo, S. Behera and S. Sabut, “Multiresolution wavelet transform based feature extraction and ECG classification to detect cardiac abnormalities”, Measurement, 2017 Oct 1, vol. 108:55-66.

[214] M. Merah, T. A. Abdelmalik and B. H. Larbi, “R-peaks detection based on stationary wavelet transform”, Computer methods and programs in biomedicine, 2015 Oct 1, vol. 121, no. 3, pp. 149-160.

[215] A. Sharma, S. Patidar, A. Upadhyay and A. R. Acharya, “Accurate tunable-Q wavelet transform based method for QRS complex detection”, Computers & Electrical Engineering, 2019 May 1, vol. 75, pp. 101-111.

[216] T. Chanwimalueang, W. Rosenberg and D. P. Mandic, “Enabling R-peak detection in wearable ECG: Combining matched filtering and Hilbert transform”, In 2015 IEEE International Conference on Digital Signal Processing (DSP), 2015 Jul 21, pp. 134-138, IEEE.

[217] O. B'charri, R. Latif, A. Abenaou, K. Elmansouri and W. Jenkal, "A Reliable QRS Detection Method Based on Dual-Tree Wavelet Transform", International Journal of Engineering and Technology, 2018, vol. 8, no. 4, pp. 307-320.

[218] A. Ahmadian , S. Karimifard , H. Sadoughi and M. Abdoli, "An efficient piecewise modeling of ECG signals based on Hermitian basis functions", In 2007 29th Annual International Conference of the IEEE Engineering in Medicine and Biology Society 2007 Aug 22, pp. 3180-3183, IEEE.

[219] D. Berwal, A. Kumar and Y. Kumar, "Design of high performance QRS complex detector for wearable healthcare devices using biorthogonal spline wavelet transform", ISA transactions, 2018 Oct 1, vol. 81, pp. 222-230.

[220] E. A. Junior, R. A. Valentim and G. B. Brandão, "Real-time premature ventricular contractions detection based on Redundant Discrete Wavelet Transform, Research on Biomedical Engineering", 2018.

[221] I. S. N. Murthy and G. S. D. Prasad, "Analysis of ECG from Pole-zero models", IEEE Trans, on BME, 1992, vol. 39, no. 7, pp. 741-751.

[222] A. Sharma, S. Patidar, A. Upadhyay and U. R. Acharya, "Accurate tunable-Q wavelet transform based method for QRS complex detection", Computers & Electrical Engineering, 2019 May 1, vol. 75, pp. 101-111.

[223] R. J. Martis, C. Chakraborty and A. K. Ray, "An integrated ECG feature extraction scheme using PCA and wavelet transform", In 2009 Annual IEEE India Conference, 2009 Dec 18, pp. 1-4. IEEE.

[224] J. S. Sahambi, S. N. Tandon and R. K. P. Bhatt, "Wavelet based ST-segment analysis", Medical & Biological Engineering & Computing, September 1998, vol. 36, pp. 568-572.

[225] J. S. Sahambi, S. N. Tandon and R. K. Bhatt, "Using wavelet transforms for ECG characterization; An on-line digital signal processing system", IEEE Engineering in Medicine and Biology Magazine, 1997 Jan, vol. 16, no. 1, pp. 77-83.

[226] P. Vaidyanathan, "Optimal design of linear phase FIR digital filters with very flat passbands and equiripple stopbands", IEEE transactions on circuits and systems, 1985, vol. 32, no. 9, pp. 904-917.

[227] T. Saramaki, T. Neuvo, and S. K. Mitra, "Design of computationally efficient interpolated FIR filters", IEEE Transactions on Circuits and Systems, 1988, vol. 35, no. 1, pp. 70-88.

[228] R. S. Powell and M. C. Paul, "Efficient narrowband FIR and IFIR filters based on powers-of-two sigma-delta coefficient truncation", IEEE Transactions on Circuits and Systems II: Analog and Digital Signal Processing, 1994, vol. 41, no. 8, pp. 497-505.

[229] Y. Yong, L. Zhang, and C. C. Ko, “An improved frequency response masking approach for designing sharp FIR filters”, Signal Processing, 2001, vol. 81, no. 12, pp. 2573-2581.

[230] L. O. Batista, J. T. Orlando, and S. Rui, “A fully adaptive IFIR filter with removed border effect”, In 2008 IEEE International Conference on Acoustics, Speech and Signal Processing, pp. 3821-3824. IEEE.

[231] J. D. Gordana and F. Alfonso, “Novel droop-compensated comb decimation filter with improved alias rejections”, AEU-International Journal of Electronics and Communications, 2013, vol. 67, no. 5, pp. 387-396.

[232] I. Singh and P. Mehta, “Joint optimization of interpolated FIR Filter,” International Journal of Engineering, vol. 2, no. 1, 2013.

[233] A. Hanrahan, J. J. M. C. Reddy and P. V. Sankar, “Interpolating cubic spline filter and method,” U.S. Patent, 7, 2011.

[234] W. Lu, and H. Takao, “A unified approach to the design of interpolated and frequency-response-masking FIR filters”, IEEE Transactions on Circuits and Systems I: Regular Papers, 2016, vol. 63, no. 12, pp. 2257-2266.

[235] L. Richard, “Interpolated narrowband lowpass FIR filters”, IEEE Signal Processing Magazine, 2003, vol. 20, no. 1, pp. 50-57.

[236] A Mehrnia and N. A Willson, “On optimal IFIR filter design”, In 2004 IEEE International Symposium on Circuits and Systems (IEEE Cat. No. 04CH37512), vol. 3, pp. III-133. IEEE, 2004.

[237] H. Xiangdong, S. Jing, Z. Wang, X. Yan and Z. Youquan, “Closed-form FIR filter design based on convolution window spectrum interpolation”, IEEE Transactions on Signal Processing, 2016, vol. 64, no. 5, pp. 1173-1186.

[238] A. Mehrnia and A. N. Willson, “Optimally Factored IFIR Filters”, Circuits, Systems, and Signal Processing, 2019, vol. 38, no. 1, pp. 259-286.

[239] A. Mehrnia and A. N. Willson, “A lower bound for the hardware complexity of FIR filters”, IEEE Circuits and Systems Magazine, 2017, vol. 18, no. 1, pp. 10-28.

[240] A. Mehrnia and A. N. Willson, “FIR filter design using optimal factoring: a walkthrough and summary of benefits”, IEEE Circuits and Systems Magazine, 2016, vol. 16, no. 1, pp. 8-21.

[241] A. Mehrnia and A. N. Willson, “Optimal factoring of FIR filters”, IEEE Transactions on Signal Processing, 2015, vol. 63, no. 3, pp. 647-661.

[242] A. Mehrnia and A. N. Willson, “Optimally Factored Interpolated FIR Filter Design”, U.S. Patent Application 14/641,234, filed September 10, 2015.

[243] C. Wangqian, H. Mo and L. Xin, “Sparse FIR Filter Design Based on Interpolation Technique”, In 2018 IEEE 23rd International Conference on Digital Signal Processing (DSP), pp. 1-5. IEEE, 2018.

[244] I. Raghu and E. Elias, “A Low Complexity Reconfigurable IFIR Filter for Software Defined Radio Channelizers”, In Proceedings of the 2nd International Conference on Vision, Image and Signal Processing, 2018, pp. 40, ACM.

[245] M. G. C. Jiménez, E. T. R. David and D. J. Gordana, “An efficient design of baseband filter for mobile communications”, In 2016 IEEE International Conference on Electro Information Technology (EIT), 2016, pp. 0368-0371. IEEE,

[246] R. C. Lamare, R. Sampaio-Neto, “Adaptive reduced-rank MMSE filtering with interpolated FIR filters and adaptive interpolators”, IEEE Signal Processing Letters. 2005, Mar, vol. 12, no 3, pp. 177-180.

[247] G. Capizzi, C. Salvatore, L. S. Grazia and N. Christian, “A new iterative FIR filter design approach using a Gaussian approximation”, IEEE Signal Processing Letters, 2018, vol. 25, no. 11, pp. 1615-1619.

[248] C. Meng, and J. Tuqan, “High-Performance Low-Cost DFE using IFIR Filters”, In 2007 Conference Record of the Forty-First Asilomar Conference on Signals, Systems and Computers, 2007, pp. 1154-1158, IEEE.

[249] D. L. C. Rodrigo and S. Raimundo, “Adaptive Interference Suppression for CDMA Systems using Interpolated FIR Filters with Adaptive Interpolators in Multipath Channels”, arXiv preprint arXiv:1301.5003, 2013.

[250] O. J. Coleman, “Nonseparable Nth-band filters as overlapping-subarray tapers”, In 2011 IEEE Radar Con (RADAR), 2011, pp. 141-146, IEEE.

[251] S. Sharma, S. Kulkarni, V. K. Pujari, P. Lakshminarsimhan and R. Seshaiah, “High data rate filter design for satellite communication”, In 2007 3rd International Conference on Recent Advances in Space Technologies, 2007, pp. 546-550, IEEE.

[252] H. P. Singh, S. Singh, R. K. Sarin, and J. Singh, “Evaluating the perceived voice quality on VoIP network using interpolated FIR filter algorithm”, International Journal of Electronics, 2012, vol. 99, no. 10, pp. 1449-1469.

[253] Y. Kuo, L. Tay-Jyi, Y. Li and C. Liu, “Design and implementation of low-power ANSI S1. 11 filter bank for digital hearing aids”, IEEE Transactions on Circuits and Systems I: Regular Papers, 2010, vol. 57, no. 7, pp. 1684-1696.

[254] V. J. Ogale and A. Jain, “Cosine Modulated Non-Uniform Filter Bank with Improved Computational Efficiency”, International Journal of Image, Graphics and Signal Processing, 2012, vol. 4, no. 2.

[255] S. S. Kaur and P. Saini, “Optimal interpolated FIR (IFIR) digital filter design with spectral estimation for radar and sonar system,” IJERA, 2013, pp. 866-871.

[256] G. Hatch, “Modulator having direct digital synthesis for broadband RF transmission”, U.S. Patent 5,412,352, issued May 2, 1995.

[257] S. Chandra and A. Sharma, “A computationally efficient approach for ECG signal denoising and data compression”, In 2017 IEEE 8th Control and System Graduate Research Colloquium (ICSGRC), pp. 22-27, IEEE.

[258] W. Omar, “Filter design”, Classical Circuit Theory, 2009, pp. 1-50.

[259] R. Koilpillai, R. David and P. P. Vaidyanathan, “Cosine-modulated FIR filter banks satisfying perfect reconstruction”, IEEE Transactions on signal processing, 1992, vol. 40, no. 4, pp. 770-783.

[260] Q. T. Nguyen, “Near-perfect-reconstruction pseudo-QMF banks”, IEEE Transactions on signal processing, 1994, vol. 42, no. 1, pp. 65-76.

[261] D. C. Creusere, and S. K. Mitra, “A simple method for designing high-quality prototype filters for M-band pseudo QMF banks”, IEEE Transactions on Signal Processing, 1995, vol. 43, no. 4, pp. 1005-1007.

[262] M. Abo-Zahhad, “Current state and future directions of multirate filter banks and their applications”, Digital signal processing, 2003 Jul 1, vol. 13 no. 3, pp. 495-518.

[263] Bergen and W. A. Stuart, “A design method for cosine-modulated filter banks using weighted constrained-least-squares filters”, Digital Signal Processing, 2008, vol. 18, no. 3, pp. 282-290.

[264] A. Kumar , G. K. Singh and R. S. Anand, “A simple method for the design of cosine-modulated pseudo-QMF banks”, International Journal of Signal and Imaging Systems Engineering, 2010, vol. 3, no. 4, pp. 236-245.

[265] M. Abo-Zahhad, “New Approach to the Design of Orthogonal M-Channel Perfect Reconstruction FIR Quadrature Mirror Filter Banks”, In Inter. Conf. On Computational Aspects and Their Application in Electrical Engineering, CATAEE'97, 1997 Jul.

[266] A. Kumar, G. K. Singh and R. S. Anand, “Design of Quadrature Mirror Filter bank using constrained optimisation”, International Journal of Signal and Imaging Systems Engineering, 2009, vol. 2, no. 3, pp. 126-133.

[267] A. Kumar, G. K. Singh and R. S. Anand, “A simple design method for the cosine-modulated filter banks using weighted constrained least square technique”, Journal of the Franklin Institute, 2011, vol. 348, no. 4, pp. 606-621.

[268] A. Kumar , S. Suman and G. K. Singh, “A new closed form method for design of variable bandwidth linear phase FIR filter using different polynomials”, AEU-International Journal of Electronics and Communications, 2014, vol. 68, no. 4, pp. 351-360.

[269] A. Kumar, G. K. Singh and R. S. Anand, "An improved closed form design method for the cosine modulated filter banks using windowing technique," Applied Soft Computing, 2011, vol. 11, no. 3, pp. 3209-3217.

[270] A. Vishwakarma, A. Kumar and G. K. Singh, "Design of near-perfect-reconstructed transmultiplexer using different modulation techniques: a comparative study, J King Saud Univ Eng Sci, vol. 29, pp. 257–263.

[271] I. Sharma, A. Kumar and G. K. Singh, "Adjustable window based design of multiplier-less cosine modulated filter bank using swarm optimization algorithms", AEU-Int J Electron C, 2016, vol. 70, pp. 85–94.

[272] K. Shaeen and E. Elias, "Prototype filter design approaches for near perfect reconstruction cosine modulated filter banks: a review", J Signal Process Syst, 2015, vol. 81, pp. 183–195.

[273] I. Sharma, A. Kumar and G. K. Singh, H. N. Lee, "Design of multiplierless cosine modulated filterbank using hybrid technique in sub-expression space," In 2016 IEEE International conference on digital signal processing (DSP), 16-18 Oct. 2016, pp. 360–364.

[274] K. Sharma and A. Sharma, "Design of Cosine Modulated Filter Banks exploiting spline function for spectrum sensing in Cognitive Radio applications, In: 2016 IEEE 1st international conference on power electronics, intelligent control and energy systems (ICPEICES), 2016, vol. 4, pp. 1–5.

[275] K. Baderia, A. Kumar and G. K. Singh, "An improved method for designing cosine modulated filter bank using polyphase components, In 2016 3rd International conference on signal processing and integrated networks (SPIN), 2016, 11-12 Feb, pp. 9–13.

[276] T. S Bindiya and E. Elias, "Design of multiplier-less sharp transition width non-uniform filter banks using gravitational search algorithm", Int J Electron 2015, vol. 102, pp. 48–70.

[277] T. S. Bindiya and E, Elias, "Design of FRM-based MDFT filter banks in the canonic signed digit space using modified meta-heuristic algorithms", 2016, vol. 9, no. 1, pp. 20-37

[278] P. Chris and S. K Dasgupta, "An iterative design with variable step prototype filter for cosinemodulated filter bank", Radio engineering, 2016, vol. 25, pp. 156–160

[279] S. Kalathil, E. Elias, "Non-uniform cosine modulated filter banks using meta-heuristic algorithms in CSD space", J Adv Res, 2015, vol. 6, pp. 839–849.

[280] S. Kalathil and Elias, "Design of multiplier-less sharp non-uniform cosine modulated filter banks for efficient channelizers in software defined radio," Eng Sci Technol Int, 2016.

[281] S. Kalathil, B. S. Kumar and E. Elias, “Efficient design of multiplier-less digital channelizers using recombination non-uniform filter banks”, J King Saud Univ Eng Sci, E 2018, Jan 1, vol. 30, no.1, pp. 31-37.

[282] B. Kuldeep, A. Kumar and G. K. Singh, “Design of multi-channel cosine-modulated filter bank based on fractional derivative constraints using cuckoo search algorithm. 2015a.

[283] A. R. Verma and Y. Singh, “Design of the Multi-Channel Cosine-Modulated Filter Bank Using the Bacterial Foraging Optimization Algorithm”, IETE Journal of Education, 2018, pp.1-12.

[284] G. Ozdemi, and N. Karaboga, “The effect of the increase in the number of channels to the performance in the Cosine Modulated Filter Bank design”, 26th Signal Processing and Communications Applications Conference (SIU), 2018, IEEE.

[285] A. Kumar, R. Pooja, G. K. Singh, “Performance of different window functions for designing quadrature mirror filter bank using closed form method”, International Journal of Signal and Imaging Systems Engineering, 2015, vol. 8, no. 6, pp. 367-379.

[286] A. S. Mehr and T. Chen, “Optimal design of nonuniform multirate filter banks”, Circuits, Systems and Signal Processing, 1999, vol. 18, no. 5, pp. 505-521.

[287] X. M. Xie, X. Y. Chen, and G. M. Shi, “A simple design method of linear-phase nonuniform filter banks with integer decimation factors”, In 48th Midwest Symposium on Circuits and Systems, 2005, pp. 724-727. IEEE.

[288] G. Shi, X. Xuemei, X. Chen, and W. Zhong, “Recent advances and new design method in nonuniform filter banks”, In 2006 International Conference on Communications, Circuits and Systems, IEEE, 2006, pp. 211-215.

[289] R. K. Soni, A. Jain, and R. Saxena, “An Optimized Design of Non-uniform Filterbank using Blackman Window Family”, International Journal of Signal & Image Processing, 2010, vol. 1, no. 1.

[290] N. C. Rajeev and J. Dale and Shpak, “Bi-criterion optimization of non-uniform filter banks for acoustic echo cancellation”, In 2011 IEEE International Symposium of Circuits and Systems (ISCAS), 2011, pp. 1073-1076, IEEE.

[291] A. Kumar, G. K. Singh and S. Anurag, “Design of nearly perfect reconstructed non-uniform filter bank by constrained equiripple FIR technique”, Applied Soft Computing, 2013, vol. 13, no. 1, pp. 353-360.

[292] P. Rani, “Performance of Different Adjustable Window Functions for Designing of Multirate Filter Bank,” M.tech Thesis, IIIT Jabalpur, 2013.

[293] A. Kumar, G. K. Singh and S. Anurag, “Design of nearly perfect reconstructed non-uniform filter bank by constrained equiripple FIR technique”, Applied Soft Computing, vol. 13, no. 1, 2013, pp. 353-360.

[294] R. K. Soni, A. Jain, and R. Saxena, "An optimized design of nonuniform filter bank using variable-combinational window function," AEU-International Journal of Electronics and Communications, 2013, vol. 67, no. 7, pp. 595-601.

[295] L. Condat, "Reconstruction from non-uniform samples: A direct, variational approach in shift-invariant spaces," Digital Signal Processing, 2013, vol. 23, no. 4, pp. 1277-1287.

[296] Z, Zhang and Y. Yun, "A simple design method for nonuniform cosine modulated filter banks," In 2007 International Symposium on Microwave, Antenna, Propagation and EMC Technologies for Wireless Communications, pp. 1052-1055. IEEE.

[297] S. Dhabal, S. M. L. Chowdhury and P. Venkateswaran, "A novel low complexity multichannel Cosine Modulated Filter Bank using IFIR technique for Nearly Perfect Reconstruction," In 2012 1st International Conference on Recent Advances in Information Technology (RAIT), pp. 208-213. IEEE.

[298] R. K. Son, A. Jain, and R. Saxena, "Design of M-band NPR cosine-modulated filterbank using IFIR technique," Journal of Signal and Information Processing, 2010, vol. 1, no. 01, pp. 35

[299] S. Kumar, A. Jain and R. Saxena, "A design of IFIR prototype filter for Cosine Modulated Filterbank and Transmultiplexer", AEU-international Journal of Electronics and Communications, 2013, vol. 67, no. 2, pp. 130-135.

[300] K. Rajgopal and S. Venkataraman, "A delayless adaptive IFIR filterbank structure for wideband and narrowband active noise control", Signal processing, 2006, vol. 86, no. 11, pp. 3421-3431.

[301] K. Rajgopal, J. D. Babu and S. Venkataraman, "Generalized adaptive IFIR filter bank structures", Signal Processing, 2007, vol. 87, no. 7, pp. 1575-1596.

[302] E. L. Batista, Eduardo, J. T. Orlando and R. Seara, "Efficient implementation of adaptive FIR-IFIR filters uses the LMS algorithm", In 2010 18th European Signal Processing Conference, 2010, pp. 1713-1717, IEEE.

[303] A. Antoniou, "Digital signal processing", McGraw-Hill; 2016 Sep 30.

[304] V. Britanak and K. R. Rao, "Perfect Reconstruction Cosine/Sine-Modulated Filter Banks in the Dolby Digital (Plus) AC-3 Audio Coding Standards", In Cosine-/Sine-Modulated Filter Banks 2018, pp. 327-413, Springer, Cham.

[305] D. L. Donoho I. M. Johnstone, "Adapting to unknown smoothness via wavelet shrinkage", Journal of the american statistical association, 1995 Dec 1, vol. 90, no. 432, pp. 1200-1224.

[306] S. Chandra, "A New IFIR Technique for Designing Digital Filter and Filter Bank," Indian Institute of Information Technology, Jabalpur, India, 2014.